Attitude control of flexible spacecraft

Design, implementation and evaluation of control strategies targeting flexible structures in the space domain, based in an analytical modeling of these structures

Jose Luis Redondo Gutiérrez

TUDelft

Attitude control of flexible spacecraft

Design, implementation and evaluation of control strategies targeting flexible structures in the space domain, based in an analytical modeling of these structures

by

Jose Luis Redondo Gutiérrez

to obtain the degree of Master of Science
at the Delft University of Technology,
to be defended publicly on Tuesday January 22^{nd} 2019 at $10:00$.

Student number:	4570332	
Project duration:	May 1, 2018 – November 30, 2018	
Supervisors:	Dipl.- Ing. A. Heidecker ,	German Aerospace Center (DLR)
	Dr. J. Guo,	TU Delft
Thesis committee:	Dr. A. Cervone,	TU Delft
	Dr. J. Guo,	TU Delft
	Dipl.- Ing. A. Heidecker ,	German Aerospace Center (DLR)
	Dr. E. Mooij,	TU Delft

An electronic version of this thesis is available at `http://repository.tudelft.nl/`.

TU Delft

Acknowledgement

Throughout my MSc thesis, I was helped, guided and inspired by several people I would like to thank before starting this report.

First of all, I would like to thank Ansgar Heidecker for his supervision and guidance during the whole project. His continuous support and feedback was essential for the work presented here. His constant interest in pushing the research forward, always introducing new challenges, was a source of new ideas and inspiration.

I also want to express my deepest gratitude to Jian Guo, who supervised the project's most relevant milestones and whose feedback contributed greatly to defining the direction of the research and to improving it.

Further, I would like to thank Patric Seefeldt for the opportunity of being part of the GoSolAr mission and for all the valuable inputs to the project. I would like to extend my thanks to the German Aerospace Center (DLR), as it was a great pleasure to be involved in such an inspiring company.

I also want to thank the members of the committee, for taking time to evaluate the work performed and providing with interesting additional perspectives.

Finally, I wish to thank my family and friends, for being a constant source of support and happiness.

Jose Luis Redondo Gutiérrez
Bremen, November 2018

Preface

During the last decades, large deployable structures are starting to be seen as a plausible configuration to multiple space missions, such as solar sailing, LEO (Low Earth Orbit) deorbiting missions or solar power generation. The potential of this kind of structures lays in their high area-to-mass ratio and their low launch volume, which decreases the overall cost of the mission. Technological advances in key areas, such as thin film solar cells or new deployment methods, as well as the miniaturization of satellites and their components, have considerably increased the usefulness of this design. The research presented in this document aims to contribute to these technological developments, helping to unfold the whole potential of this structural solution. This research comprises the MSc thesis of the author, in partial fulfillment of the MSc in Aerospace Engineering by the Technical University of Delft. The research was conducted during an internship at the department of Guidance Navigation and Control (GNC) Systems, Institute of Space Systems, German Aerospace Center (DLR). The research focuses in the study of the behavior of large thin flexible structures (LTFSs) in space from the perspective of the attitude determination and control system (ADCS). This work was performed in close relation to the DLR's mission GoSolAR (Gossamer Solar Array), which targets the technical developments that are necessary to unfold large flexible photovoltaic arrays in space.

The contributions of the research can be classified in two areas, related to the modeling of the structure and to the design of the ADCS. In relation to the first one, a methodology to integrate the flexibility of a structure into its equations of motion is explained from a theoretical perspective and implemented over a flexible spacecraft. This methodology is based in Lagrange's equations and can be applied to diverse structures, allowing modeling accurately the dynamics of the system while maintaining the model comprehensive and of relatively low order. The implementation of this approach leads to equations of motion containing both rigid and flexible motion and provides a guideline to apply the procedure to other structures. These equations enable to conduct an evaluation of the impact of the flexibility of a structure on its dynamics in a space environment. This way, the vibrations induced in the system due to, for example, actuators specifications or sudden changes in the external disturbances can be studied both qualitatively and quantitatively.

The second major area in which this thesis aims to contribute to the body of knowledge is related to the design and evaluation of attitude controllers targeting flexible satellites. Different controller's designs are proposed, based in: 1) a linear-quadratic regulator (LQR) approach, 2) robust control theory, particularly in the minimization of H_∞ and H_2 norms, and 3) a control approach based in analytical dynamics, known as the Udwadia–Kalaba approach. The performance of these designs was evaluated not only in relation to control instructions related to the rigid motion of the satellite, e.g. angular rate, but also to the capability of each controller of damping the system, reducing the vibrations that appear due to its flexibility. The particularities that need to be considered when implementing each controller are also studied, in order to give a clear idea of when would each controller be an adequate control solution. The result is a set of different control designs, including for each of these designs: 1) the methodology to derive the controller, 2) the performance of the controller and 3) the particularities and limitations of its implementation. This gives a clear basis to make a decision on which control approach to use in each particular scenario.

Contents

List of Figures ix

List of Tables xiii

Acronyms & Symbols xv

1 Introduction 1
- 1.1 Flexible structures in space . . . 2
- 1.2 Related research topics . . . 4
  - 1.2.1 Modeling flexible structures . . . 4
  - 1.2.2 Attitude control of LTFSs . . . 5
  - 1.2.3 Additional fields of interest . . . 6
- 1.3 Research specifications . . . 7
- 1.4 Structure . . . 8

2 Case of Study 9
- 2.1 GoSolAr's ADCS . . . 9
- 2.2 GoSolAr's specifications . . . 11
- 2.3 GoSolAr and research objective . . . 13

3 Basic Rigid Body Analysis 15
- 3.1 Simulation environment . . . 15
  - 3.1.1 Sensors and estimator . . . 15
  - 3.1.2 Controller and actuator . . . 16
  - 3.1.3 External disturbances . . . 17
  - 3.1.4 Equations of motion . . . 18
  - 3.1.5 Structural configurations and initial conditions . . . 19
- 3.2 Results . . . 20
  - 3.2.1 Basic analysis . . . 20
  - 3.2.2 Extended results . . . 23
- 3.3 Conclusions. . . . 27

4 Flexible model 29
- 4.1 Theoretical background. . . . 29
- 4.2 Flexible model . . . 31
  - 4.2.1 Structure and variables . . . 31
  - 4.2.2 Generic equations of motion. . . . 33
  - 4.2.3 Particularized equations of motion . . . 36
- 4.3 Model improvements . . . 39
- 4.4 Verification of the model . . . 40
  - 4.4.1 Single boom . . . 40
  - 4.4.2 Satellite's model . . . 40
- 4.5 Conclusions. . . . 42

5 Attitude Controller Design 45
- 5.1 LQR & b-dot controllers . . . 46
  - 5.1.1 Performance w.r.t. mission requirements . . . 47
  - 5.1.2 Impact of flexibility . . . 48
  - 5.1.3 Frequency domain . . . 50
- 5.2 Linearization of the plant . . . 52
  - 5.2.1 Analytical linearization . . . 53
  - 5.2.2 Numerical linearization . . . 54

5.3 Potential changes in the system . . . 55
5.4 Robust control . . . 56
5.4.1 Generic configuration . . . 57
5.4.2 H_2 norm . . . 59
5.4.3 H_∞ norm . . . 59
5.4.4 H_∞ vs. H_2 . . . 61
5.5 Non-linear controller . . . 66
5.5.1 Rigid approach . . . 67
5.5.2 Flexible approach . . . 69
5.6 Controllers' implementation . . . 73
5.6.1 Sensibility . . . 73
5.6.2 Feasibility . . . 76
5.7 Conclusions . . . 77

6 Conclusions and recommendations for future work 81
6.1 Conclusions . . . 81
6.2 Recommendations for future work . . . 83

Bibliography 85

A Simulator strucuture 87

B Tunning weights used in LQR controller. 89

C Altitude limitations 91

D Analysis of different orbits 95

E Interaction with eclipse and magnetorquer's duty cycle 97

F Verification of boom model. Example. 101

G Verification of flexible plant. 103

H Reducing order of robust controller. Example. 109

I Extended results. Robust control. 111

J Extend state vector's estimations 119

K Extended results of non-linear controller 121

L Extended results of the sensibility analysis 127

List of Figures

1.1 Artist's rendering of Gossamer-1 demonstrator [24]. 1
1.2 Solar-sailing IKAROS [28]. 2
1.3 Deployed ROSA [2]. 3
1.4 Schematic work flow for the MSc Thesis. 7

2.1 Different elements of the deployed configuration of the GoSolAr satellite, from a structural perspective. 11

3.1 Measuring process analysis. Comparison of actual state variables (up), measured state variables (center) and error (down). 16
3.2 Schematic view of the satellite structure used in the computation of surfaces forces (solar pressure and drag) for the deployed configuration. 17
3.3 Comparison of the external disturbances (torques) over stowed (right) and deployed (left) configurations. 550 km of altitude. 19
3.4 Module of the angular velocity throughout the detumbling phase for 5 different initial conditions. Stowed configuration. 21
3.5 Module of the angular velocity throughout the detumbling phase for 5 different initial conditions. Deployed configuration. 21
3.6 Pointing error [rad] throughout the pointing stage for 10 different initial conditions. Stowed configuration. 22
3.7 Pointing error [rad] throughout the pointing stage for 10 different initial conditions. Deployed configuration. Progressive acceleration. 23
3.8 Angular velocity [rad/s] throughout the pointing stage for 10 different initial conditions. Deployed configuration. Progressive acceleration. 23
3.9 Periodicity of the pointing error in the long term. 24
3.10 Study of the pointing phase for an inclination of 97 deg and different right ascensions of the ascending node. Altitude: 550km. 25
3.11 Orientation of the solar cells. A: nominal plane, B: alternative plane. 26
3.12 Evolution of the angle w.r.t. the sun vector for two different guidance instructions and initial conditions. h=550km, i=97 deg. 27

4.1 Procedure followed for the derivation of the flexible model. 31
4.2 Schematic drawing of the targeted structure. 32
4.3 Schematic drawing of a boom. 33
4.4 Shape functions for the first 5 modes. 37
4.5 Evolution of the state variables, as resulting from the analytical model. Case 0. 41
4.6 Evolution of the state variables, as resulting from the numerical model. Case 0. 42

5.1 Schematic view of the control loop. 46
5.2 Evolution of the angular velocity's norm during the detumbling phase. Flexible model. 5 cases. Initial orbit as in figure 3.5. 47
5.3 Evolution of the pointing error during the pointing stage. Flexible model. 5 cases. Initial orbit as in figure 3.7. 48
5.4 Properties of the evolution of the pointing error throughout time for the flexible and rigid plants. 48
5.5 Vibration of the booms (boom 1) due to entering or coming out an eclipse. 49
5.6 Interaction of the flexible structure (boom 1) with the control torque (magnetorquer). 50
5.7 Variables studied in the analyses in the frequency domain. 50
5.8 Bode analysis over flexible (F) and and rigid (R) open plants. 51
5.9 Bode analysis over the open and controlled (LQR controller) flexible plant. 52

5.10 Additive perturbation configuration [14]. 55
5.11 Bode analysis on the variation of the disturbance induced by the flexibility of the booms. Input: torque in x-axis direction. Output: angular rate in x-axis direction. 56
5.12 Generic configuration of the closed plant [14]. 57
5.13 Effect of different weight functions in the error signal. In expression 5.18, a is the number in the legend. 59
5.14 Comparison of the performance of H_2 and LQR controller. Responses in the left, difference in response in the right. 59
5.15 Comparison of the performance of robust controllers computed with different error weighting functions ($f(s) = af_0(s)$, where a is the number in the legend) and LQR controller. 60
5.16 Analysis shown in figure 5.15, including the first 5 modes. 61
5.17 Pole placement for the controller derived based on different error weighting functions. $f(s) = af_0(s)$, where a is the number in the legend, 0 in the constant case. 61
5.18 Comparison of the measurement signal for H_∞ (blue) and H_2 (red) 62
5.19 Comparison of the the boom deformation for H_∞ (blue) and H_2 (red) 63
5.20 Control torque for Kv controller, for 1 mode (red) and 5 modes (blue). 63
5.21 Evolution of measurements and boom deformation under the action of disturbance force and torque for H_∞ (blue) and H_2 (red). 64
5.22 Evolution of the pointing error during the pointing phase, using H_∞ and H_2. 65
5.23 Evolution of the deformation in boom 1, using H_∞ and H_2. 65
5.24 Evolution of the angular rate error, using H_∞ and H_2. 65
5.25 Evolution of the pointing error for 10 different initial conditions (angular rate and attitude). Stowed configuration. h: 600 km, i: 97 deg, Ω: 0. 68
5.26 Evolution of the pointing error under LQR and non-linear controllers. Deployed configuration. h: 600 km, i: 60 deg, Ω: 0. 69
5.27 Evolution of the pointing error under non-linear controller with different specifications. Deployed configuration. h: 600 km, i: 97 deg, Ω: 0. 71
5.28 Analysis of the short term oscillations of the angular rate under non-linear controller with different specifications. Deployed configuration. h: 600 km, i: 97 deg, Ω: 0. 71
5.29 Analysis of the evolution of the boom's deformations under non-linear controller with different specifications. Z-axis. Deployed configuration. h: 600 km, i: 97 deg, Ω: 0. 72
5.30 Analysis of the evolution of the boom's deformations under non-linear controller with different specifications. X,Y-axes. Deployed configuration. h: 600 km, i: 97 deg, Ω: 0. 72
5.31 Analysis of the control force exerted over the spacecraft by controller 3. X-axis (blue), Y (red) and Z (yellow). Deployed configuration. h: 600 km, i: 97 deg, Ω: 0. 73
5.32 Difference in the pointing accuracy due to errors in the estimation of the moment of inertia. LQR controller. 74
5.33 Difference in the pointing accuracy due to the addition of noise to the measurements. LQR controller. 7 different cases. 75
5.34 Difference in the pointing accuracy due to the addition of noise to the measurements. H_∞ controller. 76
5.35 Difference in the pointing accuracy and in the vibration of the booms (U) due to errors in the estimation of bending stiffness (EI) and length of the booms (L) and limitation in control information (N=1 only first mode available). Non-linear flexible controller. 77

A.1 Simulink model. 87

B.1 Evolution of pointing error and angular rate for different weights of the pointing error (5 cases per weight). 90

C.1 Deorbiting profiles launching at solar minimum (1996) and maximum (2014). Initial altitude 550 km. 91
C.2 Study of the detumbling stage for altitudes between 650 and 800 km. Rigid plant. B-dot controller. 3 initial conditions per case. 92
C.3 Study of the pointing stage for altitudes between 400 and 800 km. Rigid plant. LQR controller. 2 initial conditions per case. 93

D.1 Study of the detumbling stage for different inclinations and right ascensions of the ascending node. Rigid plant. B-dot controller. h: 600km. 95
D.2 Study of the pointing stage for different inclinations and right ascensions of the ascending node. Rigid plant. LQR controller. h: 600km. 96

E.1 Zoom in of figure 5.5 97
E.2 Vibration of the booms due to entering or coming out an eclipse. 98
E.3 Zoom in of figure 5.6 99
E.4 Interaction of the flexible structure (booms) with the control torque (magnetorquer). 100

F.1 Comparison of the responses of Lagrange equations and simscape model. Number of modes: 1-10. Number of elements: 1-20.I. 101
F.2 Comparison of the responses of Lagrange equations and simscape model. Number of modes: 1-10. Number of elements: 1-20.II. 102

G.1 Comparison of the evolution of the deformation of the booms using analytical (right) and numerical (left) models. Case 1: no external disturbances. 104
G.2 Comparison of the evolution of the deformation of the booms using analytical (right) and numerical (left) models. Case 2: steady external disturbances. 104
G.3 Evolution of the state variables, as resulting from the analytical model. Case 3: zero initial conditions 105
G.4 Evolution of the state variables, as resulting from the numerical model. Case 3: zero initial conditions 105
G.5 Evolution of the state variables, as resulting from the analytical model. Case 4: different disturbances and initial conditions 106
G.6 Evolution of the state variables, as resulting from the numerical model. Case 4: different disturbances and initial conditions 106
G.7 Schematic view of the model built in MATLAB/Simscape for verification purposes. 107

H.1 Hankel singular values on the successive order reductions of the controller. 109
H.2 Bode analysis of the successive order reductions of the controller. 110

I.1 Effect of different cost functions in the error signal. $f(s) = af_0(s)$, where a is the number in the legend. Extended figure 5.13. 111
I.2 Comparison of the performance of H_2 and LQR controller. Responses in the left, difference in response in the right. Extended figure I.2. 112
I.3 Comparison of the performance of robust controllers computed with different error weighting functions ($f(s) = af_0(s)$, where a is the number in the legend) and LQR controller. Extended figure 5.15. 113
I.4 Analysis shown in figure 5.15, including the first 5 modes. Extended figure 5.16 114
I.5 Comparison of the the boom deformation for H_∞ (blue) and H_2 (red). Extended figure 5.19. . . 114
I.6 Evolution of measurements under the action of disturbance force and torque for H_∞ (red), H_2 (blue) and LQR (black) controllers. 115
I.7 Evolution of the angular rate error during the pointing phase, using H_∞ and H_2. 115
I.8 Evolution of the deformation in the booms, using H_2. 116
I.9 Evolution of the deformation in the booms, using H_∞. 117

J.1 Options for obtaining a more complete estimation of the state vector. 119

K.1 Evolution of the pointing error for 9 different initial conditions (angular rate, attitude and Ω). Deployed configuration. h: 600 km, i: 97 deg. 121
K.2 Evolution of the pointing error under LQR and non-linear controllers. Deployed configuration. h: 550 km, i: 97 deg, Ω: 0. 122
K.3 Additional comparison based in figure K.2. h: 600 km, i: 60 deg, Ω: 0. 122
K.4 Consequences of adding the constrain on the torque (expression 5.31) 123
K.5 Analysis of the short term oscillations of the angular rate under non-linear controller with different specifications. Deployed configuration. h: 600 km, i: 97 deg, Ω: 0. Extended figure 5.28 . . . 123

K.6 Analysis of the evolution of the boom's deformations under non-linear controller with different specifications. Z-axis. Deployed configuration. h: 600 km, i: 97 deg, Ω: 0. Extended figure 5.29 . 124
K.7 Analysis of the evolution of the boom's deformations under non-linear controller with different specifications. X,Y-axes. Deployed configuration. h: 600 km, i: 97 deg, Ω: 0. Extended figure 5.30 125
K.8 Analysis of the control force exerted over the spacecraft by controller 3. X,Y-axes. Deployed configuration. h: 600 km, i: 97 deg, Ω: 0. Extended figure 5.31 126

L.1 Difference in the pointing accuracy due to errors in the estimation of the moment of inertia. Non-linear rigid controller. 2 different initial conditions. 127
L.2 Difference in the pointing accuracy due to errors in the estimation of the moment of inertia of the central part of the satellite and in the length and linear density of the booms. Non-linear flexible controller. ae states for linear density. 2 different initial conditions. 128
L.3 Pointing accuracy and difference in the pointing accuracy due to errors in the estimation of the moment of inertia of the central part of the satellite and in the length and linear density of the booms. H_∞ controller. ae states for linear density. 128
L.4 Difference in the pointing accuracy due to errors in the estimation of the moment of inertia. LQR controller. 7 different initial conditions. Additional cases in relation with figure 5.32. 129
L.5 Difference in the pointing accuracy due to the addition of noise to the measurements. Non-linear rigid controller. 2 different cases. 130
L.6 Difference in the pointing accuracy due to the addition of noise to the measurements. Non-linear flexible controller. 2 different cases. 130
L.7 Zoom in figure 5.35. 131
L.8 Difference in the pointing accuracy and in the vibration of the booms (U) due to errors in the estimation of bending stiffness (EI) and length of the booms (L) and limitation in control information. H_∞ controller. 132

List of Tables

2.1 Geometrical data. 12
2.2 Mass data. 12
2.3 Non-rigid dynamics (booms). 12
2.4 Interaction with environment. 12
2.5 Sensor specifications. 12
2.6 Actuator specifications. 12

3.1 Initial conditions for the satellite's attitude. 20

5.1 Relation between constrained and controlled systems. 66

Acronyms & Symbols

Acronyms

ESA European Space Agency

NASA National Aeronautics and Space Administration

e.g. exempli gratia (for example)

w.r.t. with respect to

GPS Global Positioning System

FoV Field of View)

MoI Moment of Inertia

RFI Inertial Eath Reference Frame

RFB Body-fixed reference frame

LMI Linear Matrix Inequalities

RFL Local Reference Frame

SISO Single Input Single Output

MIMO Multiple Input Multiple Output

i.e. id est (that is)

LEO Low Earth Orbit

MSc Master of Science

GNC Guidance Navigation and Control

DLR German Aerospace Center

LTFS Large Thin Flexible Structures

ADCS Attitude Determination and Control System

GoSolAr Gossamer Solar Array

LQR Linear Quadratic Regulator

JAXA Japan Aerospace Exploration Agency

General symbols

$\vec{b}$ Local magnetic field

$\vec{\omega}$ angular rate

$\dot{x}$ Time derivative of variable x

t Magnetorquer time constant

$\vec{x}_u$ Unitary vector in the direction of x

T_g Gravity gradient torque

S Stowed configuration

D Deployed configuration

I_{ij} Component ij of the matrix of inertia

CoG Center of mass

EI Bending stiffness

k_d Damping coefficient

α Ratio between bending stiffness and damping coefficient

C_D Drag coefficient

m Magnetic dipole

f_r Solar radiation force

f_d Drag

ρ Atmospheric density

v Velocity

L Angular momentum

T Torque

Q Attitude quaternion

$\vec{e}$ Euler vector

ϕ Euler angle

r Position

μ Gravity constant

T_m Magnetic field torque

i_r Solar irradiance

C_{sr} Spectral reflectivity coefficient

C_{dr} Diffusive reflectivity coefficient

A Area

θ Incidence angle

s Sun vector

Flexible model symbols

F Damping matrix

$E_{k,T}/E_{k,R}/E_{k,b}$ Kinetic energy (total/rigid body/boom)

v Velocity

s Longitudinal coordinate of the booms

u_{ij} Bending deformation of boom i in the j dimension

L Length boom

L Lagrangian

Q Non conservative (external) forces

T Kinetic energy

V Potential

W_{nc} Work of non conservative (external) forces

q Generalized coordinate

D Dissipative function

M Mass matrix

K Elastic matrix

ρ Linear density boom

ϕ_{ijk} Shape function (dimension i/ boom j/ mode k)

q_{ijik} Generalized coordinate (dimension i/ boom j/ mode k)

Control symbols

x State vector

J Cost function

α Angular acceleration

H_2/H_∞ Norms related to robust control theory

y Measurements signal

u Control command

z Error signal

w Disturbances signal

K Gain matrix / controller

1

Introduction

The last decades have witnessed the introduction of flexible structures in the space field, a conceptual change in design from the compact rigid structures satellites conventionally consist of. Even though this idea is not new, its potential applicability in the space domain is rapidly evolving. Its current emergence is caused by two main factors: 1) technological advances in key related areas, e.g. thin film solar cells or ultra-light sail films, and 2) miniaturization of satellites and their components, which is driving a decrease in weight and size [35]. Despite of the enabling effect of the progress in these areas, there are still many technological advances needed to be able to fully materialize the potential of these structures. Throughout this research, the author aims to contribute to this scientific effort, adding his bit to unfolding the complete capability that flexible structures have in relation to space.

Among the current projects and missions within this field, the DLR's (German Aerospace Center) GoSolAr (Gossamer Solar Array) demonstrator mission is particularly relevant in relation to this study. This relevancy is driven by the fact that this study was conducted as an intern at DLR and collaborator in the GoSolAr mission. Further details regarding the mission, its objectives and specifications are given in chapter 2. Figure 1.1 shows an example of a DLR's project related to the GoSolAr mission and with a considerable degree of similarity from an ADCS perspective.

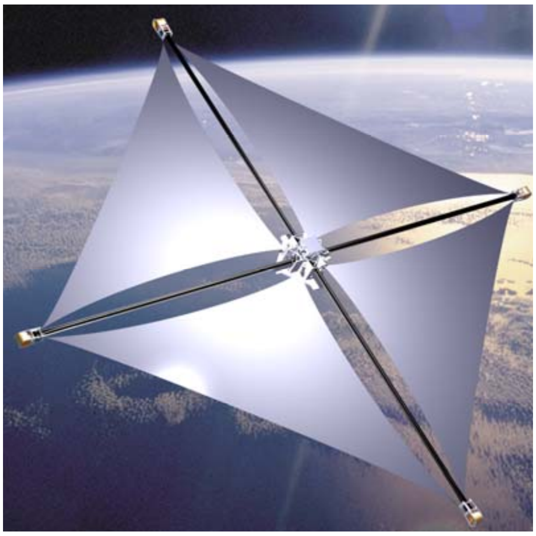

Figure 1.1: Artist's rendering of Gossamer-1 demonstrator [24].

The GoSolAr project provided a useful and representative case of study. This case of study, in combination with software tools already developed by DLR, provided with the base from where to initiate this study. These software tools consist on a simulation environment suitable to study the performance of the ADCS (Attitude Determination and Control System). The use of this environment allows avoiding the need to build and verify new software tools, saving this effort for the actual research. However, as it plays a relevant role in the validity of the results obtained and the conclusions drawn, it is to be explained in detail. This is done in chapter 3. In this chapter, an initial analysis of a proposed ADCS for the GoSolAr mission is also shown. The design of this ADCS is conventional and its analysis aims to give an initial idea of the expected behavior of the spacecraft from an attitude perspective.

After having defined a consistent setup which can be used to study the performance of ADCS's designs, the actual research can start. Two main topics are studied: 1) modeling of flexible structures and 2) control strategies. A brief introduction on these two topics, which are both considerably extensive and complex, is given later in this chapter. The model of the flexible structure was built based on a tradeoff between several aspects, among which the most relevant are: 1) the degree of similarity with the real structure and 2) the usefulness in relation with a potential controller. These factors drove the decision to use an analytical approach based on Lagrange's equations. The derivation of this flexible model is analyzed in chapter 4.

The second research topic consists in providing an understanding on different control strategies in relation with the model built, their performances and requirements. This is a broad topic and neither all control theories are analyzed nor absolutely realistic cases are considered. The decisions on which control concepts to study and implement were mainly motivated by solutions in the existing literature, the advice of the thesis supervisors and the previous expertise of the author. The controllers implemented were based in a linear–quadratic regulator (LQR), the minimization of H_∞ and H_2 norms (robust control) and the existing parallelism between constrained and controlled system (from an analytical dynamics perspective). Detailed descriptions of each of these concepts are given in chapter 5, which also includes analyses on their performance and assessments on their potential uses.

Finally, the main conclusions of the research are drawn (chapter 6), aiming to give a clear overview of the main achievements of the study, and providing at the same time with options for further studies in the field.

The rest of this chapter aims to cover four main areas, linked to providing the reader with: 1) an understanding of the reason this project was chosen, 2) a general overview of the state of the art, 3) detailed research questions and objectives and 4) the structure of the rest of the report. In order to justify the interest of the project, an introduction to the role of flexible structures in space in given, including different technological uses and examples of missions (section 1.1). Regarding the state of the art of the fields of interest (section 1.2), two main areas are covered: 1) modeling of flexible structures and 2) attitude determination and control of large thin flexible structures (LTFSs) in space. Additionally, comments are made regarding the influence of the space environment in the dynamics of a satellite and generic information on ADCS designs. These two last areas are considered to be common knowledge and, thus, are not covered in detail in this report. Finally, the research objective and research questions are defined in section 1.3 and the structure of the report is shown in section 1.4.

It is to be highlighted that this chapter is based in two previous documents that were developed as a previous step to starting the actual MSc thesis. These documents are: 1) Literature Study (May 2018. Literature Study assignment. TU Delft.) and 2) Project Proposal and Plan (April 2018. Research Methodologies course. TU Delft.). The changes w.r.t. these documents are driven by the additional knowledge and expertise gained throughout the study, which gives a clearer perspective of the research.

1.1. Flexible structures in space

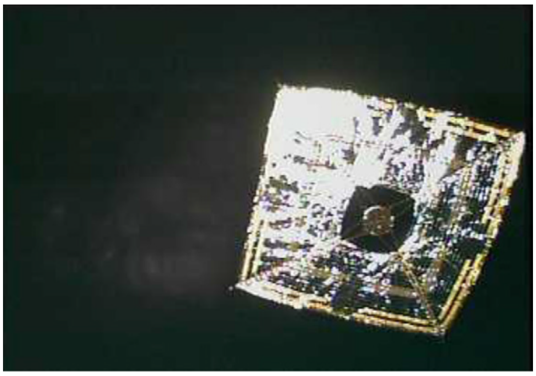

Figure 1.2: Solar-sailing IKAROS [28].

The fact that every structure is, to some degree, flexible, broadens the scope of this research and imposes the need of further limiting it, via a more precise definition of what kind of structures are to be studied. The type of structures that are within the scope of this thesis are large thin flexible structures (LTFSs). These structures are characterized by having a extremely high area-to-mass ratio compared to more conventional structures (compact). This increase is generally caused by the use of film-like bodies. The structural stability of the system can be ensured using different rigidizing strategies, such as a structure composed of several booms or via the centrifugal force appearing due to imposing a spin in the spacecraft. It is to be highlighted that this definition do not include multiple types of structures (e.g. robotic arms) where, due to strict performance requirements, flexibility may have a non-negligible effect.

The use of LTFSs in space has two main potential advantages: 1) low launching volume and 2) generate large lightweighted structures [21]. The low launching volume is caused by the two configurations that this kind of structures usually has, stowed and deployed. The low mass of the structure in relation with its final (deployed) size depends on both the film-like body, which will be called membrane from this point on, and the additional rigidizing components. It can be concluded that the main benefit of these structures is that they allow decreasing the cost of getting large areas/volumes in space. Therefore, the main question to be asked regarding their potential is what these large areas can be used for. The number of applications is rather high, going from large antennas to deployable telescopes. Three of these applications, chosen due to the similarity between the structures they use and that used in the case of study (GoSolAr), are explained further: 1) solar sailing, 2) drag sailing and 3) solar power. This aims to give an idea of the past evolution of this technology and the opportunities that it presents.

Solar sailing consists in using the solar radiation to propel the spacecraft, to generate a Δv. The solar radiation pressure is highly dependent on the properties of the surface exposed to the sun but it remains always considerably low (of the order of 1 $\mu N/m^2$ close to Earth orbit). This drives the need for large lightweighted surfaces, i.e. LTFSs, if a meaningful acceleration is to be obtained. An example of a mission using this concept is the JAXA mission IKAROS (figure 1.2), launched in 2010 [28]. With its 20-meter-span square solar sail, it was used to verify the solar radiation pressure and several GNC (guidance, navigation and control) concepts. In the last decade, the tendency towards miniaturization of satellites (e.g. CubeSats) is driving a decrease in their mass and, therefore, the size of the solar sail needed. This influences directly the complexity and risk associated with the use of this technology, increasing its potential uses.

Regarding drag sailing, two main applications can be pointed out: 1) aerobraking and 2) deorbiting. Aerobraking is already a well-established method of changing the orbiting when arriving to a planet and, whether it could benefit time-wise from the use of LTFSs, more conventional structures have been successfully used. The increase of the population of space debris and the collision risk associated with it is driving a growth in the interest for active deorbiting strategies [26]. The use of LTFSs to increase the effective area of the spacecraft, thus increasing the drag and the rate of decay of the orbit, is among the potential solutions for this problem. An example of the interest in this kind of application is the Deployable Gossamer Sail for Deorbiting by ESA [8].

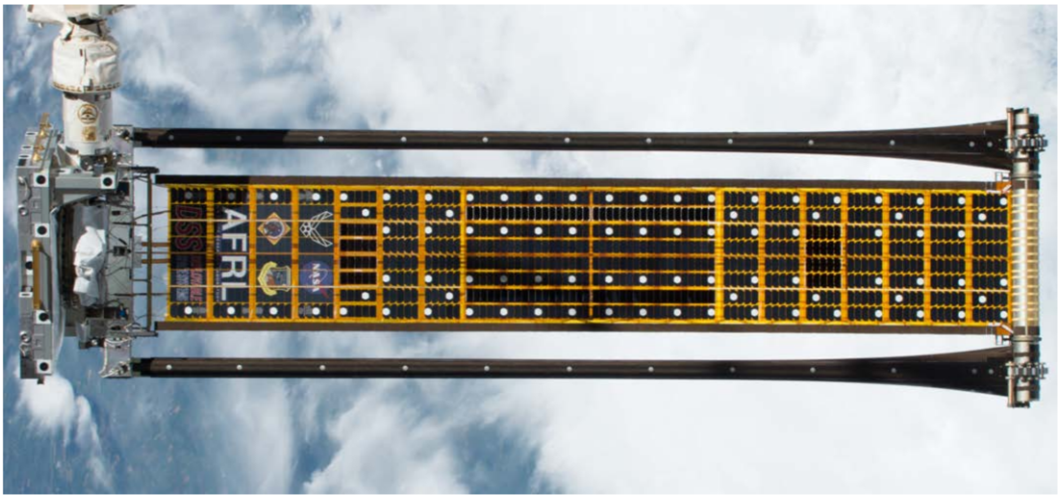

Figure 1.3: Deployed ROSA [2].

The third and last application considered here is the generation of solar-based power. The amount of power generated from solar radiation is driven by two main factors: 1) the efficiency of the solar cells and 2) the area covered by solar cells exposed to the solar radiation. The evolution of thin film solar cells has opened the door to using them in LTFSs, potentially increasing the power production and lowering the weight of the structure, and, thus, the cost. Examples of missions where this technology was implemented are the Hubble telescope, where vibrations thought to be caused by these solar panels drove the decision to change them for conventional rigid panels [9], and the NASA demonstrator mission ROSA (figure 1.3), in which a roll of thin solar panels was deployed and folded. More information about the ROSA mission can be found in [2], where the advantages of this kind of power generation are also pointed out, as well as other missions and configurations which have implemented it. Finally, the mission which is used as the main case of study of this thesis, GoSolAr, also aims to demonstrate and contribute to the development of this technology (more information in chapter 2).

1.2. Related research topics

The aim of this section is not to cover completely and in depth the state of the art of all the areas touched throughout the research. That would require a few thousand pages and is considered to be out of the scope of this thesis. Instead, the objective is to give an overview on the most relevant topics, which can be useful to understand the alternatives that were faced during the project as well as the reasoning behind the decisions made.

Two main topics are introduced: 1) modeling of flexible structures and 2) attitude control particularities when applied to LTFSs. These two areas comprise most of the research done, which is shown in chapters 4 and 5. Another two areas are briefly introduced, as they may be of help to understanding the research problem but are not directly linked to it: 1) space environment, particularly disturbances that may influence the attitude of a spacecraft, and 2) components and operation of the ADCS.

1.2.1. Modeling flexible structures

The objective behind modeling something is, usually, to be able to analyze different cases without the need of running actual experiments, allowing to gain knowledge about a problem at a much lower cost. In our case, the knowledge that is pursued is related to the effect of the flexibility in the dynamics of the satellite, mainly, but not limited to, rotational dynamics (i.e. related to the attitude). Alternatively, this effect could be studied from an experimental perspective, but that would increase the cost associated with the study from a very early stage. In the general topic of simulations versus experiments, the optimal approach seems to be to combine both, using experimental data to improve the accuracy of the simulations and simulations to be able to study a greater number of more complex cases. In our case, the role of the model is clear, to provide with a first idea of the behavior of these structures, useful from a control perspective.

The model is intended to represent the dynamics of a spacecraft. This can be done in a number of ways, depending not only in the structure of the spacecraft, but also in the accuracy that is required and in the purpose of the model. However, one first decision that clearly differentiate between existing possibilities is how, or if, the flexibility of the structure is taken into account. Several possibilities are pointed out below [4]:

- Rigid motion. It is the simplest approach and the most commonly used. It assumes the relative position between the different points of the structure remains constant throughout time, unaffected by the forces and torques exerted over it. Depending on the case it can be useful as a first insight or even be an approximation good enough. Its simplicity allows a low computational cost, as the number of state variables remains low and the relation between them simple.

- Rigid motion + flexible motion. An initial solution to study the non-rigid motion of certain parts of the body was to divide the problem in two. In this separation, the first problem solved was that of a rigid body. The second consisted then in modeling the behavior of the flexible parts under the force and stress field which had been obtained from the first problem. This division decreases the computational power needed to solve the problem, but it has one main limitation: the interaction between flexible and rigid motion is not considered [25].

- Flexible motion. This approach integrates flexible and rigid motion and solves the complete problem simultaneously, taking into account the interconnection between the different variables defining rigid and flexible dynamics. It is more complex and computationally costly.

It can be clearly observed in the options given that a tradeoff is needed, assessing mainly the accuracy required, the computational power procurable and the time available to build the model. Historically, most LTFSs have been modeled as rigid bodies, and this has very rarely (e.g. Hubble telescope) posed a problem throughout the mission. The main justification for neglecting the effect of the flexibility is the high natural frequencies of the system, due to the small size of the structures. Examples of studies related with the ADCS of LTFSs in which the structure was modelled as a rigid body are [22][34]. However, in other studies the potential influences of the flexible modes in case they are coupled with other rigid-motion frequencies are pointed out [5] [20]. Example of studies including the flexibility on their analyses are [27] and [7].

In the particular case analyzed in this study, the flexibility inherent to the structures studied makes it necessary to evaluate the interaction between rigid and flexible dynamics. This is necessary in order to understand how the structures behave and to design and implement control strategies targeting that behavior. However, integrating the flexibility of the structure into the dynamics and kinematics of the system is not an easy task and it is still a research area. Some of the options for performing this integration are shown below [17].

1. Defining a set of rigid bodies connected by joints, giving the system a flexible behavior.
2. Defining the structure as a set of interconnected flexible bodies with simple geometries.
3. Defining the structure as a small set of interconnected flexible bodies with complex geometries.

It is important to understand the evolution of three main characteristics of the model when going from option 1 to option 3: 1) the mathematical complexity increases, increasing the difficulty linked to building the model, 2) the possibility to use the same functions/model to structures with different geometries decreases, as the model becomes more specific, and 3) the order of the model derived decreases, as less elements are considered.

These are some of the decisions that need to be made before starting to build the model. There are, however, still numerous aspects that need to be evaluated before being able to actually model the structure. An example easy to comprenhend is which kinematic formulation to use. There are several possibilities when defining the coordinates and reference frame(s), e.g. floating reference frame, finite segment method and incremental finite element formulations, and they influence enormously the applicability of the different methods to solve the problem [25].

In this thesis, the approach that was implemented consists on implementing the Lagrange equations in combination with an assumed modes method and a simplified model of the spacecraft. More information about the particularities of the implementation can be found in chapter 4 and in [17]. Additionally, a numerical model based on defining the spacecraft as a set of rigid bodies interconnected via flexible joints was built using the MATLAB tool SimScape, in order to verify the analytical model.

1.2.2. Attitude control of LTFSs

The second main topic that has been studied throughout this MSc thesis is related with the design of an attitude determination and control system (ADCS) addressing the particularities of this kind of structures (LTFSs). In order be able to successfully go through this designing process, it is first necessary to understand these particularities and how they influence the behavior of the satellite. There are two main characteristics of LTFSs that affect the attitude dynamics of a spacecraft with this type of structure: 1) high area-to-mass ratio and 2) effect of the flexibility. Both of them where introduced in previous sections and will now be explained in more detail, focusing in their influence over the ADCS design.

The increase of the area-to-mass ratio is caused by the use of big structures (from a dimensional perspective) with low-mass and thin components (such as composite booms or thin-film solar cells). The size of the structure influences the interaction of the spacecraft with the environment (i.e. gravity and magnetic fields, atmosphere, solar radiation...etc), increasing the torque and force disturbances that are exerted over the satellite. Particularly relevant is the increment in the torque disturbances, not only caused by a direct increase in the forces (e.g. increase on effective area drives an increase on drag), but also by the fact that the distance between the center of pressure and the center of mass can increase considerably. This, in combination with the rise in the moment of inertia (high when compared to a compact satellite of similar mass), makes it necessary to be able to provide a significantly higher control torque (compared to compact structures) to be able to achieve the same control accuracy. Producing this torque is not a trivial task, specially if the following two limitations, which apply for most conventional satellites, are kept: 1) the control torque must be applied in the central part of the spacecraft and 2) the actuators should have low mass and volume [35].

This structural particularity drives a need to develop new concepts and strategies to control the satellite in a efficient way. Two main solutions can be found in the existing literature: 1) alternative actuators and 2) alternative control strategies. The use of alternative actuators is usually based in using the big size of the structure to generate a higher torque, e.g. shifting the center of mass away from the center of pressure or generating diferential forces far away from the center of mass. Abundant examples of these alternative actuators can be found in [11] and [33]. Another option is to use more conventional actuators in combination with alternative control strategies, e.g. passive stabilization using a spin in the main axis of inertia. This last option was the one chosen at the beginning of the project, as it does not imposes additional requirements in the design of the spacecraft and is compatible with the requirements of the mission. More details are given in chapter 2.

Regarding the effect of the flexibility in the dynamics of a spacecraft, several studies have considered it and tried to define in which cases it needs to be taken into account (see [32]). The importance of this effect in a mission, and, thus, the possibility of neglecting it, is mainly linked to two factors:

- Potential interaction between the natural frequencies of the system, flexible modes of the structure, with either the external disturbances or the control input. (Most of) the external disturbances have low frequencies, related to the orbital period. An example of an external disturbance with high frequency is when the spacecraft goes in or out an eclipse. According to [17], the overlap between the control bandwidth and the natural frequencies is the distinguishing factor of the problems in which the flexibility may pose a problem, which is likely the case for the next generation of large space structures.
- Strictness of the mission requirements. In case of high pointing accuracy requirements or requirements related with the vibrations of the structure, the flexibility may need to be included in the analysis of the mission in order to guaranty complying with those requirements.

It can be deduced from the points above, that the influence of the flexibility could range from adding small vibrations compromising the requirements of the mission (e.g. high accuracy Earth observation) to generating instabilities in the system which could potentially endanger the spacecraft structural stability. For the cases where the flexibility of the structure can pose a problem, there are two main options to approach the issue:

- Passive control. It does not add much complexity to the system and it is, usually, robust from a stability perspective. However, it can add weight and its performance is limited. Examples of this strategies are spinning the spacecraft and passively damping the booms by adding a layer of a highly damped material.
- Active control. It is considerably more complex and has several inherent difficulties not easy to overcome, among which are: 1) control theories applicability, as most of these assume all state variables known, which may very well not be the case, 2) computational cost linked to the high order of the systems and problems related with reduced orders, and 3) modeling errors and inaccuracies [17].

Throughout this study, passive control is not studied in detail, although the effect of different damping coefficients is addressed. Most of the research effort is invested towards evaluating diverse active control possibilities, their performances and their requirements (chapter 5).

1.2.3. Additional fields of interest

Even though the two fields just explained cover most of the innovative work performed throughout this thesis, knowledge and understanding of some other areas was needed in order to successfully conduct the research. These areas are mainly two: 1) ADCS components and operation and 2) space environment characteristics.

It is necessary to understand how the different ADCS components are interconnected and how they operate in order to be able to efficiently design this system. In this regards, knowledge about the following topics was gained in the initial stage of the thesis:

- Process of obtaining measurements. This involves understanding what sensors may be available (e.g. magnetometer), what they measure (e.g. magnetic field) and what errors are inherent to those measurements (e.g. noise).
- Processing of the measurements. Two main operations are conducted over the raw measurements in order to give an estimation of the state vector as accurate as possible. The first one relates the measured variables with the state variables (e.g. sun vector to pointing error), while the second reduces the effect of noise and biases via estimators (e.g. Kalman filter).

- Connection between state vector estimation and control command (controller). Different mathematical constructs, or control theories, can be used for this connection, leading to completely different behaviors of the system (e.g. robust control).

- Application of the control command. The control command is exerted via actuators, which impose their own limitations regarding the nature of the actuation (e.g. maximum angular acceleration of a reaction wheel).

Even though the focus of the thesis is in the controller, the influence of the other components of the ADCS should not be underestimated, and the problem is to be addressed as a whole. For additional information about specifications of particular sensors and actuators the author refers to [32], for more information regarding measurements processing to [10] and for an overview on control design to [19].

Regarding space environment, only two main areas are considered: 1) disturbances affecting the dynamics of a spacecraft in LEO (Low Earth Orbit) and 2) limitations affecting the ADCS. In relation to the disturbances influencing a spacecraft in LEO and their influence over the dynamics of the satellite the author refers to [31]. Four main disturbances are considered: gravity gradient, atmospheric drag, solar pressure and magnetic field. With respect to the limitations on the ADCS, they can be divided into: hardware limitations (requirements in weight, volume, power consumption...etc.), affecting the choosing of actuators and sensors, and software limitations (computational cost), influencing the design of the controller. This limitations are addressed in a qualitative way throughout the report.

1.3. Research specifications

For this subsection, the author refers to a previous document done in partial fulfillment of the MSc in Aerospace Engineering at TU Delft. This document was developed as part of the course on Research Methodologies and aimed to provide with a clear understanding of the MSc thesis. Even though some changes have been implemented throughout the research, most of its initial structure has been maintained. This way, the research objective can be enunciated as:

The research objective is to contribute to the development of attitude control concepts applicable to large thin flexible structures in space. This aim is achieved by evaluating the performance of different control concepts applied to this type of structures. This evaluation is based initially in existing literature, evolving then into simulations in a MatLab/Simulink environment.

Sub-goals were defined in relation with this research objective in order to move gradually towards it. These sub-goals are: 0) gain knowledge about related technologies, sofware tools and mathematical concepts related to the research area, 1) define and study a reference scenario, 2) model the dynamics of the LTFSs, 3) design, implement and evaluate the performance of different ADCS concepts. This sub-goals were further developed into specific tasks. The highest level tasks are shown in the work flow on figure 1.4.

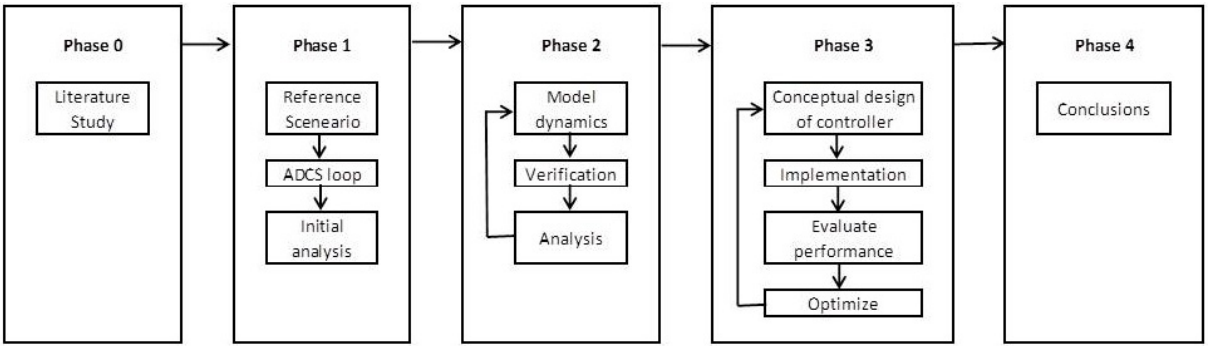

Figure 1.4: Schematic work flow for the MSc Thesis.

The ultimate research question that is targeted with this work is the following:

What attitude controllers, of those designed, are applicable to thin flexible structures (LTFSs) in space, and to what degree?

As this question is considerably complex, lower level sub-questions where defined in order to give some insight on the way the research was approached:

1. What are the relevant properties and requirements of the case of study (GoSolAr), in relation with the ADCS?
2. What influences, other that those related with the flexibility, does the particular structure of the GoSolAr satellite (LTFS) has over the ADCS performance?
3. How can the flexibility of the structure be modeled?
    (a) How and why was the approach for modeling the structure chosen?
    (b) What assumptions, simplifications and errors are inherent to the model built?
    (c) How can the model be improved?
4. Which ADCS concepts, of those designed, is optimal for each case?
    (a) What ADCS concepts are to be designed and why?
    (b) What is the performance of each concept?
    (c) What are the requirements (e.g. sensors) that each concept imposes in the ADCS?

The resources used to answer this questions are mainly two: 1) existing literature and 2) analyses in a simulated environment. The simulations were performed using a DLR's simulation environment as a basis, and implementing changes in the dynamics of the spacecraft and in the ADCS design, when necessary.

1.4. Structure

This report is organized in 5 chapters, not taking into account the conclusions. Each chapter presents a particular area of the research. This chapter (chapter 1) introduces the research's relevancy, area and objectives. This way, it explains some potential uses of large thin flexible structures in space, illustrating each use with mission examples. Then, the two main topics targeted by the research, i.e. modeling of flexible structures and attitude control of flexible structures, are briefly explained, aiming to provide an overview of the possibilities in these areas. Finally, the research is further defined by enunciating the research objective and research questions.

Chapter 2 describes the DLR's (German Aerospace Center) mission GoSolAr (Gossamer Solar Array). This mission is used as the main case of study throughout the research, being used to define some of the requirements for the controller (e.g. pointing accuracy attainable) and the specifications of the satellite. These specifications include not only the structure of the spacecraft but also the set of sensors and actuators available and the orbit chosen.

Chapter 3 contains an initial analysis of the case of study, considering the structure of the satellite rigid. This chapter also includes a descriptions of the simulation environment used, i.e. the control loop used to evaluate the performance of different controllers. In this initial analysis, the controllers used are: a b-dot controller for the detumbling phase and LQR-based controller for controlling orientation of the satellite. This analysis already points out some limitations in the performance of the controller, due to the structure of the satellite and to the ADCS's hardware used.

In chapter 4, the methodology used to integrate the flexibility of the satellite's structure in its equations of motion is explained in detail. This is done in order to ease the application of this methodology to diverse structures. Then, it is implemented over a simplification of the structure of the GoSolAr satellite. Some comments are made over potential improvements in the model used. Finally the equations of motion obtained were verified using a numerical model.

Chapter 5 contains the performance of different controllers, this time taking into account the flexibility of the satellite. First of all, the performance of the b-dot and LQR-based controllers is studied and the effect of flexibility in the behavior of the satellite pointed out. Then, the flexible plant is linearized, both analytically and numerically, in order to enable deriving linear robust controllers based in H_∞ and H_2 norms. The resulting robust controllers are introduced into the simulation environment and their performance evaluated. The last controllers obtained are derived using an analytical dynamics approach. This last approach is implemented using both the rigid and the flexible equations of motion, and the different performances are studied. Finally, an analysis of the sensibility of these controllers to noise and error is conducted, assessing also the particularities of their implementation.

2

Case of Study

The aim of this section is to introduce the case of study used throughout this thesis, the DLR's mission GoSolAr. Defining a case of study can be of great help when researching a topic as broad in options and possibilities as the one chosen, as it allows focusing on an specific case, without an excessive number of 'free' variables. E.g. the structure of the satellite of the GoSolAr mission consists on a square membrane with four booms attached to the central part of the satellite and to the tips of the membrane, therefore, that is the configuration considered. It also provides realistic estimations of the data needed, as those data are also defined as part of the mission (e.g. moment of inertia or drag coefficient). This grants that the results obtained are not based in ideal configurations, distant from real applications. Even though the use of a case study may seem to be limiting the applicability of the research, it does quite the opposite: by applying the methodology described to a particular case, a clear and structured way of applying it to any other case is provided. Additionally, the use, as case of study, of a mission under development can also provide a useful insight to that mission.

As previously pointed out, the main case of study of the MSc thesis is based in the GoSolAr (Gossamer Solar Array) demonstrator mission. This mission focuses in the 'gossamer deployment systems for huge thin-film photovoltaic array' [13]. This is particularized into two objectives: 1) developing of a flexible photovoltaic array and 2) deploying a $25m^2$ gossamer solar power generator. The goal of this mission is to demonstrate (in orbit) the two-dimensional deployment of this flexible array of thin-film photovoltaics. The general objectives and characteristics of this mission can be found in [13] and will only be discussed in this document when they have an influence to the ADCS. The rest of this section will cover three main topics: 1) ADCS in the GoSolAr mission, 2) relevant data regarding the GoSolAr satellite and 3) usefulness of this case of study in relation with the research objective.

2.1. GoSolAr's ADCS

Three main aspects of the GoSolAr mission are studied w.r.t. the ADCS. First of all, the top level requirement for the ADCS, which is to maintain an orientation w.r.t. the sun with an accuracy of 10 degrees, during operation. The reasoning behind this requirement is that the membrane is assumed not to be completely flat. This lack of flatness is assumed to affect the local orientation of each point of the membrane up to 10 degrees. As the objective of pointing towards the sun is to be able to study the performance of the solar cells in the membrane, further accuracy is assumed to superfluous. Neither the demonstration of the wrinkling of the membrane nor the justification of the requirement are within the scope of this study.

Additional requirements that may be considered related to the ADCS are: 1) guaranty safe deployment and 2) minimum deorbiting time. In the case of the deorbiting time, it could be maximized by controlling the relative orientation between the spacecraft and its velocity w.r.t. the atmosphere. However, it would interfere directly with the pointing requirement, so it is not considered. Regarding the deployment phase, its dynamics are considered to be beyond the scope of the work due to its complexity and highly non-linear character.

The second aspect to be considered is related with the different modes that appear throughout the mission, as well as with the changes in the structure configuration of the satellite (deployment). In order to give a clear idea of this different ADCS's stages, a timeline of the mission w.r.t. the main ADCS's action is explained below. Four main stages are distinguished:

1. Detumble. After launch, the satellite has an (arbitrary) angular velocity, which is expected to be of the

order of 12 degrees per second. The first task of the ADCS is to stabilize the spacecraft, reducing this angular rate.

2. Deployment. The deployment is done in two stages, deploying first the booms along one of the diagonals of the membrane and then along the other. For the analyses shown throughout this report, this dual process is not considered and only two configurations of the spacecraft are taken into account: stowed and deployed. It is recommended to study also the behavior of the 'semi'-deployed configuration in further stages of the project.

3. Reach and maintain operation point. This includes both pointing towards the sun and performing additional actions to stabilize the satellite around that orientation. In our case, the initial idea, which was afterwards included in the final design, was to spin the satellite. It is to be noticed that this process can be conducted also before the membrane and booms of the spacecraft are deployed. However, in this case a small reorientation and manipulation of the spin needs to be conducted again after deployment.

4. The rest of the mission consists initially in maintaining the orientation to the sun within the accuracy required (10 degrees). Additionally, the possibility of modifying the relative orientation to the sun (initially the objective was defined as pointing the normal of the membrane plane towards the sun) is considered. This would allow a more exhaustive characterization of the flexible solar array. This process can be conducted on several occasions.

After deriving the ADCS main tasks throughout the mission, it is necessary to analyze what is available for fulfilling this objectives. An initial (optional) requirement was to try to comply with the requirements using only a magnetorquer. This was proven to be enough, in combination with an induced spin in the mayor axis of inertia, to achieve the required performance. The reason for selecting this actuator, if able to comply with the requirement, are self-evident: it is cheap, simple and light.

Among the sensors needed to address the requirements are the following: 1) fine sun sensor, 2) gyroscope and 3) magnetometer. The fine sun sensor should have the same orientation as the solar cells, in order to ensure that the sun in within the FoV (field of view) of the sensor at the operating point (solar cells directed to the sun). The gyroscope is used to control the spin of the satellite as well as to estimate the change in attitude during eclipses. The magnetometer is use in combination with the magnetorquer to generate the control torque. It can also be used to provide provide an estimation on the attitude, if necessary. Additional sensors that could benefit the performance of the satellite from an ADC perspective are: 1)GPS and 2) coarse sun sensors. The GPS is to be included among the satellite's sensor even if not needed for the ADCS. It enables to compute the attitude, which is not a requirement for this mission, of the satellite using the magnetometer and the sun sensor. A set of coarse sun sensors covering a full angle can be used to estimate the pointing error w.r.t. the sun when it is outside the FoV of the fine sun sensor. However, this can also be done using information of the power generated by the solar panels positioned in the different surfaces of the satellite.

Having characterized the ADCS that is to be implemented, its particularities can now be further described. The challenges in this mission w.r.t. the ADCS, part of which have already been introduced, are shown below:

- High area-to-mass ratio. With a nominal membrane area of $25ms^2$ and a estimated total weight of around 60 kg, this ratio is considerably higher that for conventional satellites (e.g. before deployment the effective area is around 0.3 m^2, two orders of magnitude lower). As a consequences, external disturbances generate higher torques and the moment of inertia is higher than other satellites of similar mass.

- The use of magnetorquers as the only actuators. The reason this control strategy is unusual in this type of satellites is that most missions involving LTFSs are deep space missions or demonstrator for technology enabling for deep space missions. In the case studied, the main goal is to generate power using a light flexible structure. As this objective does not exclude LEO orbits and the demonstrator mission is planed to have this type of orbit, using only magnetorques reduces cost and launching weight. However, a direct consequence is that the control torque is limited both by the maximum dipole that can be generated and by the direction and intensity of the local magnetic field.

- The potential interaction of the flexible modes of the structure with the rigid motion of the spacecraft. This influence can be driven both by external disturbance (e.g. eclipse) and by the control torque (e.g. duty cycle of the magnetorque).

2.2. GoSolAr's specifications

In order to further define the case of study to be analyzed, a considerable amount of aspects of the satellite and of the mission needs to be described in detail. It is necessary to keep in mind that the mission is still in a very early stage and, therefore, relevant changes in the design can still occur. This section aims to include the most relevant specifications of the mission in relation to the design of the ADCS. Among these aspects are:

1. Information w.r.t. the structure of the satellite, including the geometrical specifications. As previously mentioned, two configurations will be studied: stowed (S) and deployed (D). In the deployed configuration some components can be differentiated from a structural perspective (see figure 2.1), being: central part, membrane and booms. In the stowed configuration the membrane is stowed and the booms rolled inside of the central part. Geometrical specifications are included in table 2.1.

2. Mass properties of the different components and throughout the different configurations explored. Include three main aspects of the spacecraft in both stowed and deployed configurations: mass, moment of inertia and position of the center of gravity. Table 2.2.

3. Properties related with the non-rigid motion of selected components. These properties are only studied in relation with the booms. As the selection of which booms to use is not yet taken, several options are included here (table). However, throughout the study, and for the purpose of coherence in the results, the boom implemented is that with a zero sub-index. The data includes the bending stiffness (EI), the density of the boom (just for giving an idea of the cost in weight of increasing the stiffness) and the dissipation coefficient (k_d), which is expressed as a function of the bending stiffness.

4. Interaction with disturbances. Here the coefficients and properties of the (operating) spacecraft with an influence over the way the satellite interacts with its environment are studied. The main disturbances included in this study were previously defined as the gravity gradient, the atmospheric drag, the magnetic field and the solar radiation. In light of this, information about the drag coefficient, magnetic dipole and optical properties of the membrane is included in table 2.4. These values may diverge slightly from the actual mission.

5. Specifications of the sensors used. A number of sensors in relation to the GoSolAr ADCS have already been introduced. Their main characteristics are included in table 2.5.

6. Similarly to the previous point, the specifications regarding the actuator used (magnetorquer) are included in table 2.6.

7. Finally the orbit(s) that are to be studied are to be defined in order to be able perform further analyses. As these are not yet defined, different orbits will be studied throughout the report, aiming to give an understanding on how changes in this aspect of the mission would potentially influence the ADCS performance.

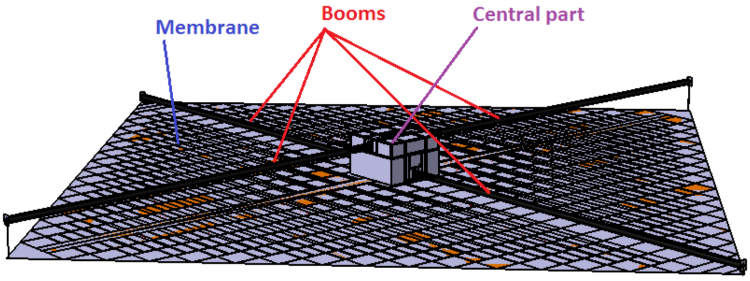

Figure 2.1: Different elements of the deployed configuration of the GoSolAr satellite, from a structural perspective.

Property [units]	Magnitude	Property [units]	Magnitude
Dimensions(S) [m^3]	0.5x0.5x0.5	Membrane area [m^2]	25
Boom length [m]	3.5355		

Table 2.1: Geometrical data.

Property [units]	Magnitude	Property [units]	Magnitude
Stowed mass [kg]	60.8	Membrane mass [kg]	6.2
Central part mass [kg]	53.1	Boom mass [kg]	0.38
Ixx(S) [kgm^2]	3.19	Ixx(D) [kgm^2]	17.3130
Iyy(S) [kgm^2]	3.42	Iyy(D) [kgm^2]	18.9068
Izz(S) [kgm^2]	2.92	Izz(D) [kgm^2]	31.7930
Ixy(S) [kgm^2]	0.005	Ixy(D) [kgm^2]	0.005
Ixz(S) [kgm^2]	-0.01	Ixz(D) [kgm^2]	-0.01
Iyz(S) [kgm^2]	-0.011	Iyz(D) [kgm^2]	-0.004
CoG(S) [m]	[0 0 0]	CoG(D) [m]	[0 0 0.05]

Table 2.2: Mass data.

Property [units]	Magnitude	Property [units]	Magnitude
EI_0 [Nm^2]	1320	ρ_0 [kg/m]	0.0785
EI_1 [Nm^2]	113.36	ρ_1 [kg/m]	0.019
EI_2 [Nm^2]	397.71	ρ_2 [kg/m]	0.03
EI_3 [Nm^2]	5156	ρ_3[kg/m]	0.102
k_d [Nm^2/s^2]	α EI	α [-]	0-0.01

Table 2.3: Non-rigid dynamics (booms).

Property [units]	Magnitude	Property [units]	Magnitude
C_D (drag coefficient) [-]	1.2	Magnetic dipole module [Am^2]	0.1
Spectral reflectance coefficient[-]	0.5	Diffuse reflectance coefficient [-]	0.5

Table 2.4: Interaction with environment.

Sensor	Property [units]	Magnitude
Coarse sun sensor	FoV [deg^2]	Full view
Coarse sun sensor	Noise [deg]	10
Coarse sun sensor	Bias [deg]	3
Fine sun sensor	FoV [deg^2]	30 (conical)
Fine sun sensor	Noise [deg]	0.2
Fine sun sensor	Bias [deg]	0.5
Magnetometer	Noise [T]	8.5e-9
Magnetometer	Bias [T]	250e-9
Gyroscope	Noise [deg/s]	0.025
Gyroscope	Bias [deg/s]	5e-3
GPS	Noise [m]	0
GPS	Bias [m]	10
All sensors	Measuring frequency [Hz]	5

Table 2.5: Sensor specifications.

Actuator	Property [units]	Magnitude
Magnetorquer	Max dipole [Am^2]	10
Magnetorquer	Time constant [s]	0.05
Magnetorquer	Duty cycle [%],[s]	90%, 5

Table 2.6: Actuator specifications.

2.3. GoSolAr and research objective

This final section of the chapter aims to highlight the relation between the GoSolAr mission and the research objective that is targeted by this thesis. By doing so, the selection of this mission as a case of study is justified and the relevance in relation with the research questions that we aim to answer is sustained.

When looking at the structure of the GoSolAr's satellite (figure 2.1), it is clear that it is far from a conventional compact spacecraft. Looking at the specifications of the structure it can be observed that this satellite qualifies for being considered a large thin flexible structure (LTFS). Particularly meaningful among this specifications are:

- Thin membrane with an area of 25 m^2.
- Composite booms with a length of 3.5 meters aiming to rigidize the structure.
- High moment of inertia and low weight (table 2.2).

Having shown that this satellite can be considered an LTFS, and considering that this kind of structures is the main target of the research, the relation between the GoSolAr mission and the thesis becomes self-evident. Furthermore, the selection of GoSolAr as a case of study allows to derive more concrete research questions, which can be helpful to define a path towards fulfilling the research objective. The main questions specified are shown below.

- To what degree can the mission requirements be fulfilled with the set of sensors and actuators defined?
- How can the structural particularities, i.e. flexibility, of the structure be modeled?
- What is the influence of these particularities in the ADCS performance?
- How can this change in behavior be approached from a control perspective?

3

Basic Rigid Body Analysis

As it can be deduced from its title, this chapter aims to provide with an initial analysis of the case of study. The objective of this basic analysis is to give an approximate idea on the performance to be expected in relation to the ADCS. The specifications of the analysis are those of a conventional ADCS analysis, i.e. assuming the satellite is a rigid body.

As a prerequisite to performing this analysis, a simulation environment was built. This environment was based in the Attitude control system simulator for Compact Satellite (CS) developed by the German Aerospace Center (DLR). This tool is implemented in Simulink (MATLAB). Its main characteristics are described in section 3.1, with a particular emphasis in the changes driven by the particularities of the GoSolAr mission (e.g. particular sensors used).

Among the main insights resulting from this analysis are the following:

- Limitations inherent to the use of the defined set of sensors and actuators.
- Challenges in relation to the particularities of the spacecraft's structure, without taking into account the flexibility.

In addition, the results obtained will be allow to, in further stages of the research, isolate and analyze the effect the flexibility of the structure has on the performance of the ADCS. Within this analysis, a search for the limitations of the GoSolAr mission w.r.t. aspects such as the altitude of the orbit is also conducted.

3.1. Simulation environment

As has been pointed out, the simulation tool used to conduct the analyses is built in a Simulink environment. This tool is based in the Attitude control system simulator for Compact Satellite (CS) developed by the German Aerospace Center (DLR). Due to its internal use at DLR, this tool is assumed verified. The main changes implemented throughout the study were: 1) the controller's block, 2) the satellite's plant, once the flexibility is introduced, and 3) the structure of the satellite, affecting its interaction with the external disturbances. The high level components of the this tool are shown in figure A.1 in appendix A. This section introduces each of those components, explaining their role in the control loop shown and their most relevant characteristics.

3.1.1. Sensors and estimator

Two main processes are included in the sensors' block, related to simulating the measuring process and deriving the state variables from those measurements. This way, a first sub-block generates each sensor's measurements from the actual state of the spacecraft. The possibility of taking into account noise and biases (data based in table 2.5) into the measurements of each of the sensors is considered and implemented. This implementation is done so that the decision of whether to consider ideal or real measuring process is an input variable. Additionally, two particularities of the sun sensors, i.e. the lack of measurements during eclipse and when the sun is outside the field of view, are also taken into account.

The second process that occurs inside this block aims to construct the state vector from the measurements. In order to be able to do this, the variables that are included in the state vector need first to be defined. One self-evident variable is the angular rate (w.r.t. the body fixed reference frame). When going through the existing literature it may seem equally obvious that the other variable is to be a quaternion defining the attitude of the satellite w.r.t. the inertial reference frame. This was the initial strategy followed, computing this quaternion using sun sensor's and magnetometer's measurements combined with a deterministic algorithm (TRIAD) [3]. However, it was noticed that this approach go beyond the mission requirements, which only aims to control the relative orientation of an axis in the body fix reference frame w.r.t. the sun vector. Therefore, this strategy, which involves also estimating the magnetic field and sun vector in the inertial reference frame based in the position, was considered unnecessarily complex. The decision was then made to use the sun vector as the second state variable. In the absence of measurements (eclipse) the change in this variable is estimated based in the angular rate. In figure 3.1, the effect of considering the real measuring process is shown. It can be seen that, while the error in the angular rate remains of similar magnitude, there are three distinguishable error behavior areas in the case of the sun vector. These areas are: 1) coarse sun sensor, up to 500 seconds, 2) fine sun sensor, 1000-1500 and 4000-5000 seconds, and 3) estimation based in angular rate, 2000-3500 seconds. Particularly relevant is the steady increase in the error during eclipse time, caused by the bias in the angular rate.

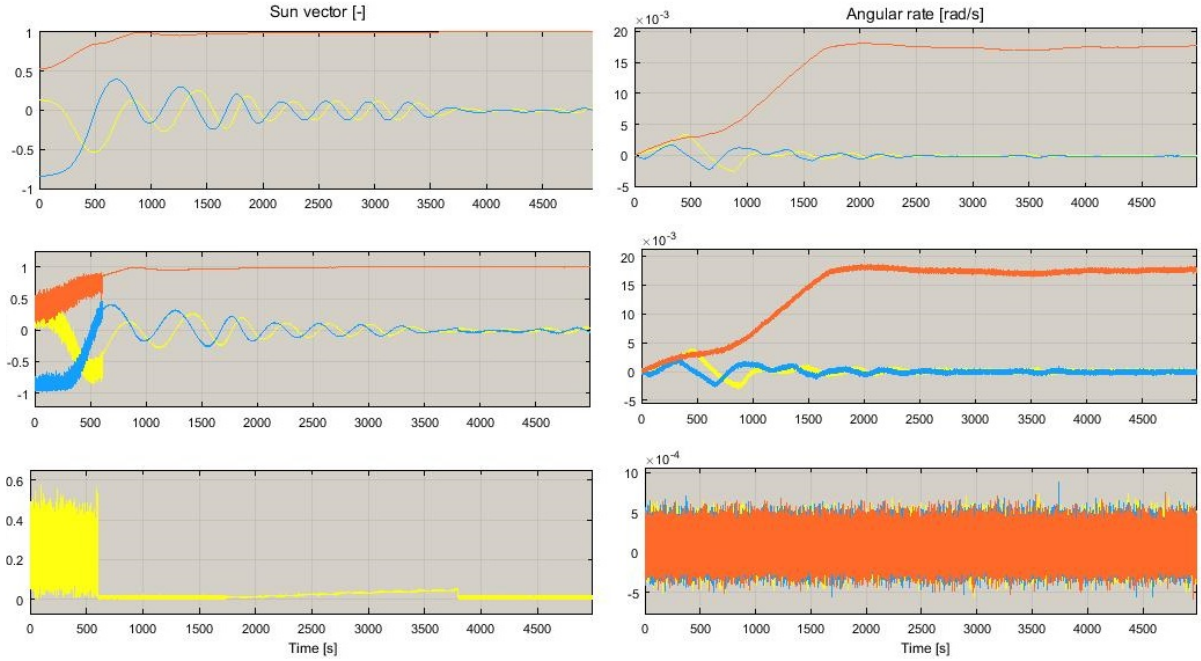

Figure 3.1: Measuring process analysis. Comparison of actual state variables (up), measured state variables (center) and error (down).

This 'raw' (unfiltered) state vector goes then through the estimator's block. In the event that the sensors are assumed ideal this block is commented off. In case the measuring process includes the noise and biases of the sensors, an extended Kalman filter is used to improve the accuracy of the state vector. The mathematical derivations involved in this filter are not included in this report. Furthermore, with the objective of simplifying the problem and avoid a potential interference in the results, during most of the research the measuring process is assumed ideal and the filter is not used.

3.1.2. Controller and actuator

As previously mentioned, there are two main tasks for the ADCS throughout the mission: 1) detumbling and 2) pointing and maintaining a relative orientation w.r.t. the sun. For each of these tasks a different controller is designed. The reason for doing this is that the controller needed for detumbling is considerably simpler than the one used during operation. For the detumbling phase, the controller used is commonly known as b-dot controller. It aims to reduce the angular velocity of the spacecraft by generating a dipole with the form shown in expression 3.1 [1]. This equation is based in the assumption that the change of the magnetic field in the inertial reference frame is negligible when compared to that in the body fixed reference frame.

$$\vec{m} = -k_{\omega}\dot{\vec{b}}_u \approx -k_{\omega}\frac{\vec{b}\times\vec{\omega}}{b} \tag{3.1}$$

For the second stage, pointing and maintaining a relative orientation w.r.t. the sun, the controller was derived using a linear quadratic regulator (LQR) approach to compute static gains, which relate the control variables with the control command. Further explanations on how the gains have been computed are included in section 3.2.1. It is to be reminded that this controller aims to generate an angular velocity in the body fix reference frame and control the orientation of the rotating axis in the inertial reference frame. The control variables are computed from the guidance instructions (spin and relative orientation between rotation axis and sun vector) and the state estimation (sun vector and angular rate). This computation is based on direct substraction in the case of the angular rate and in the method explained in [6] for the pointing error. This method gives an approach to express the difference between two axis that are to be aligned (according to guidance instructions). The equations resulting from the application of this method are shown in expression 3.2, where v_1 and v_2 are the axes to be aligned and cv the control variable related to the pointing error. With respect to the linearization points used for the LQR controller, two points are used, varying the angular rate: 1) $\omega = 0$ and 2) $\omega = \omega_g$, where ω_g is the guidance angular rate for the spacecraft.

$$\begin{gathered}\vec{e} = \frac{v_1 \times v_2}{|v_1 \times v_2|}; \quad \theta = arccos(v_1 \cdot v_2); \quad [e\times] = \begin{bmatrix} 0 & -e_3 & e_2 \\ e_3 & 0 & -e_1 \\ -e_2 & e_1 & 0 \end{bmatrix}; \\ E = I + sin\theta[e\times] + (1 - cos\theta)[e\times]^2 \rightarrow \vec{cv} = [E_{23} - E_{32}; E_{31} - E_{13}]; \end{gathered} \tag{3.2}$$

After computing the desired control torque, the controller takes into account that the actuator use (magnetorquer) is only able to provide a torque in a plane normal to the local magnetic field. This is taken into account by the conventional approach of projecting the desired torque into that plane. Other alternatives can be found in literature but are not considered here [23]. Then, based on the information regarding the magnetic field, the command torque is transform into a command dipole, which is to be generated by the magnetorquer.

The actuator used is a three axis magnetorquer, aligned with the main axis of the satellite. The specifications of the actuator are shown in table 2.6. However, as the impact or meaning of some of these specifications may not be that intuitive, they deserve further explanation. The time constant is linked to the velocity at which the magnetorquer can change the dipole it is generating. Therfore, for a time constant t, the transfer function of the magnetorquer is $1/(ts+1)$. The duty cycle is meant to switch on and off the magnetorquer so the magnetometer can measure the unaffected local magnetic magnetic field. This measurement is directly necessary for the b-dot controller and indirectly for the LQR controller, as it is the base for the relation between the torque desired and the command dipole.

3.1.3. External disturbances

For computing the external disturbances, a simplified model of the structure is used. This model is a cube in the case of the stowed configuration and a body like that shown in figure 3.2 for the deployed configuration. It does not take into account the interaction between different parts of the structures (e.g. shade projected by the central part over the membrane). Four origins of disturbance torques (gravity field, magnetic field, atmosphere and radiation pressure) and two of disturbance forces are considered (atmosphere and radiation pressure). The following expressions for these disturbances were already implemented in the attitude control system simulator for Compact Satellite provided by the German Aerospace Center and have not been modified. The gravity gradient is computed as shown in equation 3.3, where MoI is the moment of inertia and r_u the unitary position vector. The magnetic disturbance calculation is given in equation, where m is the satellite's dipole and b the local magnetic field.

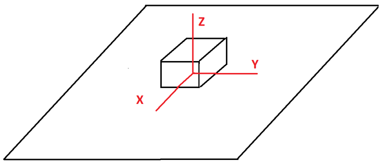

Figure 3.2: Schematic view of the satellite structure used in the computation of surfaces forces (solar pressure and drag) for the deployed configuration.

$$\vec{T}_g = 3\frac{\mu}{|r|^3}(\vec{r}_u \times (MoI\vec{r}_u)); \tag{3.3}$$

$$\vec{T}_m = \vec{m} \times \vec{b}; \tag{3.4}$$

The value of the of the solar irradiance (i_r) used to compute the solar pressure is assumed constant and with a value of 1358 W/m^2. This is an approximation, as it actually varies (variations <10%) throughout the year and solar cycle (≈11 years). Both the disturbance torque and disturbance force are computed based in the simplified structure previously mentioned and in expression 3.5, used to compute the distributed force over the surfaces exposed to the solar radiation. In this expression, s is the sun vector, n the normal of the surface, θ the angle between both, C_{sr} the spectral reflectivity coefficient, C_{dr} the diffusive reflectivity coefficient and A the area.

$$\vec{f}_r = i_r((1 - C_{sr})\vec{s} + 2(C_{sr} cos\theta + \frac{1}{3} C_{dr})\vec{n}) A cos\theta; \tag{3.5}$$

The atmospheric density is defined at the beginning of each simulation and considered constant throughout it. It is computed at the initial altitude based on the Harris-Priester model [16], assuming a value of 111 $W/m^2/Hz$ of the F10.7 cm flux level and taking the maximum density. This value (F10.7 cm flux level) shows considerable variations during the solar cycle, from 65 to 275, having a great influence in the density (up to 2 orders of magnitude), which increases as the flux level increases. The assumption is optimistic, in the sense that it is assumed that the satellite is operating at a time with low solar activity, but still strict, as it takes into account the maximum densities to be found under that solar activity. The consequences of this assumption will be evaluated in section 3.2.2. Once the atmospheric density is defined, the force and torque caused by the drag can be computed using equation 3.6 combined with the definition of the structure.

$$\vec{f}_d = -\frac{1}{2} C_D \rho v^2 A cos\theta \vec{v}_u; \tag{3.6}$$

Figure 3.3 compares external disturbance torques generated for stowed and deployed configurations. In the stowed configuration only gravity gradient and magnetic torque generate torque, as the center of mass matches the center of pressure (nominal case). In the deployed configuration the gravity gradient and atmospheric drag generate the highest torques (of the order of 5e-5 Nm), followed by solar pressure (5e-6) and finally magnetic torque (5e-8). Due to the similarity in the moments of inertia in x and y axes, the gravity gradient is smaller in the z-axis. The internal magnetic dipole is assumed not to change due to the deployment. Therefore, the magnetic torque remains of a similar magnitude. Evidently, during the eclipse there is no solar pressure.

3.1.4. Equations of motion

The plant of the satellite contains the equations of the dynamics and kinematics of the spacecraft. Even though the equations related to linear motion are also included in the model, only those related to the angular motion are shown here. The expressions shown throughout this subsection were obtained from [32], where more detailed derivations can be found. In this initial analysis, the satellite was assumed to behave as a rigid body. Taking this assumption into account (i.e. the moment of inertia is constant), the dynamics of the spacecraft can be derived from the angular momentum (L) as shown in equation 3.7. In this equation, ω is the angular rate, MoI the moment of inertia and T the external torque.

$$\begin{gathered}\vec{L} = MoI\vec{\omega} \\ \frac{d\vec{L}}{dt} = \vec{T} - \vec{\omega} \times \vec{L} = MoI\frac{d\vec{\omega}}{dt} \\ \dot{\vec{\omega}} = MoI^{-1}(\vec{T} - \vec{\omega} \times (MoI\vec{\omega}))\end{gathered} \tag{3.7}$$

Regarding the kinematics of the spacecraft, it is necessary to choose how to describe the attitude of a rigid body, i.e. the relative orientation of two three-axes reference frames. It was decided to use Euler symmetric parameters, which describe this relative orientation using a quaternion. The four elements of this quaternion (Q) contain information regarding the Euler axis ($[e_1, e_2, e_3]$) and angle (ϕ) (see expression 3.8). The rotation needed to go from one reference frame to the other is then described as a rotation of the Euler angle in the Euler axis.

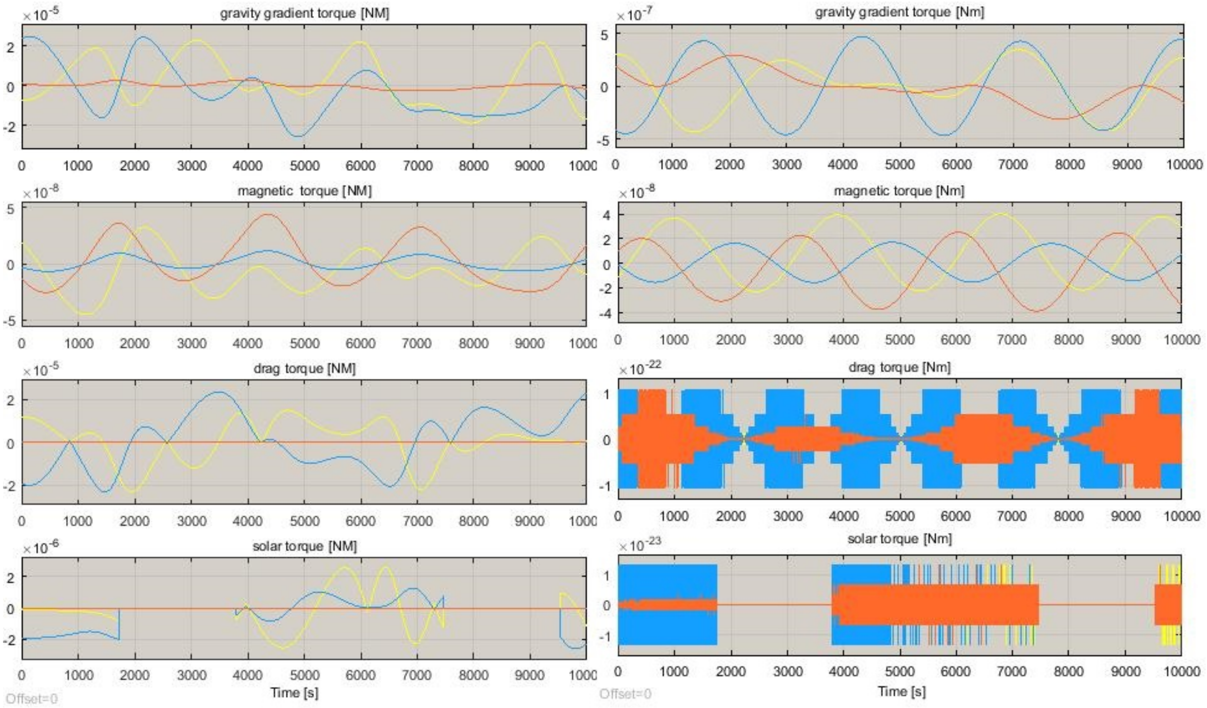

Figure 3.3: Comparison of the external disturbances (torques) over stowed (right) and deployed (left) configurations. 550 km of altitude.

$$Q_1 = e_1 sin\frac{\phi}{2}; \quad Q_2 = e_2 sin\frac{\phi}{2}; \quad Q_3 = e_3 sin\frac{\phi}{2}; \quad Q_4 = cos\frac{\phi}{2}; \tag{3.8}$$

Using this parametrization leads to the expression of the kinematics of the spacecrafts shown in equation 3.9. In this equation Q is the quaternion and Ω is the extended angular rate. The conversion of the angular rate (ω) into the extended angular rate (Ω), consists in adding a forth component equal to zero. More information about quaternion algebra (e.g. quaternion product) can be found in [18].

$$\dot{Q} = \frac{1}{2} Q\Omega; \tag{3.9}$$

These two equations (3.7 and 3.9) define the motion of the satellite assuming it is a rigid body. In chapter 4, this assumption is eliminated and, therefore, these equations are extended to include the effect of the flexibility.

The two blocks left are less interesting from the research's perspective. The transformation block computes all relevant variables from data regarding time, position and attitude of the satellite. These variables include, for example, the local magnetic field and the sun vector in the body reference frame. The visualization block provides with a direct way of visualizing and analyzing the results.

3.1.5. Structural configurations and initial conditions

Once the ADCS loop components have been introduced, it is necessary to analyze the different set-ups or configurations that can appear during the mission and, thus, have been implemented in the simulation. First of all, regarding the structure, two main options are considered: stowed and deployed. In the first case the geometry of the spacecraft consists on a prism with the dimensions specified in table 2.1. For the deployed case, the membrane lays centered in the surface of the prism pointing to +Z-axis in the body fix reference frame and each of the four booms is connected to the central part of the satellite and to one corner of the membrane (see figure 2.1). Another aspect to be define for each simulation is the initial condition of the spacecraft. Three main possibilities are studied:

- After launch and before the detumbling phase. The assumptions made are that: 1)the norm of the angular velocity is 12 deg/s, 2) the direction of the angular velocity is aleatory and 3) the attitude of the spacecraft is aleatory. This is considered to be consistent with the actual situation expected after launch.

- After the detumbling phase has been conducted the angular rate is assumed to be reduced to 0.1 deg/s, based in the results obtained. Both the direction of this angular velocity and the attitude of the satellite are still defined in an aleatory way.
- After the spacecraft has been given a spin in the z-axis and this axis has been aligned with the sun vector, the operation phase is reached. In this case the error in the angular rate is assumed to be of the order of 0.01 deg/s and the error in the in the pointing direction of the order of 1 degree.

Finally, regarding the ADCS operation, it is necessary to consider two cases: active and inactive. In case the system is active the controller is chosen based in the initial conditions: b-dot controller if the satellite is still tumbling and LQR based controller for the rest of the scenarios.

3.2. Results

This section contains the results obtained when performing analyses based in the description given in the previous section. Therefore, the simulation environment described is used and the satellite is considered a rigid body. The analyses cover the two main tasks of the ADCS (detumbling and pointing phases) and aim to give a clear idea of the performance over the different structural configurations (stowed and deployed) for several scenarios (i.e. initial conditions, orbital parameters..etc.).

A separation is made between two set of results. The first set (section 3.2.1) contains an exhaustive analysis over the performance of the controller over the complete mission, containing all combinations of phases and structural configurations, for a defined array of orbital parameters. In the second sub-section (section 3.2.2), the analyses performed focus in the most critical aspects of the mission (as identified in 3.2.1). By focusing in these parts, it studies the limitations that may arise as well as different conceptual alternatives that could be implemented in the mission.

3.2.1. Basic analysis

This analysis is conducted in order to gain a further understanding about the ADCS role in the mission and the main challenges that will appear throughout it. To achieve this goal, is necessary to first conduct an initial analysis covering all different configurations and tasks that this system will face during the mission. To simplify this analysis, the number of variables changing for the different analyses is lowered by choosing a concrete orbit. The orbit chosen has an altitude of 600 km, inclination of 60 deg and the rest of the orbital parameters are zero. The starting date of the simulation remains also constant for all the simulations, being 01/09/2015.

All possible combinations of the two structural configurations (deployed and stowed) and control phases (detumbling and pointing) are considered. The initial condition of the spacecraft is defined based on those two parameters, as shown in table 3.1, where: ω_0 is 12 deg/s, ω_1 is 0.01 deg/s, a is a vector containing three values out of a standard normal distribution and b containing four values (computed for each run), I_S is the moment of inertia of the stowed configuration and I_D of the deployed configuration.

Control phase	Structural configuration	Angular rate	Attitude quaternion
Detumbling	Stowed	$\omega_0 \frac{a}{\lvert a\rvert}$	$\frac{b}{\lvert b\rvert}$
Detumbling	Deployed	$I_d^{-1}(I_s \omega_0 \frac{a}{\lvert a\rvert})$	$\frac{b}{\lvert b\rvert}$
Pointing	Stowed	$\omega_1 \frac{a}{\lvert a\rvert}$	$\frac{b}{\lvert b\rvert}$
Pointing	Deployed	$\omega_1 \frac{a}{\lvert a\rvert}$	$\frac{b}{\lvert b\rvert}$

Table 3.1: Initial conditions for the satellite's attitude.

The performance of the controller in the detumbling phase is measured by the reduction achieved in the module of the angular rate. This reduction is shown in figure 3.4 for the stowed configuration and in figure 3.5 for the deployed configuration. In each case, 5 different initial conditions (based in table 3.1) are considered.

It can be observed that in both configurations the b-dot controller is able to stabilize the satellite, keeping the module of the angular velocity under 0.01 deg/s for the stowed configuration and under 0.1 deg/s for the deployed configuration. The time needed for detumbling is of the order of 2 hours for the stowed configuration and 1 hour for the stowed one.

Regarding the differences between the two configurations, it can be observed that the angular velocity reduction achieved in the stowed configuration is considerably higher than in the deployed configuration. This is mainly caused by: 1) an increase in the external disturbances, due to an increase in the area exposed

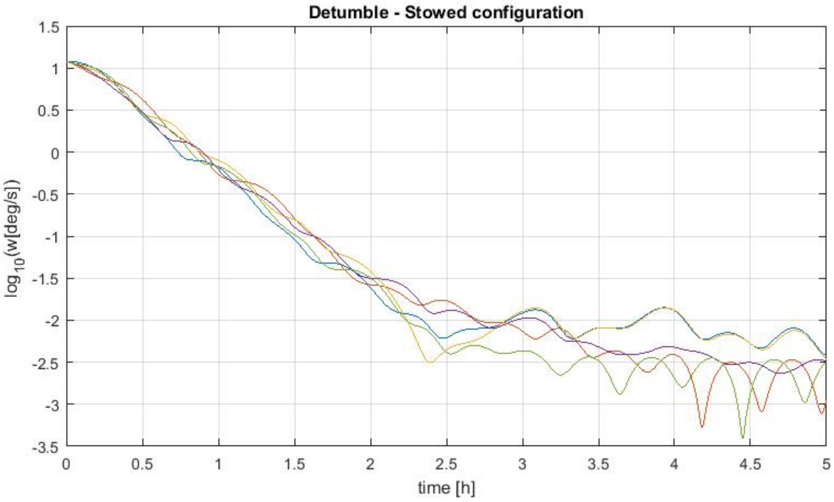

Figure 3.4: Module of the angular velocity throughout the detumbling phase for 5 different initial conditions. Stowed configuration.

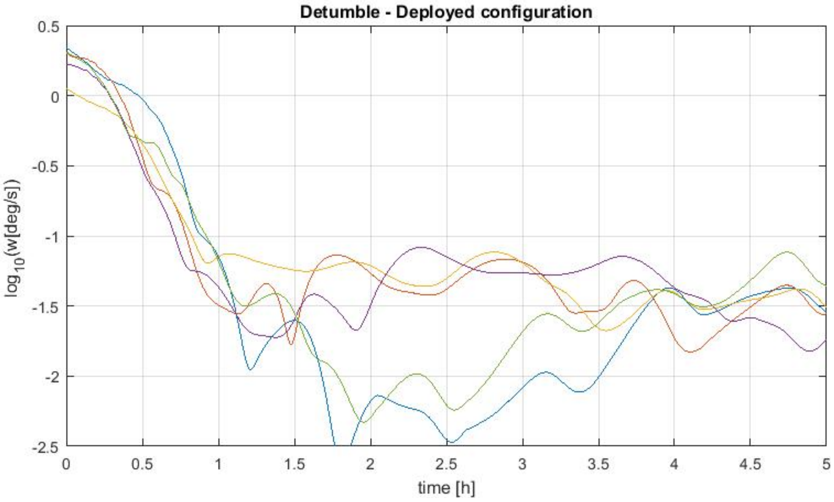

Figure 3.5: Module of the angular velocity throughout the detumbling phase for 5 different initial conditions. Deployed configuration.

to solar radiation pressure and drag, and 2) increase in the moment of inertia. As the specifications of the actuator (magnetorque) remain constant throughout the different satellite's configuration, its performance decreases as the external disturbance torque and the moment of inertia increase. Another clear difference is that the initial angular rate is lower for the deployed configuration, as the increase of the moment of inertia of the spacecraft throughout the deployment phase slows the spinning of the satellite, conserving the angular momentum. This leads to a lower time for reaching the final detumbled stage.

After considering these two main possibilities regarding when to conduct the detumbling of the spacecraft w.r.t. the mission timeline (before and after deployment), no clear 'winner' is discovered. As the results are considerably similar from an ADCS perspective, the decision on which one to implement must be based in other factors, such as loads induced during deployment or influence in later ADCS' phases.

The other control phase to be studied is the pointing towards the sun. As part of this phase, the satellite is also given a spin in order increase its stability w.r.t. the direction of the spin axis. As previously mentioned, during this phase the controller uses static gains computed using an LQR approach. As explained in section 5.1, this approach aims to find a gain matrix K, such that function J is minimum when applied over a linear system (see expression 3.10). This function depends on the state vector, the control command and the weighting matrices Q, R and N, which define the importance of each state and control variable.

$$\dot{x} = Ax + Bu \quad \rightarrow \quad J = \int_0^{\infty} (x^T Q x + u^T R u + 2x^T N u) dt \quad \rightarrow \quad u_{min(J)} = Kx \tag{3.10}$$

The minimization of the J function is done using a built-in Matlab function (*lqr*). However, in order to be able to implement this function, the weighting matrices need first to be defined. This is done experimentally, analyzing the performance of the controller for several combinations of weights for the pointing error, angular rate error and commanded torque. The most promising weights are then selected. An example on how this was done can be seen in appendix B. The final weights selected are: 5e-3 for the pointing error, 1e4 for the angular rate error and 1e5 for the control torque. Regarding the linear plant used, two linearization points were implemented, giving two different sets of gains. The first point is centered in zero angular rate and the second one in the desired final angular rate. The change between these sets of gains is implemented automatically by the controller once the spacecraft reaches the desired angular rate.

The performance of the controller in this control phase (pointing) is now evaluated, over both stowed (figure 3.6) and deployed (3.7) configurations. There is one difference in the control strategy used in each configuration: while in the stowed configuration the satellite is accelerated to the final desired spin from the beginning, in the deployed configuration the acceleration is progressive (see figure 3.8). This is done in order to avoid reaching a highly stable configuration far from the desired orientation. These simulations were run under the assumption of ideal measurements. 10 different cases were run for each configuration, changing the initial condition according to table 3.1.

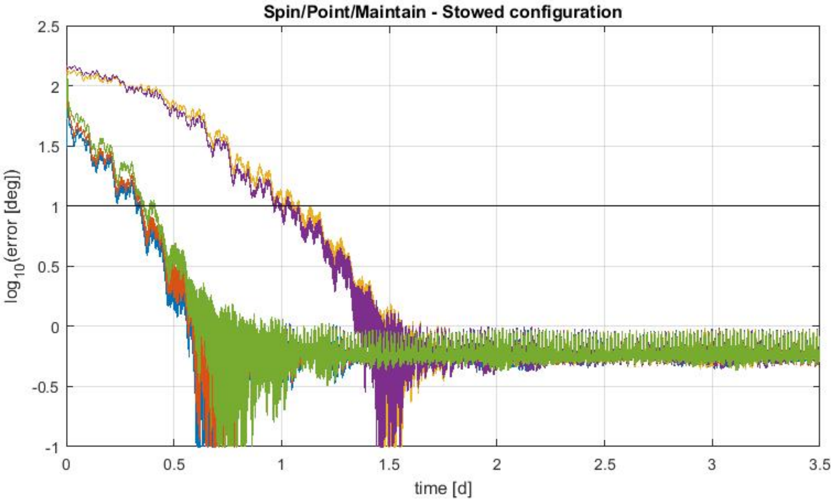

Figure 3.6: Pointing error [rad] throughout the pointing stage for 10 different initial conditions. Stowed configuration.

The main conclusion that can be extract from these results is that the mission attitude requirements regarding pointing accuracy can be fulfilled (for the particular orbit studied) with the ADCS design proposed. This design comprises the set of sensors and actuators as well as the controller, previously described. It is also to be mentioned that further optimization of the gains and a more precise use of the progressive spin may have the potential of decreasing the time needed to reach the operating point and even to increase the attainable accuracy.

Two main aspects of the results are to be studied: 1) the convergence speed towards the operating point and 2) the accuracy with which the spacecraft can be maintained in that point. Regarding 2, when comparing the results obtained for both configurations (stowed and deployed), it can be observed that, similarly to the results for the detumbling phase, the accuracy achieved in the stowed configuration is considerably better than the one in the deployed configuration. The explanation is, a priori, similar: increase in the external disturbances and in the moment of inertia. In relation with the time needed to reach the operation point, it can be noticed that it is highly dependent on the initial attitude, ranking between 0.5 and 1.5 days for both stowed and deployed configurations. Again, no clear benefits are observable for conducting the pointing stage before or after the deployment has taken place.

It was also noticed that, in the deployed configuration, the error shows a periodic behavior linked in frequency with the orbit of the spacecraft. A more detailed view of this behavior is shown in figure 3.9. This periodic behavior appears to be divisible in two main distributions: 1) higher period ($\approx 1.6h$), in relation with the orbital frequency and therefore with most external disturbances, and 2) higher frequency (twice the previous one), in relation with the limitation to the control torque imposed by the local magnetic field (locally underactuated).

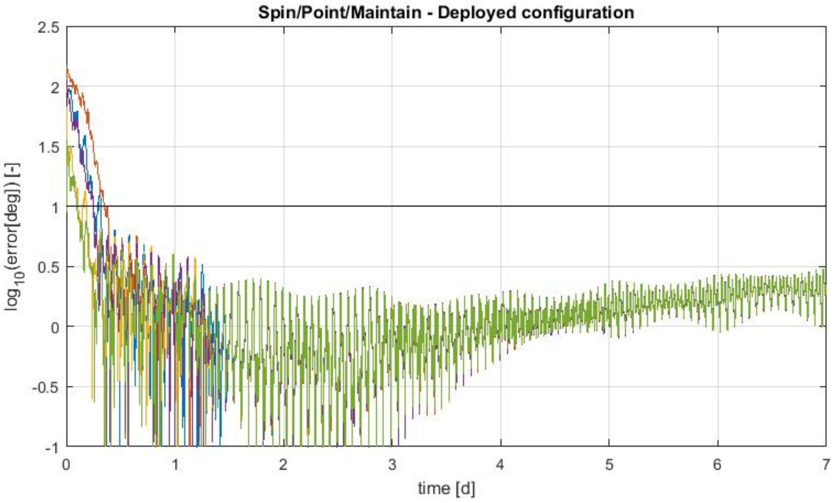

Figure 3.7: Pointing error [rad] throughout the pointing stage for 10 different initial conditions. Deployed configuration. Progressive acceleration.

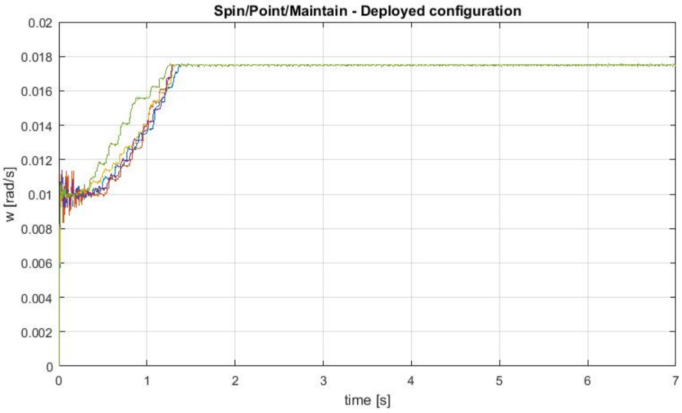

Figure 3.8: Angular velocity [rad/s] throughout the pointing stage for 10 different initial conditions. Deployed configuration. Progressive acceleration.

Finally, it is important to remark that the ADCS system is able to maintain the deployed satellite pointing towards the sun within the limits specified in the requirements. In figure 3.7, the results show that the pointing error remains below 3 degrees after the first attitude correction. However, further analyses are needed in order to prove the stability of the configuration for broader time spans, different initial altitudes and orbital parameters.

3.2.2. Extended results

The analysis conducted in the previous section can be used to understand qualitatively the performance of the ADCS, pointing out which are the critical phases and main potential limitation that may appear. It is now safe to state that the most critical structural configuration for the ADCS is the deployed configuration and that the most demanding control phase is pointing.

Throughout this section, additional analyses are shown with the aim of giving an additional insight to the GoSolAr mission and, therefore, to missions with similar characteristics. These additional analyses focus in two main aspects of the mission: 1) orbit selection and 2) conceptual alternatives for the design of the mission.

With respect to the selection of an orbit, two main limitations are studied, both related to the interaction of the spacecraft with the space environment:

- Altitude.

- Inclination and right ascension of the ascending node.

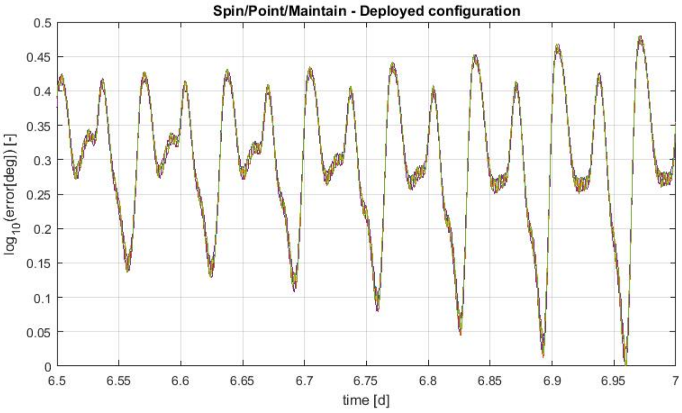

Figure 3.9: Periodicity of the pointing error in the long term.

W.r.t. the altitude, the objective is to define both the upper and lower limits that allow complying with the mission requirements on pointing accuracy. The results of the simulations used to draw conclusions in relation this limitation are included in appendix C.

The upper constrain in the attitude is caused by two main factors: 1) strength of the magnetic field and 2) code of conduct (which aims to contain the increase of orbital debris). As at higher altitudes the magnetic field's strength lowers, the control torque that can be applied also decreases. However, the decrease of the magnetic field is followed by a decrease in the disturbances caused by the gravity gradient and the atmospheric drag, which are dominant for lower altitudes. Therefore, the decrease in the control torque attainable is not considered to be critical for altitude within the range considered for this mission. This is confirmed in figures C.2, which shows that the detumbling phase can be successfully conducted up to 800 km, and C.3, which shows that the pointing error can be keep within requirements for altitudes up to 750 km. On the other hand, the current code of conduct limits the deorbiting time of the nominal configuration to 25 years. This nominal configuration can be assumed to be the worst case scenario (i.e. failure in deployment) or the actual nominal scenario (i.e. successful deployment). This decision makes a considerable impact, as in the first case the initial altitude is limited to around 600 km while in the second one it can go up to almost 800 km. Therefore, it can be concluded that the main limitation regarding the upper limit of the initial altitude is related to the application of the code of conduct and not to the ADCS requirements.

Regarding the lower constrain in altitude, the main cause is the fast (exponential) increase of the atmospheric density when decreasing the altitude. Even thought, the magnetic field strength also increases, at a certain altitude the magnetorquer will not be able to cope with the torque generated by the drag. This limits the operative lifetime of the mission, as below this altitude the controller will not be able to ensure that the satellite is pointing towards the sun within the accuracy required. The results (appendix C) indicate that the altitude limit for controlling the spacecraft with the selected ADCS design is slightly below 450 km. For the flux level (F10.7) assumed, this altitude states for a mean density of 2.2E-12 kg/m^3. It is to be highlighted that, throughout the solar cycle, the mean density at 450 km of altitude can vary from 1.1E-11 (high solar activity) to 9E-13 (low solar activity). This means that the altitude limitation for the mission changes with time, pointing out to the possibility of ensuring the lifetime and the deorbiting time simultaneously, by launching the spacecraft to a low orbit in a period of low solar activity. Two main options to extend the lifetime of the spacecraft to lower altitudes can be observed: 1) to ensure it operates in a timeframe where the solar activity is low and 2) to reduce the membrane area.

An analysis on the deorbiting time of the satellite is shown also in appendix C. This analysis shows the deorbiting profile (altitude as a function of time) for different initial conditions, including: 1) date (linked to the solar cycle), 2) initial altitude and 3) success/failure of the deployment. The only external disturbance taken into consideration is the drag. The density is computed using Harris Priester atmospheric model, estimating the radio flux based on data from the Space Weather Prediction Center (U.S. Dept. of Commerce). In case of failure of deployment the effective area is assumed constant (0.25 m^2). In case of success of deployment the effective area is compute in two phases: 1) For densities lower than 3E-12 kg/m^3 the membrane is assumed to be pointed towards the Sun and, therefore, the effective area is computed based on the satellite's velocity and the position of the sun, and 2) for higher densities the membrane is assume oriented perpendicularly to the velocity (constant effective area equal to the area of the membrane). This analysis shows that, in case the nominal case is assumed to be a failure in deployment, there are two main possibilities, if the requirements on maximum an minimum deorbiting time are kept at 25 years and 6 months: 1) ensure launching at an epoch with low solar activity or 2) reduce the membrane area. In case the nominal case is assumed to have successfully deployed the membrane, both requirements can easily be met by choosing an initial higher altitude.

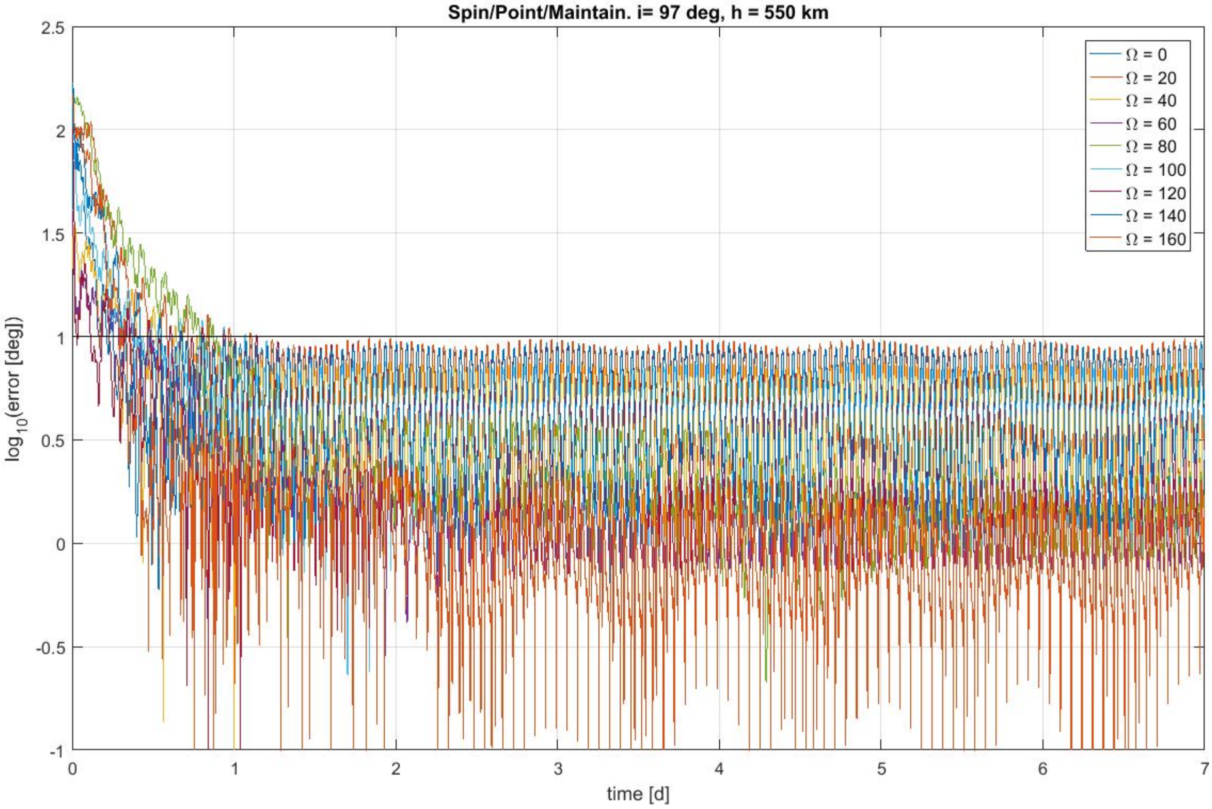

Figure 3.10: Study of the pointing phase for an inclination of 97 deg and different right ascensions of the ascending node. Altitude: 550km.

The second main factor to be taken into account when choosing the orbit is that, in order for the magnetorquer to be able to properly control the attitude of the satellite, the direction of the magnetic field should not be steady. As pointed out in previous sections, the exclusive use of magnetorquers to control the attitude of the satellite leads to a locally underactuated spacecraft. In order to be able to minimize the effect of this local phenomena, the orbit of the spacecraft needs to be such that the magnetic field varies throughout the orbit allowing exerting control torques in any direction. Taking into account that Earth's magnetic dipole (simplification of the actual magnetic field, which is considerably more complex) has an inclination of around 11 degrees, it can be deduced that orbits with low inclinations may encounter this kind of problem. In this orbits the magnetic field remains close to an axis normal to the orbital plane, imposing a hard limitation in the torque applicable in that direction, making the spacecraft less controllable or even uncontrollable. In appendix D, several analyses over a range of orbital inclinations and right ascensions of the ascending node are run. These analyses confirm the lack of controllability (with the controller developed) of the system for some orbits with low inclinations.

It is also to be noted that, even for orbits with high inclination, the accuracy obtained differs considerably for different right ascensions of the ascending node. The reason behind this is that, as the membrane plane is pointed towards the sun, its relative orientation w.r.t. its orbital velocity is determined by this orbital parameter (right ascension of the ascending node). This relative orientation influences the both the evolution of the effective area determining the drag and the distance between the center of pressure and center of mas, having a considerable effect in the disturbance torque generated by the drag. This can be seen in figure 3.10, were the pointing accuracy obtained changes between 3 and 10 degrees as a function of the right ascension of the ascending node.

When studying the design of the mission, three main potential changes are considered, listed below. These changes are explained in the remaining of this section using mainly a qualitative approach.

- Change in the orientation of the solar cells.
- Reorientation phases throughout the mission.
- Changing the pointing objective at low altitudes.

The reason to evaluate the possibility of changing the orientation of the solar cells is that this orientation defines the vector that is to be aligned (in direction and orientation) with the sun vector. The two alternatives are shown in figure 3.11 as A, the orientation chosen initially, and B, the alternative to be analyzed. The main drawback of configuration A is that it leads to the operating point being an unstable equilibrium point w.r.t. the torque produced by the solar radiation. This is because the center of mass is more distant to the sun than the membrane plane. On the other hand, in configuration B, the operation point is a stable equilibrium point w.r.t. to this torque. In case the solar radiation was the dominant disturbance, this would be a critical point for improving the pointing accuracy of the satellite. In the range of altitudes considered in the GoSolAr mission and in this report, the dominant disturbance torques are caused by gravity and drag, and, thus, the benefit to be gain by this change of configuration is limited. However, for missions aiming higher altitudes it would be a point to be taken into consideration.

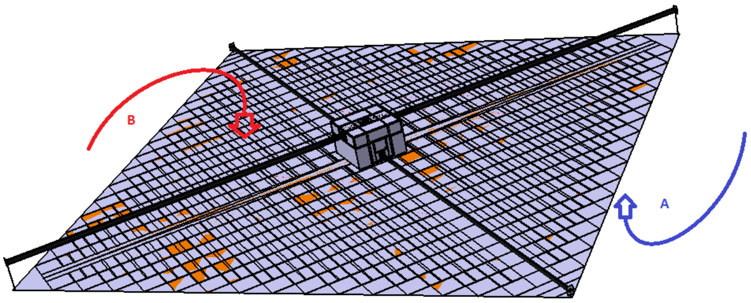

Figure 3.11: Orientation of the solar cells. A: nominal plane, B: alternative plane.

Among the objectives of the GoSolAr mission is to characterize the solar array. In order to allow a more complete characterization of this array, it seems to be optimal to study different orientations of it w.r.t. the incident solar radiation. From a control perspective, re-orientating the rotation axis towards an aleatory fixed axis in the inertial reference frame, expressed in the body fixed reference frame, do not pose a problem. Furthermore, the proximity of the new axis to the previous one (i.e. the sun vector) increases the convergence rate, leading to a maneuver time of the order of 1-6 hours.

However, when examining in depth this new axis some challenges are found. The conditions that this axis should fulfill are: 1) fixed orientation with respect to the sun vector, which is equivalent to being (quasi) constant in the inertial reference frame, and 2) be expressed in the body fixed reference frame. Fulfilling both requirements is not trivial in the absence of complete knowledge regarding the attitude of the satellite. In the initial case, where this axis is the sun vector, it can be expressed directly in the body fixed reference frame due to the use of sun sensors. The solution for this problem is considerably immediate, computing the attitude quaternion. This is done using the TRIAD method (previously mentioned), which computes it using the relative rotation between sun and magnetic vectors in the inertial and body fixed reference frames. Even though this computation is considerably simple, it still adds some computational cost. The results (see figure 3.12) confirm the estimation on the time needed for performing this maneuvers, between 1 and 6 hours. Furthermore, they also point out the pointing accuracy achieved is not dependent of the angle w.r.t. the sun vector.

The final aspect of the mission considered is related with what control strategy to follow when the ADCS is no longer able to maintain the orientation towards the sun within the accuracy requirements. In the analyses shown previously, the controller developed aimed to continuously point towards the sun (or towards other inertially fixed direction). However, as it has been shown before, there is an lower limit in the altitude from where this is not possible anymore. In order to avoid uncontrolled tumbling, an additional phase is proposed, in which the drag is used to create an equilibrium point and stabilize the spacecraft attitude around it. This way, this additional phase consist in using the structure of the satellite and the dominant external disturbance (drag) for passive control of the spacecraft's attitude. From a conceptual perspective, this passive control is based in aligning the satellite's axis Z (see figure 3.2) as close as possible to the satellite's velocity vector w.r.t. the atmosphere. It is also to be mentioned, that the importance of this phase is low when compared to the

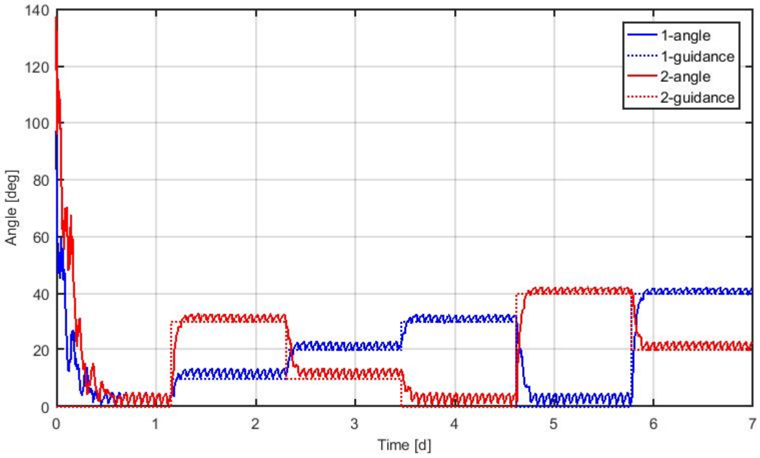

Figure 3.12: Evolution of the angle w.r.t. the sun vector for two different guidance instructions and initial conditions. h=550km, i=97 deg.

overall mission, as once the density of the atmosphere is such that the pointing requirements can't be met, the rate of orbit decay is high and the satellite deorbits in the order of days. This is the reason why this phase was not analyzed in further detail.

3.3. Conclusions

The main conclusion of this chapter is that the mission requirements in relation with the ADCS are met, in the absence of the potential effect of the flexibility, by the design proposed. The results are also meant to give an idea of the accuracy attainable and of the behavior of the structure from an attitude perspective. Furthermore, these analyses are also useful to isolate an analyze the effect of the flexibility in further stages of the study.

Additionally, several challenges, in relation with the particularities of the structure and with the proposed ADCS design, that are considered particularly relevant are pointed out below.

- The spacecraft is locally under-actuated. The control torque produced is always contained in a plane normal to the local magnetic field. Therefore, in the absence of additional actuators, the system will always be locally under-actuated.
- Low volume available to be use for potential actuators, in relation to the moment of inertia and to the effective area interacting with external disturbances. This volume limits the length of the magnetorquers and, thus, the maximum dipole that can be generated.
- In the deployed configuration, the center of mass and the center of pressure are no longer coincident. This increases the effect of the solar radiation and atmospheric drag in the final disturbance torque.

Concerning potential improvements in this area, the most relevant addition would be, from the author perspective, the implementation of either periodic control or a finite-horizon approach to address the local under-actuation.

4

Flexible model

The aim of this chapter is to improve the accuracy and completeness of the analysis shown in the previous section, as well as to take the next step towards answering the research questions. In order to be able to do this, we aim to go beyond the 'simple' dynamics of the rigid bodies, incorporating the effect of flexibility in our equations of motion.

In order to decide the approach to use when adding this effect, the objectives that are targeted with the derivation of these new equations need to be defined. Two main objectives are distinguished below. Note that a tradeoff needs to be made between achieving these two goals, as the second one prevents for using over complicated models (such as those which would be used for the study of the static deformations or load distribution over the structure).

- Increase the accuracy of the model of the satellite. This objective is related to allowing a more precise evaluation of the performance of the different ADCS designs studied.
- Generate meaningful equations that can give an insight of the behavior of the plant and be used for control purposes.

The rest of the chapter is structured starting with a brief introduction to the theoretical basis of the method used to derived these equations/model, highlighting its potential applicability to cases different than the one covered in this report. Then, the implementation of the method over a simplified version of the spacecraft's structure is explained in detailed. Several possibilities for increasing the similarity of this simplified case to the real one are also explained. After building the model for a particular case of study, the results are compared to those obtained using a numerical model, with the aim of verifying the process of deriving the equations.

4.1. Theoretical background

As explained in the first chapter of this thesis, a considerable number of approaches to modeling a flexible structure can be found in the existing literature. In this study, an analytical method was selected, as it appears to be the most suitable for covering both objectives of the model: it allows building an accurate model while maintaining the order of the system low enough for it to be comprehensible and useful in control applications.

Of course, there are several analytical approaches to derive equations of motion taking into account the flexibility of the structure. The one chosen in this study is based in the Lagrange equations and, more particularly, in one of the methods explained in [17], which was found extremely useful throughout the progression of the thesis. The reasons to select this particular approach (i.e. Lagrange's equations in combination with assumed modes method), which will be properly explained throughout this section, are the following:

- It allows a relatively easy and intuitive derivation of the equations of motions, w.r.t. other methodologies (i.e. most of the derivations are partial derivatives).
- The arbitrary selection of the coordinates makes possible to determine these coordinates in relation with the structure analyzed and with the variables of interest for each case.

The model is derived from the classical form of Lagrange equations 4.1, which has been widely used, in holonomic discrete coordinate systems, to obtain the equations of motion [17]. In this expression, L is the lagrangian, T the kinetic energy, V the potential, q a coordinate and Q the non-conservative forces over coordinate q. This expression is derived from the generalized Hamilton principle, shown in expression 4.2, assuming the virtual work of the non-conservative forces (W_{nc}) can be expressed as shown in equation 4.3.

$$\frac{d}{dt}(\frac{\partial L}{\partial \dot{q}}) - \frac{\partial L}{\partial q} = Q; \quad L = T - V; \tag{4.1}$$

$$\int_{t_1}^{t_2} \delta(T-V)dt + \int_{t_1}^{t_2} \delta W_{nc} dt = 0; \tag{4.2}$$

$$\delta W_{nc} = \sum_i Q_i \delta q_i; \tag{4.3}$$

In order to distinguish between the non-conservative internal forces (i.e. dissipation) and the external forces, expression 4.4 was defined, where D is the Rayleigh dissipation function. Finally, assuming that the potential (V) is a function only of q (and not of $\dot{q}$), this equation can expressed as shown in equation 4.5, which will be used from this point. The sub-index i points out the discrete number of coordinates to be used.

$$\frac{d}{dt}(\frac{\partial L}{\partial \dot{q}}) - \frac{\partial L}{\partial q} + \frac{\partial D}{\partial \dot{q}} = Q_{ext}; \tag{4.4}$$

$$\frac{d}{dt}(\frac{\partial T}{\partial \dot{q}_i}) - \frac{\partial T}{\partial q_i} + \frac{\partial V}{\partial q_i} + \frac{\partial D}{\partial \dot{q}_i} = Q_i; \tag{4.5}$$

Once this initial equation has been defined, it is necessary to go through the terms that appear in it. In order to enable the derivation of the equations of motion, we aim to describe the kinetic energy (T), potential (V) and dissipation function (D) as shown in expression 4.6. In this expression N is the number of coordinates (which will be called generalized coordinates from this point on), q_i is the generalized coordinate i, $\dot{q}_i$ its time derivative and M, K and F are NxN matrices.

$$\begin{aligned} T(q,\dot{q},t) =& \frac{1}{2}\sum_{i=1}^{N}\sum_{j=1}^{N} M_{ij}(q)\dot{q}_i(t)\dot{q}_j(t) \\ V(q,t) =& \frac{1}{2}\sum_{i=1}^{N}\sum_{j=1}^{N} K_{ij}q_i(t)q_j(t) \\ D(\dot{q},t) =& \frac{1}{2}\sum_{i=1}^{N}\sum_{j=1}^{N} F_{ij}\dot{q}_i(t)\dot{q}_j(t) \end{aligned} \tag{4.6}$$

Assuming expressions for M, K and F can be found, expression 4.5 can be further developed, leading to expression 4.7. This assumption is later on validated by deriving the three matrices. Equation 4.7 contains the equations of motion of the system and will be used throughout the rest of the study as the basic expression of the model. Three main terms appear to be added w.r.t. the conventional and well-known expression for the dynamics of a simple flexible system (i.e. $M\ddot{q}+F\dot{q}+Kq = Q$). These additional terms are caused by the dependency of the mass matrix (M) on time ($\dot{M}(q,\dot{q},t)\dot{q}(t)$) and on the generalized coordinates ($\frac{1}{2}\dot{q}^T(t)\frac{\partial M(q,t)}{\partial q}\dot{q}(t)$) and by effect of the time derivative taking into account the rotating character of the system ($R(q,\dot{q},t)$). Note that $\frac{\partial M}{\partial q}$ is a tensor in with dimension NxNxN, and, therefore, the result of the term involving that quantity is a vector as well as the rest of the terms.

$$M(q,t)\ddot{q}(t) + \dot{M}(q,\dot{q},t)\dot{q}(t) + R(q,\dot{q},t) - \frac{1}{2}\dot{q}^T(t)\frac{\partial M(q,t)}{\partial q}\dot{q}(t) + Kq + F\dot{q} = Q \tag{4.7}$$

This expression (4.7) is generic and can be applied to different geometries and structures by defining an adequate set of generic coordinates, in line with the structure and with the objectives of the study. This implementation over a particular structure can be done following the process shown in figure 4.1. This process is now briefly introduced and later on explained in detail for the case of study analyzed in this thesis.

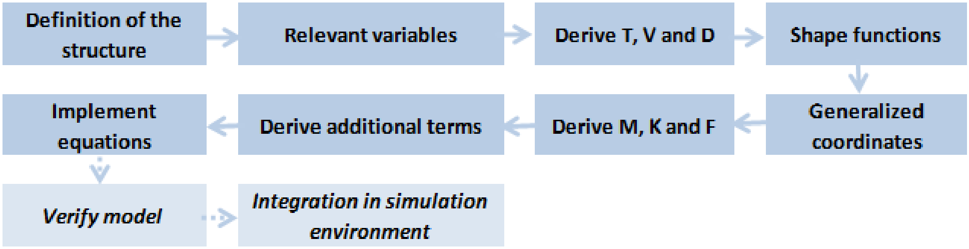

Figure 4.1: Procedure followed for the derivation of the flexible model.

First of all, in order to be able to study the dynamics of a structure, the structure itself needs to be define. This definition process includes the assumptions that are being made to simplify the actual structure as well as complete definition of the different bodies and their relevant structural properties (e.g. density or bending stiffness). Having defined the structure, the objective the model is built for is to be evaluated. By analyzing this objective the relevant variables that need to be included in the model can be obtained (e.g. if the vibrations of a boom are to be studied, its deformation needs to be included as a variable). Once these variables are defined, it is necessary to evaluate if the kinetic energy, potential and dissipation function can be expressed as a function of them, taking into account the assumptions made. If this is not possible, it may be necessary to consider adding variables.

When expression for T, V and D as functions of the study variables have been found, several options are possible to obtain the matrices M, K and F. The method used here is called assumed modes method and is based in selecting a set of shape functions, which represents the different flexible modes that appear in the structure, using discrete number of generalized coordinates. The nature and implementation of these functions will be further explained throughout this chapter. After obtaining matrices M, K and F, the rest of the terms of expression 4.7 need to be computed. Particularly relevant is the conversion of external forces into generalized forces (Q), which is here done using the virtual work principle. The process concludes with the implementation of the equations. Two additional phases are shown here, as they play a relevant role for the particular case of study: 1) verification of the equations obtained and 2) integration of the model in the simulation environment described in the previous chapter.

4.2. Flexible model

This section aims to explain the process followed for deriving the equations of motion for a particular set of assumptions in relation with the structure. As shown in figure 4.1, this process starts by defining the structure that is to be modeled and the variables which have a relevant role in the analysis. Then, through deriving the kinetic energy, the potential and the dissipation function, and defining a consistent set of generalized coordinates, the terms involved in expression 4.7 can be expressed in a generic form. This generic form means that the precise form of the shape functions have not been defined up to this point. Finally, the shape functions are defined and the actual equations of motion obtained.

4.2.1. Structure and variables

Due to the high complexity of the modeling of the flexibility of the membrane, it was decided to (initially) define the structure to be modeled including only the flexibility of the booms. The possibility of including the flexible dynamics of the membrane at later stages of the project was left open but finally not implemented. Even though this limits considerably the accuracy with which the equations of motion obtained model the behavior of the actual spacecraft, it is considered a considerable improvement w.r.t. assuming a rigid body in the sense that:

- It provides with an understanding on how the flexible and rigid modes interact with each other, including qualitative and quantitative results.

- It enables to estimate the effect of the flexibility in the performance of the ADCS.

- It can be used to study different possibilities for addressing the particularities of a flexible structure from an ADCS perspective.

- It describes a methodology to model this kind of structures, which can also be used in relation to more complex setups.

As mentioned before, this analysis only included the flexibility of the booms, considering the spacecraft as a combination of rigid and flexible bodies. This way, the structure analyzed consists on a rigid body to which four flexible bodies (booms) are attached (see figure 4.2). Initially, the rigid body was assumed to contain the mass and moment of inertia of both the central part of the spacecraft and the membrane. However, in light of further analyses (see section 4.3), it was decided to increase the density of the booms, incorporating there part of the membrane's mass and moment of inertia. The reasoning behind this explained in section 4.3 and does not play a role in deriving this equation of motions but just in the final coefficients that will appear in the matrices.

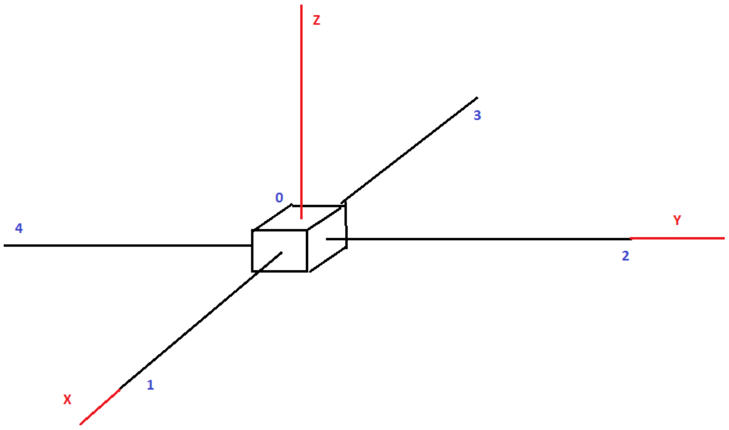

Figure 4.2: Schematic drawing of the targeted structure.

Additional general assumptions that were made when defining the structure are:

- The rigid body geometry is assumed constant throughout time and independent from the motion of the booms.
- In relation with the evaluation of the interaction between the membrane and the external disturbances (drag and solar pressure), the membrane is assumed rigid and maintains a fixed relative position w.r.t. the central part of the satellite.
- The distributed forces and torques applied in the membrane are assigned to the central part and the tip of the booms. This distribution is done by dividing the membrane in 4 rigid triangular membranes, each one laying on 2 boom tips and the central hub.
- The only elastic deformations studied are those of the bending of the booms. Therefore, no torsion or axial deformation is considered.
- The mass distribution of the booms is assumed to be concentrated along its longitudinal dimension.

Once the structure targeted by the model has been defined, the variables of interest need to be taken into account. Two main categories of variables can be distinguish, related with: 1) rigid motion and 2) flexible motion. Those variables linked to the rigid motion describe the motion of the central part of the satellite and are those conventionally used for this purpose: position, attitude, velocity and angular rate. Of particular interest for this analysis are those related with the rotation of the spacecraft (i.e. attitude and angular rate). Even thought we are linking them to rigid motion, it is to be highlighted that the evolution of these variables is, of course, affected by variables of the flexible motion. With respect to this second category, the main variables to be addressed are the deformations of the booms. These variables are continuous and contain the bending deformation of each boom along its span.

In order to consistently define these variables, three reference frames need to be used: 1) inertial reference frame, 2) body fixed reference frame and 3) boom reference frame (for each boom). The inertial reference frame (RFI) is defined as the inertial Earth reference frame. The body fixed reference frame (RFB) origin is the

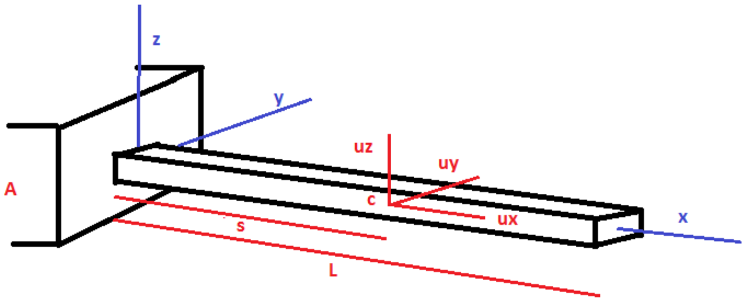

Figure 4.3: Schematic drawing of a boom.

geometrical center of the central part of the spacecraft, and the axes are defined as shown in figure 4.2. These two reference frames (RFI and RFB) are used to define the rigid motion variables (e.g. the attitude describes the rotation between RFB and RFI). The third reference frame(s) used is defined for each boom (RFL), it has the same origin as RFB but the orientation of the axes is such that the x-axis is aligned with the longitudinal dimension of the boom (see figure 4.3)

4.2.2. Generic equations of motion

The objective of this section is to explain how the generic equations of motion were obtained. It is organized starting the derivation of the kinetic energy as a function of the selected variables (previous section). Then, this expression is converted into an expression with the form shown in equations 4.6. In order to do this, generalized coordinates have been defined using the assumed modes method, which will be explained later. This allows reformulating the expression of the kinetic energy and computing the mass matrix (M) and the terms related with this matrix. Obtaining of the the potential and dissipation functions (V and D) and matrices (K and F) is then explained. Finally, the conversion of the external forces to generalized forces (forces applied over the generalized coordinates) is analyzed. This conversion is not immediate and requires the application of the virtual work principle.

The reason the kinetic energy is computed before defining the generalized coordinates is that, even though the main aim of these coordinates is to be able to study the variables of interest, they should also allow to represent completely the the matrices M, F and K. Out of these matrices, M is the most complicate. As it is linked to the kinetic energy, it is advantageous to derived first and expression for this energy and then study the possibilities regarding the generalized coordinates.

The kinetic energy of a system can be expressed as the sum of the kinetic energy of the different bodies included in that system. The case studied consists on five bodies: one rigid body and four flexible booms. Therefore, the kinetic energy can be expressed as shown in equation 4.8, where $E_{k,T}$ is the total kinetic energy, $E_{k,R}$ that of the rigid body and E_{k,B_i} the one of boom i. The computation of the kinetic energy related to the rigid body ($E_{k,R}$) is well known and it can be expressed as shown in equation 4.9. ω is the angular velocity of RFB with respect to RFI, I is the moment of inertia, m the mass and v_o is the velocity of the origin of RFB.

$$E_{k,T} = E_{k,R} + \sum_{i}^{4} E_{k,B_i}; \tag{4.8}$$

$$E_{k,R} = \frac{1}{2}\omega^T I \omega + \frac{1}{2} m v_o^2 \tag{4.9}$$

The kinetic energy of each boom can be expressed in relation with the velocity of each of its massive points. This leads to the integral shown in expression 4.10., where ρ is the longitudinal density, L the length of the boom, s the integration variable covering the longitudinal dimension of the boom and v is the velocity w.r.t. RFI. This velocity can be divided in two parts, assigned to: 1) the rigid motion of the central part of the satellite (v and ω) and 2) the velocity of deformation of the booms. The deformation of the booms is expressed as u and, therefore, the velocity of deformation as $\dot{u}$. This two terms are shown in equation 4.11. Introducing expression 4.11 into 4.10 leads to the expression for the kinetic energy of a boom shown in equation 4.12.

$$E_{k,b} = \int_0^L \frac{1}{2} \rho v^2(s) ds \tag{4.10}$$

$$
\begin{aligned}
v(s) =& v_o + \omega \times r(s) + \dot{u}(s);\\
r(s) = [s,0,0] + u(s); &\quad \dot{u}(s) = [\dot{u}_x, \dot{u}_y, \dot{u}_z];
\end{aligned}
\tag{4.11}
$$

$$
E_{k,b} = \frac{1}{2}\rho \int_0^L \left[(v_{ox} + \omega_y u_z - \omega_z u_y + \dot{u_x})^2 + (v_{oy} + \omega_z ac - \omega_x u_z + \dot{u}_y)^2 + (v_{oz} + \omega_x u_y - \omega_y ac + \dot{u}_z)^2 \right] ds \tag{4.12}
$$

Having computed the two terms that appear in the expression of the total kinetic energy (expression 4.8), this can be expressed as shown in equation 4.13. However, it is to be reminded that the objective of this derivation is not to obtain an expression for the kinetic energy but rather for the mass-matrix (M). In order to do this, the terms involved in expression 4.13 are classified depending on whether they contain the velocity (v), angular rate (ω) or the deformation velocity ($\dot{u}$). This differentiation is shown in expression 4.14.

$$
\begin{aligned}
&E_{k,b} = \frac{1}{2}\omega I \omega + \frac{1}{2} M v_o^2 +\\
&\frac{1}{2}\rho \int_{b1} \left[(v_{ox} + \omega_y u_{1z} - \omega_z u_{1y} + \dot{u_{1x}})^2 + (v_{oy} + \omega_z (s + u_{1x}) - \omega_x u_{1z} + \dot{u}_{1y})^2 + (v_{oz} + \omega_x u_{1y} - \omega_y (s + u_{1x}) + \dot{u}_{1z})^2 \right] ds +\\
&\frac{1}{2}\rho \int_{b2} \left[(v_{oy} - \omega_x u_{2z} + \omega_z u_{2x} + \dot{u_{2y}})^2 + (-v_{ox} + \omega_z (s + u_{2y}) - \omega_y u_{2z} - \dot{u}_{2x})^2 + (v_{oz} - \omega_y u_{2x} + \omega_x (s + u_{2y}) + \dot{u}_{2z})^2 \right] ds +\\
&\frac{1}{2}\rho \int_{b3} \left[(-v_{ox} - \omega_y u_{3z} + \omega_z u_{3y} - \dot{u_{3x}})^2 + (-v_{oy} + \omega_z (s - u_{3x}) + \omega_x u_{3z} - \dot{u}_{3y})^2 + (v_{oz} + \omega_x u_{3y} + \omega_y (s - u_{3x}) + \dot{u}_{3z})^2 \right] ds +\\
&\frac{1}{2}\rho \int_{b4} \left[(-v_{oy} + \omega_x u_{4z} - \omega_z u_{4x} - \dot{u_{4y}})^2 + (v_{ox} + \omega_z (s - u_{4y}) + \omega_y u_{4z} + \dot{u}_{4x})^2 + (v_{oz} - \omega_y u_{4x} - \omega_x (s - u_{4y}) + \dot{u}_{4z})^2 \right] ds
\end{aligned}
\tag{4.13}
$$

$$
\begin{aligned}
&v, -\rightarrow \frac{1}{2} M v_0^2 + 2 m_b v_0^2 + \rho \int_0^L v_o^T ((\sum R_{bi})\omega) ds + \rho \int_0^L v_o^T (\sum \dot{u}_i) ds\\
&\omega, -\rightarrow \rho \int_0^L v_o^T ((\sum R_{bi})\omega) ds + \frac{1}{2}\omega^T (I\omega) + \frac{\rho}{2} \int_0^L \omega^T ((-\sum R_{bi}^2)\omega) ds + \rho \int_0^L \dot{u}^T ((\sum R_{bi})\omega) ds\\
&\dot{u}_i, -\rightarrow \rho \int_0^L v_o^T \dot{u}_i ds + \rho \int_0^L \dot{u}_i^T (R_{bi}\omega) + \frac{\rho}{2} \int_0^L \dot{u}_i^2 ds
\end{aligned}
\tag{4.14}
$$

$$
R_{bi} = \begin{bmatrix} 0 & d_{iz} & -d_{iy} \\ -diz & 0 & d_{ix} \\ d_{iy} & -d_{ix} & 0 \end{bmatrix}; d_1 = \begin{bmatrix} s + u_{1x} \\ u_{1y} \\ u_{1z} \end{bmatrix}; d_2 = \begin{bmatrix} u_{2x} \\ s + u_{2y} \\ u_{2z} \end{bmatrix}; d_3 = \begin{bmatrix} -s + u_{3x} \\ u_{3y} \\ u_{3z} \end{bmatrix}; d_4 = \begin{bmatrix} u_{4x} \\ -s + u_{4y} \\ u_{4z} \end{bmatrix} \tag{4.15}
$$

In expression 4.14, it can be seen that even though the kinetic energy has been defined as a function of the selected variables, the matrix M is not obtainable. This is because the variable u and $\dot{u}$ are function of both time and the longitudinal distance (s). This means it is not possible to solve this integrals or to take these variables outside of the integrals. In order to overcome this issue, the deformation of the booms are expressed as a combination of time dependent (q) and space dependent (ϕ) functions. In equation 4.16, i defines the coordinate, j the boom and k the mode.

$$
\begin{aligned}
u_{ij}(s,t) &= \sum_{k=1}^{N} q_{ijk}(t) \phi_{ijk}(s); \quad i: x,y,z; \quad j: 1,2,3,4; \quad k: 1,2...N\\
\Phi_{j,k} &= \begin{bmatrix} \phi_{xjk} & 0 & 0 \\ 0 & \phi_{yjk} & 0 \\ 0 & 0 & \phi_{zjk} \end{bmatrix}
\end{aligned}
\tag{4.16}
$$

The strategy followed to define these shape functions is known as the assumed modes method, and consists in expressing the deformation of the booms as shown in expression 4.16. There is another alternative, which consists in lowering the number of modes and dividing the boom into multiple flexible elements (finite element method). The reason to choose the first method is that it leads to a lower order system. This enables to use the resulting equations not only in the modeling of the plant but also in its control. In the finite element method, in the other hand, the number of elements increases considerably fast and, thus, the order of the system. This leads to an increase in the computational cost, becoming inefficient for using it for control purposes. The method used also has, however, some inconveniences. Particularly important are: 1) need to derived the shape functions for each particular geometry and 2) complicated shape functions [17].

Introducing the shape functions shown in expression 4.16 into the expressions in 4.14, leads to the expression for the mass matrix (M) shown in equation 4.17. Additionally, the definition of the shape function makes possible to define the generalized coordinates, which include: 1) position, 2) attitude quaternion and 3) q_{ijk}, with i:x,y,z, j:1-4 and k:1-N (see expression 4.16). The $\dot{q}$ shown in expression 4.6, is then expressed as shown in equation 4.18.

$$M = \begin{bmatrix} (M+4m_b)I_u & \rho\int_0^L \sum R_{bi} ds & \rho\int_0^L \Phi_{1,1} & \rho\int_0^L \Phi_{1,2} & \dots & \rho\int_0^L \Phi_{4,N-1} & \rho\int_0^L \Phi_{4,N} \\ -\rho\int_0^L \sum R_{bi} ds & I+\rho\int_0^L -\sum R_{bi}^2 ds & \rho\int_0^L R_{b1}^T \Phi_{1,1} ds & \rho\int_0^L R_{b1}^T \Phi_{1,2} ds & \dots & \rho\int_0^L R_{b4}^T \Phi_{4,N-1} ds & \rho\int_0^L R_{b4}^T \Phi_{4,N} ds \\ \rho\int_0^L \Phi_{1,1} & \rho\int_0^L \Phi_{1,1} R_{b1} ds & \rho\int_0^L \Phi_{1,1}^2 & \rho\int_0^L \Phi_{1,1}\Phi_{1,2} & \dots & 0 & 0 \\ \rho\int_0^L \Phi_{1,2} & \rho\int_0^L \Phi_{1,2} R_{b1} ds & \rho\int_0^L \Phi_{1,1}\Phi_{1,2} & \rho\int_0^L \Phi_{1,2}^2 & \dots & 0 & 0 \\ \dots & \dots & \dots & \dots & \dots & \dots & \dots \\ \rho\int_0^L \Phi_{4,N-1} & \rho\int_0^L \Phi_{4,N-1} R_{b4} ds & 0 & 0 & \dots & \rho\int_0^L \Phi_{4,N-1}^2 & \rho\int_0^L \Phi_{4,N-1}\Phi_{4,N} \\ \rho\int_0^L \Phi_{4,N} & \rho\int_0^L \Phi_{4,N} R_{b4} ds & 0 & 0 & \dots & \rho\int_0^L \Phi_{4,N-1}\Phi_{4,N} & \rho\int_0^L \Phi_{4,N}^2 \end{bmatrix} \tag{4.17}$$

$$\dot{q} = [v_{0x}; v_{0y}; v_{0z}; \omega_x; \omega_y; \omega_z; \dot{q}_{x,1,1}; \dot{q}_{y,1,1}; \dot{q}_{z,1,1}; \dot{q}_{x,1,2}; \dot{q}_{y,1,2}; \dot{q}_{z,1,2}; \dots; \dot{q}_{x,4,N-1}; \dot{q}_{y,4,N-1}; \dot{q}_{z,4,N-1}; \dot{q}_{x,4,N}; \dot{q}_{y,4,N}; \dot{q}_{z,4,N}] \tag{4.18}$$

Once the mass matrix (M) has been derived, the terms in relation with it in the general expression for the equations of motion (equation 4.7) can be obtained. Differentiating this matrix w.r.t. time is relatively simple, as the only time dependent variables involved in M are the deformation of the booms. As these deformations are expressed as a combination of shape and time dependent functions (see equation 4.16), their derivation with respect to time is immediate. The term $\dot{q}^T \frac{\partial M}{\partial q} \dot{q}$ is considerably more complex. In order to simply its addition to the final expressions and avoid including tensors in the implementation, it has been divided in two parts: $\dot{q}^T \frac{\partial M}{\partial q}$ and $\dot{q}$. The first of these parts was derived and the expression for its non-zero rows is shown in equation 4.19. In this expression i is the axis (x,y,z), k the mode (1-N), j the boom (1-4) and N the total number of modes included). Finally, the term addressing the rotation of the reference frame (R) includes the non-zero terms shown in expression 4.20.

$$\begin{gathered} \dot{q}^T(t)\frac{\partial M(q,t)}{\partial q}(a,:) = \frac{1}{2}\begin{bmatrix} (\rho\int_0^L \frac{\partial \sum R_{bi}}{\partial q_{ijk}} ds)\omega \\ (-\rho\int_0^L \frac{\partial \sum R_{bi}}{\partial q_{ijk}} ds)v - (\rho\int_0^L \frac{\partial \sum R_{bi}^2}{\partial q_{ijk}} ds)\omega + \sum_{lmn}((\rho\int_0^L \frac{\partial R_{bl}^T}{\partial q_{ijk}} \Phi_{l,m} ds)\dot{q}_{nml}) \\ (\rho\int_0^L \Phi_{1,1}\frac{\partial R_{b1}}{\partial q_{ijk}} ds)\omega \\ (\rho\int_0^L \Phi_{1,2}\frac{\partial R_{b1}}{\partial q_{ijk}} ds)\omega \\ \dots \\ (\rho\int_0^L \Phi_{4,N}\frac{\partial R_{b4}}{\partial q_{ijk}} ds)\omega \end{bmatrix}^T \\ a = 6+i+3(k-1)+3N(j-1); \quad i = x,y,z; k = 1\dots N; j = 1\dots 4; \end{gathered} \tag{4.19}$$

$$\begin{aligned} R(q,\dot{q},t)(1:3) &= \omega \times (M(1:3,1:3)v) \\ R(q,\dot{q},t)(4:6) &= \omega \times (M(4:6,4:6)\omega) \end{aligned} \tag{4.20}$$

Regarding the potential energy, only that related with the elastic deformation of the booms is taken into account. The potential (V) can be expressed (following the derivations shown in [17]) as shown in equation 4.21, where i defines the coordinate, j the boom and k the mode. This expression leads to a general form of K as shown in expression 4.22. The dissipation force can be approximated using a Rayleigh equation, leading to a expression of F similar proportional to that of K, changing EI for k_d. This coefficient needs to be obtained experimentally.

$$V(t) = \sum_j \int_0^L EI(\frac{\partial^2 u_j}{\partial s^2})^2 ds = \sum_j \sum_i \int_0^L EI(\frac{\partial^2 u_{ji}}{\partial s^2})^2 ds; \quad j \in [1,4], i \in [1,3] \tag{4.21}$$

$$K = \begin{bmatrix} 0 & 0 & 0 & 0 & ... & 0 & 0 \\ 0 & 0 & 0 & 0 & ... & 0 & 0 \\ 0 & 0 & \int_0^L EI(\frac{\partial^2 \Phi_{1,1}}{\partial s^2})^2 ds & \int_0^L EI \frac{\partial^2 \Phi_{1,1}}{\partial s^2} \frac{\partial^2 \Phi_{1,2}}{\partial s^2} ds & ... & 0 & 0 \\ 0 & 0 & \int_0^L EI \frac{\partial^2 \Phi_{1,1}}{\partial s^2} \frac{\partial^2 \Phi_{1,2}}{\partial s^2} ds & \int_0^L EI(\frac{\partial^2 \Phi_{1,2}}{\partial s^2})^2 ds & ... & 0 & 0 \\ ... & ... & ... & ... & ... & ... & ... \\ 0 & 0 & 0 & 0 & ... & \int_0^L EI(\frac{\partial^2 \Phi_{4,N-1}}{\partial s^2})^2 ds & \int_0^L EI \frac{\partial^2 \Phi_{4,N-1}}{\partial s^2} \frac{\partial^2 \Phi_{4,N}}{\partial s^2} ds \\ 0 & 0 & 0 & 0 & ... & \int_0^L EI \frac{\partial^2 \Phi_{4,N-1}}{\partial s^2} \frac{\partial^2 \Phi_{4,N}}{\partial s^2} ds & \int_0^L EI(\frac{\partial^2 \Phi_{4,N}}{\partial s^2})^2 ds \end{bmatrix} \tag{4.22}$$

The next step is to convert the real forces (Q_r) that are exerted over the structure (satellite) into a vector of generalized forces(Q_g). This is done by calculating the virtual work that the real forces will perform as a function of the general coordinates (see expression 4.3). It has been assumed that the forces and torques exerted over the satellite are: 1) force over the central part ($F_0 = Q_r(1:3)$), 2) torque over the central part ($T_0 = Q_r(4:6)$), 3) forces over the tip of the booms ($F_1, F_2, F_3, F_4 \rightarrow Q_r(7:18)$) and 4) torques over the tip of the booms ($T_1, T_2, T_3, T_4 \rightarrow Q_r(19:30)$). The location of each of these disturbances in the vector of real forces is also indicated. The redistribution of the loads on the membrane over the hub and the tip of the booms is assumed to take place before this step. The virtual work can be then expressed as shown in equation 4.23, where R_{bi} is defined in expression 4.15, F indicates force, T torque, r position, θ atittude, u bending deformation, 0 rigid motion and 1-4 booms. This derivation was done following the reasoning shown in [17]. This expression can be further developed into matrix C, in expression 4.25, which relates the real and the generalized forces.

$$\begin{aligned} \delta W =& F_i \delta r_i + T_i \delta \theta_i = F_0 \delta r_0 + F_1 \delta r_1 + F_2 \delta r_2 + F_3 \delta r_3 + F_4 \delta r_4 + T_0 \delta \theta_0 + T_1 \delta \theta_1 + T_2 \delta \theta_2 + T_3 \delta \theta_3 + \\ & T_4 \delta \theta_4 = F_0 \delta r + T_0 \delta \theta + F_1(\delta r + R_{b1} \delta \theta + \delta u_1) + F_2(\delta r + R_{b2} \delta \theta + \delta u_2) + F_3(\delta r + R_{b3} \delta \theta + \\ & \delta u_3) + F_4(\delta r + R_{b4} \delta \theta + \delta u_4) + T_1(\delta \theta + \delta d_1) + T_2(\delta \theta + \delta d_2) + T_3(\delta \theta + \delta d_3) + T_4(\delta \theta + \delta d_4) \end{aligned} \tag{4.23}$$

$$d_1 = \begin{bmatrix} 0 \\ -u'_{1z} \\ u'_{1y} \end{bmatrix}; \quad d_2 = \begin{bmatrix} u'_{2z} \\ 0 \\ -u'_{2x} \end{bmatrix}; \quad d_3 = \begin{bmatrix} 0 \\ u'_{3z} \\ -u'_{3y} \end{bmatrix}; \quad d_2 = \begin{bmatrix} -u'_{4z} \\ 0 \\ u'_{4x} \end{bmatrix} \tag{4.24}$$

$$Q_g = CQ_r; \quad C = \begin{bmatrix} I_u & 0 & I_u & I_u & I_u & I_u & 0 & 0 & 0 & 0 \\ 0 & I_u & -Rb_1 & -Rb_2 & -Rb_3 & -Rb_4 & I_u & I_u & I_u & I_u \\ 0 & 0 & \Phi_{1,1}(L) & 0 & 0 & 0 & H_{1,1}(L) & 0 & 0 & 0 \\ 0 & 0 & \Phi_{1,2}(L) & 0 & 0 & 0 & H_{1,2}(L) & 0 & 0 & 0 \\ ... & ... & ... & ... & ... & ... & ... & ... & ... & ... \\ 0 & 0 & 0 & 0 & 0 & \Phi_{4,N-1}(L) & 0 & 0 & 0 & H_{4,N-1}(L) \\ 0 & 0 & 0 & 0 & 0 & \Phi_{4,N}(L) & 0 & 0 & 0 & H_{4,N}(L) \end{bmatrix} \tag{4.25}$$

$$H_{1,k} = -H_{3,k} = \begin{bmatrix} 0 & 0 & 0 \\ 0 & 0 & \phi'_{y1k} \\ 0 & -\phi'_{z1k} & 0 \end{bmatrix}; \quad H_{2,k} = -H_{4,k} = \begin{bmatrix} 0 & 0 & -\phi'_{x2k} \\ 0 & 0 & 0 \\ \phi'_{z2k} & 0 & 0 \end{bmatrix} \tag{4.26}$$

4.2.3. Particularized equations of motion

After the generic expression for the equations of motions has been obtained, there is one main decision left: the shape functions that are to be used. This decision is necessary to be able to define the terms on equation 4.7 and, thus, to define the actual equations of motion of the system. Another decision to be made is related to the number of modes. However, with the aim of leaving the tradeoff between accuracy and model complexity for further stages of the project, the equations are derived and implemented for a generic number of modes.

Another decision to be made is in which reference frame to compute the kinetic energy. In this regard, the decision was made to use a reference frame with the center coincident with the geometric center of the central part of the satellite and with the same linear velocity, but no acceleration or angular velocity. This decision is based in the high values of the velocity w.r.t. the inertial reference frame, which can cause numerical problem if the time step of the simulation is not small enough.

As previously mentioned, the deformation of the booms is expressed as the sum of space dependient and time dependent functions 4.16. The space dependent functions are calle shape functions. The decision of which shape functions to use is critical and their derivation is not trivial. For the work presented here, these functions were extracted from [17] and are defined as shown in equation 4.27 and figure 4.4.

$$\phi_k(s) = 1 - cos(\frac{k\pi s}{L}) + \frac{1}{2}(-1)^{k+1}(\frac{k\pi s}{L})^2 \tag{4.27}$$

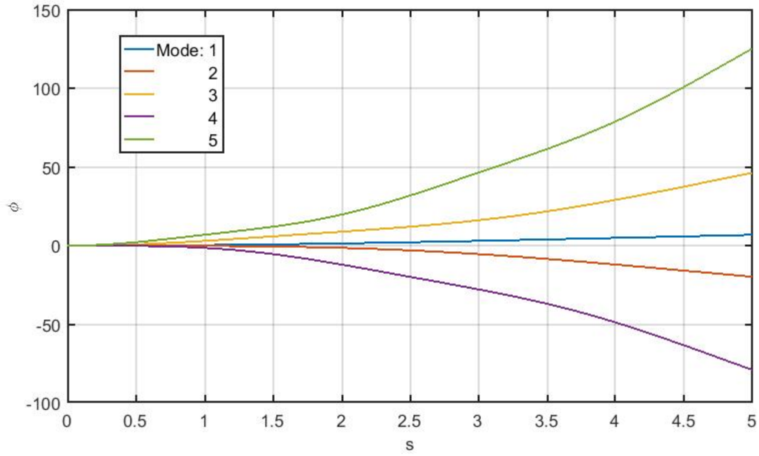

Figure 4.4: Shape functions for the first 5 modes.

These shape functions address the bending deformation of the booms. As was mentioned in the initial assumptions regarding the structure that is to be modeled, no axial deformation or torsion of the booms is considered. Furthermore, in order to simplify the shape functions, it was assumed that there is no displacement of the tip of the boom in the axial direction (see x-axis in figure 4.3). In reality these two conditions are not consistent, but for case of study this inconsistency in negligible due to the extremely low values of the deformation w.r.t. the total length of the boom.

In the expressions of the terms that appear in the equation of motion (expression 4.7) some terms related to the shape functions appear. These terms involve applying different manipulation processes over these functions, such as integrating them or particularizing them over a certain point of the structure. In order to be able to compute the actual equation of motion, those terms are obtained here, as functions of the mode (k,l) and the length of the boom (L).

$$\int_0^L \phi_k = L(1 + \frac{1}{6}(-1)^{k+1}(k\pi)^2) \tag{4.28}$$

$$\int_0^L \phi_k\phi_l = L(1 + (-1)^{k+l}((\frac{k}{l})^2 + (\frac{l}{k})^2) + \frac{1}{2}\delta_{kl} + (-1)^{k+1}\frac{k^2\pi^2}{6} + (-1)^{l+1}\frac{l^2\pi^2}{6} + (-1)^{k+l}\frac{k^2 l^2\pi^4}{20}) \tag{4.29}$$

$$\int_0^L s\phi_k = L^2(\frac{1}{2} + \frac{1}{8}(-1)^{k+1}(k\pi)^2 - ((-1)^k - 1)\frac{1}{(k\pi)^2}) \tag{4.30}$$

$$\int_0^L \phi_k''\phi_l'' = ((-1)^{k+l} + \frac{1}{2}\delta_{kl})\frac{k^2 l^2\pi^4}{L^3} \tag{4.31}$$

$$\phi_k(L) = 1 + (-1)^{k+l} + \frac{1}{2}(-1)^{k+l}(k^2\pi^2) \tag{4.32}$$

$$\phi'_k(L) = (-1)^{k+l}\frac{k^2\pi^2}{L} \tag{4.33}$$

After defining this quantities, the equations of motion can be computed by substituting in the generic expressions derived in section 4.2.2. The matrices can be considerably big, as its final dimension is equal to nxn, with $n = 6 + 12N$, being N the number of modes. It is necessary to keep in mind the the shape function assigned to the axial direction of each boom is zero, i.e. $\phi_{x1k} = \phi_{y2k} = \phi_{x3k} = \phi_{y4k} = 0$. As an example, an because it is the most complex matrix, the expression for the mass matrix (M) is shown in detail in equations from 4.34 to 4.44.

$$M = \begin{bmatrix} M_{1,1} & M_{1,2} & M_{1,3} & ... & M_{1,N} \\ M_{2,1} & M_{2,2} & M_{2,3} & ... & M_{2,N} \\ M_{3,1} & M_{3,2} & M_{3,3} & ... & M_{3,N} \\ ... & ... & ... & ... & ... \\ M_{N,1} & M_{N,2} & M_{N,3} & ... & M_{N,N} \end{bmatrix} \tag{4.34}$$

$$M_{1,1} = (M + 4m_b)\begin{bmatrix} 1 & 0 & 0 \\ 0 & 1 & 0 \\ 0 & 0 & 1 \end{bmatrix}; \tag{4.35}$$

$$M_{1,2} = M_{2,1}^T = \rho\sum_{j=1}^{4}\begin{bmatrix} 0 & \sum_{k=1}^N q_{zk}\int\phi_{zk}ds & -\sum_{k=1}^N q_{yk}\int\phi_{yk}ds \\ -\sum_{k=1}^N q_{zk}\int\phi_{zk}ds & 0 & \sum_{k=1}^N q_{xk}\int\phi_{xk}ds \\ \sum_{k=1}^N q_{yk}\int\phi_{yk}ds & -\sum_{k=1}^N q_{xk}\int\phi_{xk}ds & 0 \end{bmatrix}_j; \tag{4.36}$$

$$M_{l,1} = M_{1,l}^T = \rho\begin{bmatrix} \int_0^L\phi_{xl} & 0 & 0 \\ 0 & \int_0^L\phi_{yl} & 0 \\ 0 & 0 & \int_0^L\phi_{zl} \end{bmatrix}; \quad l \in [3, 4N+2] \tag{4.37}$$

$$M_{l,2} = M_{2,l}^T = \rho\begin{bmatrix} 0 & 0 & 0 \\ -\sum_{k=1}^N q_{zk}\int\phi_{zk}\phi_{yl}ds & 0 & \int s\phi_{yl}ds \\ \sum_{k=1}^N q_{yk}\int\phi_{yk}\phi_{zl}ds & -\int s\phi_{zl}ds & 0 \end{bmatrix}; \quad l \in [3, N+2] \tag{4.38}$$

$$M_{l,2} = M_{2,l}^T = \rho\begin{bmatrix} 0 & \sum_{k=1}^N q_{zk}\int\phi_{zk}\phi_{xl}ds & -\int s\phi_{xl}ds \\ 0 & 0 & 0 \\ \int s\phi_{xl}ds & -\sum_{k=1}^N q_{xk}\int\phi_{xk}\phi_{zl}ds & 0 \end{bmatrix}; \quad l \in [N+3, 2N+2] \tag{4.39}$$

$$M_{l,2} = M_{2,l}^T = \rho\begin{bmatrix} 0 & 0 & 0 \\ -\sum_{k=1}^N q_{zk}\int\phi_{zk}\phi_{yl}ds & 0 & -\int s\phi_{yl}ds \\ \sum_{k=1}^N q_{yk}\int\phi_{yk}\phi_{zl}ds & \int s\phi_{zl}ds & 0 \end{bmatrix}; \quad l \in [2N+3, 3N+2] \tag{4.40}$$

$$M_{l,2} = M_{2,l}^T = \rho\begin{bmatrix} 0 & \sum_{k=1}^N q_{zk}\int\phi_{zk}\phi_{xl}ds & \int s\phi_{xl}ds \\ 0 & 0 & 0 \\ -\int s\phi_{xl}ds & -\sum_{k=1}^N q_{xk}\int\phi_{xk}\phi_{zl}ds & 0 \end{bmatrix}; \quad l \in [3N+3, 4N+2] \tag{4.41}$$

$$\begin{gathered} M_{2,2} = I + \rho[\int_0^L 2s^2ds\begin{bmatrix} 1 & 0 & 0 \\ 0 & 1 & 0 \\ 0 & 0 & 2 \end{bmatrix} - \begin{bmatrix} 0 & s(u_{1y}+u_{2x}-u_{3y}-u_{4x}) & s(u_{1z}-u_{3z}) \\ s(u_{1y}+u_{2x}-u_{3y}-u_{4x}) & 0 & s(u_{2z}-u_{4z}) \\ s(u_{1z}-u_{3z}) & s(u_{2z}-u_{4z}) & 0 \end{bmatrix} + \\ \begin{bmatrix} u_{1z}^2+u_{2z}^2+u_{3z}^2+u_{4z}^2+u_{1y}^2+u_{3y}^2 & 0 & -u_{2z}u_{2x}-u_{4z}u_{4x} \\ 0 & u_{1z}^2+u_{2z}^2+u_{3z}^2+u_{4z}^2+u_{2x}^2+u_{4x}^2 & -u_{1z}u_{1y}-u_{3z}u_{3y} \\ -u_{2z}u_{2x}-u_{4z}u_{4x} & -u_{1z}u_{1y}-u_{3z}u_{3y} & u_{2x}^2+u_{4x}^2+u_{1y}^2+u_{3y}^2 \end{bmatrix}] \\ su_{ij} = \sum_{k=1}^N q_{ijk}\int_0^L s\phi_{ijk}ds; \quad u_{ij} * u_{iw} = \sum_{k=1}^N\sum_{l=1}^N q_{ijk}q_{iwl}\int_0^L \phi_{ijk}\phi_{iwl}ds; \end{gathered} \tag{4.42}$$

$$M_{wv} = \rho \begin{bmatrix} 0 & 0 & 0 \\ 0 & \int \phi_{yw}\phi_{yv} ds & 0 \\ 0 & 0 & \int \phi_{zw}\phi_{zv} ds \end{bmatrix}; \qquad w, v \in [3, N+2; 3, N+2] \quad or \quad w, v \in [2N+3, 3N+2; 2N+3, 3N+2] \tag{4.43}$$

$$M_{wv} = \rho \begin{bmatrix} \int \phi_{xw}\phi_{xv} ds & 0 & 0 \\ 0 & 0 & 0 \\ 0 & 0 & \int \phi_{zw}\phi_{zv} ds \end{bmatrix}; \qquad w, v \in [N+3, 2N+2; N+3, 2N+2] \quad or \quad w, v \in [3N+3, 4N+2; 3N+3, 4N+2] \tag{4.44}$$

4.3. Model improvements

After having derived the equations of motion for a structure which includes the flexibility of the booms, it is considered beneficial to analyze potential ways to increase the fidelity of this model w.r.t. the actual spacecraft. In order to do this, the first objective is to find what is the main driver of the lack of accuracy of the model. This is implicit in the description of the structure modeled, where 'only' the flexibility of the booms is considered. The main limitation of the model is, thus, that it does not take into account the flexibility of the membrane, which is considered a rigid body fixed to the central part of the satellite. There are several consequences of this assumption, among which the most relevant (to the author's best knowledge) are listed below.

- The constraints that the membrane imposes in the bending of the booms are not considered. This would mainly affect the motion in the membrane's plane but could also affect the effective bending stiffness of the booms, by inducing axial load in their tips.
- The moment of inertia of the membrane is constant.
- The interaction with the environment (i.e. drag and solar pressure) does not take into account potential deformations in the membrane.

Even though these problems are initially considered to be out of the scope of this thesis, some ideas for future developments are pointed out here. These concepts are analyzed in relation to: 1) the difficulty of implementing them into the equations of motion and 2) the increase in accuracy that it would bring to the model. Both factors are analyzed only from a qualitative perspective. The study of these possibilities is meant to be helpful for future research in this area. The concepts analyzed are mentioned below.

1. Transfer part of the inertia/mass of the membrane to the booms, without further changes in the equations of motion. This increases the inertia linked to the bending deformations as well as the change in the total moment of inertia due to these deformations. The complexity of the model is not increase and the main difficulty consists on how to mathematically conduct this transfer. This option addresses the second point highlighted previously, the steadiness of the membranes's moment of inertia.
2. Change in the number of bodies considered in the model. Instead of 1 rigid body and 4 booms attached to it, consider 5 rigid bodies (central part plus 4 rigid triangular membranes attached to the central hub and to the tip of two booms) and 4 booms. This concept would include the variation of the membrane's moment of inertia as well as provide with a more accurate geometry w.r.t. the interaction with the environment. However, it is to be highlighted that it does not include the flexibility of the membrane, but only links it to the booms. From a mathematical perspective, additional terms would need to be added to the kinetic energy and, thus, the expression of the mas matrix (M) would have to be recalculated. This change in the expression would be considerably simpler than that proposed in option 4.
3. W.r.t. the interaction of the membrane with the external loads, another possibility is to define instantaneously rigid geometries for the membrane as a function of those external loads. These would be useful to study the dynamics of the plant as it would allow a more accurate computation of the changes in the moment of inertia as well as provide with a more accurate geometry for computing the effect of drag and solar pressure. These rigid geometries would have to be computed previously (e.g. using a finite element model). Being these geometries a function of the external loads, as well as considerably complex, it would be difficult to use this information in the design of the ADCS controller.

4. This option consists in following the same procedure used for introducing the flexibility of the booms but in relation to the membrane. Therefore, set of generalized coordinates and shape functions able to represent the motion of the membrane would need to be defined. These would be then introduced into the kinetic, potential and dissipation functions, leading to a new definition of matrices M, K and F. This would be the most complete approach, providing with an accurate evolution of the membrane's geometry w.r.t time as well as considering the effect of its structural properties (e.g. density) in the dynamics of the system. However, the complexity of finding a suitable set of generalized coordinates and shape functions is considerably high, and so is obtaining the different terms involved in the equations of motion.

The conclusions of this analysis pointed towards option 1 as the best tradeoff between: 1) increasing the accuracy of the model, 2) create a model useful from a control perspective and 3) avoid overcomplicating the model in excess. Regarding the transfer of the moment of the inertia of the membrane to that of the booms, it was done based in two assumptions: 1) in the absence of deformation, the moment of inertia of the flexible body is equal to that of the rigid body, and 2) the moment of inertia of the membrane is, when symmetrically possible, distributed between the booms, by increasing their linear density.

4.4. Verification of the model

As it can be observed in the expressions shown of the mass matrix (equations 4.34 to 4.44), the terms appearing in the equations of motion (expression 4.7) can reach a high complexity. Furthermore, several assumptions and long derivations are also involved in the computation of these equations, which were then implemented as a MATLAB function. These derivations, assumptions and implementation are potential sources of error. In order to verify the final equations obtained, a verification procedure needs to be conducted. This procedure is based in comparing the behavior of the model previously explained (which will be called 'analytical' model throughout this section) and a model built using a MATLAB tool named Simscape Multibody ('numerical' model). This last model is based in a finite element's approach and was also developed by the student. More information about the elements of the numerical model can be found in appendix G. Two comparison are performed: 1) single boom and 2) spacecraft model.

4.4.1. Single boom

The first stage of the verification process targets the implementation of the equations of motion (expression 4.7) over a single boom, particularly a candeliver boom. The model built in using the Simscape Multibody tool consists on several rigid bodies (arbitrary number to be defined as an input) linked to each other by joints which include stiffness and damping coefficients (see figure G.7 in appendix G).

The response of analytical and numerical models of the boom are studied for two external disturbances: 1) force in the tip of the boom and 1) torque in the tip of the boom. The evolution of these disturbances throughout time is modeled in three different ways: 1) delta, 2) step and 3) sine with variable frequency. In addition, different number of elements is considered in the numerical model (from 1 to 20) and different number of modes in the analytical model (from 1 to 10). The results of these comparison (i.e. the responses of the different models to the external disturbances) are included in appendix F.

In these results, it can be observed that the behavior of both models is highly similar and that this similarity increases with the number of modes/elements. It can also be seen that the analytical model converges faster to the actual solution w.r.t. the number of modes, than the numerical model w.r.t. the number of elements. The final conclusion of this comparison is that the analytical model for a single boom is verified.

4.4.2. Satellite's model

The second model built aims to represent the actual flexible plant developed in section 4.2. Therefore, it consist on a central rigid body with 4 candeliver booms attached. The physical properties (moment of inertia, bending stiffness...etc) are defined accordingly to those used for the analytical model. An schematic view of this model is shown in appendix G, figure G.7.

Numerous comparisons were run in order to verify the similarity between the models. This was an arduous and time-consuming task throughout which several inconsistencies were found and solved. One of the most representative cases is included here, while more extensive examples are included in appendix G. It is thought to be representative due to sharing the order of magnitude with the actual case of study both in the initial conditions and in the external disturbances. The results of both analytical and numerical models are shown in figures 4.5 and 4.6 respectively. In these figures, r states for position, v velocity, T attitude quaternion, ω angular rate and u_i deformation on the tip of the boom. The units are those of the International System and the x-axis contains time. The specifications, i.e. initial conditions and external disturbances, of this particular example (named case 0) are shown below.

- Initial conditions: $v = [3;2;5]km/s; \omega = [-0.1;0.1;1.75] * 1E-2rad/s$.
- External disturbances: pulses of a period of 10 s, pulse width of 1% and a phase delay of 1 second. The magnitude of the total force is $2[0.9649;0.1576;0.9706] * 1E-5N$ uniformly applied over the membrane. The magnitude of the torque is $2[0.2785;0.5469;0.9575] * 1E-5Nm$.

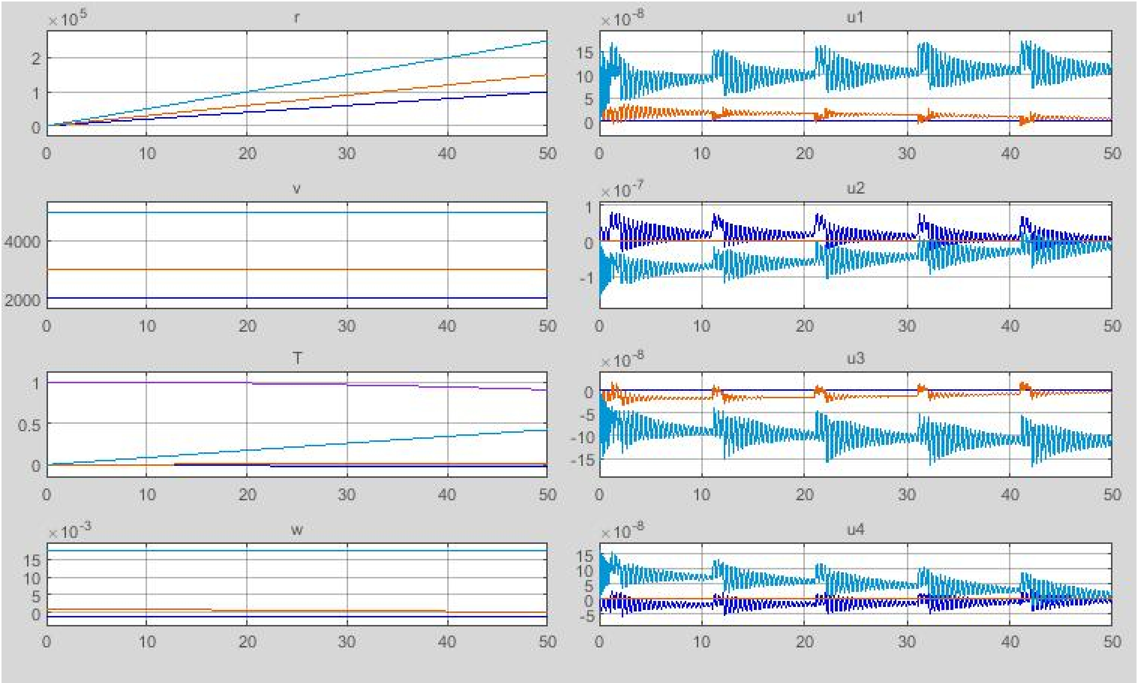

Figure 4.5: Evolution of the state variables, as resulting from the analytical model. Case 0.

Among the analyses shown in appendix G are the following (only differences w.r.t. the case above are mentioned): 1) absence of external disturbances, 2) static external disturbances (instead of periodic), 3) initial conditions equal to zero and 4) different initial conditions and external disturbances. The analysis of these, and multiple other cases, led to the conclusion that the dynamics of both models have a high degree of similarity, at least for cases of the order of magnitude of the case of study. The analytical equations are therefore considered verified. However, it is necessary to keep in mind that there are some differences inherent to the definition of the models, which can pose a problem under certain circumstances:

- The analytical model assumes no axial displacements. This creates an inconsistency in the length of the boom proportional to the square of the bending deformation divided by the length of the boom. Therefore, an error in the moment of inertia arises, increasing with the bending deformation and the mass of the booms.
- While the deformation in the analytical model is continuous, the deformation in the simscape model is defined by the relative rotation between a set of rigid boom elements.

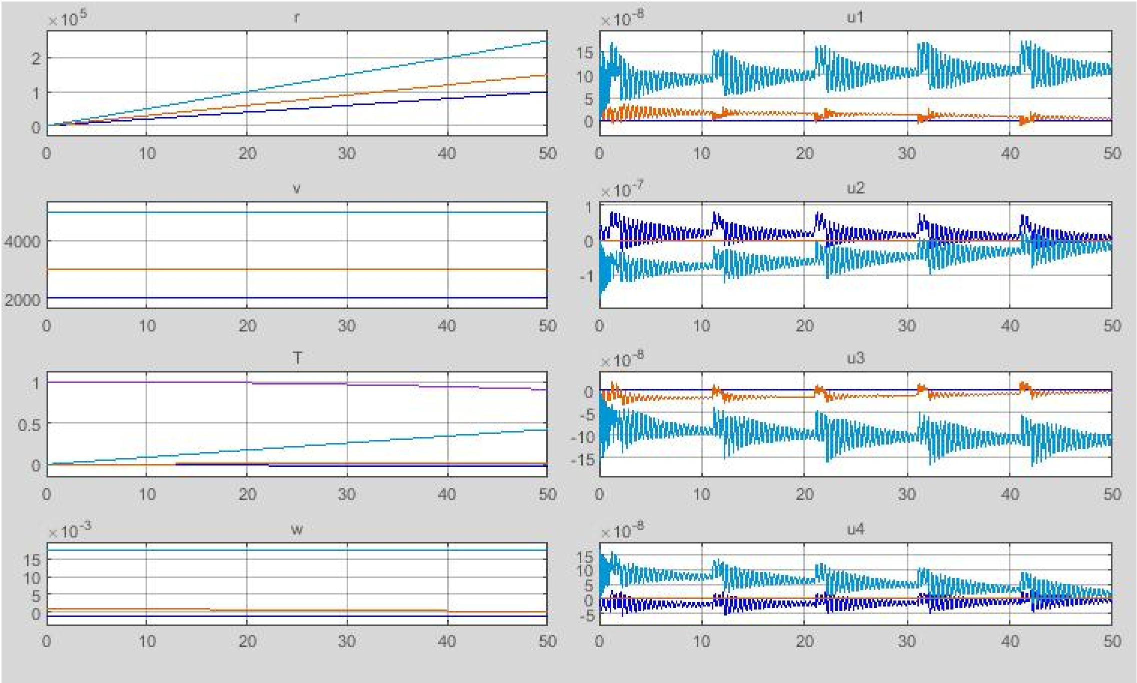

Figure 4.6: Evolution of the state variables, as resulting from the numerical model. Case 0.

4.5. Conclusions

This section has one main objective: integrate the flexibility of the structure into the equations of motion. This objective can be further developed into two main tasks: 1) explain in detail a procedure to derive, implement and verify a dynamic model of a flexible structure, and 2) apply this procedure to a simplified model of the GoSolAr spacecraft.

In relation with the general explanation of the procedure, an schematic analysis is shown in figure 4.1. There are 5 main milestones on this process: 1) defining the structure to be analyzed and the variables targeted in the analysis (e.g. deformation of the booms), 2) deriving kinetic energy, potential and dissipation function using those variables, 3) choose generic coordinates such that the variables chosen are represented in a finite (low when possible) number of coordinates, 4) making sure that there are shape functions that can relate the generic coordinates with the variables in an accurate way (not trivial for complex structures) and 5) obtain the terms of the equations of motion. The verification procedure can be done in a number of ways and with a considerably high number of software resources. Similarly, the actual implementation can be done in multiple ways.

Three main ideas are to be highlighted w.r.t. this procedure. The equations of motion derived are based in Lagrange's equations (see expression 4.1). The procedure involves complex mathematical derivations but aims to obtain a relatively simple and representative set of equations of motion for the structure. The process explained can be applied to other structures, assuming that a suitable set of shape functions and generalized coordinates can be found.

Implementing this procedure for the GoSolAr mission has, therefore, a dual objective. First of all, and more importantly, it allows to study the flexibility of a spacecraft in relation with the ADCS. The second aim is to provide with an example on how to apply the procedure of deriving the equations of motion to a real case. The model is meant to integrate flexible and rigid motion of the defined structure, from a dynamic perspective. This means that both the rigid and flexible variables are interconnected and their evolution throughout time affects each other (e.g. vibrations in the booms to the magnetorquer duty cycle are transmitted to the angular rate). This interconnection is visualized in the equations of motion (e.g. mass matrix terms shown in expression 4.34 to 4.44), where it can be seen that disturbances in any point of the structure affects both the rigid (position and attitude) and flexible variables (deformations of the booms) as well as their derivatives w.r.t. time.

Through this integration of flexible and rigid motion, the behavior of the structure from a dynamic's perspective can be consistently studied. Furthermore, the relative simplicity and low order of the final model (depending on the number of flexible modes taken into consideration) allows: 1) gaining an understanding on the dynamics of this type of structures from a conceptual perspective, and 2) using the model in relation with the development of a controller.

5

Attitude Controller Design

In the previous chapter a model (i.e. equations of motion) of a simplified version of the GoSolAr spacecraft has been derived and implemented, integrating the flexible and rigid motion of this structure. Throughout this section different designs for the attitude controller are derived and their performance over these extended equations of motion studied.

First of all, the effect that the introduction of flexible terms in the model of the satellite has on the performance of the initial controller design has been analyzed (see section 3.2.1). The performance indexes used to evaluate this controller go beyond the mission requirements of the GoSolAr mission, studying also the vibrations introduced in the system due to its flexibility.

After studying the effect of the flexibility of the structure in the dynamics of the close (with an LQR controller) and open plants, this chapter aims to study potential improvements in the performance of the attitude controller, by using alternative designs. This improvement in performance is evaluated in relation to two main indexes: 1) degree of compliment with the mission requirements (i.e. pointing accuracy) and 2) capability of reducing the vibrations in the booms and, more important from an ADCS perspective, in the attitude and angular rate.

Two additional analyses are conducted before diving into alternative controllers: 1) linearization of the equations of motion and 2) change in the behavior due to changes in the plant specifications. The derivation of the linearized plant is meant not only to provide with additional insight in relation with the dynamics of the system, but also to verify the implementation of the numerical linearization. The effect of changes in the specifications of the structure (e.g. length of the booms) in the behavior of the system is studied in order to analyze whether it is possible or not to extrapolate the results to similar cases.

The first alternative to the controller based in an LQR approach is based in the application of robust control theory, deriving controllers based in both H_2 and H_∞ norms. These controllers have the capability of focussing in particular frequencies, i.e. the natural frequencies of the system to be controlled. The performance of these controllers is studied in frequency and time domains, integrating them in the simulation environment described in chapter 3. After having evaluated the potential of this approach, the possibility of extending the information available to the controller, including the deformation of the booms, is considered. This additional information makes it feasible to try to minimize not only the vibration in the angular rate, but also the vibration of the booms. The last controller studied is a non-linear controller developed from the existing relation between constrained and controlled motion, studied from an analytical dynamics approach. This approach is known as the Udwadia-Kalaba approach.

After deriving and evaluating the performance of each controller, some additional comments on the differences between the controllers in aspects such as the computational cost or sensibility to errors in the parameters' estimation are made. This is meant to provide with a broader perspective when coming to decide which controller to use for a particular case.

The different controller designs are explained based in the structure shown in figure 5.1. In this figure each block simulates a part of the control loop, being: the controller (K), the actuators (A), the satellite's equations of motion (P), the sensors (S) and the weighting function (W). The signals that are inputs and outputs of this blocks are: the guidance signal (yg), the measurements (y), the error signal (e), the control command (u), the control actuation (ua), the external disturbances (w), the external forces and torques (Q), the state vector (x) and the cost signal (z).

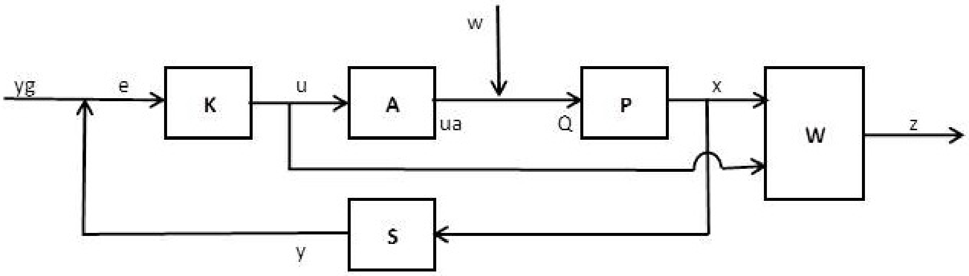

Figure 5.1: Schematic view of the control loop.

Except in cases where the contrary is explicitly stated: 1) the measurements signal (y) contains the angular rate and the sun vector, 2) the error signal (e) contains two magnitudes related with the pointing error (see equation 3.2) and three with the angular rate error, and 3) the control command (u) is linked to the torque that is to be generated by the magnetorquer (in the three axes).

5.1. LQR & b-dot controllers

At this stage of the study, a model of the satellite addressing the flexibility of part of its structure has been derived, implemented and verified. This model was then implemented into the simulation environment described in section 3.2.1 in order to be able to study the changes w.r.t. the case studied in that section, where the satellite is assumed to be a rigid body. In the model implemented, the membrane moment of inertia has been incorporated to the that of the booms as explained in section 4.3.

The objective of this analysis is to evaluate the consequences of the flexibility w.r.t. the ADCS performance. Therefore, the differences in the behavior of the flexible and rigid plants w.r.t. the ADCS have been studied. These differences are first studied in relation with the requirements of the mission (GoSolAr), i.e. pointing requirement, and then from a more general approach, evaluating any existing difference. Additionally, and in order to clarify the impact of the flexible modes in the dynamics of the system, both open (uncontrolled) and close (LQR controller) plants are analyzed in the frequency domain.

But before evaluating the performance of these controllers, the process of deriving the LQR controller is briefly introduced in relation to figure 5.1. The derivation of the LQR controller is done in two steps: 1) linearize the equations of motion and 2) minimize a cost function. In this case, the equations of motion linearized are those of the rigid motion (see expression 3.7). The linearization leads to a linear system as the one shown in equation 5.1, where: 1) x, u and y are the same as in figure 5.1 and 2) A (state matrix), B (input matrix), C (output matrix) and D (feedthrough matrix) are constant matrices. In this case the linear system was derived analytically and, for the linearization, the actuator's block was not considered (i.e. $ua = u$). More information about the basis of this analytical linearization can be found in section 5.2.1.

Once the linear system is defined, a cost function J is defined based on weighting matrices linked to the state vector (x) and to the control command (u). These matrices (Q,R and N) are equivalent to a weighting function (W) in figure 5.1 and are related to the relative importance of errors in each variable and combination of variables. The controller (K) is then derived as a constant control gain which minimizes the cost function J. This optimization problem is solved with the help of the MATLAB's function *lqr*, which solves it by solving a Ricatti equation. As previously mentioned, the selection of Q, R and N was done in an iterative way, by studying the performance of the controller (K) resulting from different values of these matrices (see appendix B). Additional information regarding the derivation of the LQR controller can be found in [12].

$$\dot{x} = Ax + Bu; \quad y = Cx + Du; \tag{5.1}$$

$$J = \int_0^{\infty} (x^T Q x + u^T R u + 2x^T N u) dt \quad \rightarrow \quad [u = Kx]_{min(J)} \tag{5.2}$$

In relation with the b-dot controller, the explanation included regarding expression 3.1 is considered enough. More information about this controller can be found in [1].

5.1.1. Performance w.r.t. mission requirements

As previously mentioned, the ADCS has two main purposes within the GoSolAr mission: 1) detumbling the satellite after launch and 2) pointing towards an inertially fixed (or slowly varying) axis (initially the sun vector) with an accuracy of 10 degrees. In this section, these two phases will be conducted over the new model derived ('flexible' model) and the results will be studied in relation with that over the previous model ('rigid' model). The controllers used are the same as in section 3.2.1, i.e. a b-dot controller and LQR-based controller. In order to limit the computational cost of the simulations, the model used for these analysis includes only the first flexible modes of each boom.

First of all, the detumbling phase is studied. This phase consists in lowering the angular rate of the spacecraft, which starts with an uncontrolled angular rate as a result of its launch. In this case, the satellite is assumed to be deployed, as otherwise there is no flexible part to be included. This way, figure 5.2 shows the performance of the b-dot controller over the flexible plant for a set of different initial conditions. These initial conditions are defined in the same way they were for the analysis of the rigid plant (see section 3.2.1).

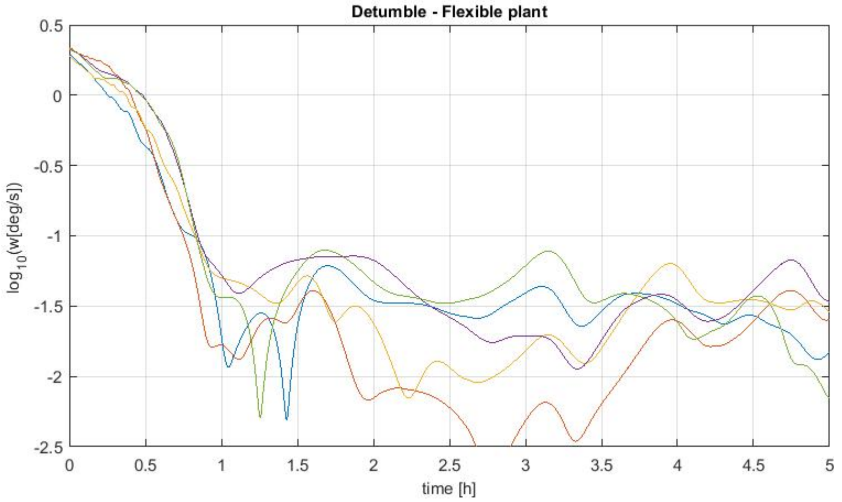

Figure 5.2: Evolution of the angular velocity's norm during the detumbling phase. Flexible model. 5 cases. Initial orbit as in figure 3.5.

When comparing it to the results shown in the previous chapter (see figure 3.5), it can be observed that the performance of the b-dot controller does not deteriorate appreciably due to the flexibility of the structure, for the nominal plant. In both cases, the angular velocity is reduced to around 0.1 deg/s. This result is relevant even if the detumbling phase is conducted over the stowed spacecraft, as it provides with a safe mode controller in case the satellite angular rate is disturbed throughout the mission. The detumbling phase has not be considered in further analyses of the different controller, as no need for damping the vibrations of the system is expected at this stage.

The next analysis targets the pointing phase. During this phase the spacecraft is to be given a spin and the spin axis to be pointed towards a defined axis (i.e. sun vector). This is done using a controller which computes the control command from the error in the pointing direction and in the angular rate, combined with steady gains defined using an LQR approach (section 3.2.1). Figure 5.3 shows the performance of the controller over the flexible plant for different initial conditions. The simulation's initial conditions are those shown in section 3.2.1.

From a first observation, the controller seems to be able to provide the spin required and maintain an orientation w.r.t. the sun within the accuracy required. Furthermore, there is no appreciable difference between the performance of the controller over the rigid plant (see figure 3.7) and over the flexible plant, giving both an approximate long term accuracy of 3 degrees (pointing error).

The evolution of the pointing error was further analyzed in order to evaluate the difference. This was done by studying the distribution of the pointing error throughout the second half of the simulation (from times 2E5 to 6E5 seconds). The selection of the time frame is motivated by a desire of minimizing the influence of the initial conditions. The standard deviations and means of these distributions, 10 for the rigid and 5 for the flexible plants, are shown in figure 5.4.

From this analysis, no significant deterioration of the controller's behavior is noticeable w.r.t. the mission requirements. Therefore, no additional challenges in relation with the flexibility of the structure can be de-

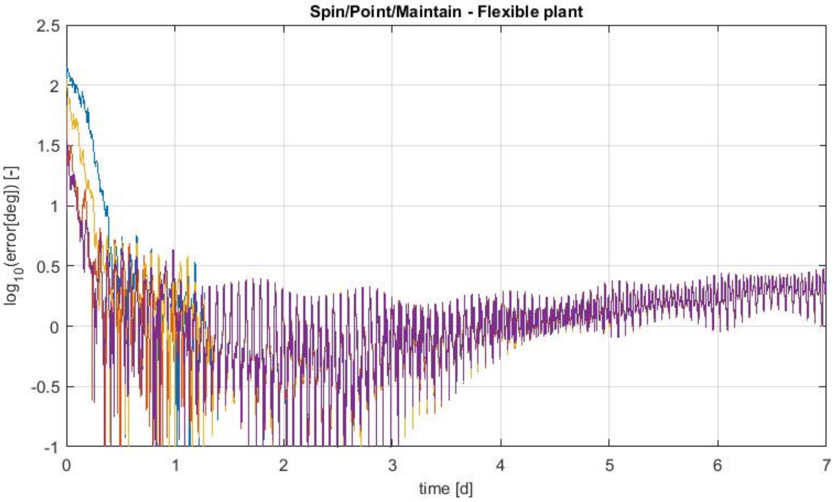

Figure 5.3: Evolution of the pointing error during the pointing stage. Flexible model. 5 cases. Initial orbit as in figure 3.7.

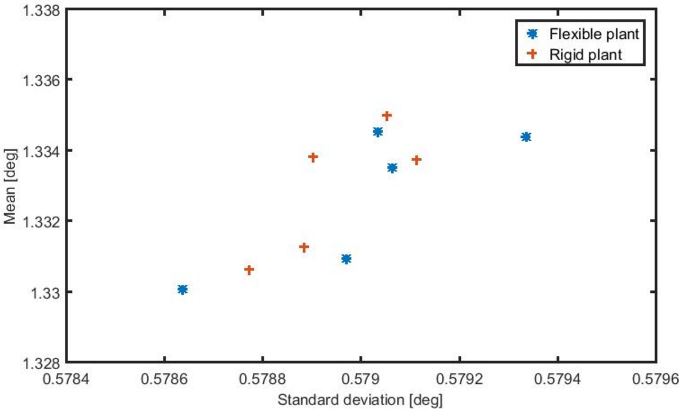

Figure 5.4: Properties of the evolution of the pointing error throughout time for the flexible and rigid plants.

duced. In the following section, these analyses are expanded in order to address other possible effects of the flexibility of the structure.

5.1.2. Impact of flexibility

The aim of this section is to provide with a more complete understanding of the effects that the flexibility inherent to the structure have (or may have) in relation with the ADCS. In order to do this, two main topics are addressed: 1) explain the reason of the low impact of the flexibility w.r.t. the mission requirements (see section 5.1.1) and 2) noticeable consequences of the flexibility.

As shown in the previous section, the requirements of the mission are met even if the controller is design based on a purely rigid body. In order to understand this, the problem needs to be studied in the frequency domain. As mention in [32] and [17] the flexibility becomes a relevant problem when the natural frequencies of the system interact with the frequencies of the controller or of the external disturbances. For the following analyses, the frequency of the controller was divided into the frequency of the control process and the frequency inherent to the use of a magnetorquer, i.e. duty cycle. In our case, these four sets of frequencies take the following values: 1) natural frequencies, the lowest frequency (nominal case) is 14 Hz, 2) the control process frequency is linked to the time step of the simulation and, thus, higher than the highest frequency included, 3) the frequency of the external disturbances can be, with some exceptions that will be explained later, related to the orbital frequency (period of around 1.5 hours), and 4) the period of the magnetorquer is defined as 5 seconds. It can be observed that these bandwidths do not interact. Therefore, it is consistent that the effect of the system's flexibility is considerably limited.

However, the flexibility of the systems is still noticeable and affecting the behavior of the ADCS and of the whole system in a number of ways, when looking closer. These analyses aim to conduct this closer look on the behavior of the structure by studying the evolution of two main variables (i.e. deformation of the booms and angular rate) under the three main perturbations previously metioned (external disturbances, control process and magnetorquer's duty cycle).

The frequencies of the external disturbances are in the order of the orbital frequency, which is considerably lower than the natural frequencies of spacecrafts of the type considered. For a nominal altitude of 600 km this frequency is 1.1E-3 Hz, while the satellite studied has, in its nominal configuration, its lowest frequency at 14.5 Hz. Revised literature also indicates that these two bandwidth of frequencies are considerably distant for current satellites. There is, however, an exception to this: the immersion or coming out of Earth's projected shadow (eclipse). The rate at which the forces change in this events can be related to the velocity of the satellite and to it's size, and the equivalent frequency is considerably higher. Therefore, the potential induced vibrations in the booms in considerable (see figure 5.5). However, as it is not a continuous perturbation, it happens only twice per each orbit, a minimum passive damping at the booms is able to minimize its effect. Furthermore, as this perturbation is aligned with the rotation axis (in the operation point the spin axis points towards the sun), its effect over the angular rate is minimum. Figure 5.5 is analyzed more in detail in appendix E, where figure E.1 zooms in figure 5.5 and figure E.2 contains the deformations of the four booms. It can be seen that the deformations are mainly in the z-axis, as the period of time shown is selected once the operating point has been reached (pointing towards the sun). Furthermore, it can be concluded that this phenomena (eclipse) generates high frequency vibrations with a considerably high amplitude. Even though for the particular case of study (GoSolAr) this is not critical, it can be for other missions.

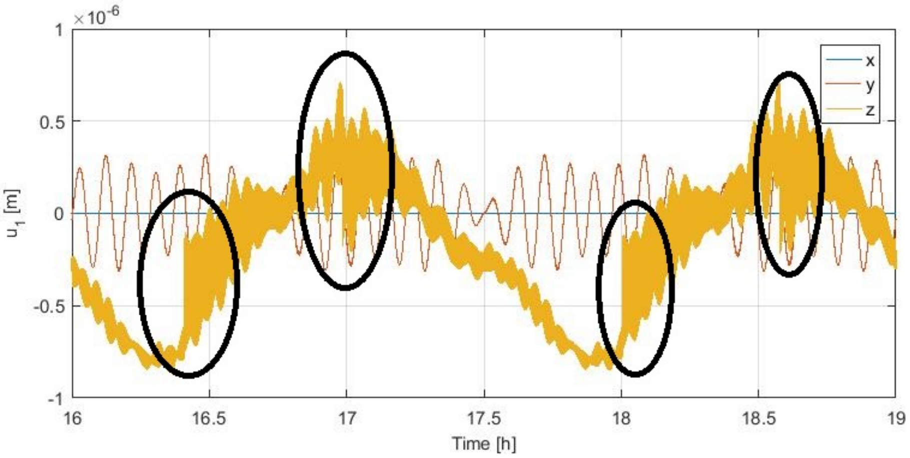

Figure 5.5: Vibration of the booms (boom 1) due to entering or coming out an eclipse.

The frequency of the controller in a real spacecraft is limited by the bus specifications and influenced by the computational cost of the estimators and controllers involved. This frequency can be defined in order not to interact with the eigen modes of the satellite. In the case of study, the limitations in the frequency of the controller are not studied. Furthermore, the frequency of the controller is assumed, ideally, same as the time step. This decision is based in the possibility of tuning it to avoid interaction with the natural modes of the structure.

The vibrations due to the interaction between the magnetorquer and the lowest modes of the booms were not expected to be particularly relevant around the operating point, as the relatively low control torque applied is not enough to generate relevant vibrations (w.r.t. the mission requirements). However, even thought the effect of this vibrations is not affecting the mission requirements, it is still noticeable. In figure 5.6 an example of the vibrations induced in one of the booms due to the magnetorquer duty cycle is shown. It can be seen that this duty cycle is affecting considerably the deformation of the boom, inducing fast vibrations.

In appendix E, the example in figure 5.6 is extended. First to the deformations on the rest of the booms (figure E.4) and then to a more in detail analysis of the deformations in boom 1, also in relation with the angular rate (figure E.3). Looking at the deformations in the different booms, it can be seen that they are opposite in phase between the pair 'boom 1-boom 3' and 'boom 2-boom 4'. This is caused by the nature of the duty cycle, which consists in 'stopping' the control torque and then 'starting' it again, cyclically. The deformations caused by a torque are antisymmetric, causing this opposition in phase. This opposition is also the reason why it

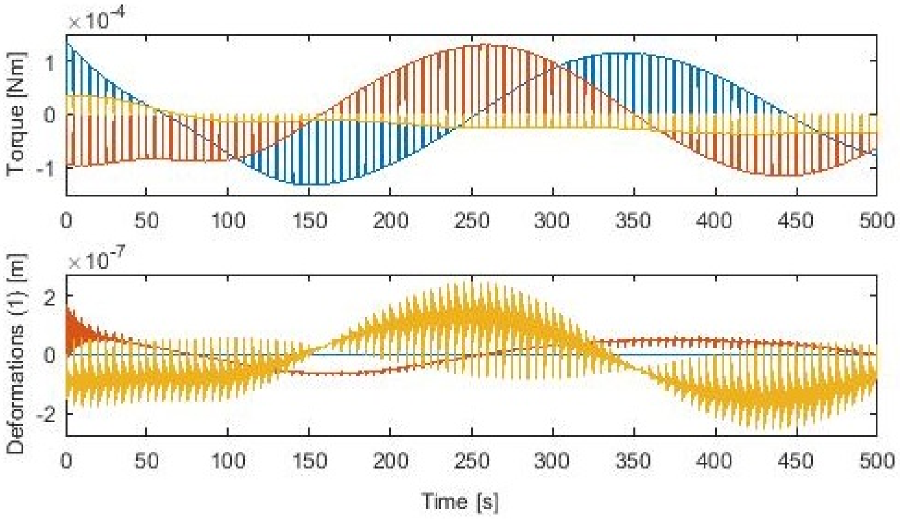

Figure 5.6: Interaction of the flexible structure (boom 1) with the control torque (magnetorquer).

does not affect the long term evolution of the angular rate and attitude. In relation with the vibrations on each boom, they are analyzed in more detail in figure E.3. It can be observed in this figure that the flexibility of the boom also generates vibrations in the angular rate. The amplitude of these vibrations is considerably low ($\approx 1E-7$[m] for the booms and $\approx 1E-7$[rad/s] in the angular rate) and does not show a divergent behavior. This amplitude is mainly affected by the maximum dipole that the magnetorquer can provide, increasing as it increases. Several cases for different initial conditions and controllers (LQR and b-dot) were run showing qualitatively the same behavior. Furthermore, changes (between 0% and 100%) in the damping coefficient (which is the parameter with a higher degree of uncertainty) do not change qualitatively this behaviour, but only damp the vibration of the booms faster.

5.1.3. Frequency domain

This section focuses in analyzing two topics in the frequency domain. This topics are: 1) effect of the flexibility in the dynamics of the structure and 2) performance of the LQR controller.

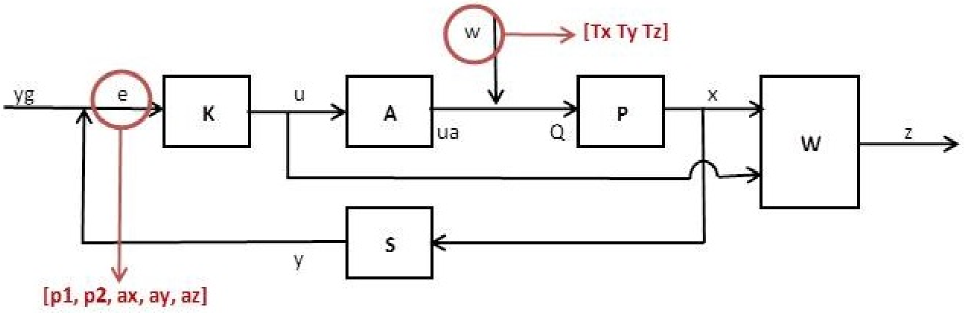

Figure 5.7: Variables studied in the analyses in the frequency domain.

All analyses in the frequency domain included in this chapter focus in the same variables, which are pointed out in figure 5.7. As it can be observed, the variables that are use in these analyses output are: 1) pointing error (2 components: p1, p2) and 2) angular rate error (3 components: ax, ay, az). These variables are defined as explained in section 3 and are considered to contain all relevant information in relation with the attitude of the satellite. The input initially contained both distributed forces and torques. However, it was noted in the first analyses that the effect of the forces in the error variable is extremely low, so it was decided, for the sake of simplicity, to focus only in the torques (Tx, Ty, Tz). The disturbances are scaled according to previous results (see figure 3.3), so the torque magnitude is scaled with a factor of 1e-5. This selection of input and output variables leads to a final input-output system of dimensions 3x5 (see for example figure 5.8). The analyses are then conducted by studying the response in the frequency domain of the system, using a Bode diagram. This response is the amplification (in dB) of the input signal in each of the output signals over a range of frequencies.

In relation with the first topic to be analyzed, the response of the open plant (i.e. without a feedback loop with a controller), is studied for both rigid (see section 3) and flexible (section 4) models. The analysis is conducted by studying the response in the frequency domain of the linearization (centered in the operating point) of the two models. The range of frequencies studied goes from 1E-11 to 1E3 rad/s. In the operating point the satellite has a spin in the z-axis (normal to the membrane plane) and this axis is pointing towards an axis quasi-static in the inertial reference frame (the sun vector changes considerably slow). The flexible plant is modeled taking into account the first 5 modes of each boom. The variables used for the analysis are those pointed out in figure 5.7 and the results are shown in figure 5.8.

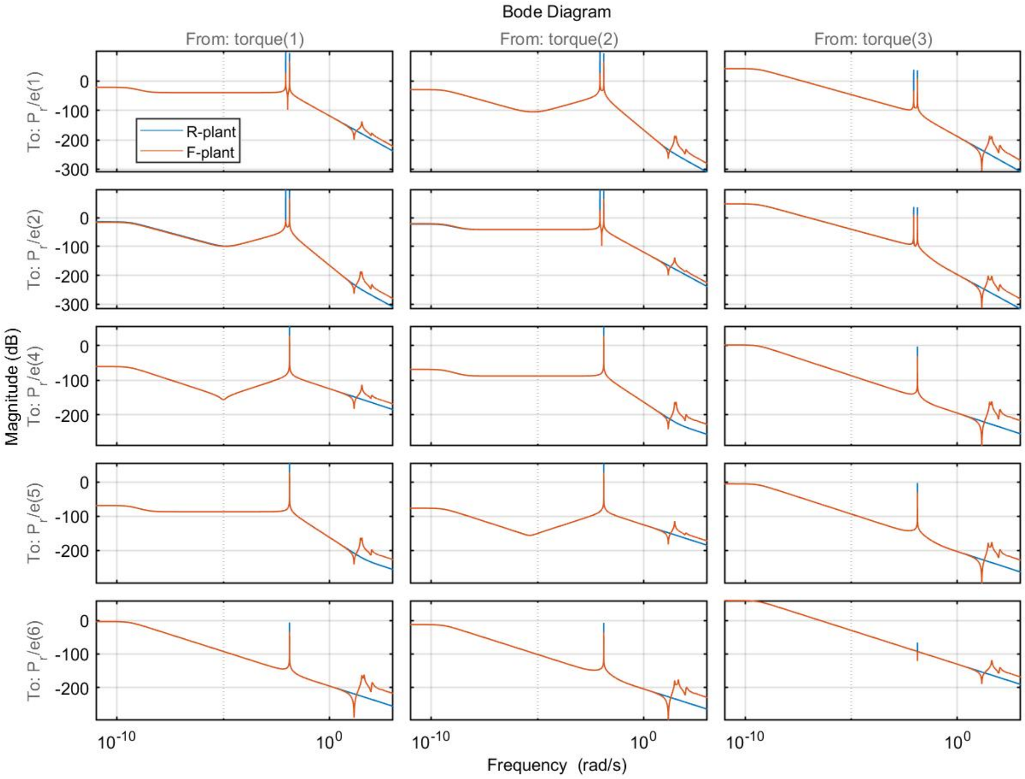

Figure 5.8: Bode analysis over flexible (F) and and rigid (R) open plants.

There are two main aspects to be highlighted from this results, regarding the behavior at low and high frequencies. It can be observed that the response on low frequencies (lower than 1 Hz) is extremely similar. This supports the conclusions previously stated, saying that: if the external disturbances frequencies are low enough w.r.t. the natural frequencies, they do not affect the behavior of the plant in a relevant manner. When the response at higher frequencies is studied, the differences between flexible and rigid plants appear. It can be seen that at the frequencies of the natural modes of the plant, the response has local maximums. However, two other aspects in relation with these peaks need to be taken into consideration: 1) they are local maximums but still considerably far away from the absolute maximum, meaning that their relative importance is probably low, and 2) even though the first 5 modes of the booms are considered, only the first 2 are visible, which means that the higher modes are damped considerably faster than the lower ones (the analysis is run with the nominal damping coefficient, i.e. 1.32).

After this initial analysis, where the effect of the flexibility is explained by comparing rigid and flexible models of the satellite, all further analyses will be conducted over the flexible plant (i.e. the equations of motion derived in chapter 4). Having analyzed the behavior of the open plant, it is time to study the close plant, evaluating the performance of the LQR controller. In order to do this, the response of the flexible plant is analyzed with (close plant) and without (open plant) the LQR controller. In this case, only the first two modes of the booms are included, without any noticeable effect in the results. The input and output variables are those pointed out in figure 5.7. The results of the analysis are shown in figure 5.9.

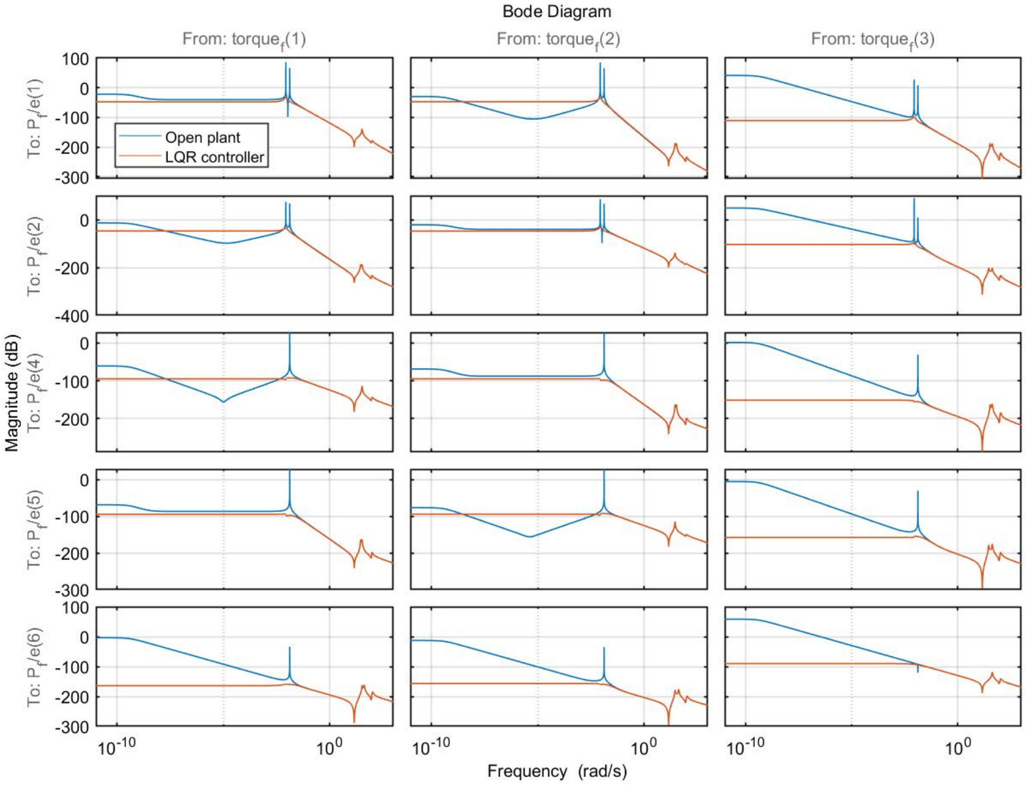

Figure 5.9: Bode analysis over the open and controlled (LQR controller) flexible plant.

It can be observed that the response over low frequencies, which is related to the rigid body motion, is considerably improved. However, the response at higher frequencies remains the same as in the open plant. It can be therefore concluded that this controller is not able to reduce the response at higher frequencies and, thus, is not able to reduce vibrations at frequencies in the range of the natural modes. Despite of this, as shown in previous sections, the controller is able to fulfill the requirements of the GoSolAr mission.

This analysis shows that the current ADCS design is not able to deal with the vibrations of the system induced by the flexibility of the structure. Therefore, further controllers are to be studied in order to provide an alternative, able to reduce the effect of these vibrations. With this objective, two main control strategies have been analyzed: 1) robust control and 2) non-linear controller. However, before diving into these additional control options, two analyses are conducted. First of all, in order to gain a deeper understanding on the dynamics of the flexible plant and the linearization processes, the linearization of this plant is studied. Secondly, regarding the potential extrapolation of the results to other cases, the influence of variations of the physical parameters (e.g. bending stiffness) of the system is studied.

5.2. Linearization of the plant

As explained in the previous section, the comparisons in the frequency domain are performed over linearized plants. In order to further understand the meaning and limitations of operating over the linearized plant instead of over the actual plant, the linearization of the flexible plant is studied in detail throughout this section.

Linearization states for the process of building a linear plant, such as that shown in equation 5.4, which accurately models the behavior of the actual (non-linear) plant in the proximity of the linearization point. Obtaining a linearized plant is a prerequisite to implementing several linear control approach, such as LQR or the H_∞ approach used.

Three main objectives are targeted in this section: 1) gain further understanding of the main drivers of the flexible plant behavior, 2) gain expertise in the use of MATLAB built-in linearizing function and 3) validate the numerical results via an analytical derivation of the linear plant. In order to achieve these goals, the linearized plant is first derived analytically and then numerically.

5.2.1. Analytical linearization

The linearization procedure followed is based in a Taylor expansion of first order (see equation 5.3). The meaning of this equation is considerably intuitive, in the sense that it states that: the value of the function F when leaving point x_0 in the x direction, can be approximated by the value of F in x_0 plus the rate of change of F in the x direction ($\frac{\partial F}{\partial x}$) multiplied by the distance covered Δx. The objective of the linearization is to obtain a system with the form shown in expression 5.4, with a behavior as similar as possible to the actual system. In this expression x is the state vector, y the variables measured and u the control variables. Matrixes A, B, C and D are functions of linearization point and are commonly know as: dynamic matrix (A), input matrix (B), output matrix (C) and feedthrough matrix (D). In this particular case, the point chosen is that shown in expression 5.5.

$$F(x_0 + \Delta x) \approx F(x_0) + \frac{\partial F}{\partial x}_{x_0} \Delta x \tag{5.3}$$

$$\dot{x} = Ax + Bu; \quad y = Cx + Du; \tag{5.4}$$

$$r = r_0; v = v_0; Q = Q_0; \omega = \omega_0; q_{ijk} = q_{ijk0}; \dot{q}_{ijk} = \dot{q}_{ijk0}; u = u_0; \tag{5.5}$$

The state vector (x) comprises (in this order) the position (r), attitude quaternion (Q), bending deformations of the booms (q), velocity (v), angular rate (ω) and time derivative of the bending deformations ($\dot{q}$). Vector y contains the position, attitude quaternion, velocity and angular rate. In order to simplify the calculations, the equation involving A, B and x is decomposed as shown in equation 5.6, where x_1 contains the position, attitude quaternion and bending deformations of the booms, and x_2 the rest of the state vector.

$$\begin{bmatrix} \dot{x_1} \\ \dot{x_2} \end{bmatrix} = \begin{bmatrix} A_{11} A_{12} \\ A_{21} A_{22} \end{bmatrix} \begin{bmatrix} x_1 \\ x_2 \end{bmatrix} + \begin{bmatrix} B_1 \\ B_2 \end{bmatrix} u; \quad \begin{bmatrix} y_1 \\ y_2 \end{bmatrix} = \begin{bmatrix} C_{11} C_{12} \\ C_{21} C_{22} \end{bmatrix} \begin{bmatrix} x_1 \\ x_2 \end{bmatrix} + \begin{bmatrix} D_1 \\ D_2 \end{bmatrix} u; \tag{5.6}$$

The nonlinear expressions that are to be linearized are shown in expression 5.7 and were derived in chapter 4. R_2 is an additional term that rotates the velocity vector in order to 'conserve' it in the inertial reference frame and not in the body reference frame (which is where the instantaneous kinetic energy is computed). The expressions for the matrices mentioned in expression 5.6 are shown in expressions 5.8 to 5.17. The terms not defined are zero. The parameter n states for the the length of x_2. The term-by-term expressions for A_{21} and A_{22} are not shown here due to their extension.

$$\begin{gathered} x_1 \rightarrow \dot{r} = v; \quad \dot{Q} = \frac{1}{2} Q\omega; \quad \dot{q} = dq; \\ x_2 \rightarrow \dot{x}_2 = M^{-1}(x_1)(-\dot{M}(x_1, x_2)x_2 + (\frac{\partial M(x_1)}{\partial x_1} x_2)^T x_2 - Kx_1 - Fx_2 + Q(x_1, u) + R(x_1, x_2)) + R_2(x_2); \end{gathered} \tag{5.7}$$

$$A_{11}(1:3, 4:7) =$$

$$\begin{bmatrix} 2(v(1)Q(1) + v(2)Q(2) + v(3)Q(3)) & -2(-v(1)Q(2) + v(2)Q(1) + v(3)Q(4)) & 2(v(1)Q(3) + v(2)Q(4) - v(3)Q(1)) \\ 2(-v(1)Q(2) + v(2)Q(1) + v(3)Q(4)) & 2(v(1)Q(1) + v(2)Q(2) + v(3)Q(3)) & 2(v(1)Q(1) + v(2)Q(2) + v(3)Q(3)) \\ -2(v(1)Q(3) + v(2)Q(4) - v(3)Q(1)) & -2(-v(1)Q(4) + v(2)Q(3) - v(3)Q(2)) & 2(-v(1)Q(4) + v(2)Q(3) - v(3)Q(2)) \\ -2(-v(1)Q(4) + v(2)Q(3) - v(3)Q(2)) & 2(v(1)Q(3) + v(2)Q(4) - v(3)Q(1)) & 2(-v(1)Q(2) + v(2)Q(1) + v(3) * Q(4)) \end{bmatrix}^T; \tag{5.8}$$

$$A_{11}(4:7, 4:7) = \frac{1}{2} \begin{bmatrix} 0 & \omega(3) & -\omega(2) & \omega(1) \\ -\omega(3) & 0 & \omega(1) & \omega(2) \\ \omega(2) & -\omega(1) & 0 & \omega(3) \\ -\omega(1) & -\omega(2) & -\omega(3) & 0 \end{bmatrix}; \tag{5.9}$$

$$A_{12}(1:3, 1:3) = (Q(4)^2 - Q(1:3)^2)I(3) + 2Q(1:3)Q(1:3)^T - 2Q(4) \begin{bmatrix} 0 & Q(3) & -Q(2) \\ -Q(3) & 0 & Q(1) \\ Q(2) & -Q(1) & 0 \end{bmatrix}; \tag{5.10}$$

$$A_{12}(4:7,4:6) = \frac{1}{2}\begin{bmatrix} Q(4) & -Q(3) & Q(2) \\ Q(3) & Q(4) & -Q(1) \\ -Q(2) & Q(1) & Q(4) \\ -Q(1) & -Q(2) & -Q(3) \end{bmatrix}; \tag{5.11}$$

$$A_{12}(8:n+1,7:n) = \begin{bmatrix} 1 & 0 & ... & 0 \\ 0 & 1 & ... & 0 \\ ... & ... & ... & ... \\ 0 & 0 & ... & 1 \end{bmatrix}; \tag{5.12}$$

$$\begin{aligned} A_{21} =& \frac{\partial M^{-1}}{\partial x_1}(-\dot{M}x_2 + \frac{1}{2}(\frac{\partial M}{\partial x_1}x_2)^T x_2 - Kx_1 - Fx_2 + R + Q) + M^{-1}(-\frac{\partial \dot{M}x_2}{\partial x_1} + \frac{1}{2}\frac{\partial(\frac{\partial M}{\partial x_1}x_2)^T x_2}{\partial x_1} - \frac{\partial Kx_1}{\partial x_1} - \frac{\partial Fx_2}{\partial x_1} + \frac{\partial R}{\partial x_1} + \frac{\partial Q}{\partial x_1}) = \\ =& - M^{-1}\frac{\partial M}{\partial x_1}M^{-1}(-\dot{M}x_2 + \frac{1}{2}(\frac{\partial M}{\partial x_1}x_2)^T x_2 - Kx_1 - Fx_2 + R + Q) + M^{-1}(\frac{1}{2}\frac{\partial(\frac{\partial M}{\partial x_1}x_2)^T x_2}{\partial x_1} - K + \frac{\partial R}{\partial x_1} + \frac{\partial Q}{\partial x_1}); \end{aligned} \tag{5.13}$$

$$\begin{aligned} A_{22} =& M^{-1}(-\frac{\partial \dot{M}x_2}{\partial x_2} + \frac{1}{2}\frac{\partial(\frac{\partial M}{\partial x_1}x_2)^T x_2}{\partial x_2} - \frac{\partial Kx_1}{\partial x_2} - \frac{\partial Fx_2}{\partial x_2} + \frac{\partial R}{\partial x_2} + \frac{\partial Q}{\partial x_2}) + \frac{\partial R_2}{\partial x_2} = \\ =& M^{-1}(-\frac{\partial \dot{M}x_2}{\partial x_2} + \frac{1}{2}\frac{\partial(\frac{\partial M}{\partial x_1}x_2)^T x_2}{\partial x_2} - F + \frac{\partial R}{\partial x_2}) + \frac{\partial R_2}{\partial x_2}; \end{aligned} \tag{5.14}$$

$$B_1 = 0; \quad B_2 = M_l^{-1}C;^1 \quad D = 0; \tag{5.15}$$

$$C_{11}(1:7,1:7) = \begin{bmatrix} 1 & 0 & ... & 0 \\ 0 & 1 & ... & 0 \\ ... & ... & ... & ... \\ 0 & 0 & ... & 1 \end{bmatrix}; \quad C_{12} = 0; \tag{5.16}$$

$$C_{22}(1:3,1:3) = A_{12}(1:3,1:3) = C_{22}(4:6,4:6); \quad C_{21}(1:3,4:7) = H_{(\omega=\upsilon)}; \quad C_{21}(4:6,4:7) = H; \tag{5.17}$$

These matrices and the system they represent were implemented as a function of the linearization point as a MATLAB function. From the final equations obtained it can be derived that there are 4 main parameters in relation with the booms affecting the behavior of the system: linear density, length, bending stiffness and damping coefficient.

5.2.2. Numerical linearization

The linearization is here performed numerically instead of analytically. For this purpose, built-in MATLAB functions were used, particularly: 1) $linio$, which is used to define the state input (u) and output (y) vectors, and 2) $linearize$, used to linearize the system defined by $linio$. The particular value of $linio$ is that it allows defining inputs and output in multiple ways, e.g. if they are defined as 'open' the feedback loop, if any, is not considered.

The resulting linear model is first compared to that obtained in the previous section (5.2.1). The input data for the model is that stated in section 4.4.2. The comparison is performed by using a ν-gap metric, which was introduced by Vinnicombe in [30]. This metric is meant to be used to find the stability margin of a perturbed system. However, in this report, it is only used to express numerically the difference between two systems. This difference ranks from 0 to 1, increasing as the difference between the systems increases. The computation of the metric is done using the MATLAB's funtion $gapmetric$. The comparison is done over three different linearization points and the values of the ν-gap metric for each case are shown below. These results are the basis to considered verified the derivation and implementation of the analytical derivation.

- For arbitrary attitudes and an arbitrary deformation of each boom of order 1E-5 m, ν-gap remains on the order of 5E-7.

---

[1] C extracted from equation 4.25

- For arbitrary attitudes and an angular rate equal to $[0,0,0.0175]+\Delta(\approx 1E-3)$, ν-gap remains on the order of 5E-4.

- For arbitrary attitudes, an angular rate equal to $[0,0,0.0175]+\Delta(\approx 1E-3)$ and an arbitrary deformation of each boom of order 1E-5 m, ν-gap remains on the order of 5E-4. According to the results previously obtained, the operating point will remain within this ranges.

Analogously, this linearized plant is compared with a linearization of the plant built in simscape [2]. An schematic view of the numerical model is shown in figure G.7 in appendix G. The number of modes and elements per boom used in this comparison are 5 and 10, respectively. Linearizing at an aleatory attitude and for zero angular rate, the value of ν-gap is around 0.25. The higher values can be explained based on numerical errors and the slightly different assumptions made. This is considered an additional verification of the analytical equations of motion derived in chapter 4. Some additional aspects to be considered in relation with this last comparison are:

- Reducing the system output (y) to the attitude quaternion and the angular rate (avoiding including the position and velocity) leads to a higher degree of accuracy measured in terms of the ν-gap. This way, for the same case, it is lowered from 0.25 to 0.03. This points out that the main differences in the linear models are regarding the velocity/position of the spacecraft, which are not that relevant from an ADC perspective.

- Effect of the damping. Higher damping leads to a higher degree of similarity of the models, probably due to decreasing the importance of higher modes, which have a lower accuracy.

5.3. Potential changes in the system

Throughout this section, potential changes in the design are addressed in order to analyze whether the behavior remains qualitatively similar. This is done in order to justify potential extrapolations of the results to other cases with a similar structure. This study focuses only in the peaks in response related to the flexibility and in how these peaks are affected by perturbations in the specifications of the boom.

This way, instead of studying the response of the complete flexible plant, only the difference w.r.t. the rigid plant is studied. A plant is built with the configuration shown in figure 5.10, where G_0 is the rigid plant and Δ the effect of the flexibility. Δ is estimated so that: $G_f \approx G_0 + \Delta$, where G_f is the flexible plant. This estimation is done numerically, by obtaining the response in frequency of rigid and flexible plants and computing the difference. The MATLAB function *idfrd* is used to store the difference in response over frequency. Additionally, the function *tfest* has been used to estimate a transfer function based in that difference. It is important to highlight that, even though this configuration is similar to that used in relation with H_2, H_∞ or $\mu-$synthesis, this is not what it is used for here.

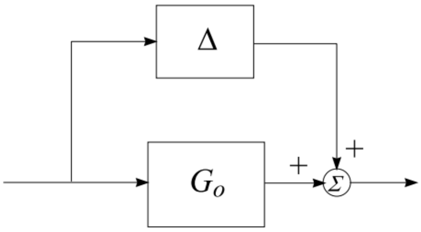

Figure 5.10: Additive perturbation configuration [14].

The selection of the boom parameters that are varied is based in the results of the analytical linearization, and comprises the following:

- Bending stiffness. 2 cases: 20% and 100% of nominal value.

- Damping coefficient. 3 cases: 1%, 10% and 100% of nominal value.

- Linear density. 3 cases: 20%, 100% and 500% of nominal value.

---

[2] In order for the simscape model to obtain the initial conditions (linearization point), the linearization time should be higher than zero.

- Length. 2 cases: 100% and 200% of nominal value.

As to avoid excessive figures, only the response of the angular rate error in the x-axis under the action of a torque in the same axis is considered, assuming only one mode (N=1). From previous results it can be seen that this is representative. Figure 5.11 shows the response of the function $\Delta(s)$ in the frequency domain for all the combinations of changes in the parameters previously mentioned.

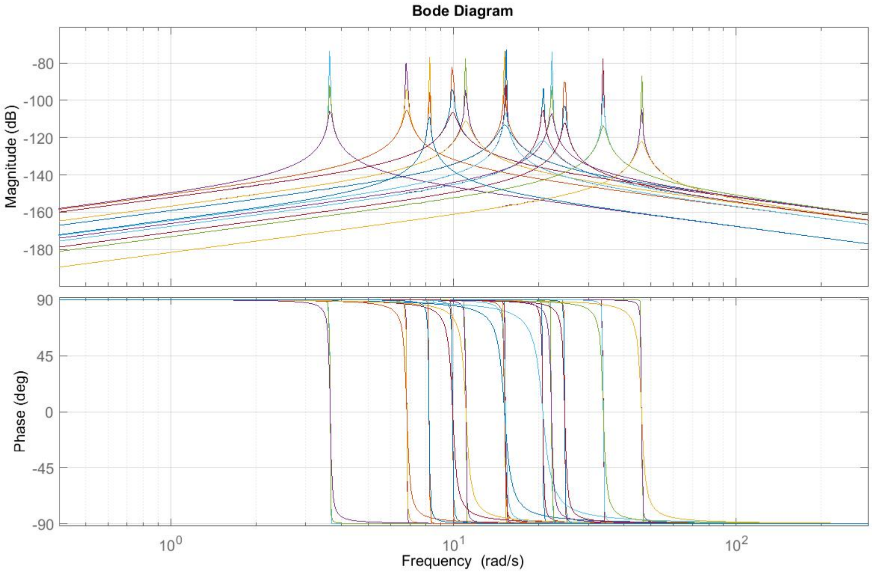

Figure 5.11: Bode analysis on the variation of the disturbance induced by the flexibility of the booms. Input: torque in x-axis direction. Output: angular rate in x-axis direction.

It can be observed that even with considerable variation in the booms used, the behavior is similar. The peaks in response remains under -120 and -60 dB and between 1 and 100 Hz. The most relevant variation is caused by the change in damping coefficient, affecting the height of the peak. This analysis leads to the conclusion that the processes used for deriving the controller can be applied to these different cases with a similar resulting performance, if they are applicable to cases with low damping coefficient. The effect of changes in the parameters in relation to the height (h) and frequency (f) of the peak in response are: 1) $\uparrow EI \rightarrow \uparrow f; \sim h$, 2) $\uparrow kd \rightarrow \sim f; \uparrow h$, 3) $\uparrow \rho \rightarrow \downarrow f; \uparrow h$, and 3) $\uparrow L \rightarrow \downarrow f; \uparrow h$.

5.4. Robust control

A more accurate title for this chapter would be 'analysis of some particular tools developed within the scope of robust control (i.e. H_2 and H_∞), in relation to the case of study'. It is not the intention of the author to dive into the mathematical derivations leading to these methods, nor to provide with a global explanation in relation with robust control theory. For this, the reader is referred to [19], which was found extremely useful to gain an understanding on the basic ideas behind robust control as well as the multiple tools that have been developed based in this approach.

Essentially, robust control aims to incorporate the uncertainties of a system in the design of the control system, ensuring stability and a level of performance. These uncertainties include, for example, uncharacterized external disturbances and errors due to simplifications in the model. There are multiple methods to describe these uncertainties (e.g. small-gain approach and Lyapunov method) and several tools to develop the controller based on the description of the uncertainties (e.g. H_2 and μ-synthesis). Only the methods and tools used in this study are explained, more complete explanations can be found at [19].

In relation to this project, there are two main aspects in which the ADCS could benefit from using a robust control approach. First of all, it allows reaching a higher certainty w.r.t. the stability of the system. This is not trivial, as the system is not fully observable. A priori the only measurements are related to the attitude variables (sun vector and angular rate), while the actual plant of the system includes also variables linked to the deformation of the booms. With the set of sensors proposed in table 2.5, these last variables are not obtainable. Furthermore, the only actuation the controller can provide is a torque in the central part of the structure. The stability of the system could be proven by applying robust control methods (e.g. H_∞) to the actual system. However, these methods are applied, for the sake of simplicity, to a linearization of the system around the operating point. Therefore, this should not be considered a 'prove' of the stability of the system, but rather an indication of it.

The other potential advantage of using this approach is that it enables to easily target certain frequencies in the response of the system. This means that the controller can be designed to minimized the vibrations due to the natural modes of the system, without the need of having an estimation on the deformation of the booms. This is possible because the controller derived using this approach contains a more extensive knowledge of the dynamics of the plant.

Therefore, throughout this study, robust control tools and methods are used to design an ADCS system aiming to: 1) comply with the mission requirements, 2) minimize the effect of the flexibility in the attitude variables and 3) lead to a stable system. Additional benefits that approaching the problem from a robust control perspective could have are: 1) optimizing the performance of the controller while maintaining the stability and 2) studying the limits of the stability of the system w.r.t. variation of the system's parameters (e.g. using a μ-synthesis approach). These possibilities have not been implemented. The rest of this section covers first the design of a plant over which the robust control tools and methods can be applied and then introduces the two ADCS design proposed (i.e. H_2 and H_∞), studying their performance.

5.4.1. Generic configuration

In this section, the system to be controlled is defined, including the specifications on outputs and inputs as well as internal dynamics and external disturbances. Potential manipulations on the signal in order to increase the performance in relation with certain aspects (e.g. minimization of the vibrations) are also explained.

In this project, MATLAB built-in functions are used, when possible, to implement the robust control methods. These built in functions required the system to be controlled to be defined in a certain way. This generic configuration is shown in figure 5.12. In this figure, w is the external disturbance, z the output to be reduced by the controller, y contains the measurements and u the control command. P is the plant targeted by the controller, including the uncertainties to be studied which can be added, for example, as shown in figure 5.10. K is the controller, which aims to minimize the effect of the disturbances (w) in the output signal (z). It is to be highlighted that K is not a constant matrix, as it was in the previous control design (based in an LQR approach), but an additional linear plant (linear time invariant system). Finally, W is a weighting function, equivalent to W in figure 5.1. Each of this components of the system are further explained, in relation with the case of study, below.

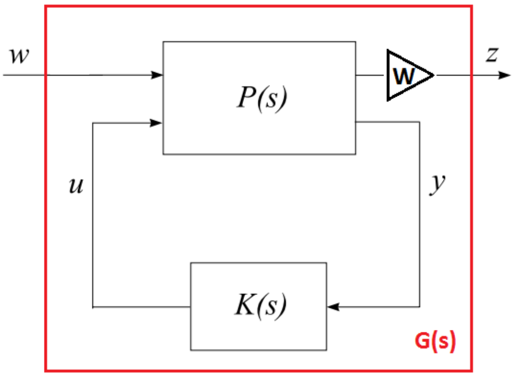

Figure 5.12: Generic configuration of the closed plant [14].

The external disturbances (w) contain the torque and, optionally, force disturbances. For simulation purposes these are modeled as white noise with a frequency of 0.01 s^{-1} and power 1. Within the plant (P) the external disturbance are escalated by a factor of 1e-5, linked to the actual external disturbances exerted in the spacecraft. The output signal (z) contains the pointing error, the angular rate error and the control torque. Each magnitude is scaled and amplified in a different way by the weighting function (W). These differences are explained in detail later in this section. W.r.t. the measurement signal, the set of sensors used is assumed to be able to provide an estimation on the pointing (w.r.t. the sun) and angular rate errors. Even though this signal is called measurements, it actually contain an estimation of the control variables. This estimation is initially assumed perfect.

The control command (u) is defined by signal y and controller K. Inside the plant (P) three modifications are done over the control command in order to simulate the magnetorquer behavior: 1) limit in the maximum torque in each axis to 5e-4 Nm (aiming to address the limitation in maximum dipole), 2) a duty cycle is imposed in the signal, with a period of 5 seconds and a pulse width of 90%, and 3) the time constant of the magnetorquer, characterizing the behavior of the signal, has been set in 0.05 seconds. These assumptions do not include the local underactuation due to the interaction with the magnetic field.

The controller (K) is derived implementing robust control theory. It consists on a linear MIMO (multiple input-multiple output) system with 5 inputs (measurements) and 3 outputs (control command). The plant (P) of the system is the linearization of the flexible model around the operating point (error signal equal to zero). The deformations of the booms in the linearization point are assumed to be zero. The linearization is performed numerically, as described in section 5.2.2.

Among the most relevant decisions influencing this controller's derivation and its performance is the definition of the weighting function (W) for the output signal. This function defines the importance given by the controller to the response of the system to error in each control variable at each which is the signal the controller targets. The objectives of this weighting function, in the case studied, are two: 1) determine the relative weight of the error in the pointing orientation and angular rate, w.r.t. the control effort (control torque), and 2) graduate the importance given to damping the vibrations induced by the vibrations of the booms. The first objective is met based in the gains computed iteratively for the LQR controller (see appendix B). The second objective is considerably more complex, as it aims to obtain a controller which is able to damp high-frequency vibrations maintaining a certain performance at low frequencies. In order to be able to do this, the weighting functions need to amplify the output signal z at certain frequencies, e.g. using a band-pass filter. It can be deduced that there are two qualitatively different approaches to define W:

- Constant gain for each signal. The pointing, angular rate and control torque error are scaled with gains that represent the importance they are given from a control perspective. This is done in a similar way as when deriving the LQR controller.
- Define the gain as a function of the frequency. The gain is designed as a transfer function, amplifying the signal at those frequencies in need of a more strict control.

Both approaches are implemented and the resulting controllers studied. In relation with the constant gains, their values are assigned in relation to the LQR controller. When the gains are defined as function of the frequency, they have the form shown in expression 5.18. In this expression, W_0 is the value of the constant gain assigned to that variable, a is a scalar multiplying tf and tf is a transfer function. This transfer function was defined so that it: 1) amplifies the response in the frequencies of the first natural modes of the system (i.e. from 10 to 100 Hz.) and 2) has a low impact in the response at low frequencies (below 1 Hz.) and at high frequencies (above 1000 Hz). The actual selection of these ranges of frequencies depends on the natural modes of the plant that is targeted by the controller. The two conditions that are to be fulfilled by the transfer functions drive the decision to use a band-pass filter or order 4.

$$W(s) = W_0(1 + atf(s)) \tag{5.18}$$

In figure 5.13, the transfer function between the disturbance signal (w) and the output signal (z) in the absence of controller is presented for various values of the parameter a (see expression 5.18). In this figure, only the first pointing error signal (see figure 5.7), is included. The rest of the signals in the output signal are shown in figure I.1 in appendix I. The effect of the frequency dependent weighting functions can be clearly noticed and has the behavior desired. These frequency-dependent weighting functions are only applied to the angular rate and pointing errors, and not to the control command. The gains for the control command are initially assumed constant.

After the two options regarding the definition of the weighting functions (block W in figure 5.12 have been defined, two main strategies for deriving the robust controller are studied. These strategies are based in minimizing two different norms: H_2 and H_∞. The particularities of each approach are explained in the subsections that follows. The theoretical expressions shown are taken from [19]. No uncertainties in the parameters of the system (e.g. bending stiffness of the booms) are accounted for, thus, only nominal plant is analyzed.

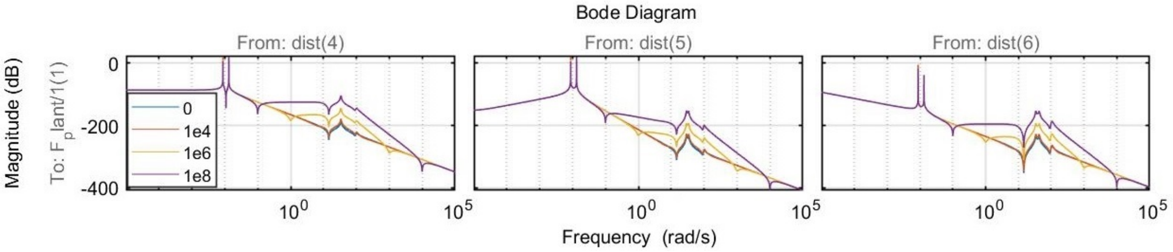

Figure 5.13: Effect of different weight functions in the error signal. In expression 5.18, a is the number in the legend.

5.4.2. H_2 norm

The controller derived using this approach aims to minimize the norm shown in expression 5.19, where Tr is the trace of the matrix and ω the frequency. G is the transfer function between disturbances (w) and output (z) signals (see figure 5.12). It is to be highlighted that the plant of the system (P) contained in this figure is the linearized flexible plant. It can be observed that the aim of this controller is to minimize the response over all frequenciesThe MATLAB built-in function that is used to derive the controller which minimizes this norm is *h2syn*.

$$||G||_2 = \sqrt{\frac{1}{2\pi}\int_{-\infty}^{\infty} Tr[G^*(j\omega)G(j\omega)]d\omega} \tag{5.19}$$

Among the options for the weighting function (W) described in the previous section (section 5.4.1), only constant gains are used in the derivation of this controller. As mentioned, this gains are related to those used in the initial LQR controller, being approximately their square root. The numerical values of these gains are: 1) pointing error: 0.07, 2) angular rate error: 100 and 3) command torque: 300.

In figure 5.14 (extended in figure I.2, appendix I), the resulting closed plant is compared to that resulted of the use of the LQR controller. This comparison is done based in the transfer functions between the inputs and output shown in figure 5.7, taking into account that the controller (K) is in one case the one resulting from minimizing the H_2 norm and in the other the previous LQR controller. As expected, the performance of the H_2 controller, with the error gains defined, is considerably similar to that of the LQR based controller.

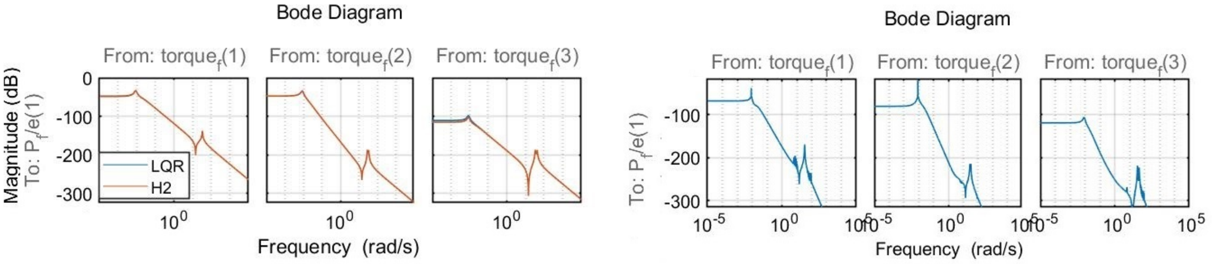

Figure 5.14: Comparison of the performance of H_2 and LQR controller. Responses in the left, difference in response in the right.

5.4.3. H_∞ norm

In this case, the norm to be minimized is shown in expressions 5.20 (for SISO systems) and in 5.21 (for MIMO systems), with u being the input vector. The single input - single output version (SISO) is shown in order to show in a comprehensive way that this norm aims to minimized the maximum response in frequency, reducing the peaks in response. The derivation of the robust controller is done using the MATLAB function *hinfsyn*, using an LMI-based (linear matrix inequalities) algorithm. Similarly as in section 5.4.2, the transfer function G is that shown in figure 5.12.

$$||G||_\infty = \sup_{\omega} |G(j\omega)| \tag{5.20}$$

$$||G||_\infty = \sup_{u\in\mathbb{C}^m;||u||\leq 1} ||Gu||_\infty; \quad ||Gu||_\infty = \sup_{\omega} ||G(j\omega)u||_2 \tag{5.21}$$

For the derivation of this controller, both strategies presented in relation with the weighting function are implemented: 1) constant gains and 2) frequency-dependent gains. The constant gains were found iteratively and are the following: 5e-3 for the pointing error, 1e1 for the angular rate error and 1e2 for the control torque. The frequency dependent weighting functions were already introduced in relation with equation 5.18. In order to reduce the numerical complexity of obtaining the controller (K), which is computed via the MATLAB function *hinfsyn*, the plant (P) targeted is the linearization of the flexible plant taking into account only the first mode of the booms. The parameters of the booms are the nominal ones.

In the following results, four different controllers are studied and compared: 1) the H_2 controller explained in the previous section, 2) an H_∞ controller computed using constant weighting function, 3) an H_∞ controller computed using a weighting function as the one shown in expression 5.18, with parameter a equal to $10^{6.5}$, and 4) same as 3 but with a equal to 10^8.

Figure 5.15 (extended in figure I.3, appendix I), contains the response of the close plants resulting of implementing these 4 different controller. The inputs and outputs of the transfer functions shown are those in figure 5.7. Figure in the left cover a broad range of frequencies while the figure in the right zooms in the responses at the frequencies close to the natural frequencies of the system. In this analysis the damping coefficient is reduced to 1% of its value in order to evaluate the performance of the controller in worse conditions.

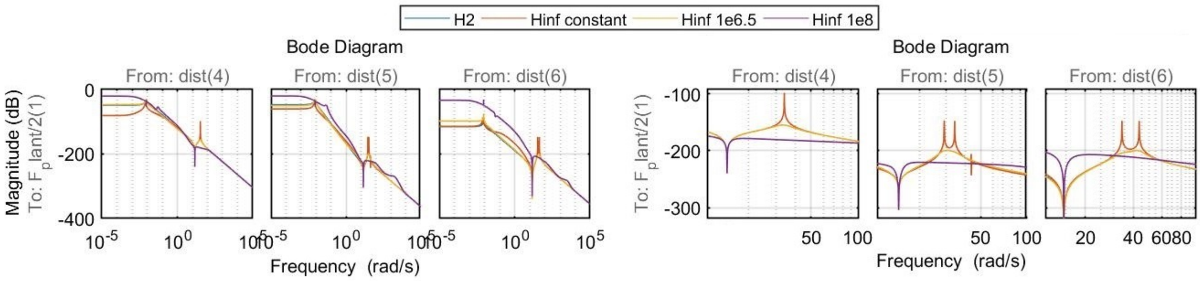

Figure 5.15: Comparison of the performance of robust controllers computed with different error weighting functions ($f(s) = af_0(s)$, where a is the number in the legend) and LQR controller.

Several conclusions can be extracted from comparing the different controllers analyzed in figure 5.15. First of all, when comparing the behavior of the close plant with the H_2 controller and with H_∞ using a constant weighting function, it can be observed that both controllers have a considerably similar performance. Further analyses showed that the H_∞ controller derived in this manner is able to slightly increase the performance of the H_2 controller at low frequencies. However, neither of these two controllers is affecting the peaks in response at high frequency. The reason for this is that, even with really low damping coefficients, these peaks are considerably lower than those at lower frequencies, related to the rigid dynamics (see figure 5.9). As the controller is derived based in the H_∞ norm, it focuses in minimizing the maximum response over frequency, and leaves the response at high frequencies untouched.

Having concluded that the H_∞ derived with constant error weighting functions is not targeting the vibrations at high frequencies, the consequences of adding frequency-dependent weighting functions is studied. It can be observed in figure 5.15, that an amplification of the response at higher frequencies generates a higher control effort in this area. This is a direct consequence of the implementation of a controller based in the H_∞ norm, which aims to reduce the highest peaks in response. The two controllers obtained with this approach (i.e. Hinf 1e6.5 and Hinf 1e8) are able to reduce considerably the peak in response over at the natural frequencies. Increases in the relative weight of the band pass filter (i.e. increases in the parameter a in expression 5.18), lead to a higher reduction in the magnitude of these peaks. However, it is also to be pointed out that, as more control effort in invested in high frequency vibrations, there is a decrease in the performance of the controllers at low frequencies.

As previously mentioned, the controller (K) was obtained taking into account only one mode. In analyses shown before, the plant (P) to be controlled also includes only the first mode and, thus, the effect of this limitation are not visible. In order to study the potential problem that this may pose, the performance of the controllers (the four controllers in figure 5.15) over a more accurate flexible plant, including the 5 first modes, is studied. The behavior of the close plant is shown in figure 5.16, and more extensively in figure I.4 in appendix I. It can be seen that the peak reduction is considerably similar to that shown in figure 5.15 and no negative consequences are noticeable. Furthermore, the peaks linked to higher modes are also reduced.

Based in this first analysis it would seem that increasing the amplification of the error signal at high fre-

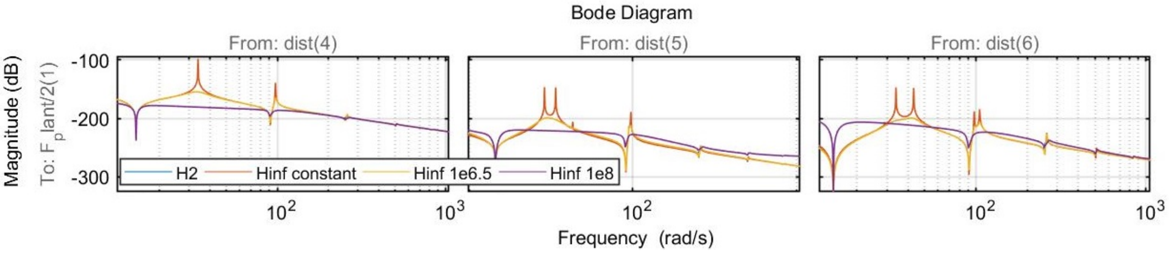

Figure 5.16: Analysis shown in figure 5.15, including the first 5 modes.

quencies is always contributing to minimize the response at high frequencies and, thus, the vibrations of the structure. However, there are two main negative consequences of increasing it in excess: 1) the performance at low frequencies is decreased, implying that the ADCS design is not able to fulfill the mission requirements, and 2) the closed system becomes unstable. This last drawback is caused by the controller, which is a linear system on its own, becoming unstable. The stability of three different controllers computed using the H_∞ approach is studied in figure 5.17, by studying the location of their poles. These controllers are computed in the same way as those in figure 5.15, but with changes in the coefficients of the weighting function. This way, one controller is computed with constant gains (constant) and the other two with the component frequency dependent component ($f(s)$) of the weighting function scaled multiplying it by 10^6 (F1e6) and 10^7 (F1e7).

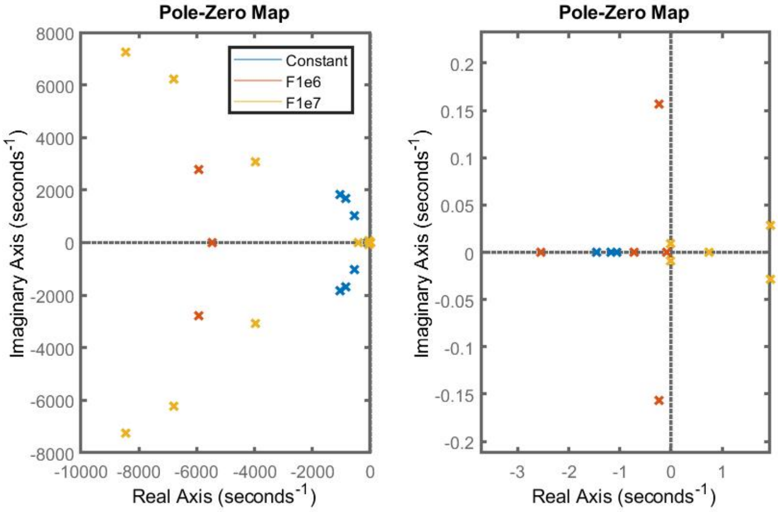

Figure 5.17: Pole placement for the controller derived based on different error weighting functions. $f(s) = af_0(s)$, where a is the number in the legend, 0 in the constant case.

It can be observed that in the case with the highest amplification at high frequencies (F1e7), the controller is not stable. This is not noticeable in a bode analysis, where it performance is increased, but creates a divergence when implemented over the actual plant in the time domain. Of the controllers shown in figure 5.15, the controller labeled as *F1e8* is unstable.

It can be concluded that the vibrations appearing in the pointing and angular rate errors due to the natural frequencies of the system can be targeted and controlled using an H_∞ approach. However, this control strategy can also be linked to a decrease in the performance of the controller w.r.t. the mission requirements.

5.4.4. H_∞ vs. H_2

It has been seen in the previous analyses in the frequency domain that the H_∞ controller was able to reduce the vibrations in the booms and in the attitude variables. In this section this capability is further analyzed, comparing it to the performance of the H_2 controller. These analyses are conducted in the time domain. The variables used to study the behavior of the close plant and to measure the performance of the controller are: 1) measurement signal, related to the rigid motion, 2) control torque, linked to the control effort, and 3) deformation of the booms, related to the flexible motion. Three main analyses are presented throughout this section, listed below. In all of these analyses the damping coefficient is defined as 0, in order to evaluate the worst case scenario.

- Comparison between H_2 and H_∞ (weighting function*F1e65*) controllers, in the absence of force disturbances.
- Influence of higher modes. This measures the influence that simplifications of the model when computing the controller have over its performance.
- Comparison between H_2 and H_∞ (weighting function*F1e65*) controllers, with force disturbances. The force disturbances cause a decoupling between the vibrations of the booms and of the attitude variables.
- Comparison between H_2 and H_∞ in relation to the mission requirements, when integrated into the simulation environment described in chapter 3.

First of all, the performance of the H_2 and H_∞ controllers previously described is analyzed. For the rest of the section the H_2 controller will be referred to as H_2 and the H_∞ controller as H_∞, in order to simplify the text. It is also to be remember that, due to the similarity between the perfomance of H_2 and the LQR controller, the conclusions of this analysis can be extrapolated to comparing H_∞ with the LQR controller.

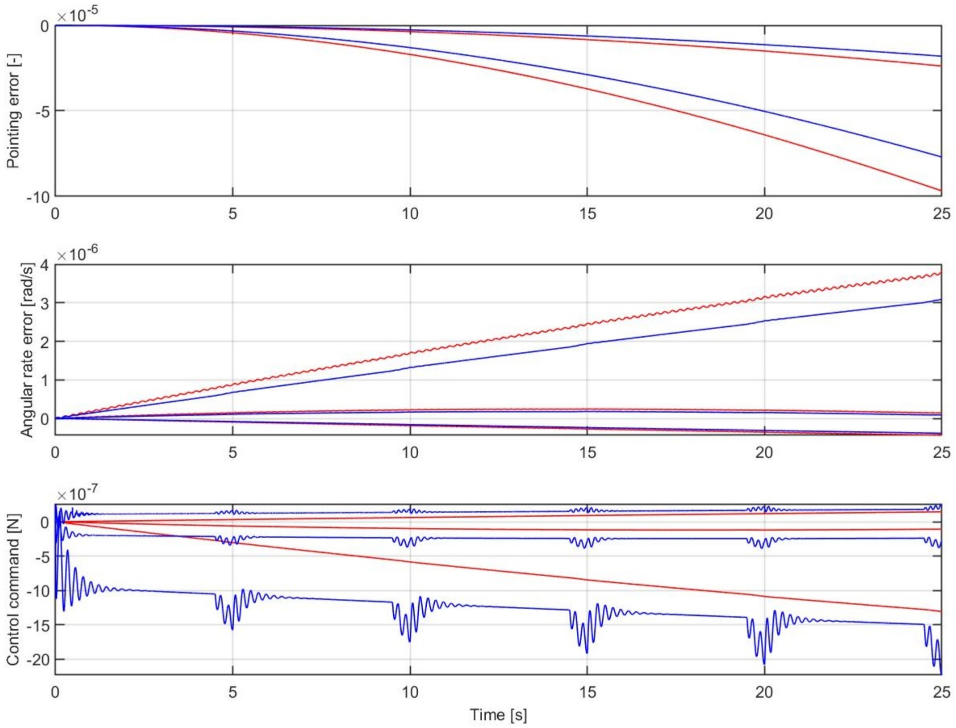

Figure 5.18: Comparison of the measurement signal for H_∞ (blue) and H_2 (red)

Figure 5.18 shows the evolution of the measurement's signal and the control torque, for both H_2 and H_∞. It is to be highlighted that the duration of the simulations shown in this figure (25 seconds) is not enough to draw any conclusions in the behavior of the controller at low frequencies. Therefore, these results are only used to provide an insight on the degree of damping achieved in relation to the vibrations of the structure. The long term variation of the error signal is studied in later figures. It can be noticed that the short term oscillations in the angular rate are highly reduced by the use of H_∞. However, in order to reduce these oscillations, the control effort increases and the oscillations in the control signal are noticeable higher. Furthermore, the response of the control signal to the error related with the rigid motion (i.e. without taking into account the short term vibrations) appears to be linked to a lower gain in the H_∞. This can be noticed in the fact that similar variations in the error signal lead to considerably higher variations in the control command with H_2 than with H_∞. This could lead to slightly longer times needed for reaching the operating point and to a decrease in pointing accuracy.

Regarding the evolution of the deformations on the booms (shown in figure 5.19 for boom 1 and in figure I.5, appendix I, for the 4 booms), it can be seen that H_∞ is considerably efficient in actively damping the vibrations of the booms. However, it is to be highlighted that this analysis is run in the absence of force disturbances. The consequence for this is that the vibrations appearing in the booms are, to a great extent, visible in the measurements (pointing error and angular rate). This enables the controller, with only information on these variables and capable only of exerting a control torque, to damp those vibrations. A more generalized case where this assumption is not considered is studied in a later analysis.

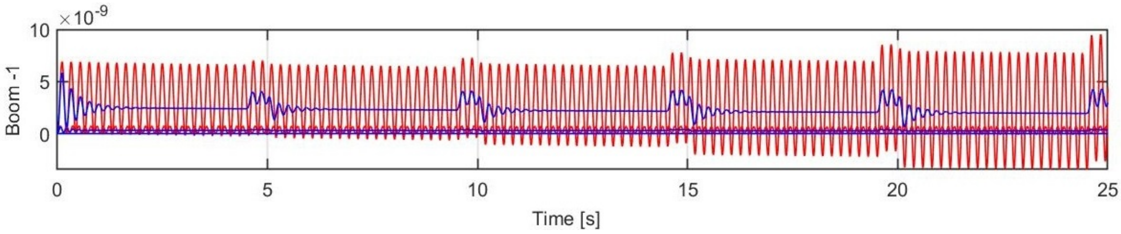

Figure 5.19: Comparison of the the boom deformation for H_∞ (blue) and H_2 (red)

The second analysis performed focuses in analyzing if there are any consequences of using a simplified plant when deriving the controller. As previously explained, the robust controllers have been obtained using a flexible plant with only the first flexible mode of the booms. In this analysis, one of controller (H_∞) is applied over a flexible plant which considered the first 5 modes. This analysis is similar to the one shown in figure 5.16. Only the evolution of the control command is analyzed (see figure 5.20), as it is assumed to be enough to characterize the vibrations of the error variables. It can be seen in that figure that low-amplitude fast oscillations in the control command appear and remain in the system longer than the low frequency vibrations. This means that the controller is less efficient when reducing this vibrations. However, it is to be taken into account that this analysis is performed over the assumption of zero damping coefficient. This is never the real case, and even a considerably small damping coefficient will damp these high frequency oscillations considerably faster.

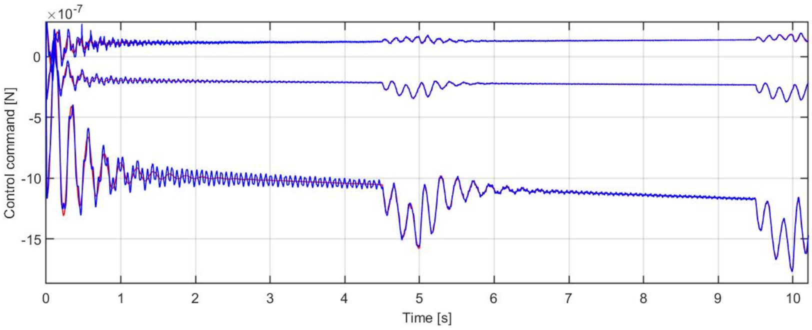

Figure 5.20: Control torque for Kv controller, for 1 mode (red) and 5 modes (blue).

Previously it was mentioned that, in a simplified case with only torque disturbances, the vibration of the booms was also minimized by H_∞. The analysis presented in figure 5.21 goes beyond that simplified case introducing also force disturbances. It can be seen that the active damping is still successful regarding the oscillations in angular rate. However, the vibrations of the booms are only partially damped. This is caused by the introduction (by the disturbance forces) of vibration modes in the booms that are not represented in the measurement signal, composed by pointing and angular rate errors. As this modes can't be measured (with the current set of sensors), it is not possible to actively damp them. The possibility of having additional sensors and actuators in order to avoid this situation is presented in the next section.

Additionally, a longer term analysis on the evolution of the measured error is run for the three controllers developed so far: LQR approach, H_2 and H_∞ (see figure I.6 in appendix I). In can be observed that the behavior of the closed plant is considerably similar under the action of the three controllers, showing only small deviations over 1 hour. The H_2 and the LQR based controller are particularly similar.

The final analysis performed over this two controllers, H_2 and H_∞, is conducted over an integration of them on the simulation environment. The objectives of this analysis are mainly two: 1) address the compli-

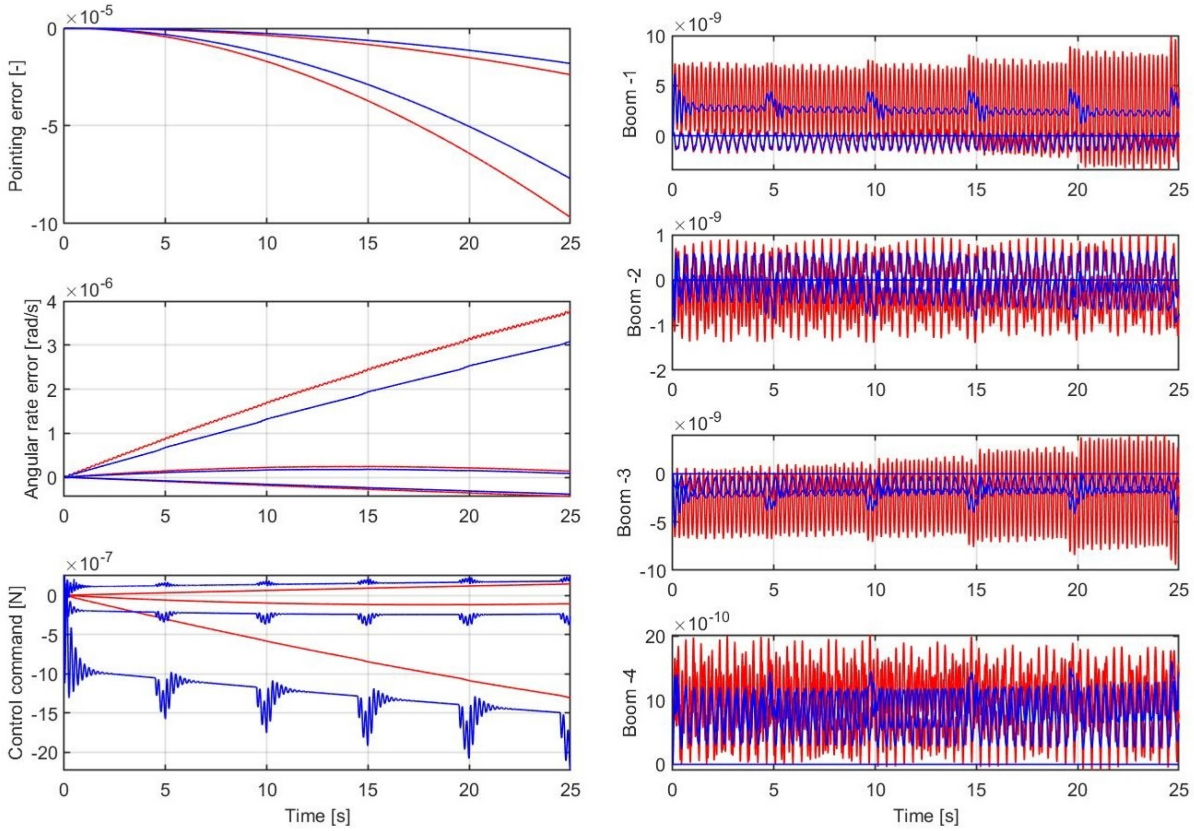

Figure 5.21: Evolution of measurements and boom deformation under the action of disturbance force and torque for H_∞ (blue) and H_2 (red).

ance of the controllers with the mission requirements and 2) study the performance of the controllers w.r.t the vibrations caused by the flexibility of the booms. Part of this analysis is included in appendix I. Figure 5.22 shows the evolution of the pointing error under both controller for the same initial conditions. It can be confirmed that the H_∞ requires more time to reach the operating point and that the long term pointing error is increased.

Figure 5.23 shows the evolution of the deformation of boom 1 for both H_2 and H_∞. It can be seen that, even thought H_∞ is not able to completely damp the vibrations, these are one order of magnitude lower than when H_2 is used. Considering that the damping coefficient is zero and that no information regarding the deformation of the booms is available, this is considered a good achievement. The deformation of the rest of the booms is included in appendix I, figures I.9 and I.8, and the same behavior can be observed.

Finally, figure 5.24 shows the evolution of the z-axis component of the angular rate using both H_2 and H_∞. When using H_∞ no vibrations are noticeable, while when using H_2 this variable is constantly oscillating (mainly due to the duty cycle of the magnetorquer). It is to be highlighted that this oscillation is considerably higher than in previous analyses run using an LQR controller, mainly due to the value of the damping coefficient (0). The evolution of the angular rate during a more extended time is shown in appendix I, figure I.7.

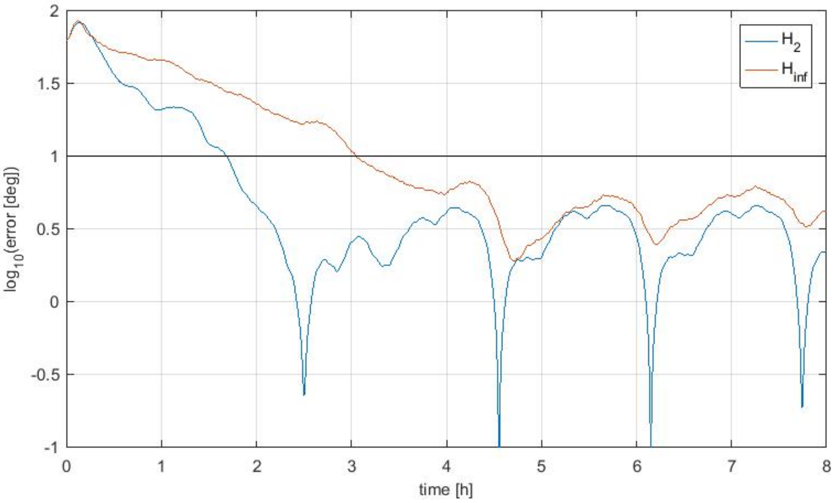

Figure 5.22: Evolution of the pointing error during the pointing phase, using H_∞ and H_2.

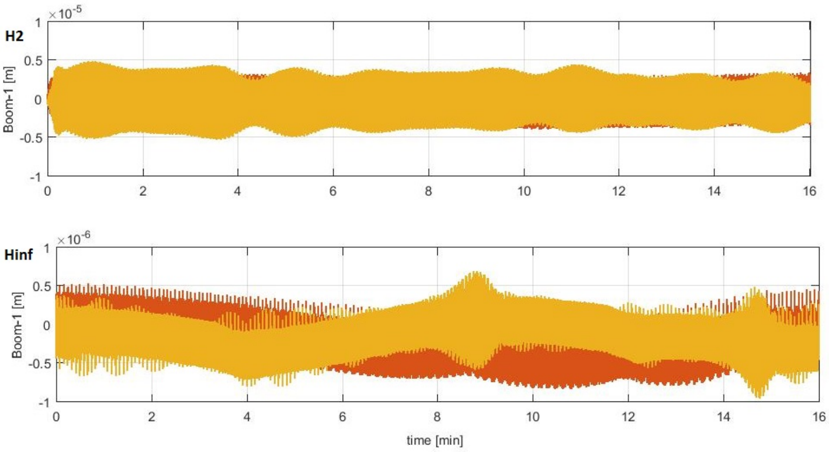

Figure 5.23: Evolution of the deformation in boom 1, using H_∞ and H_2.

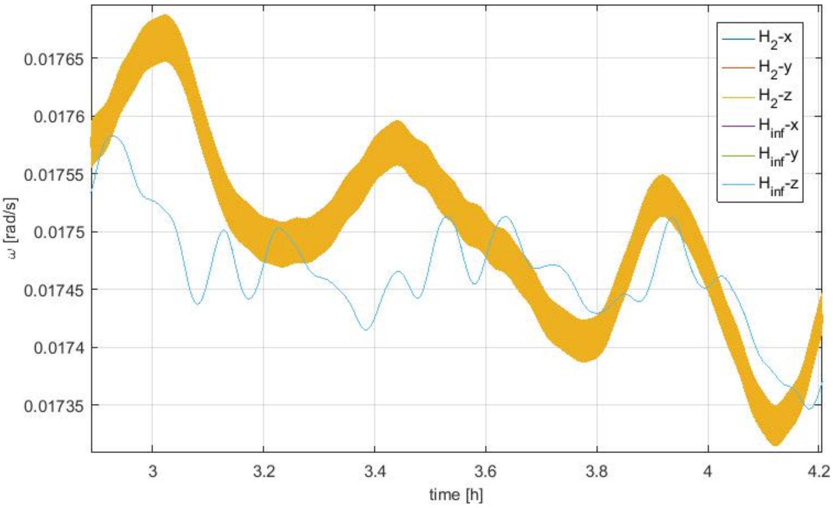

Figure 5.24: Evolution of the angular rate error, using H_∞ and H_2.

5.5. Non-linear controller

Throughout this section, the design of the ADCS is faced from a conceptually different perspective. This perspective differs from that of the previous designs in two main aspects: 1) the controller retains the non-linearity of the equations of motion, and 2) the analysis of the control problem, and, thus, the derivation of the controller, is based in analytical dynamics. These aspects are only briefly explained in this section, and the reader is encouraged to go to [29] for a more detailed explanation of this approach, known as the Udwadia-Kalaba approach.

This approach to the ADCS design is based in the existing parallelism between analytical dynamics and control theory described in [29]. This paper derives a generic formulation to compute the forces that act over a constrained system. This formulation leads to a control rule that makes the system follow the constrained motion without actual constraints. The different ways in which a constrained system and a controlled system are related can be seen in table 5.1.

Constrained system		Controlled system	Equation
Unconstrained system	↔	Uncontrolled plant	5.22
Constrained system	↔	Controlled system	5.23
Constraints	↔	Trajectory requirements	5.24
Gauss principle	↔	Control cost	5.25
Constraint force	↔	Control force	5.26

Table 5.1: Relation between constrained and controlled systems.

Starting from an uncontrolled system of the form shown in equation 5.22, the objective is to derive a control force (see Q_c in equation 5.23) such that the constrains shown in equation 5.24 are met. In these equations, q is the state vector, Q is a vector which contains both internal and external forces (or torques) faced by the system and M is the mass matrix (i.e. linking 'forces' and 'accelerations'). Matrix A and vector b need to be derived from the trajectory requirements (or guidance instructions). The method to obtain this terms (as explained in [29]) consists in deriving the initial constrain (e.g. angular rate equal to zero) w.r.t time until the double derivative of the state vector (e.g. angular acceleration) appear in the equation. The intermediate terms are also kept in the equation, to enable convergence from 'positions' that do not comply with the trajectory requirements. The resulting equation is then converted into as expression of the form shown in equation 5.24. This process is further explained in next section (section 5.5.1).

$$M(q,t)\ddot{q} = Q(q,\dot{q},t) \tag{5.22}$$

$$M(q,t)\ddot{q} = Q(q,\dot{q},t) + Q_c(q,\dot{q},t) \tag{5.23}$$

$$A(q,\dot{q},t)\ddot{q} = b(q,\dot{q},t) \tag{5.24}$$

After obtaining all this terms (M, A, b and Q), the generalized Gauss's principle is used as a cost function. The Gauss principle states that: from all possible constraint forces (Qc) that satisfy the constraints (equation 5.24), Nature chooses in each instant of time the one minimizing the cost function shown in expression 5.25 (with the weighting matrix (N) equal to the mass matrix (M)). As it may be necessary to use a weighting matrix that is not the mass matrix (e.g. due to non ideal constraints or limitations in the control actuation), the generalized Gauss principle is used. This 'generalization' is explained in detail in [29] and allows defining an arbitrary weighting matrix N> 0.

$$J(t) = [Q_c(q,\dot{q},t)]^T N(q,t)[Q_c(q,\dot{q},t)] \tag{5.25}$$

The expression of the constraint (control) force minimizing this cost function, at every instant, is presented in [29] and can be seen in equation 5.26. In this equation, a is an estimation of $\ddot{q}$ based in the knowledge of Q (internal and external forces). It can be seen in the description of the derivation of the controller, that no linearization or any other simplification of the equations of motion of the system are required (i.e. the controller can contain the actual dynamics of the plant). Another important aspect to be taken into account is that adding complex constrains (trajectory requirements) to the system is relatively easy.

$$Q_c = Ke = -N^{-1}M^{-1}A^T[A(MNM)^{-1}A^T]^+(Aa-b) \tag{5.26}$$

As can be seen in equation 5.26, the main matrices and vectors to be determined in order to compute the control command are: M, Q, A, b and N. These terms are related to the assumptions made over the equations of motion and to the control objectives. In this regard, two main options can be clearly distinguished: 1) using the 'rigid' equations of motion and 2) using the 'flexible' equations of motion. The constraints, or control objectives, are linked to the requirements of the mission and to additional requirements (e.g. reduce vibration of the booms). The rest of this section covers these two implementations of the control approach and their performance in relation to the case of study.

5.5.1. Rigid approach

In this section the non-linear control approach previously introduced is applied to the rigid equations of motion. This implementation is useful not only to study the performance of the resulting controller, but also as an example of how this control approach can be applied over a system. Two main steps are explained: 1) the definition of the system and 2) the derivation of the constraints.

The dynamics of the plant that is targeted by the controller include only the rigid motion of the satellite, particularly the attitude of this spacecraft. The uncontrolled motion (equivalent to expression 5.22), can be expressed in this particular case as shown in equation 5.27, where MoI is the moment of inertia, α the angular acceleration and T the torque. Therefore, the mass matrix (M) is equal to the moment of inertia, the vector Q is the sum of external and internal torques and the vector $\ddot{q}$ is the angular acceleration.

$$MoI\alpha = T_{int} + T_{ext} \tag{5.27}$$

The next step is related to deriving the constraints (guidance instructions). As explained in previous sections, there are two main constrains to be imposed over the motion of the satellite during the pointing stage: 1) pointing direction and 2) angular rate. The expressions for these two constraints are shown in equation 5.28, where s is the sun vector in the body reference frame, ω the angular rate and g states for guidance.

$$1) \quad s - s_b = 0; \quad 2) \quad \omega - \omega_g = 0; \tag{5.28}$$

The expressions used to define these constraints are not unique, and have a considerable impact in the performance of the resulting controller. As the quaternion is not fully known in the case studied, and in order to improve the performance of the final controller, expression 1 in 5.28 has been rewritten incorporating two assumptions. The first one is that the axis that needs to be aligned is the rotation axis ($s_g = \omega_g/|\omega_g|$). The second one is that the controller is implemented so that the desired angular velocity (w_g) is reached considerably faster than the pointing direction ($\omega_g \approx \omega$). These assumptions lead to the following expression for the constrain: $\omega_i \times s_i = 0$. It needs to be taken into account when deriving the controller that this constraint has two equilibrium points.

It can be observed that in order to obtain an expression as the one shown in 5.24, both constraints need to be derived w.r.t. time. The intermediate derivations are kept as part of the final expression (multiplied by constants c_i) to address initial conditions not fulfilling the constrains and a potential lack of knowledge regarding the external torque. The final expressions can be written as shown in expressions 5.29 (1) and 5.30 (2). Sub-index i states for inertial reference frame and the absence of it indicates body fixed reference frame. The ± in expression 5.29 is defined by the angle between ω and s being higher or lower than 90°, in order to avoid the equilibrium point at 180° angle. This way, when $\omega \cdot s < 0$ the system goes away from the nearest equilibrium point (180°) and when $\omega \cdot s > 0$ the system evolves towards the nearest equilibrium point (0°). α is the angular acceleration.

$$\alpha_i \times s_i \pm c_1(w_i \times s_i) = 0 \quad \rightarrow \quad \alpha \times s \pm c_1(w \times s) = 0; \tag{5.29}$$

$$\alpha + c_2(w - w_g) = 0; \tag{5.30}$$

The option to add an additional constraint, taking into account that there is a direction (i.e. direction of the local magnetic field) in which no control torque can be applied has also been added. This constraint is imposed by ensuring that the angular acceleration (α) in the direction of the magnetic field (m) is that of the unconstrained system (a) (see expression 5.31). The weight of this constraint can be scaled using parameter c_3.

$$c_3[m \cdot (MoI\alpha) - m \cdot (MoIa) = 0]; \tag{5.31}$$

Having defined the controller from a theoretical perspective, it was first implemented for simplified cases, in order to gain a deeper understanding of its behavior, and then in the actual ADCS simulator. From the first set of implementations, two main characteristics of the controller can be derived:

- Huge increase in performance when implementing a feed-forward strategy based on an accurate knowledge of the external (i.e. disturbances) and internal forces. In its absence, the speed of the controller needs to be considerably increased to maintain the performance.

- Overlap of constraints is automatically dealt with by the controller, and poses no additional problem if they are consistent. However, the number of constrains is directly related to the size of the matrix that needs to be inverted, so the less the better the speed of the controller.

After this initial analysis, the controller is implemented in the simulation environment and its performance analyzed throughout the rest of the section. The constants previously mentioned are defined as: $c_1 = 0.01; c_2 = 0.1; c_3 = 1$. First of all, the performance for different initial conditions (different orbits and initial attitude/angular rate) has been studied (see figures 5.25 and, in appendix K, K.1).

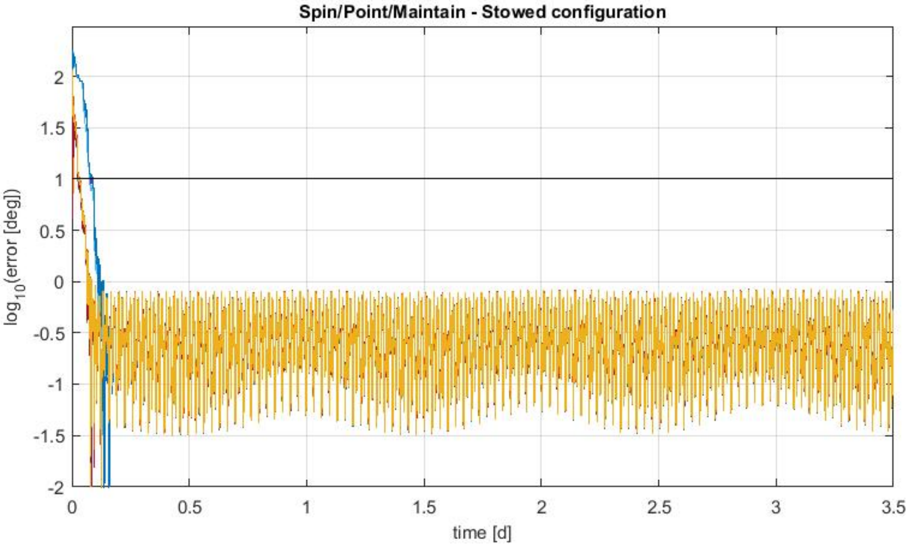

Figure 5.25: Evolution of the pointing error for 10 different initial conditions (angular rate and attitude). Stowed configuration. h: 600 km, i: 97 deg, Ω: 0.

From these results, it can be seen that the controller derived meets the performance requirements, 10 degrees pointing accuracy. A first comparison with the performance of the LQR controller (see section 3.2.1) does not give any clear difference in the long term performance. However, it appears that the non-linear controller is able to reach the desired configuration considerably faster than the LQR controller. Even though it may seem that the implementation of different weights in the cost function of the LQR controller could lead to a faster convergence to the operating point, all efforts in this direction have led to unstable controllers. A further comparison with the results shown in appendix D confirms that the operating point can be reached faster and give another interesting result. It seems that the pointing accuracy for the most critical cases (those with a highest amplitude on the periodic oscillation of the pointing error) is considerably improved.

In order to be able to confirm these differences in performance, it is necessary to conduct further analyses, applying both controllers over the same cases and initial conditions. Two examples are shown, one in which the LQR controller is able to achieve a considerably high accuracy and one where this accuracy is close to the requirements. In the first case (figure 5.26), it can be observed that, as previously indicated, the performance of both controllers is considerably similar in the long term and that the non-linear controller allows reaching faster the operating point. The second case (figure K.2, in appendix K) shows an increase in the pointing accuracy of almost 6 degrees. This can be explained by two main factors: 1) the limitations of the magnetic torque are included when optimizing the cost function of the non-linear controller, 2) the LQR controller designed relies on a discrete number of points (two in our case) and its accuracy depends on the proximity of the state vector to those points and 3) the objective angular rate (which is meant to be progressively increased once close enough to the orientation desired) is maintained at 0.01 rad/sec instead of 0.0175 rad/sec, as the condition for increasing it is not met.

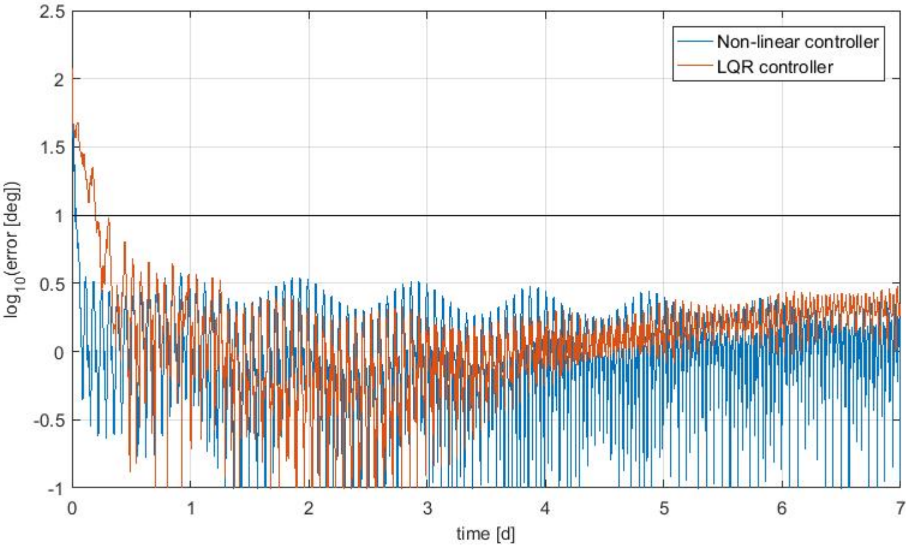

Figure 5.26: Evolution of the pointing error under LQR and non-linear controllers. Deployed configuration. h: 600 km, i: 60 deg, Ω: 0.

To evaluate the relative importance of each source of error, further analyses are conducted. The results are shown in appendix K. The effect of increasing the spin of the satellite progressively is proven to be a limitation for the pointing accuracy (see figure K.3) if the final spin is not reached. This way, an increase in the guidance angular rate has the effect of improving the stability of the pointing axis w.r.t. external disturbances, increasing the pointing accuracy. It is to be highlighted that, for the same angular rate command, the non-linear controller still improves the pointing accuracy by 1 degree in both cases shown in figure K.3, from a maximum angular error of over 5 degrees to less than 4 degrees. It can also be noticed that, while the non-linear controller allows a more accurate pointing, the oscillations of the angular rate have a higher amplitude. However, as these oscillations do not interfere with the requirements of the mission, this is not considered a relevant drawback. Finally, even though the convergence to the operating point has been found to be faster for the non-linear controller in most cases, there are still certain initial conditions which can lead to a similar convergence rate (see case 1 in figure K.3).

Additionally, the effect in the performance of adding the limitation on the control torque to the controller is studied over a series of cases (see figure K.4, appendix K). This figure compares the pointing error throughout time with and without adding this limitation in the computation of the controller. It can be observed that adding it has a positive effect, reducing the pointing error during 80% of the time for most cases and during 70 % for all cases. Leaving out 10% of the data in each side, the improvement in the pointing accuracy is between -0.2 and 0.8 degrees, which is considered a positive result.

5.5.2. Flexible approach

Up to now the proposed designs for the ADCS have been based in a considerably limited knowledge of the state of the plant, i.e. only the sun vector and the angular rate can be estimated. This means no information about the variables linked to the flexible motion (i.e. the deformation of the booms). This leads to limitations w.r.t. having a controller able to actively damp the vibrations of the booms. This can be noticed for example in the inability of the H_∞ controller to completely damp these vibrations, as they also contain modes that are not visible in the attitude variables.

These limitations are, a priori, not linked with the ADCS requirements, as the vibrations in the attitude variables can be damped with information about them. However, as the vibration of the booms is also targeted, the potential solutions to deal with this limitation by estimating the complete state vector are studied. Possible methods of obtaining this estimation are briefly introduced in appendix J.

This section aims to design a controller combining the knowledge gained in relation with the plant (flexible equations of motion) and the non-linear approach introduced at the beginning of this chapter. There are three main decisions to be made when designing a controller based in this control concept: 1) which definition of the dynamics of the plant to use, 2) which constraints to impose and 3) over which coordinates can the control be exerted. Regarding 1, two main options are considered: 1) rigid plant (see previous section 5.5.1) and 2) flexible plant (see equation 5.32, for further information go to chapter 4). Two aspects w.r.t. the feasibility of using the dynamics of the flexible plant to derive the controller are critical. The first one is the observability of the state vector, the deformation of the booms needs to be estimated. The second one is the computational power available, as the derivation of the controller becomes increasingly complex (see equation 5.26) and a considerable increase in computational speed would be needed for real time applications.

$$M = M(q(t)); \quad Q = Q_{ext} - [\dot{M}(q, \dot{q}, t)\dot{q}(t) - \frac{1}{2}(\frac{\partial M(q,t)}{\partial q}\dot{q}(t))^T \dot{q}(t) + Kq + F\dot{q} + R] \tag{5.32}$$

In relation to the definition of the constrains, four constrains have been considered. The first three were already introduced in the previous section and are linked to the angular rate, pointing direction and torque generation. The forth one aims to reduce the vibration of the booms, and is expressed as shown in equation 5.33, where q_i contains the deformation of the booms in the different axes and modes taken into account.

$$\dot{q}_i = 0; \quad \rightarrow \quad \ddot{q}_i + c_5\dot{q}_i = 0; \quad i = 1, 2, ..., n \tag{5.33}$$

Finally, w.r.t. the actuation possibilities, two options are considered: 1) using only a torque to control the spacecraft attitude (as it has been done in previous sections), and 2) introducing also a force in order to cope with vibrations decoupled from the attitude variables. The limitation on the control actuation is introduced in the controller derivation via a matrix N as shown in equations 5.25 and 5.26. It is important to highlight that, while this matrix N minimizes the control actuation over certain coordinates, it does not reduce it to zero. Therefore, this condition needs to be added outside the controller. The force command is not define directly by the the output of the non-linear controller equations, as it needs to be processed in order to avoid steady terms and provide only oscillatory forces. This is done by subtracting the moving average of the signal. More sophisticated methods to process this signal are left to further analyses, in which more detail specifications of potential actuators to be used are expected to be available. The constant c_5, in equation 5.33, is also directly connected to the actuator specifications, influencing the convergence rate of the constrain and, therefore, the peaks in the commanded control force.

Two controllers have been derived, with different performance objectives driving different decisions in the options previously described. The first controller do not target actively the vibrations caused by the flexibility of the system. Therefore, this controller is derived using the flexible equations of motion combined with the three constraints used in the previous section (expressions 5.29,5.30 and 5.31), and the only possible actuation is a control torque. The second controller aims to reduce the vibration of the booms by introducing an additional constraint (expression 5.33) and assuming a control force (in the central part of the satellite) can also be exerted. Throughout the rest of the section, the performance of these controllers (for now on controllers 2 and 3) is compared with that presented in the previous section (section 5.5.1), which was derived using the rigid equations of motion (controller 1). This performance is studied in relation with three aspects:

- Pointing accuracy achievable.
- Short term oscillations in the rigid motion variables, particularly in the angular rate.
- Deformation of the booms.

In figure 5.27, the first of these aspects is evaluated. In can be seen that controllers 2 and 3 have almost the same performance w.r.t. the pointing error. The accuracy reached with these controllers decreases considereable w.r.t that obtained with controller 1 (using the rigid equations of motion). This may be caused by the fact that the controllers using the flexible equations of motion estimate the needed control torque based in the moment of inertia of the rigid part of the satellite. This moment of inertia is one order of magnitude lower than the total moment of inertia. Furthermore, the ellipsoids of inertia of the rigid part and of the total part are not proportional. This drawback of using the flexible equations of motion to derive the controller has not been solved. It is to be highlighted, however, that the pointing accuracy is still complying with the requirements of the mission (10 degrees).

The second analysis focuses on the short term vibrations induced in the angular rate due to the interaction between the magnetorquer's duty cycle and the flexibility of the system. The results of this analysis are shown in figures 5.28 and, in appendix K, K.5. The effect of the flexible motion on the rigid motion of the structure is

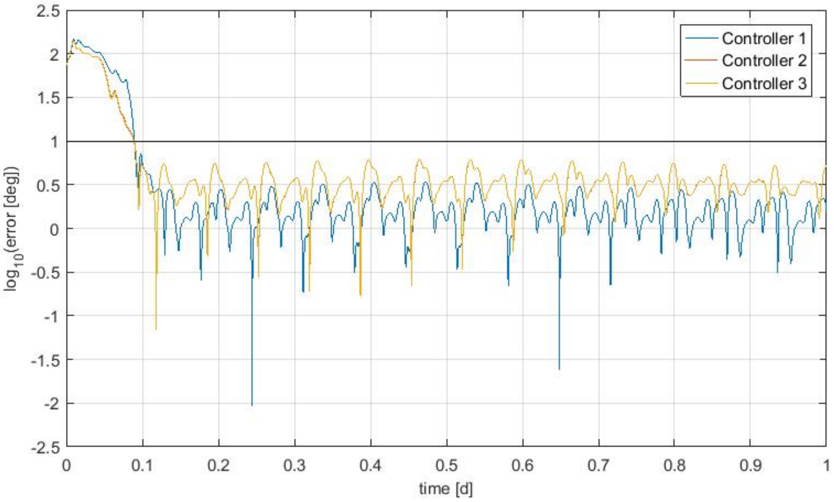

Figure 5.27: Evolution of the pointing error under non-linear controller with different specifications. Deployed configuration. h: 600 km, i: 97 deg, Ω: 0.

here clearly visible, though considerably limited. It can be seen that both controller 2 and 3 damp the vibrations on this variable faster than controller 1. This damping appears to be driven not by additional constrains or actuation capabilities, but by a more complete knowledge on the dynamics and state of the plant, as this is the only difference between controllers 1 and 2. It is to be taken into account that both in the constraint related to pointing orientation (expression 5.29) and in that related to the spin of the spacecraft (expression 5.30), the condition of angular acceleration equal to zero is imposed. The oscillations of the angular rate variables influence this acceleration, as, even though they have low amplitude, their frequency is high.

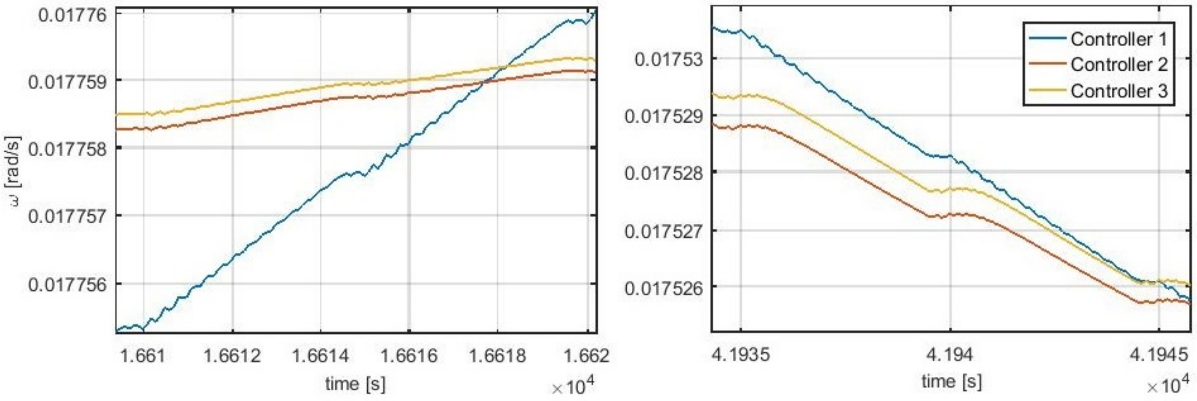

Figure 5.28: Analysis of the short term oscillations of the angular rate under non-linear controller with different specifications. Deployed configuration. h: 600 km, i: 97 deg, Ω: 0.

In relation with the vibration of the booms, several types of oscillations are expected. First of all, as the plant is initialized without been in equilibrium with the external disturbances, initial vibrations caused by the sudden exertion of these disturbances are expected. Once these vibrations have been damped, the external disturbances vary slowly over time (with the exception of eclipses), generating long term oscillations. These low frequency oscillations are not targeted by any of the controllers. There are also high frequency vibrations, linked to two main sources: 1) magnetorquer duty cycle and 2) sudden variation in the solar pressure due to the immersion or coming out of an eclipse.

In order to analyze the vibrations produced by the external disturbance related with eclipses, the deformations of the booms in the z-axis are studied. This axis is selected because it is the axis aligned with the sun vector in the operating point. The evolution of this variable, using the three different controllers mentioned, is shown in figures 5.29 and, in appendix K, K.6. It can be seen that controller 3 is able to damp the vibrations appearing after coming in or out of an eclipse. This is mainly due to the additional constrain over the deformation of the booms and is only possible due to the exertion of a control force. An example of the force needed is shown in figure 5.31. Controller 2 has a better performance than controller 1, but still radically lower than controller 3.

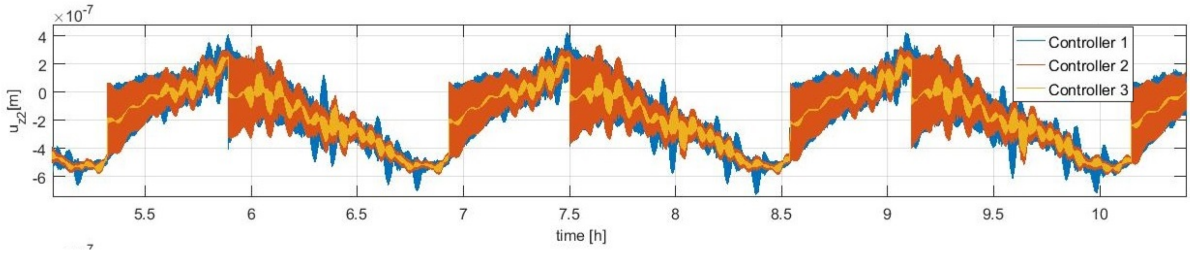

Figure 5.29: Analysis of the evolution of the boom's deformations under non-linear controller with different specifications. Z-axis. Deployed configuration. h: 600 km, i: 97 deg, Ω: 0.

In order to analyze the vibrations caused by the magnetorquer duty cycle, the deformations in the x and y axes are analyzed. This is done in order to minimize the appearance of vibrations linked to the eclipses. The results are included in figures 5.30 and, in appendix K, K.7. In those figures it is possible to see that there are long term oscillations in the deformation of the booms, which are, as previously mentioned, linked to the change in the external disturbances. Regarding the high frequency vibrations, it can be seen that both controllers 2 and 3 have a better performance than controller 1 regarding damping them. This was expected from the results shown in figure 5.28.

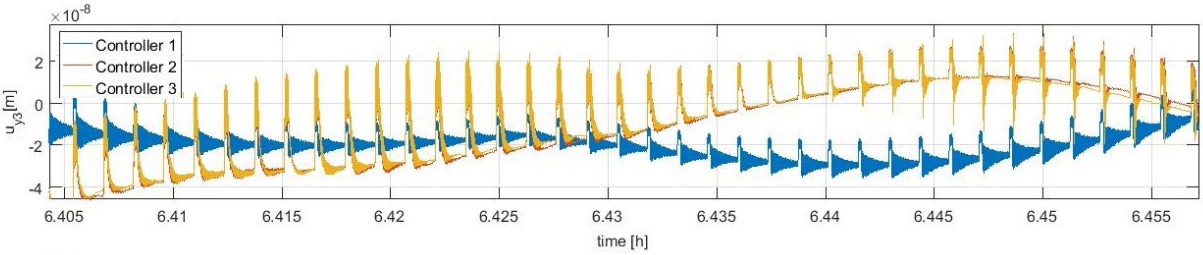

Figure 5.30: Analysis of the evolution of the boom's deformations under non-linear controller with different specifications. X,Y-axes. Deployed configuration. h: 600 km, i: 97 deg, Ω: 0.

Finally, some comments on the control force allowed in controller 3 are made. The force command resulting from the implementation of the non-linear control approach explained is manipulated to extract the steady terms. This is done by subtracting the moving average. However, more sophisticated methods can also be applied, depending the necessities of the actual actuator to be used. It is mainly used to minimize the vibrations related to eclipses. An example of the control force generated after going out of an eclipse is shown in figure 5.31 (extended in appendix K, K.8). The damping of the vibrations is considerably fast, of the order of seconds, which means that the magnitude of the force could be lowered considerably and still actively damp these vibrations. It can also be seen that the force is exerted mainly in the z-axis direction, as expected due to the alignment of this axis w.r.t the sun.

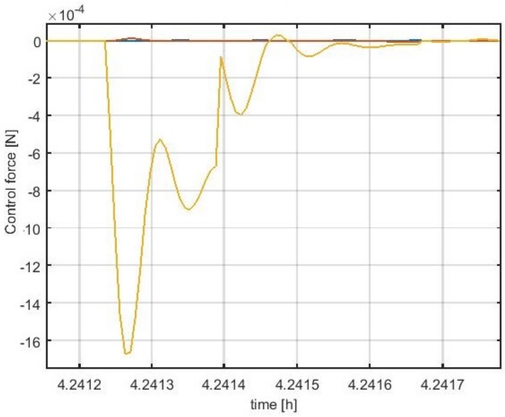

Figure 5.31: Analysis of the control force exerted over the spacecraft by controller 3. X-axis (blue), Y (red) and Z (yellow). Deployed configuration. h: 600 km, i: 97 deg, Ω: 0.

5.6. Controllers' implementation

At this stage of the project, several ADCS designs have been defined and their performances studied. There are, however, two main areas that the analyses performed do not cover. First of all, the analyses where performed over the ideal case, meaning that the controller has access to both the real values of the variables measured (ideal sensors) and to the real specifications of the plant (e.g. moment of inertia). This is never the real case. Additional analysis to evaluate how the performance of each controller would be on a more realistic situation are, therefore, to be run. The second area still to be studied includes the needs of each controller in relation with the rest of the ADCS. This topic has been already mentioned, but not covered in detail. It includes aspects such as sensors needed, computational cost and control frequency. These aspects change enormously depending on the controller and, therefore, deserve a more detailed analyses.

5.6.1. Sensibility

The most common strategy to study the sensibility of the performance of the ADCS design to errors in the system's parameters, is to conduct a Monte Carlo analysis. This analysis is based in defining the distributions that these parameters follow (e.g. normal distribution with standard deviation x and centered in the nominal value). Then the case (simulation) is run a large number of times, analyzing the distribution of the results. In each run the parameters of the system are obtained again, according to their distribution. For the case studied here, the available time and computational resources prevent from using this approach. This is mainly because the performance of the controller is linked to the long term evolution of the variables (i.e. pointing accuracy) and, therefore, each run takes a considerable amount of time. It is also important to highlight that this analysis aims only to give an initial idea of the sensibility of the controller, not to study it in detail.

It was decided then to use a deterministic approach, based on a sampling grid. This way, errors in the specifications of the system where defined, and their consequences over the performance studied. This approach allows investing a lower amount of computational and time resources. On the other hand, a Monte Carlo analysis would, most probably, allow a more complete an accurate analysis. In addition to the study of how different errors in the structure's model affect the performance of the controllers, they behavior w.r.t. noise in the measurements is also studied. Four controller are evaluated: 1) LQR controller, 2) H_∞ controller, 3) non-linear controller based in rigid equations of motion and 4) non-linear controller based in flexible equations of motion and including a control force. The sensibility analysis is composed of:

- Effect of errors related with the moment of inertia in the pointing accuracy.
- Effect of noise in the measurements in the pointing accuracy.
- Effect of errors related to the booms specifications in the damping effectiveness.
- Effect of noise in the damping effectiveness.

Figure 5.32 shows the effect of a 5% error in the estimation of the different terms of the moment of inertia when using the LQR controller. Additional cases are added in appendix L, figure L.4. It can be seen that the difference in performance is considerably small, less than 1 degree, and that the sensibility is higher for errors in the z-axis component of the moment of inertia. Furthermore, the results lead to the conclusion that this difference is not dependent in the initial conditions and it has an oscillatory nature.

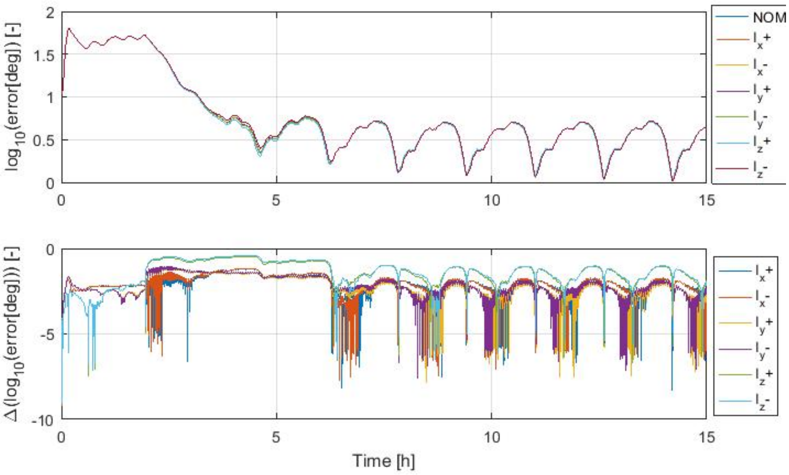

Figure 5.32: Difference in the pointing accuracy due to errors in the estimation of the moment of inertia. LQR controller.

Those conclusions (i.e. higher sensibility w.r.t the z-axis component, oscillatory nature and independence from initial conditions) are also applicable for the non-linear rigid controller (see figure L.1 in appendix L). However, the system appears to be more sensible to errors using this controller (non-linear rigid) than with the LQR controller.

In relation with the non-linear flexible controller and with the controller based in the H_∞ norm, the total moment of inertia is not an input for the controller, so errors in this variable are not directly measurable. The total moment of is computed from the moment of inertia of the central part of the satellite combined with the moment of inertia of the booms. The moment of inertia of the booms depends on their deformation, length and linear density. Therefore, the analysis is performed considering errors in: 1) the moment of inertia of the central part, 2) the length of the booms and 3) the density of the boom. The results are shown in figure L.2 (flexible non-linear) and L.3 (H_∞) in appendix L. In both cases the effect of the error in the moment of inertia of the central part of the satellite is not particularly relevant. This was expected, as their relative weight of the central part of the satellite in the total moment of inertia is considerably low ($\approx 10\%$). The parameter with a highest sensibility is the length of the booms, followed by its density. The error is still bounded and becomes considerably small after some time, being independent from the initial conditions and with an oscillatory behavior.

As a second step of the sensibility analysis, the effect of introducing noise in the measurements (which, as mentioned, are ideal in the previous analyses), is studied. Initially, only the effect over the pointing accuracy is studied. The characterization of the noise is based in the sensors' data included in table 2.5. In figure 5.33, the effect of noise on the performance of the LQR controller is shown over a number of cases. It can be seen that at initial times the error induced is considerable, due to the high noise of the coarse sun sensors. Once the spacecraft is oriented towards the sun, which then falls into the field of view of the fine sun sensor, the effect of noise is considerably reduced. This is also the case for the non-linear rigid and flexible controllers (see figures L.5 and L.6 in appendix L.

The effect of noise in the performance of the controller based in the H_∞ norm is, however, devastating. With this controller, the plant does not converge to the operating point, i.e. the satellite is not pointed towards the sun with any meaningful accuracy. For understanding this, the methods used to derived this controller need to be understood. As mentioned in section 5.4.3, for deriving this controller the weight of the response at high frequencies in the cost function is amplified. In the presence of noise, the controller shifts a considerable control effort towards damping non-existing vibrations in the booms, leading to complete loss in performance (see figure 5.34). A potential solution for this problem would be to add an additional weighting function, reducing the importance of high-frequencies in the error signal. This solution has not been applied within this report.

After studying the sensibility of the system w.r.t. the mission requirements (i.e. pointing accuracy), the

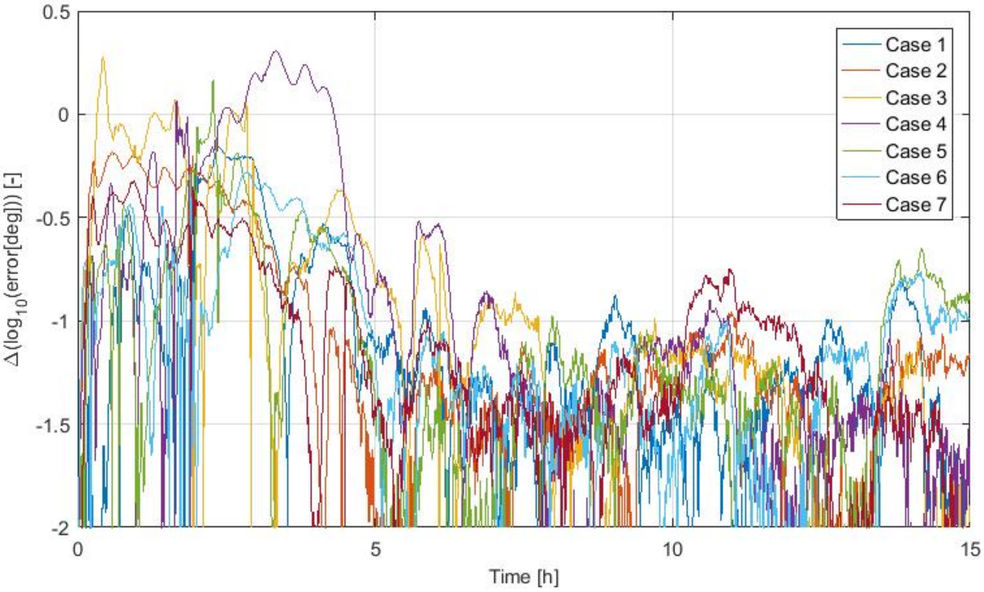

Figure 5.33: Difference in the pointing accuracy due to the addition of noise to the measurements. LQR controller. 7 different cases.

effect of errors and noise in the reduction achieved in relation with the vibrations of the structure is studied. This effect is evaluated in relation to the damping achieved in the vibration of the booms. Therefore, only the controllers targeting these vibrations are analyzed, i.e. H_∞ and non-linear flexible controller. The variable (U) is used to study the sensibility of the controller to these parameters. This variable is related to the potential energy of the booms and is expressed as shown in expression 5.34, where u_i is the deformation of boom i at its tip.

$$U(t) = \sum_{i}^{4} u_i^2(t) \tag{5.34}$$

In relation with the non-linear flexible controller, 8 different cases are studied: 1) using the non-linear rigid controller, 2) nominal case, 3) adding noise, 4-5) error in the length of the boom, 6-7) error in the bending stiffness of the boom and 8) limiting the available knowledge of the controller. It is to be highlighted that the noise is only introduced in the sensors included in table 2.5, i.e. the information regarding the deformation of the booms is ideal. This simplification would need to be reassessed after the sensors to be used to measure these deformations are defined. Case 8 consists in using a controller which only has access to the first mode, over a plant containing the first two modes. The results are shown in figure 5.35 and in figure L.7 (appendix L).

It can be concluded that this controller is not particularly sensible to the variables studied. For all cases studied, the vibrations are highly damped (w.r.t the rigid controller) independently of the estimation error. This damping is particularly noticeable when the control torque is low (i.e. once the operating point is reached). At the beginning the controller focuses more in reaching the operating point than in damping, but still the vibration is reduce considerably.

The results of performing this same analysis over the H_∞ controller can be seen in figure L.8. It can be observed that the mayor decrease in performance (higher U) is linked to the addition of noise. With this noise, the vibrations are of a similar order as when using a controller based in the rigid equations of motion. It is also noticeable, that the controller is more sensible to errors that increase the natural frequencies of the system (decrease in the length of the booms (L-) and increase in the bending stiffness (EI+)) than to those that decreases these frequencies (L+ and EI-).

These analyses in the sensibility of the controllers have identified one mayor problem in relation with one of the controller, the one based in the H_∞ norm. A solution for this challenge is also proposed from a conceptual perspective. In relation with the rest of controllers, the errors and noise analyzed are not a mayor threat to the performance of the controllers.

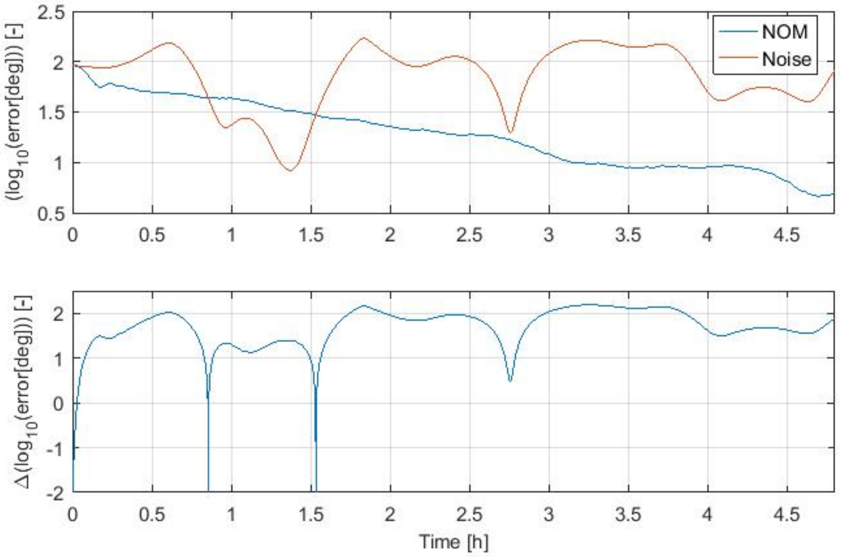

Figure 5.34: Difference in the pointing accuracy due to the addition of noise to the measurements. H_∞ controller.

5.6.2. Feasibility

The other aspect that needs to be studied in relation with each of the controllers proposed, is whether it is feasible to implement this controller in an actual satellite and at what cost. This is evaluated, only from a qualitative perspective, based in three factors:

1. Computational cost associated to computing the control command.
2. Controller time step needed.
3. Sensors and actuators needed.

The computational cost of the LQR controller is considerably low, as constant gains, obtained beforehand, are used. The restrictions on the controller time step are not strict. As no intention of damping the flexible vibrations is needed, the lowest frequency that the controller needs to deal with is linked to the angular rate of the satellite, which is considerably low. The sensors and actuators needed are those described in section 3, and are those that are nominally included in the design of the GoSolAr mission. This controller can be implemented relatively easy and no relevant problem are expected in this regard.

In relation with those controller based on robust control (i.e. H_∞ and H_2), the computational cost is considerably higher. This is because the control command is not based in the use of fixed gains but it consists in a linear time invariant system. The computational cost can be linked to the order of this linear plant. Therefore, the objective is to reduce the order of the controller as much as possible without losing performance. This is done using two approaches based in two MATLAB functions, see example in appendix H.

- *minreal*, which "eliminates uncontrollable or unobservable state in state-space models, or cancels pole-zero pairs in transfer functions or zero-pole-gain models".
- *reduce*, which reduces the order of the system based on the Hankel singular values.

In relation to the minimum frequency needed for each controller, it can be derived from its natural frequencies. This way, for example, the controllers shown in figure 5.15 have the following maximum natural frequencies: *Constant weight*: 3.7e4 Hz, *F1e65*: 1.7e3 Hz, and *F1e8*: 3.68e3 Hz. It can be seen that even without aiming to reduce the response at high frequencies, the controller operates at high frequencies. A common approach to reduce this frequency is to increase the cost of the control torque for high frequencies, in a similar way as it was done with the error weighting functions. However, the implementation of this approach has not provided any benefit, as the frequencies remain on the same range or the performance drops dramatically.

The sensors and actuators needed do not change w.r.t. the LQR controller. These controllers can be implemented relatively easy and no relevant problem are expected in this regard. It can be concluded that these

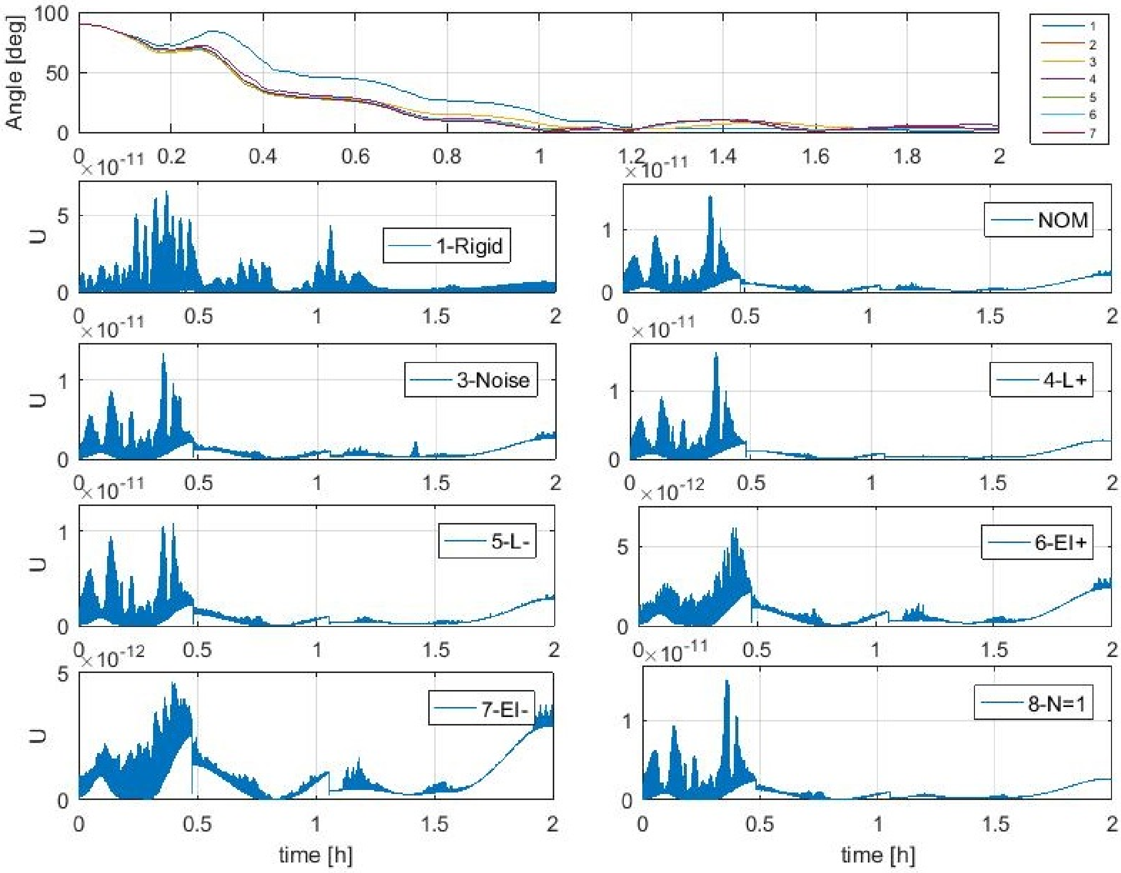

Figure 5.35: Difference in the pointing accuracy and in the vibration of the booms (U) due to errors in the estimation of bending stiffness (EI) and length of the booms (L) and limitation in control information (N=1 only first mode available). Non-linear flexible controller.

controllers (H_∞ and H_2) require an increase in the computational power available and a huge increase in the control frequency.

The non-linear controllers based in the approach presented at [29] both require an increase in the computational power needed w.r.t. the LQR controller. This increase is caused by the need to conduct a mathematical operation (including an inverse of a matrix) for each control step. The matrix to be inverted is, logically, considerably smaller for the case where the rigid equations of motion are considered. The control frequency is linked to the eigen frequencies of the equations of motion considered, being these considerably lower than the frequency needed by the robust controllers. It is also to be mentioned that, in case a feedforward including external disturbances can be accurately implemented, the need of a high frequency controller decreases. W.r.t. the sensors and actuators needed, the rigid controller operates with the set already defined, while the flexible approach requires to have an estimation of the deformation of the booms. Additionally, the capability of exerting a control force can be added.

5.7. Conclusions

In light of the results and analyses presented throughout this chapter, a conclusion in relation to the research objective can be drawn: the effect of the flexibility in a satellite with a large thin flexible structure can be minimized by the derivation and implementation of an appropriate ADCS design. This does not mean that it is convenient to implement this kind of designs to every mission, as it is possible that the effect of flexibility does not interfere with the mission requirements and the implementation of these designs comes always at a price. This cost can differ greatly from one controller to another, including, for example, the need of additional sensors or a higher computational power. Some comments are now made on the most relevant aspects of each of the ADCS designs proposed.

In relation with the GoSolAr mission, the consequences of the flexibility of the structure appear to be limited (see section 5.1.1) and, as expected from the revised literature, the flexibility does not pose an additional threat to attitude requirements of the mission. This is mainly because of the separation between the different frequencies involved: external disturbances, natural modes and controller frequencies (within the controller both the actuators, i.e. magnetorquer, and the computations are considered). It is necessary to highlight that, even though the flexibility does not affect the complying with the mission requirements, the vibrations added to the system may pose a structural problem (e.g. fatigue in joints between the booms and membrane or central part of the satellite).

It is also to be taken into account that the natural frequencies studied are those of the simplified flexible model of the spacecraft. Therefore, the influence of the membrane in the natural frequencies of the system is not considered. Numerical estimations from previous DLR's studies draw values around 0.3 Hz, which changes significantly the quantitative results. Further analyses are needed in order to address this issue.

From a generic approach, it can be concluded that the effect of the flexibility influences the behavior of the structure in three main ways: 1) external disturbances (e.g. sudden change in solar pressure) generate a vibration in the booms, which is then transmitted to the rigid variables, 2) variations in the control torque or force (e.g. due to the magnetorquer duty cycle) generate a vibration in the booms, transmitted then to the rigid variables, and 3) the control process frequency is such that in interacts with this vibrations in the rigid variables, amplifying them. Examples of 1 and 2 are shown in section 5.1.2, while 3 is considered to be out of the scope of this work. The nature of this vibrations (i.e. amplitude, frequency and damping) is affected by the properties of the structure (i.e. bending stiffness, damping coefficient and length and density of the booms). However, it is to be pointed out that several analysis were conducted, changing these parameters and obtaining the same qualitative behavior, i.e. the long term behavior remains unaffected by the flexibility. Needless to say, if these parameters change dramatically, further analyses need to be performed. For structures as the one analysed, the effect of the flexibility is mainly a challenge for missions with either a requirement of highly accurate pointing accuracy stable throughout time, or a limitation in the the vibration of the booms.

W.r.t. the controller based in an LQR approach, its main advantages are its low complexity and the low computational power it requires. In relation to the case of study, i.e. the GoSolAr mission, this controller is able to fulfill the ADCS requirements. Regarding the effect of the flexibility of the structure, is clear that it is not damping in any way the vibrations that appear in the system. This can pose a problem in cases where these vibrations interfere with the objectives/requirements of the mission.

Two additional control approaches have been studied, one based in robust control and the other one in the relation between constrained and controlled systems, from the perspective of analytical dynamics [29].

From the existing methods related to robust control, two were selected, based in the minimization of H_∞ and H_2 norms. The H_2 controller developed does not shown any particular advantage w.r.t. the LQR controller. The H_∞ controller, in the other hand, proved to be able to minimize the vibrations linked to flexible modes which are visible in the attitude variables (e.g. angular rate). This reduces the overall vibrations of the booms as well as enables a better pointing stability. Nonetheless, the pointing accuracy decreases, as part of the control effort is reallocated from minimizing the pointing error to damping the vibrations of the system. The implementation of this ADCS design does not require substantial change in the hardware used, as no additional sensors and actuators are needed. However, the computational cost increases considerably and can become a killer requirement.

The control approach proposed in [29] is not as well known as the two robust control methods just explained, and fewer implementations of this control strategy can be found in the existing literature. However, it shows a great potential in several ways: 1) the control command is based in the actual equations of motion, without simplifications, 2) relative easy implementation of complex constrains and 3) direct integration of a feed-forward component, if needed. This feed-forward was not implemented in the case of study as no real time estimation of the external disturbances is expected, but can play a major role improving the accuracy in other missions.

This approach is applied in two different ways. In the first one, the equations of motion considered are those of the rigid body. Logically, in this approach the vibrations of the system are completely ignored, as they were in the LQR controller. However, the resulting controller has a better performance than the LQR controller, reaching the operating point faster and remaining in that point within a higher accuracy. No relevant disadvantages were found to the implementation of this controller, as the computation cost remains low and no additional sensors or actuators are needed. Therefore, this is considered (a priori) an improvement w.r.t. the LQR controller for cases the flexibility does not play a relevant role.

The other alternative is implementing the control approach over the flexible equations of motion. This has two main drawbacks: 1) the computational cost increases, as a square matrix with the size of the state vector (including deformations of the booms) needs to be inverted at each control step, and 2) the deformation of the booms needs to estimated. In order to estimate these variables additional sensors are needed. However, the controller obtained is able to reduce enormously the effect of the flexibility. Similarly to the H_∞, the pointing accuracy decreases.

Two main lines of work starting from these results can be distinguish. The first one is related with defining and implementing additional ADCS designs. Particularly promising options are: 1) use of the H_∞ norm in combination with a non-linear plant (e.g. [15]), 2) design of an actuator able to provide with a control force such as the one needed by controller 3 in section 5.5.2, and 3) study further possibilities in relation with the control approach proposed in [29]. The second line of work consists in testing the controllers proposed over simple flexible structures (e.g. single candeliver boom). This would enable to analyze their performance and to identify and address any problem that may appear during the implementation in real time and over a real plant.

6

Conclusions and recommendations for future work

The aim of this chapter is to give a complete overview of the work performed during the thesis, highlighting the most relevant results in relation to the research objective (enunciated below) and to the research questions (see section 1.3). It also includes several ideas for future work.

The research objective is to contribute to the development of attitude control concepts applicable to large thin flexible structures in space. This aim is achieved by evaluating the performance of different control concepts applied to this type of structures. This evaluation is based initially in existing literature, evolving then into simulations in a MatLab/Simulink environment.

6.1. Conclusions

The close relation between the project and the GoSolAr mission provides with a realistic case of study of a spacecraft using this type of structure. The relevant properties and requirements of this case of study (research question 1) were defined in collaboration with the rest of the team working in the GoSolAr project. After defining the case of study, the use of the simulation tools already developed by DLR allowed to move fast towards the innovation elements in the research (i.e. modeling of flexible structures and attitude controller designs targeting flexible structures).

Before going through the results and conclusions over those two major topics, some aspects of the analysis shown in section 3, which does not takes into account the flexibility of the plant, are worth mentioning. That analysis, which contains the answer to research question 2, pointed out some challenges in relation to the case of study and, more generally, to the control of LTFSs (large thin flexible structures). W.r.t. a generic LTFS, two main challenges are identified: 1) strict size and mass restrictions for the actuators, when compared to the moment of inertia and size of the deployed structure, and 2) increase in the disturbance torques due to an increase in the moment of inertia and effective area. In the particular case of study evaluated, the first challenge is translated into a limitation in the length of the magnetorquer, so that it fits in the central part of the satellite. The effective area in the membrane plane increases two orders of magnitude after deployment and the moment of inertia one order of magnitude, increasing the disturbances. Furthermore, in the case of study the distance between the center of mass and pressure increases considerably after deployment (see figure 2.1), contributing also to the increase in the torque disturbances. An additional challenge, for the particular ADCS design proposed in the case of study, is using only a magnetorquer to control the attitude of the satellite. This leads to a locally under-actuated spacecraft, in which no control torque can be applied in the direction of the local magnetic field. Even thought this initial analysis assumes the spacecraft is a rigid body (i.e. neglecting the effect of the flexibility of the structure), it helped to identify different aspects in which the structural particularities of LTFSs can affect the design and performance of the ADCS. These aspects can have, depending on the specifications of the mission, a higher importance than the flexibility of the structure.

Research question 3 is answered throughout chapter 4, where a methodology for integrating the flexibility of a structure into the equations of motion is explained and implemented for a particular case. This method is based in the use of Lagrange's equations combined with the approach known as assumed modes method, which is based in decomposing the flexible motion into a series of flexible modes. The implementation of this methodology over a particular structure gives a step-by-step example on how this approach can be used to obtain a meaningful model of a flexible structure. This modeling approach leads to a definition of the equations of motion of the object containing both the flexible and the rigid motion of the structure. These equations, in combination with the simulation environment, give an insight in the behavior of LFTSs in space. This way, for example, the duty cycle of the magnetorquer and the interaction with the solar pressure before and after going through an eclipse are identified as sources of vibrations for the satellite. Even though the process to derive these equations is mathematically and conceptually complex, the final plant obtained is relatively simple and of low order. This allows to use the model to derive attitude controllers targeting not only the rigid motion of the spacecraft but also the effect of the flexibility. The most relevant challenge or limitation of this modeling approach is the availability of a suitable combination of shape functions and generalized coordinates. This combination should be able to accurately describe the continuous flexible structure using a discrete number of coordinates, related to flexible modes. In the structure studied, the only flexible elements are booms, which lowers the difficulty of finding this combination but also lowers the final accuracy. In is also to be taken into account that the inherent mathematical complexity of the derivations and assumptions, require that the final equations of motion obtained are verified.

The derivation of a model that integrates the flexibility of a structure into its equations of motion is a huge step forward in relation to the research objective. It allows to evaluate, both qualitatively and quantitatively, the effect that the flexibility has in the dynamics of an LTFS as well as the interaction of the ADCS system with the flexible modes of the system. Furthermore, it provides with the knowledge and tools to define an ADCS design able to reduce the negative effects of the flexibility. In relation to the GoSolAr mission, it was soon concluded that the flexibility of the satellite's structure does not pose a threat to the mission requirements. The limited size of the structure (5x5m^2) leads to a system with natural frequencies that do not overlap with the frequencies of the external disturbances or of the control. The relatively lenient pointing accuracy requirement (10 degrees) is, thus, not threaten by the flexibility of the satellite. Therefore, for this particular mission, a conventional ADCS design is able to comply with the mission requirements, which can be met with the set of sensors and actuators described in section 2.

Research question 4 is answered in three steps, explained in chapter 5: derive controllers (4a), analyse each controller's performance (4b) and study each controller's requirements (4c). The controllers derived are based in three main control approaches: linear-quadratic regulator (LQR) approach, robust control approach (i.e. minimization of H_2 and H_∞ norms) and analytical dynamics approach (i.e. Udwadia-Kalaba approach). The LQR controller was the first one used, due to its relative simplicity. The controllers based on robust control theory were then seen as a potential solution to redirect the controller towards damping the natural modes of the structure. Finally, the approach based in analytical dynamics was used due to its capability of integrating the knowledge of the equations of motion of the structure into the controller. The analyses performed over the different controllers derived from those three approaches lead to the conclusion that the effect of the flexibility can be minimized, i.e. the vibrations of the structure can be damped. However, it comes at the cost of lowering the performance of the ADCS in other area (e.g. pointing accuracy). Regarding the particular findings w.r.t. the ADCS designs evaluated, one main conclusion can be drawn: there is not one ADCS design which is optimal for all missions. The difference in requirements of each controller is not trivial, as aspects as the computational power required or the set of sensors and actuators needed can vary considerably. Therefore, each combination of mission requirements and available sensors, actuators and computational power leads to a different optimal design for the controller. For example, for the GoSolAr mission the optimum control solution (of those studied) appears to be the analytical dynamics controller derived from the rigid equations of motion (see section 5.5.1). However, in case rotation wheels are used (i.e. avoiding local under-actuation and the influence of the magnetorquer duty cycle) and enough computational power is available, the H_∞ controller could become the optimal one (see section 5.4.3). A more extreme case is one in which the 'cost', in terms of additional sensors and actuators and computational power, is not a critical issue and the vibration of the system needs to be minimized against all disturbances (e.g. eclipse). In this case the best option may be the analytical dynamics controller based in the flexible equations of motion (see section 5.5.2) could lead to a better performance, as it uses a more complete model of the plant.

The fact that each mission should be analyzed in detail before choosing which controller is most convenient, does not mean that the results presented in this report are inconclusive or that research question 4 is not answered. Rather the opposite, those results are a consistent basis to be used to make that choice, giving an understanding of the performance and requirements of each of the designs evaluated. This is aligned with the research objective, in the sense that multiple attitude control concepts are developed and evaluated w.r.t. large thin flexible structures in space, proving that the effect of the flexibility can be minimized and gathering knowledge and qualitative and quantitative data regarding potential ADCS designs.

Summing up, the two major achievements presented on this work are: 1) a process of integrating the flexibility of a structure (i.e. satellite) into its equations of motion, verified and giving coherent and meaningful results, and 2) an analysis of the performance and requirements of different designs of attitude controllers, accounting also for the effect of the flexibility of the structure.

6.2. Recommendations for future work

In this last section of the report, several ideas for future work in relation to the research are introduced. These ideas are those the student think most relevant and interesting. Nevertheless they are not the only possibilities and the reader is encouraged to use his/her expertise and imagination to find additional paths. The ideas here presented are only briefly introduced and no detailed technical discussions are included. There are two tasks that are considered particularly promising, having the potential to push the research considerably forward. These task are:

- Integrate the membrane into the analytical equations of motion.
- Test, experimentally, the different controllers here designed.

Several possibilities for integrating the membrane into the flexible model are considered in section 4.3. The most accurate would be applying the same procedure used for modelling the flexibility of the booms but this time with the membrane. The main difficulty facing when trying to do this is finding a set of generalized coordinates and shape functions able to accurately convert the continuous problem into a discrete one. This is not a trivial problem and would require an in-depth research. However, once (if) this set is found, the derivation of the model would be quite similar to the one shown in chapter 4, which can, therefore, be used as a guideline.

Throughout the research presented in this report, several controllers are designed and evaluated. However, this evaluation is based purely in simulations, no experimental tests were conducted. Testing the controllers over the actual structure of the satellite would be considerably difficult and expensive and, therefore, it is not the option proposed by the author. However, testing the controller over a simple flexible structure (e.g. single boom) would allow gaining a deeper understanding on the challenges that their implementations present (e.g. control frequency) as well validate the methodology followed. A relatively simple set-up that could be used for this testing consists on: 1) single boom, with all properties well known, 2) attached (candeliver) to an element to which forces and torques can be applied, 3) with sensors to estimate the deformation of the boom, e.g. piezoelectric sensors. The last condition is due to the fact that for testing some of the controllers it is necessary to know the deformation of the boom.

Bibliography

[1] Giulio Avanzini and Fabrizio Giulietti. Magnetic detumbling of a rigid spacecraft. *Journal of guidance, control, and dynamics*, 35(4):1326–1334, 2012.

[2] Jeremy Banik, Steve Kiefer, Matt LaPointe, and Pete LaCorte. On-orbit validation of the roll-out solar array. In *2018 IEEE Aerospace Conference*, pages 1–9. IEEE, 2018.

[3] Itzhack Y Bar-Itzhack and Richard R Harman. Optimized triad algorithm for attitude determination. *Journal of guidance, control, and dynamics*, 20(1):208–211, 1997.

[4] Olivier Andre Bauchau. *Flexible multibody dynamics*, volume 176. Springer Science & Business Media, 2010.

[5] A Bolle and C Circi. Solar sail attitude control through in-plane moving masses. *Proceedings of the Institution of Mechanical Engineers, Part G: Journal of Aerospace Engineering*, 222(1):81–94, 2008.

[6] Andrea Colagrossi and Michèle Lavagna. Fully magnetic attitude control subsystem for picosat platforms. *Advances in Space Research*, 2017.

[7] Ofer Eldad, E Glenn Lightsey, and Christian Claudel. Minimum-time attitude control of deformable solar sails with model uncertainty. *Journal of Spacecraft and Rockets*, 54(4):863–870, 2017.

[8] Juan M Fernandez, Lourens Visagie, Mark Schenk, Olive R Stohlman, Guglielmo S Aglietti, Vaios J Lappas, and Sven Erb. Design and development of a gossamer sail system for deorbiting in low earth orbit. *Acta Astronautica*, 103:204–225, 2014.

[9] Carlton L Foster, Michael L Tinker, Gerald S Nurre, and William A Till. Solar-array-induced disturbance of the hubble space telescope pointing system. *Journal of Spacecraft and Rockets*, 32(4):634–644, 1995.

[10] Hassen Fourati and Djamel Eddine Chouaib Belkhiat. *Multisensor Attitude Estimation: Fundamental Concepts and Applications*. CRC Press, 2016.

[11] Bo Fu, Evan Sperber, and Fidelis Eke. Solar sail technology—a state of the art review. *Progress in Aerospace Sciences*, 86:1–19, 2016.

[12] Torkel Glad and Lennart Ljung. *Control theory*. CRC press, 2014.

[13] JT Grundmann, P Spietz, P Seefeldt, and T Spröwitz. Gossamer deployment systems for flexible photovoltaics. In *67th International Astronautical Congress 2016*.

[14] Da-Wei Gu, Petko Petkov, and Mihail M Konstantinov. *Robust control design with MATLAB®*. Springer Science & Business Media, 2005.

[15] Congying Han, Jian Guo, and Alexandre Pechev. Nonlinear hinf based underactuated attitude control for small satellites with two reaction wheels. *Acta Astronautica*, 104(1):159–172, 2014.

[16] I Harris and W Priester. Relation between theoretical and observational models of the upper atmosphere. *Journal of Geophysical Research*, 68(20):5891–5894, 1963.

[17] John L. Junkins and Kim Youdan. *Introduction to dynamics and control of flexible structures*. American Institute of Aeronautics and Astronautics, 1993.

[18] Jack B Kuipers et al. *Quaternions and rotation sequences*, volume 66. Princeton university press Princeton, 1999.

[19] Kang-Zhi Liu and Yu Yao. *Robust control: theory and applications*. John Wiley & Sons, 2016.

[20] Daniele Romagnoli and Thimo Oehlschlägel. High performance two degrees of freedom attitude control for solar sails. *Advances in Space Research*, 48(11):1869–1879, 2011.

[21] Mark Schenk, Andrew D Viquerat, Keith A Seffen, and Simon D Guest. Review of inflatable booms for deployable space structures: packing and rigidization. *Journal of Spacecraft and Rockets*, 51(3):762–778, 2014.

[22] Christina Scholz, Daniele Romagnoli, Bernd Dachwald, and Stephan Theil. Performance analysis of an attitude control system for solar sails using sliding masses. *Advances in Space Research*, 48(11):1822–1835, 2011.

[23] Aaron D Schutte, David P Arndt, Patrick T Doyle, Darren W Rowen, and Richard M Dolphus. Generalized magnetic attitude control of spacecraft with application to a 0.5 u cubesat platform. *65 International Astronautical Congress*, 2014.

[24] P Seefeldt, T Spröwitz, and JT Grundmann. Verification testing of the gossamer-1 deployment demonstrator. In *67th International Astronautical Congress 2016*, 2016.

[25] Ahmed A Shabana. Flexible multibody dynamics: review of past and recent developments. *Multibody system dynamics*, 1(2):189–222, 1997.

[26] Minghe Shan, Jian Guo, and Eberhard Gill. Review and comparison of active space debris capturing and removal methods. *Progress in Aerospace Sciences*, 80:18–32, 2016.

[27] Stephanie Thomas, Michael Paluszek, Bong Wie, and David Murphy. Aocs performance and stability validation for large flexible solar sail spacecraft. In *41st AIAA/ASME/SAE/ASEE Joint Propulsion Conference & Exhibit*, page 3926, 2005.

[28] Yuichi Tsuda, Osamu Mori, Ryu Funase, Hirotaka Sawada, Takayuki Yamamoto, Takanao Saiki, Tatsuya Endo, Katsuhide Yonekura, Hirokazu Hoshino, and Jun'ichiro Kawaguchi. Achievement of ikaros—japanese deep space solar sail demonstration mission. *Acta Astronautica*, 82(2):183–188, 2013.

[29] Firdaus E Udwadia and Harshavardhan Mylapilli. Constrained motion of mechanical systems and tracking control of nonlinear systems: connections and closed-form results. *Nonlinear Dyn. Syst. Theory*, 15 (1):73–89, 2015.

[30] Glenn Vinnicombe. Frequency domain uncertainty and the graph topology. *IEEE Transactions on Automatic Control*, 38(9):1371–1383, 1993.

[31] Karel F Wakker. Fundamentals of astrodynamics. 2015.

[32] James R Wertz. *Spacecraft attitude determination and control*, volume 73. Springer Science & Business Media, 2012.

[33] Bong Wie. *Space vehicle dynamics and control*. American Institute of Aeronautics and Astronautics, 2008.

[34] Bong Wie and David Murphy. Solar-sail attitude control design for a flight validation mission. *Journal of Spacecraft and Rockets*, 44(4):809–821, 2007.

[35] Bong Wie, David Murphy, Michael Paluszek, and Stephanie Thomas. Robust attitude control systems design for solar sails (part 1): Propellantless primary acs. In *AIAA Guidance, Navigation, and Control Conference and Exhibit*, page 5010, 2004.

A

Simulator strucuture

Figure A.1 shows the structure of the simulink environment used throughout the project. This is based in the Attitude control system simulator for Compact Satellite (CS) developed by the German Aerospace Center (DLR). Further explained in chapter 3.

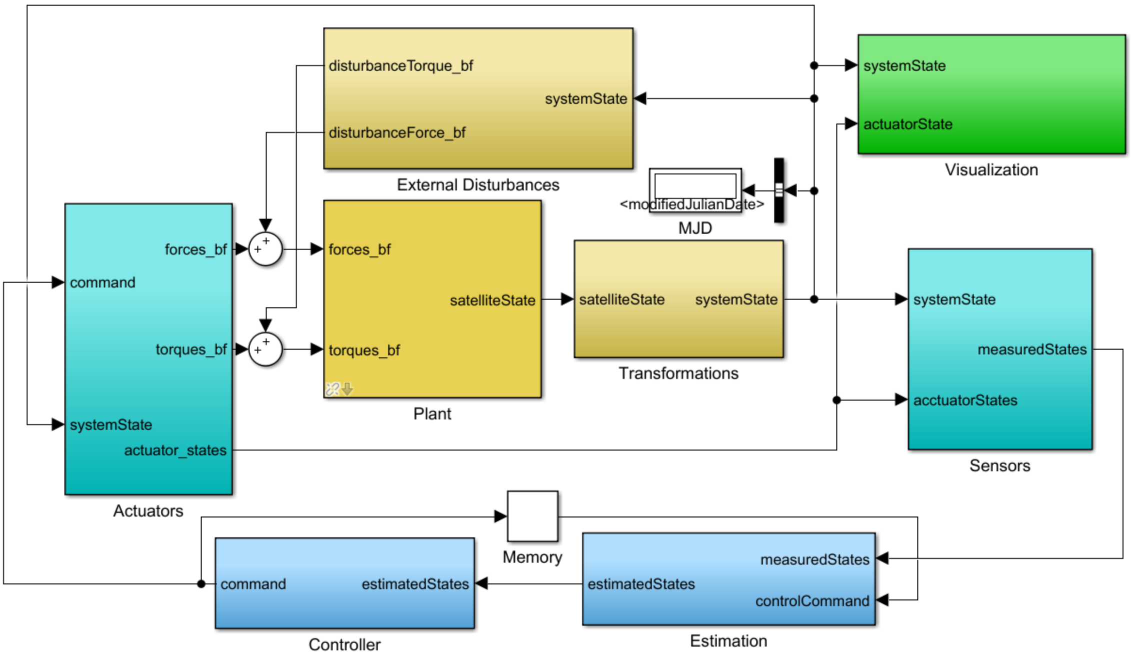
disturbanceTorque_bf
systemState
disturbanceForce_bf
External Disturbances
systemState
actuatorState
Visualization
<modifiedJulianDate>
MJD
forces_bf
command
torques_bf
systemState
actuator_states
Actuators
+
+
+
+
forces_bf
satelliteState
torques_bf
Plant
satelliteState
systemState
Transformations
systemState
measuredStates
acctuatorStates
Sensors
Memory
command
estimatedStates
Controller
measuredStates
estimatedStates
controlCommand
Estimation

Figure A.1: Simulink model.

B

Tunning weights used in LQR controller.

Figure B.1 shows the long term performance of LQR's controllers computed based in different cost matrices. In order to decide which gains to use, three main aspects are taken into account:

1. Long term pointing error. Low relative weights (pointing error w.r.t. angular rate error) make difficult to accurately follow the motion of the sun in the inertial Earth reference frame.
2. Time to convergence to the operating point. Both low and high relative weights increase this parameter, the first due to a lower importance of the pointing error and the second due to the constrains existing over the control torque.
3. Constant errors in the control variables.

Mentioned in chapter 3.

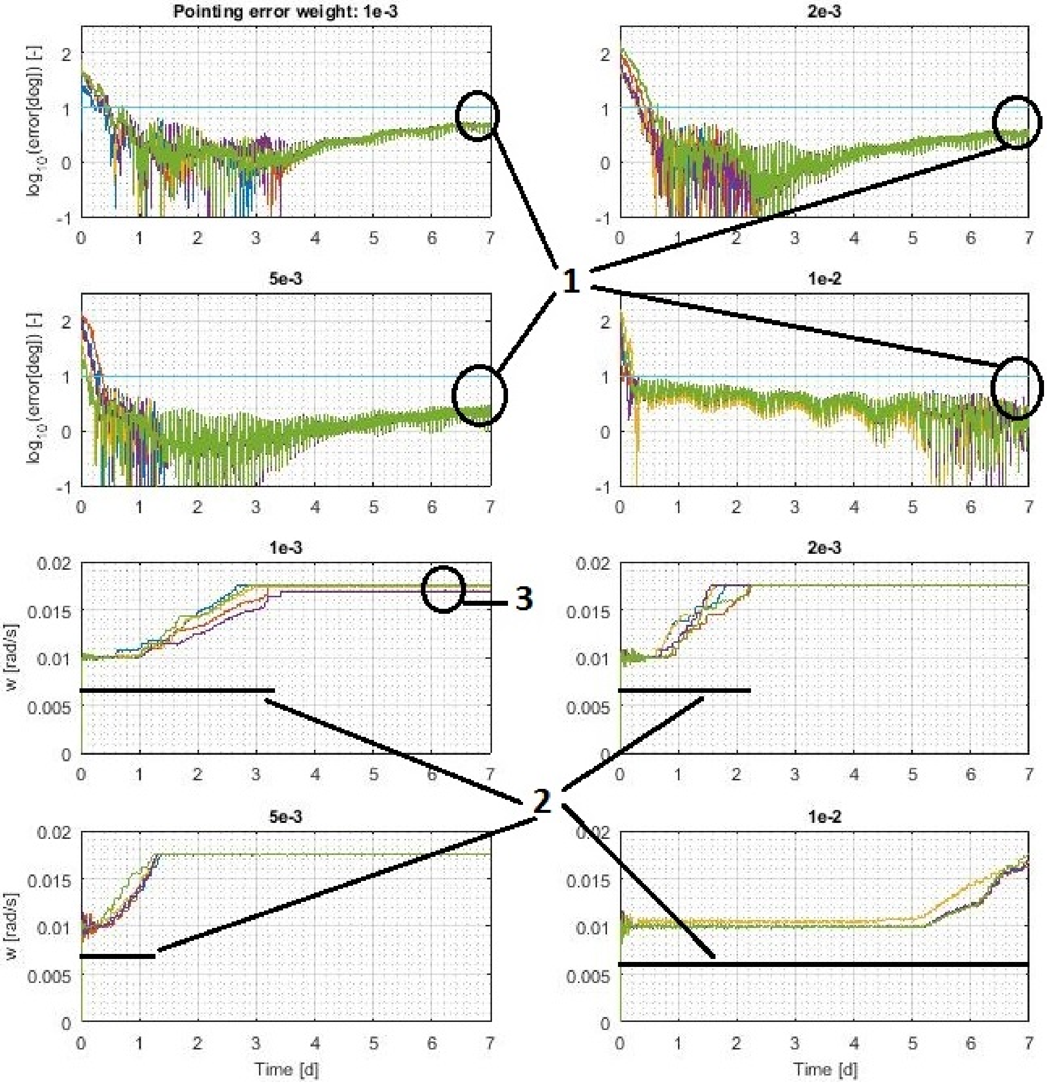

Figure B.1: Evolution of pointing error and angular rate for different weights of the pointing error (5 cases per weight).

C

Altitude limitations

The figures shown here are used for studying the altitude limitation of the mission in chapter 3. Figure C.1 contains an estimation of the deorbiting time for several cases, changing: 1) the launching date (affecting the solar cycle and, thus, the atmospheric density), 2) the success of the deployment (changing the structure of the spacecraft) and 3) the area of the membrane. Figure C.2 shows the detumbling phase of the satellite for different altitudes and for the deployed configuration. Figure C.3 shows the pointing phase of the satellite for different altitudes for the deployed configurations.

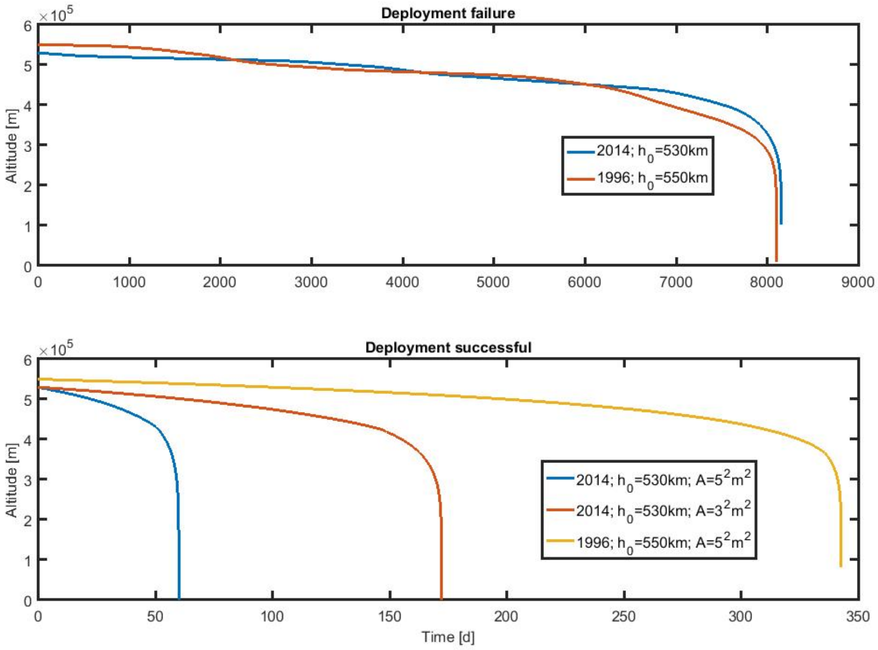

Figure C.1: Deorbiting profiles launching at solar minimum (1996) and maximum (2014). Initial altitude 550 km.

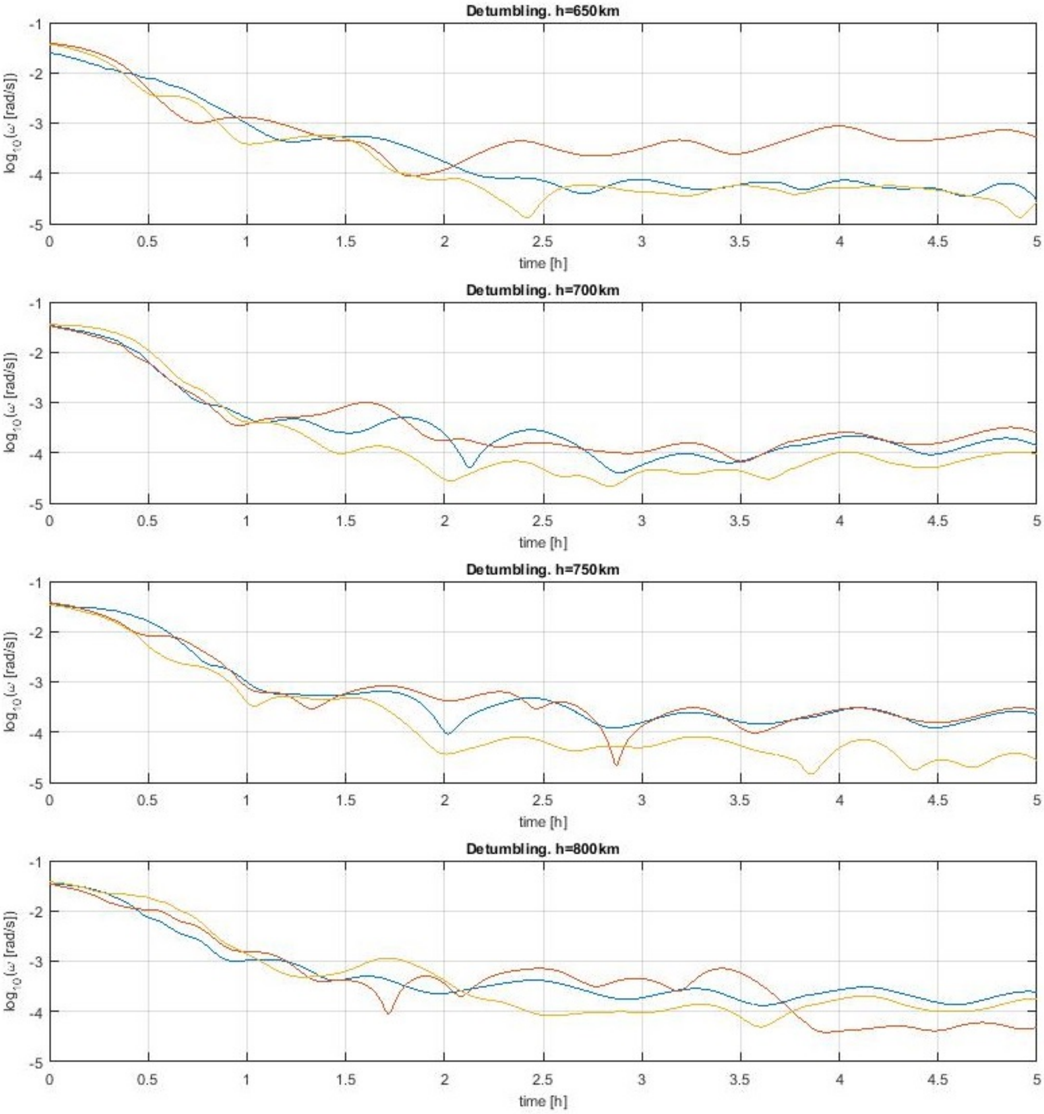

Figure C.2: Study of the detumbling stage for altitudes between 650 and 800 km. Rigid plant. B-dot controller. 3 initial conditions per case.

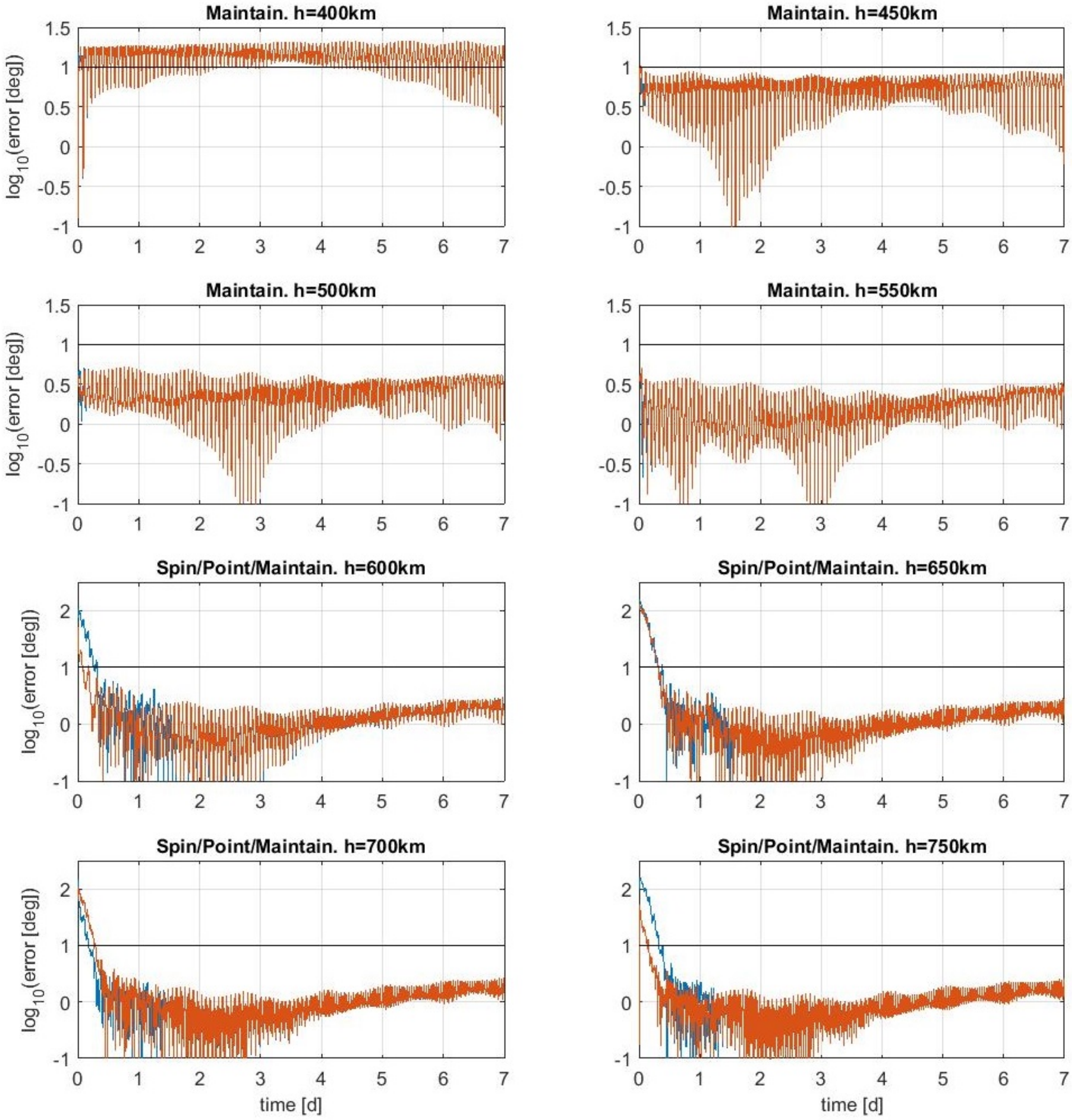

Figure C.3: Study of the pointing stage for altitudes between 400 and 800 km. Rigid plant. LQR controller. 2 initial conditions per case.

D

Analysis of different orbits

The figures contained in this appendix are used for studying potential limitations in the inclination of the orbit due to the locally underactuated satellite (magnetorquers) in chapter 3. Figure D.1 contains the evolution of the angular rate during the detumbling phase. Figure D.2 contains the evolution of the pointing error during the pointing phase.

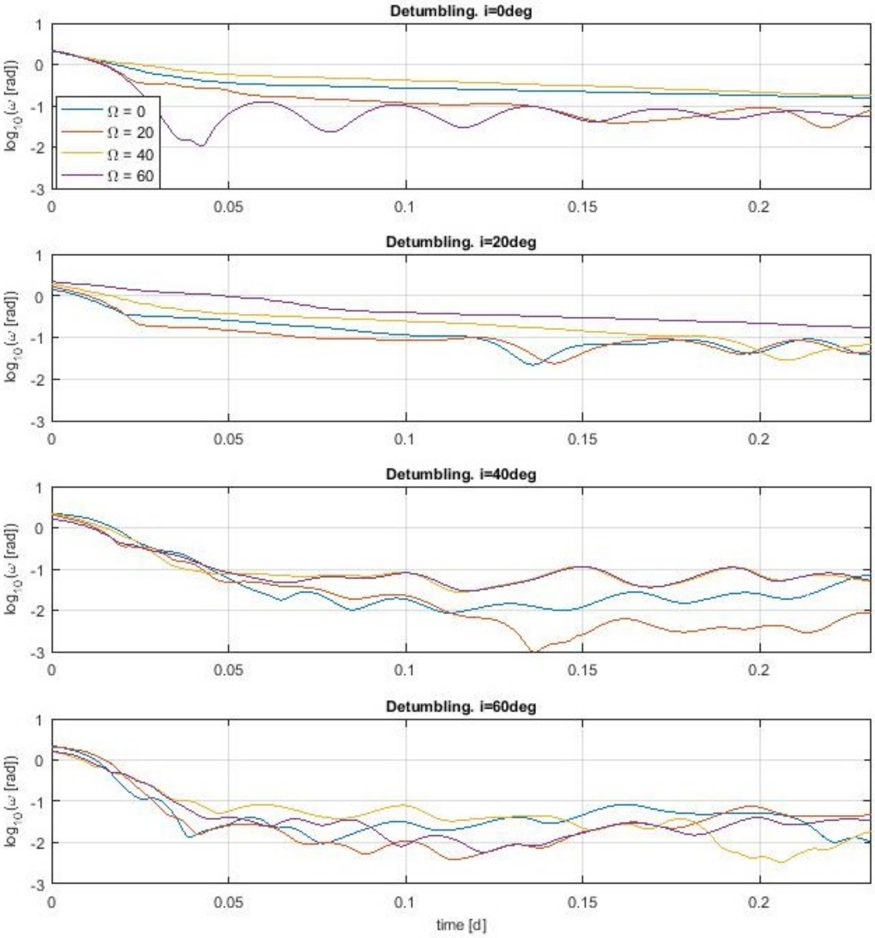

Figure D.1: Study of the detumbling stage for different inclinations and right ascensions of the ascending node. Rigid plant. B-dot controller. h: 600km.

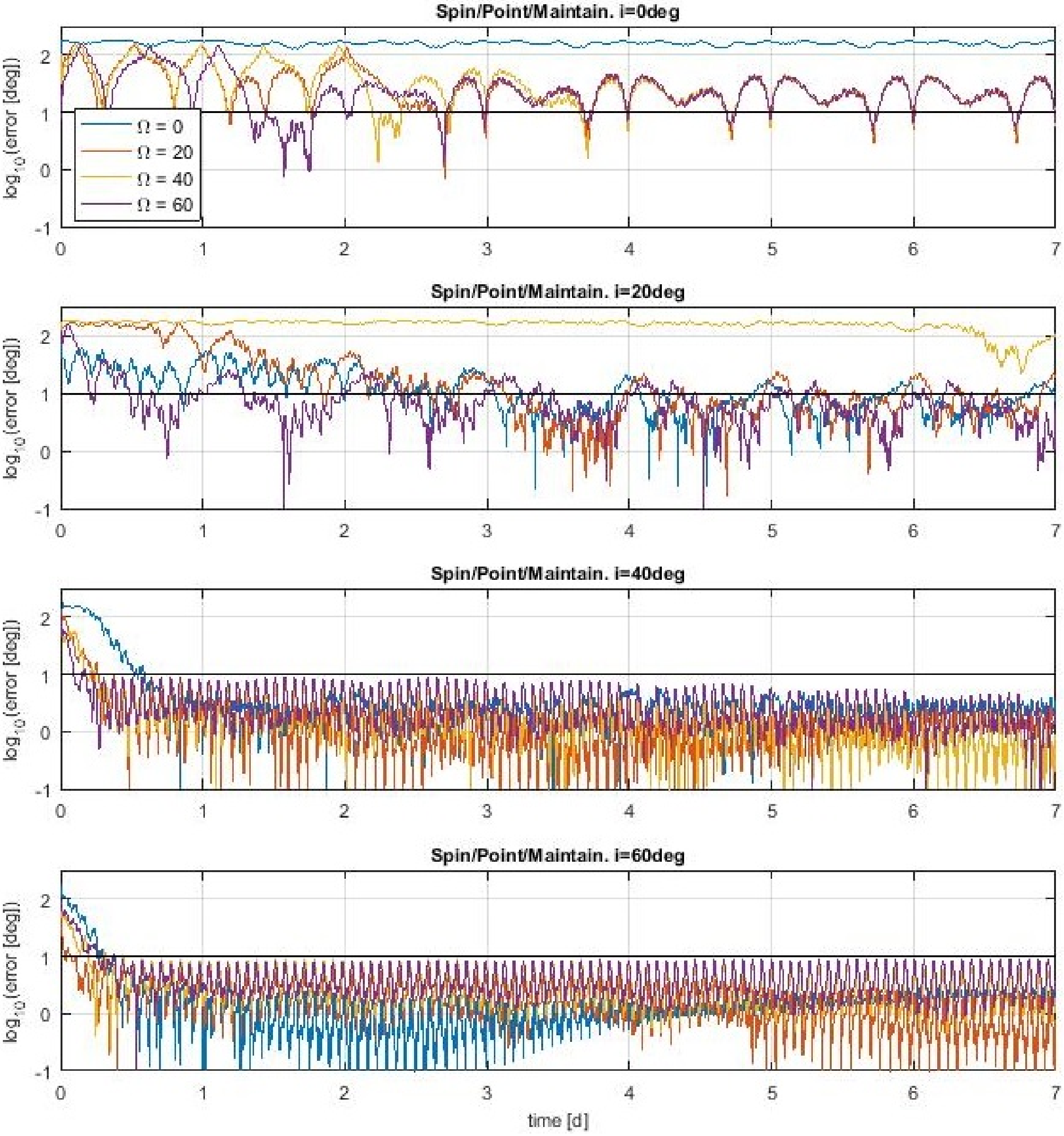

Figure D.2: Study of the pointing stage for different inclinations and right ascensions of the ascending node. Rigid plant. LQR controller. h: 600km.

E

Interaction with eclipse and magnetorquer's duty cycle

The figures shown in this appendix expand the analysis presented in section 5.1.2, explaining the effect of the flexibility in the dynamics of the spacecraft. Figures E.1 and E.2 show the vibration of the booms due to eclipses. Figures E.3 and E.4 show the vibration of the booms induced by the magnetorquer duty cycle and the way this vibration is transferred to the angular rate.

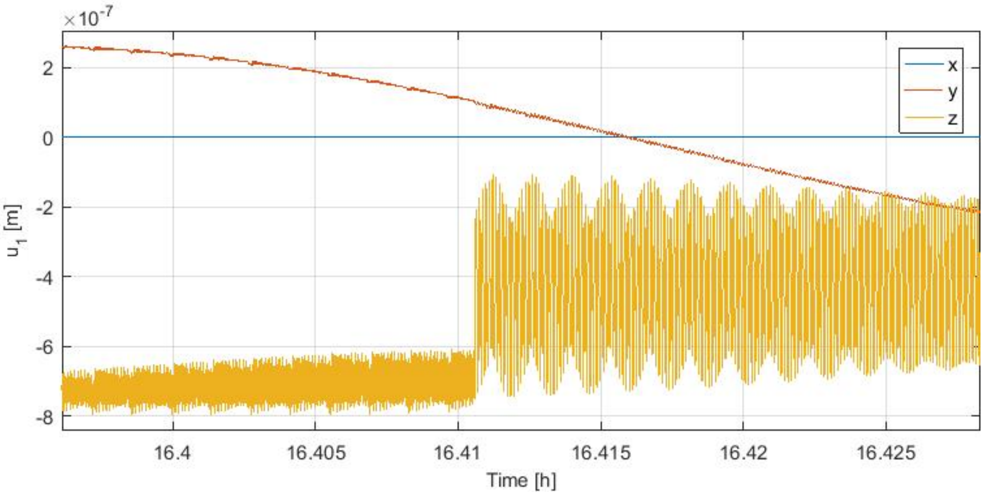

Figure E.1: Zoom in of figure 5.5

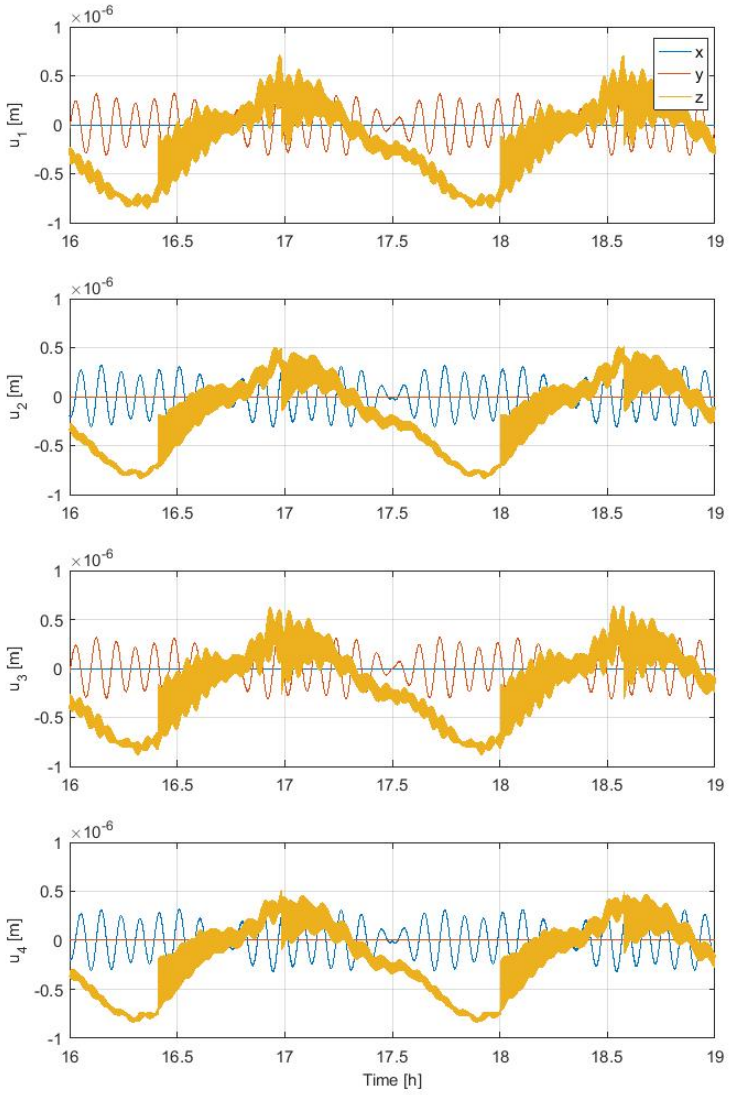

Figure E.2: Vibration of the booms due to entering or coming out an eclipse.

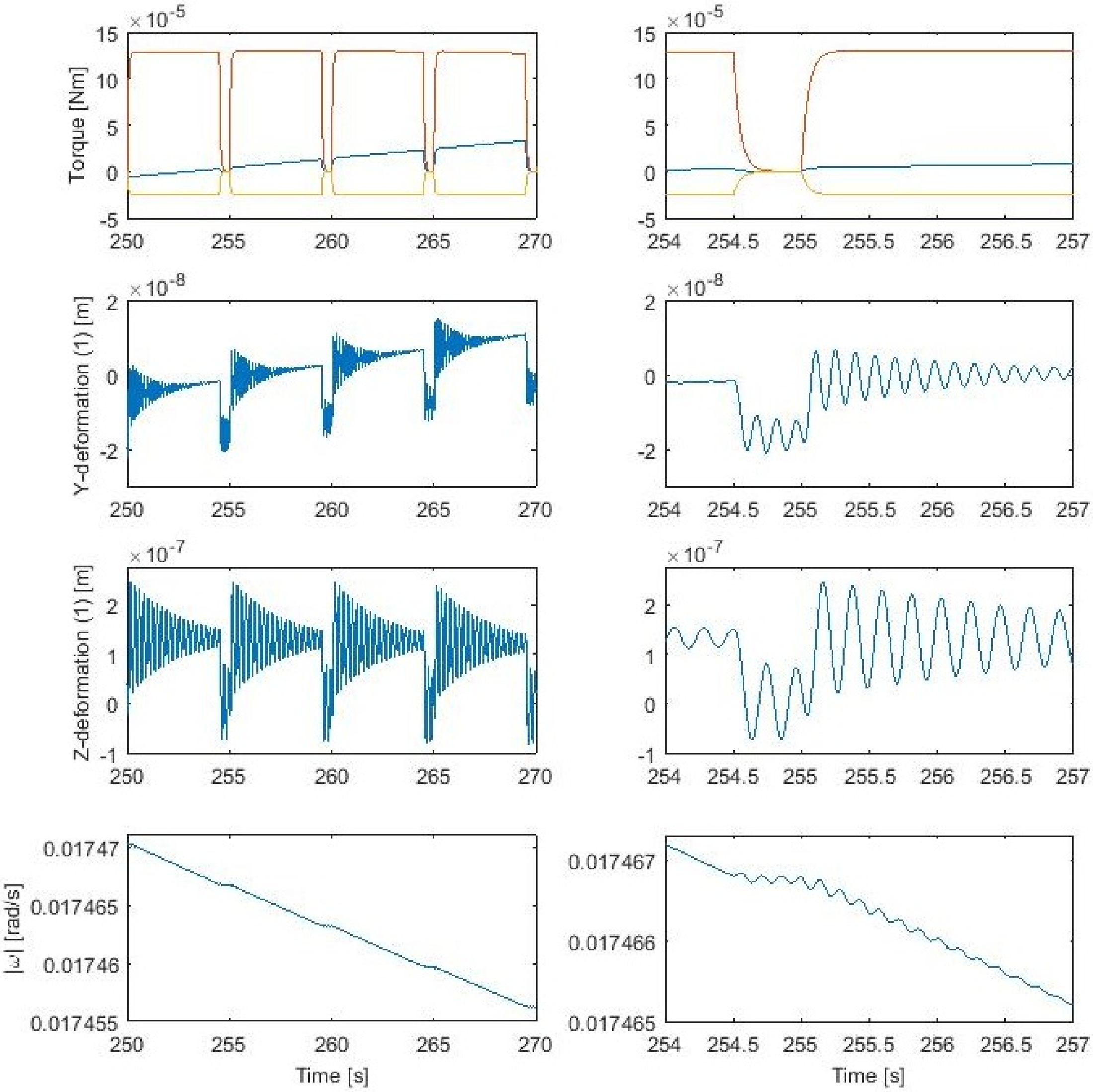

Figure E.3: Zoom in of figure 5.6

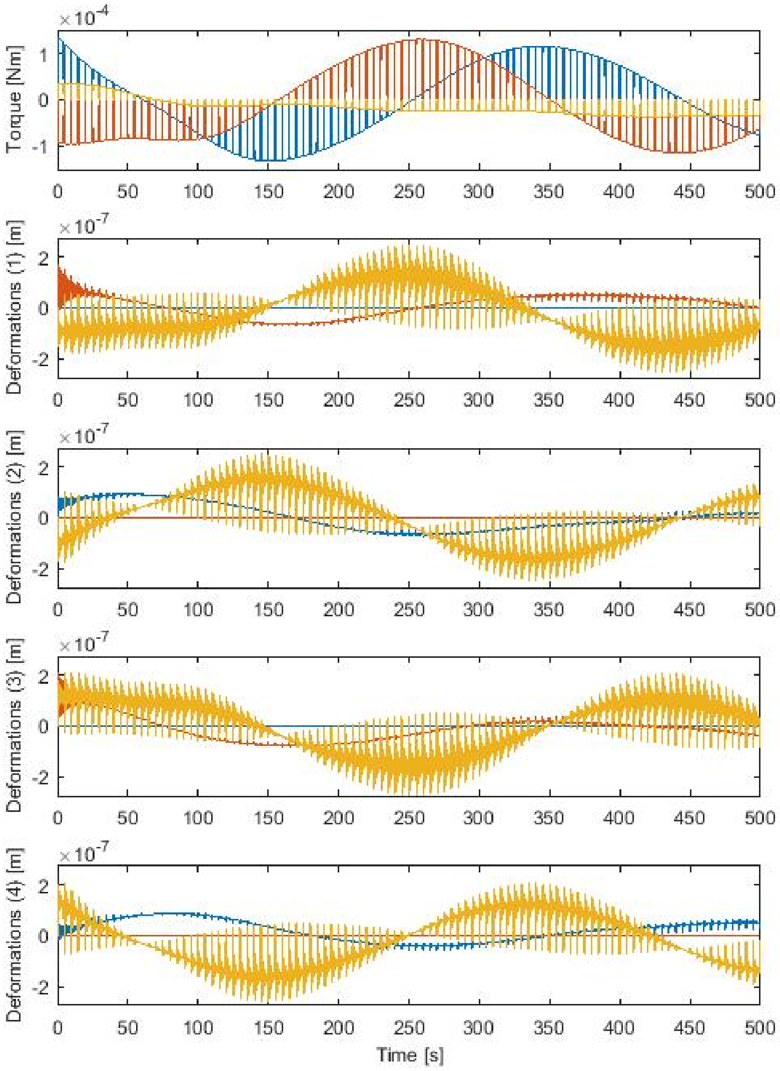

Figure E.4: Interaction of the flexible structure (booms) with the control torque (magnetorquer).

F

Verification of boom model. Example.

The figures in this appendix are related to the verification of the analytical model of a single candeliver boom, which is performed as a previous step to verifying the complete model of the spacecraft (see section 4.4). The response of both the analytical (Lagrange) and numerical (Simscape) models are studied for different number of modes (Lagrange) and elements (Simscape).

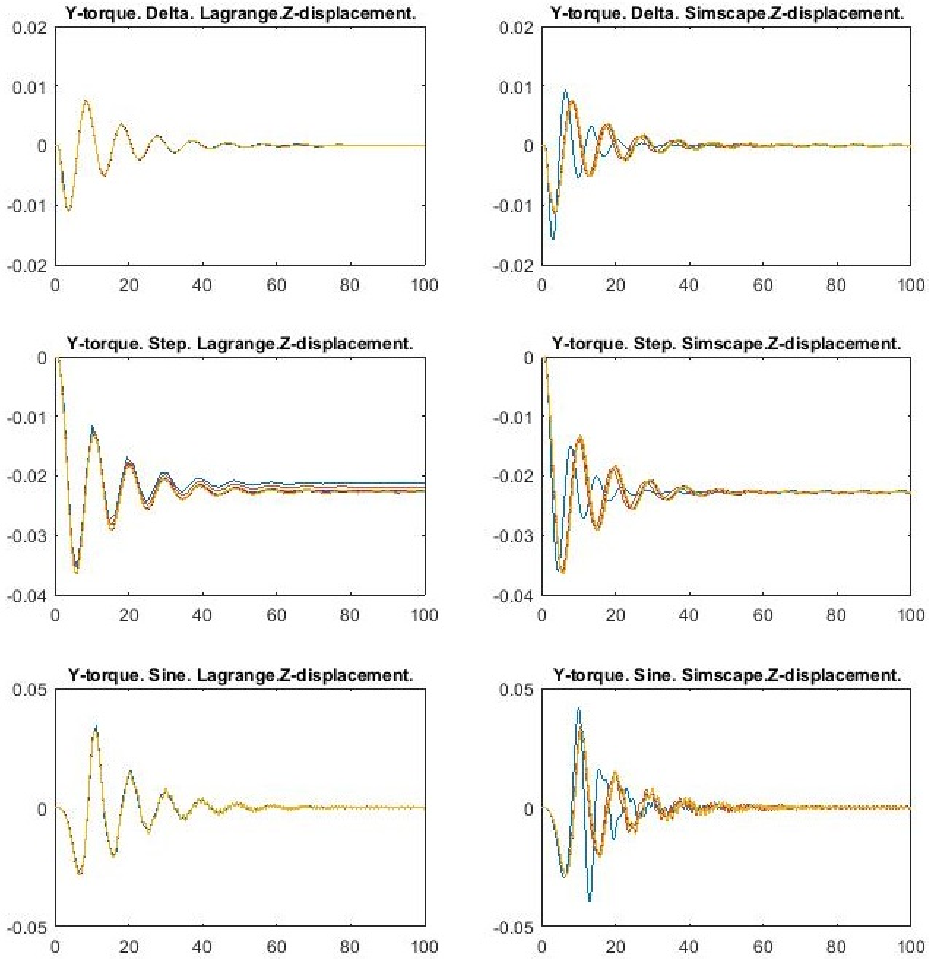

Figure F.1: Comparison of the responses of Lagrange equations and simscape model. Number of modes: 1-10. Number of elements: 1-20.I.

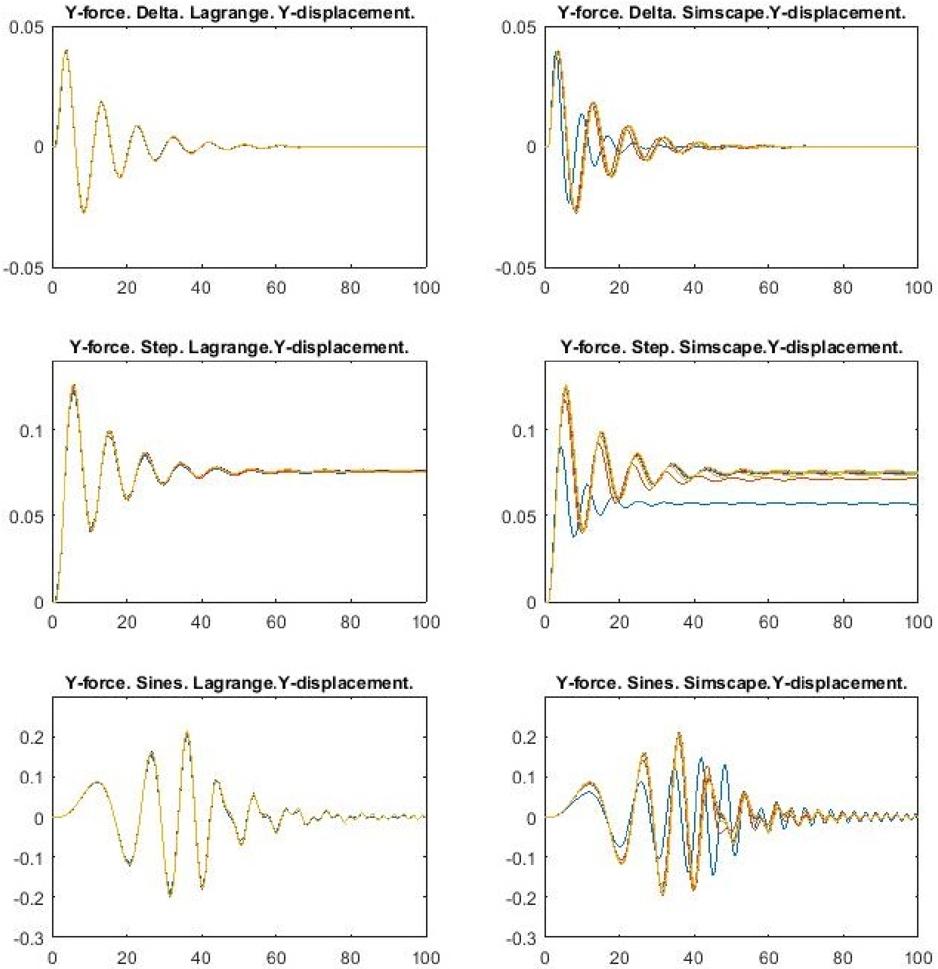

Figure F.2: Comparison of the responses of Lagrange equations and simscape model. Number of modes: 1-10. Number of elements: 1-20.II.

G

Verification of flexible plant.

The figures included in this analysis support the analysis shown in section 4.4.2, which aims to verify the analytical flexible model of the satellite. This is done comparing the evolution of: 1) position (r), 2) velocity (v), 3) attitude quaternion (T), 4) angular rate and 5) deformation of the booms at their tip (u_1 to u_4). The difference w.r.t. the case shown in section 4.4.2 are:

- Case 1: absence of external disturbances.
- Case 2: static external disturbances (instead of periodic).
- Case 3: initial conditions equal to zero.
- Case 4: different initial conditions and external disturbances.

Figure G.7 shows the numerical model built in MATLAB Simscape to verify the analytical model (derived in chapter 4). This model consists in 4 boom attached (candeliver) to a central body. Each boom has a variable number of elements (defined as an input) which are attached to each other using a joint. The rotation of these joints is linked to an elastic coefficient (K) and dissipation coefficient (kd), related to the mechanical properties of the booms. The specific simulink elements used can be seen in figure G.7.

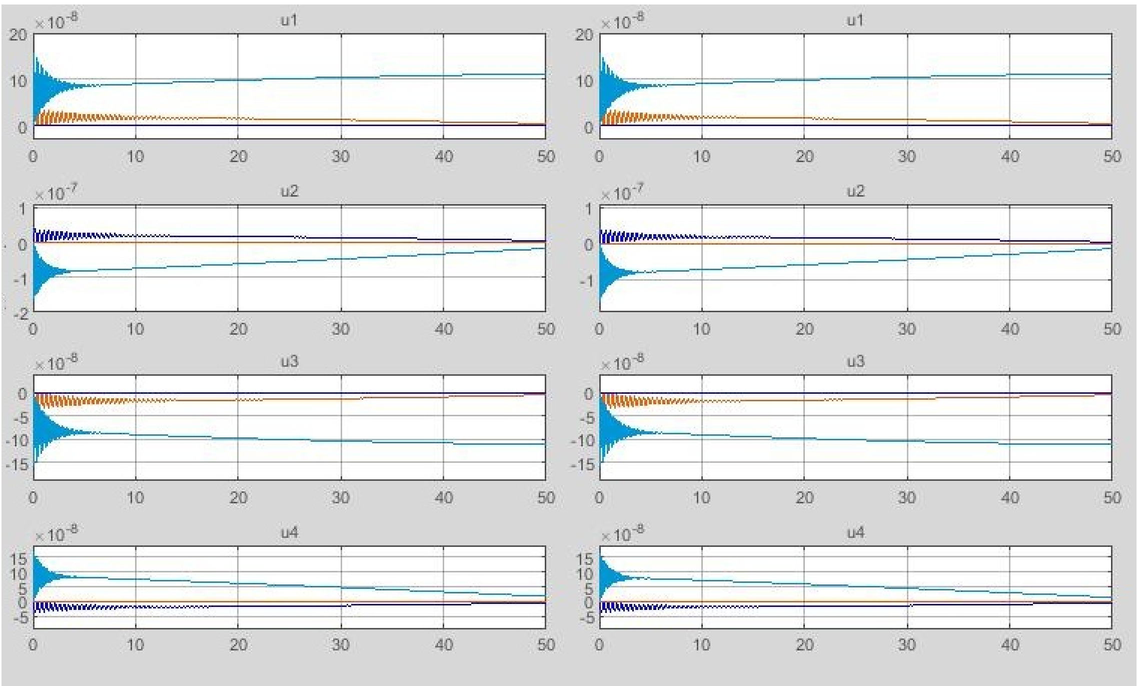

Figure G.1: Comparison of the evolution of the deformation of the booms using analytical (right) and numerical (left) models. Case 1: no external disturbances.

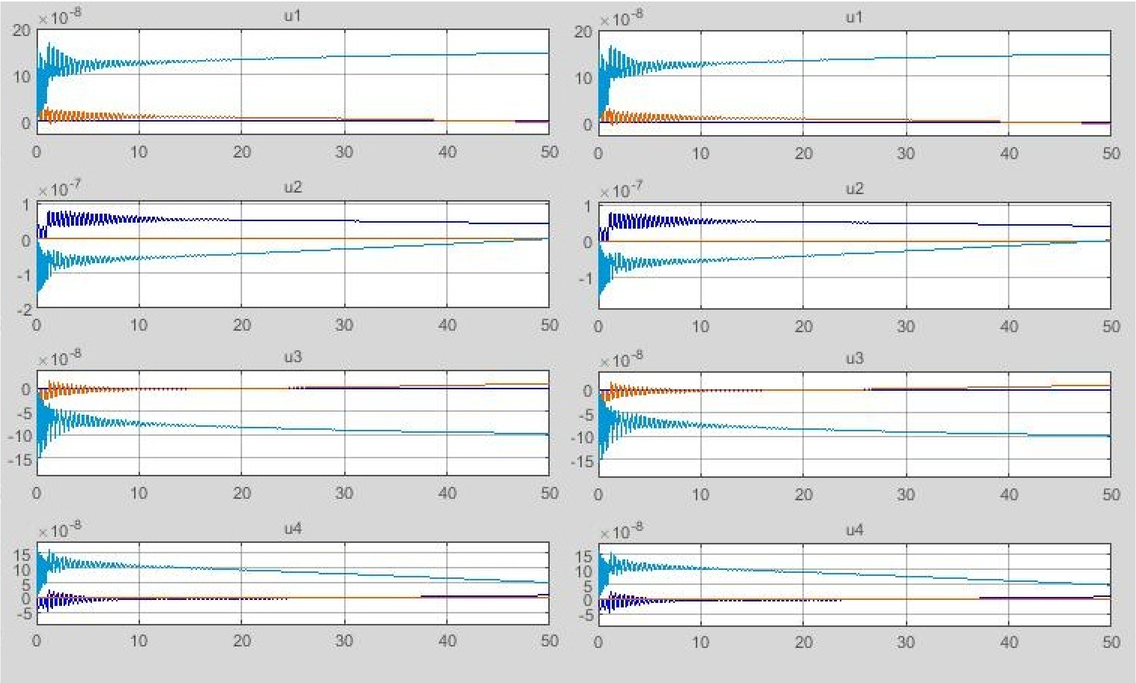

Figure G.2: Comparison of the evolution of the deformation of the booms using analytical (right) and numerical (left) models. Case 2: steady external disturbances.

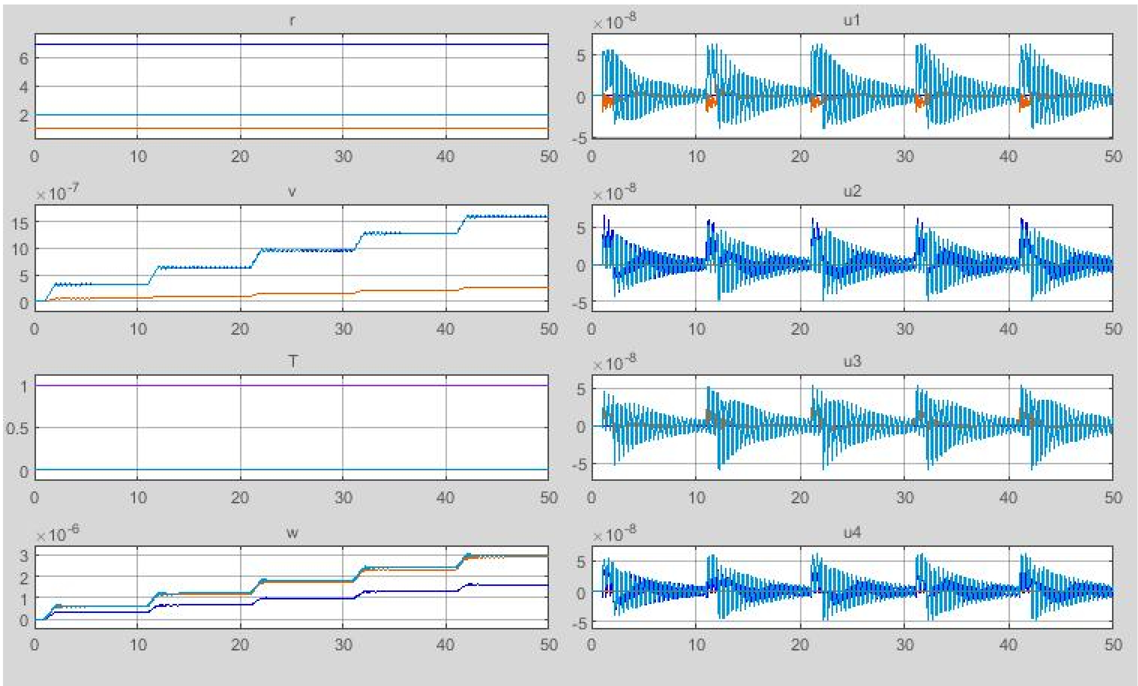

Figure G.3: Evolution of the state variables, as resulting from the analytical model. Case 3: zero initial conditions

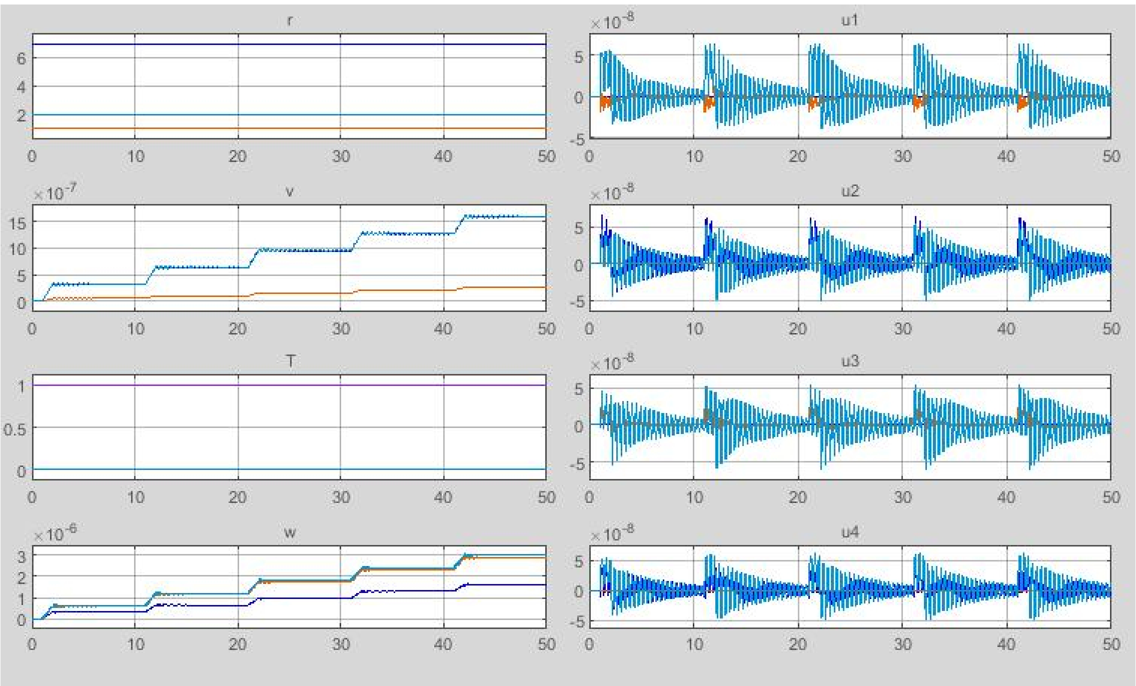

Figure G.4: Evolution of the state variables, as resulting from the numerical model. Case 3: zero initial conditions

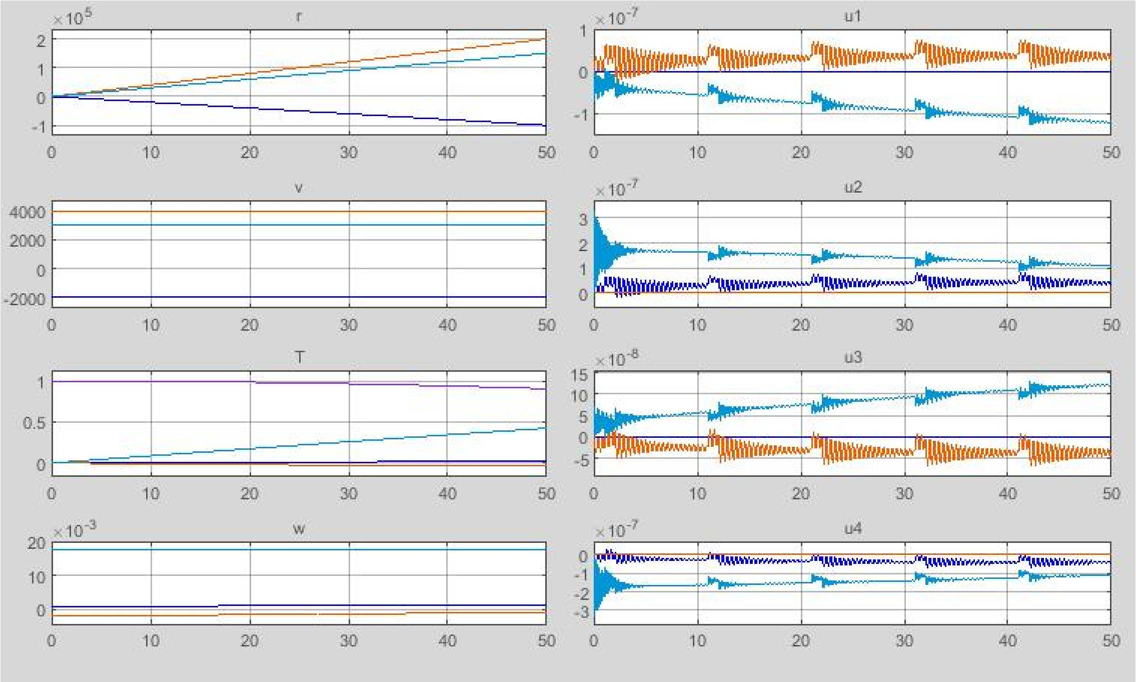

Figure G.5: Evolution of the state variables, as resulting from the analytical model. Case 4: different disturbances and initial conditions

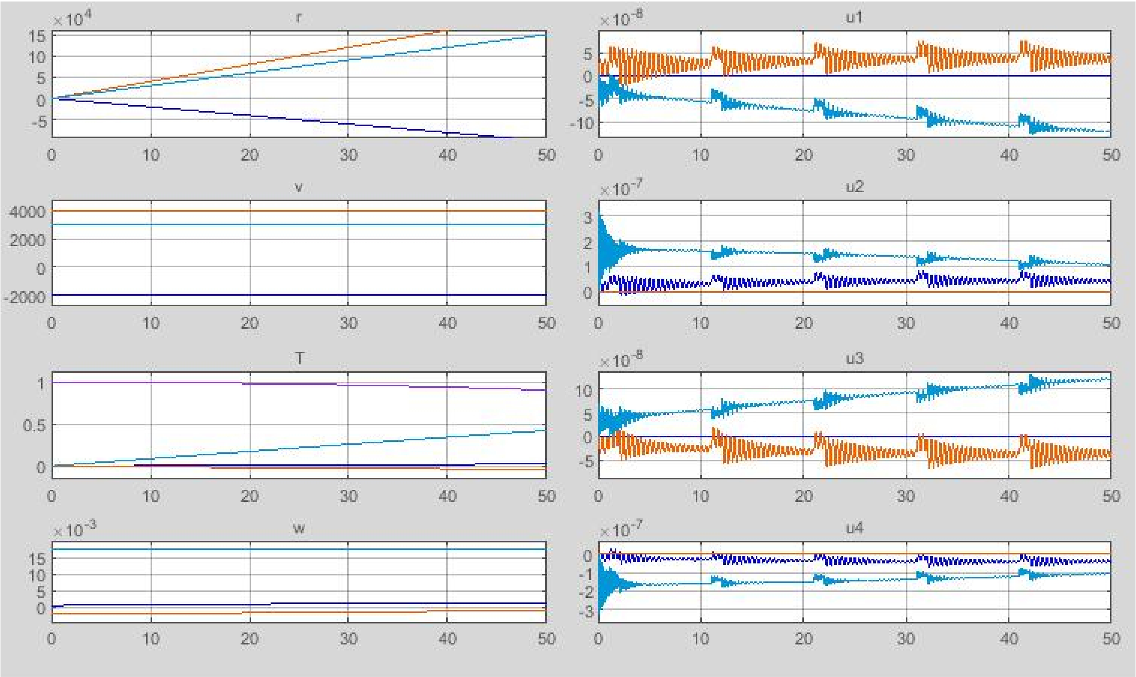

Figure G.6: Evolution of the state variables, as resulting from the numerical model. Case 4: different disturbances and initial conditions

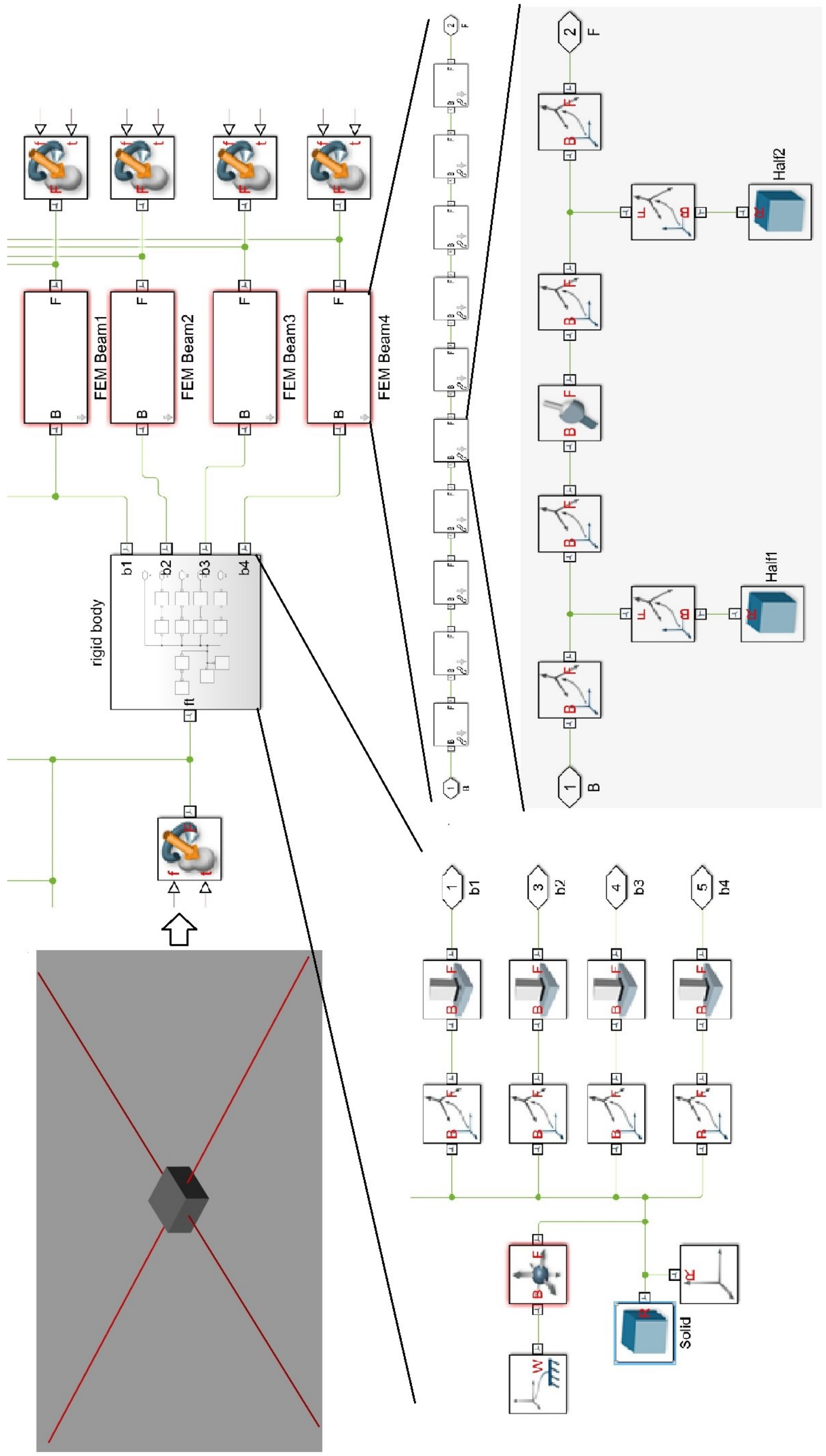
FEM Beam1
FEM Beam2
FEM Beam3
FEM Beam4
rigid body
b1
b2
b3
b4
ft
B
F
1
2
3
4
5
Half1
Half2
Solid
W
R

Figure G.7: Schematic view of the model built in MATLAB/Simscape for verification purposes.

H

Reducing order of robust controller. Example.

For reducing the order of the controller two main steps are taken. First of all, the function *minreal* is used to keep only controllable and observable states and to cancel pole-zero pairs. In this case, the order of the controller is not reduced by this function. It can be observed in figure H.1 that the initial controller does not have any extra mode when compared to *Minreal*. Secondly, based in the Hankel singular values, several reduction of order are considered. In this case 4 different reduction are considered, ending with controllers of 25, 17, 11 and 8 orders. The difference between this controller is then studied in the frequency domain (see figure H.2). In this case the results show that there are considerable differences at low frequencies and small differences at high frequencies. The objective of the reduction is, however, to choose the lowest order possible maintaining a highly similar behavior. In this case the controller chosen would be, most probably, the one of order 25.

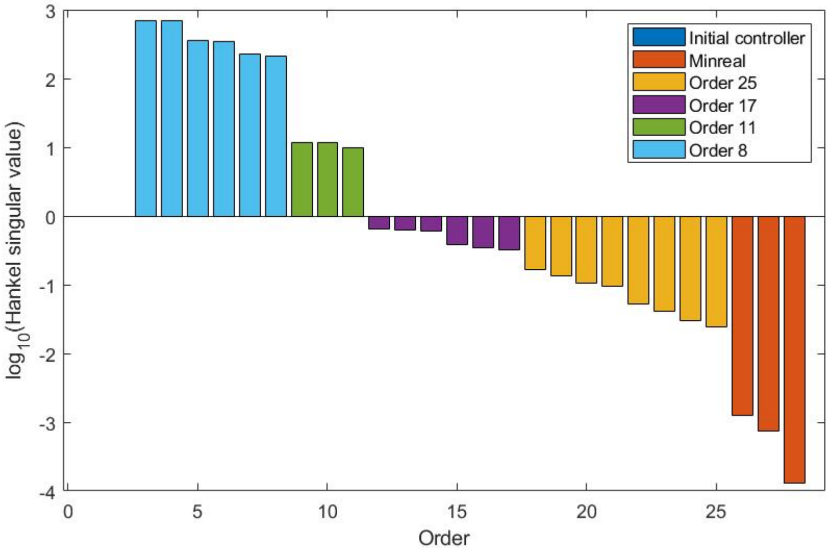

Figure H.1: Hankel singular values on the successive order reductions of the controller.

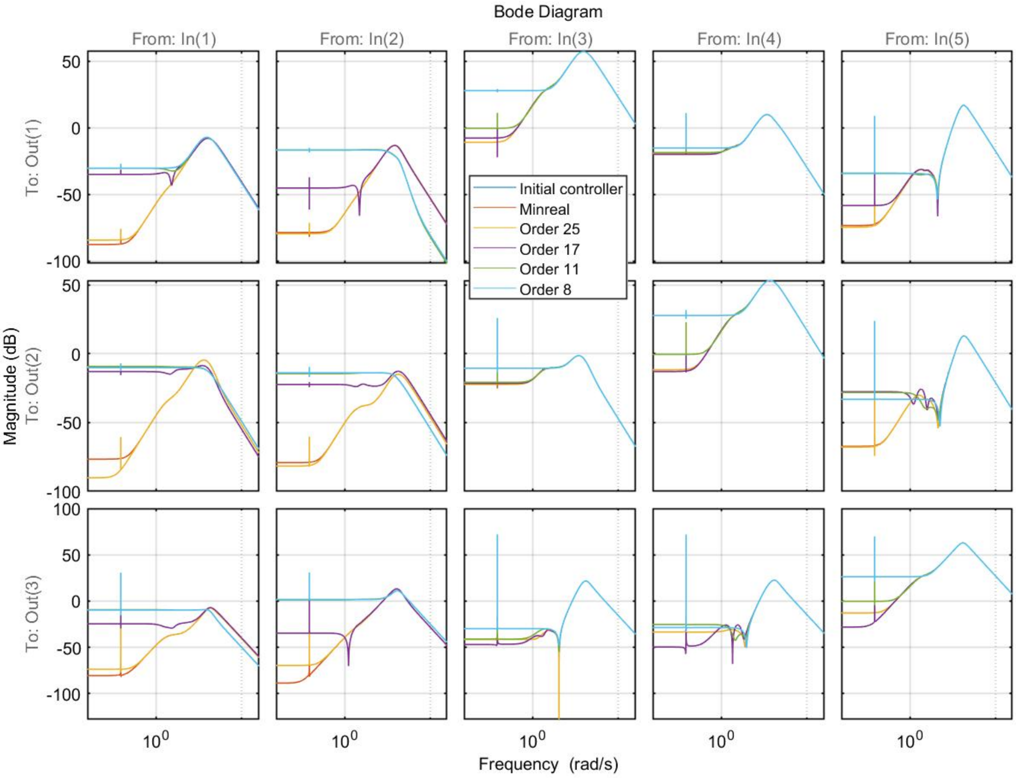

Figure H.2: Bode analysis of the successive order reductions of the controller.

I

Extended results. Robust control.

The figures in this appendix extend the analyses shown in section 5.4 in relation to the derivation and evaluation of controllers based in robust control theory. Figures I.1 to I.4 contain analyses in the frequency domain. These figures show the response in frequency of the error or measurements signal w.r.t. external torque disturbances, extending figures already explained in section5.4. Figures I.5 to I.9 compare the performance of the controller base in H_2 and that based in H_∞ in the time domain, focusing on: the deformation of the booms, the angular rate and the pointing error.

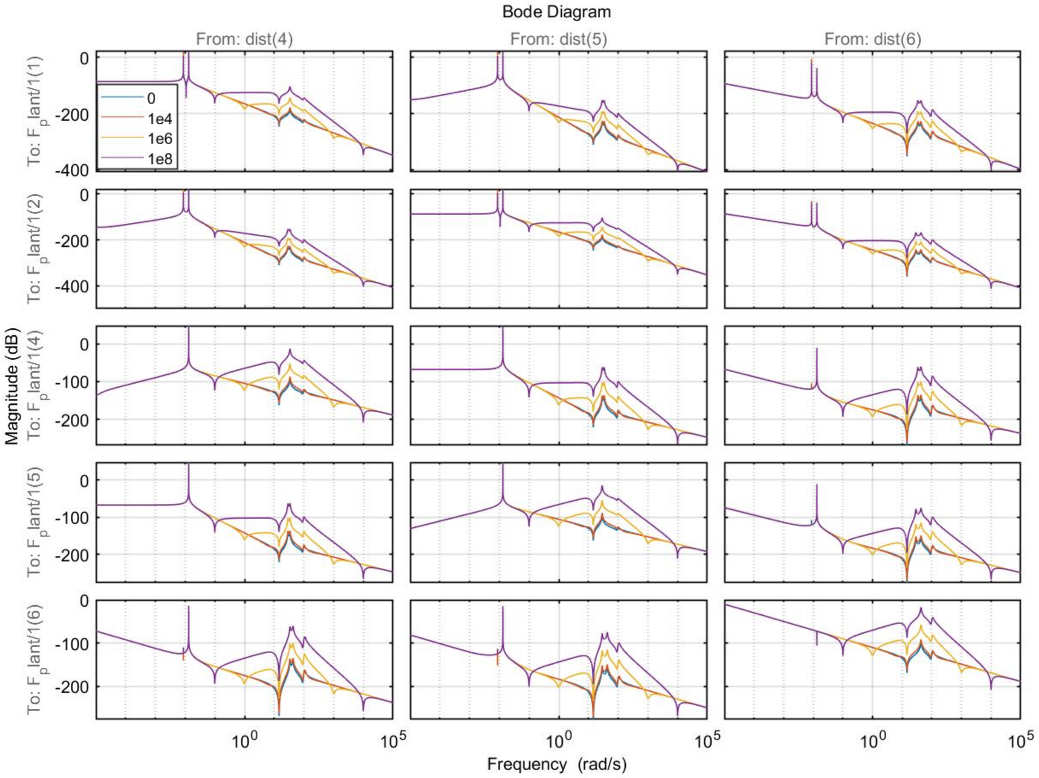

Figure I.1: Effect of different cost functions in the error signal. $f(s) = af_0(s)$, where a is the number in the legend. Extended figure 5.13.

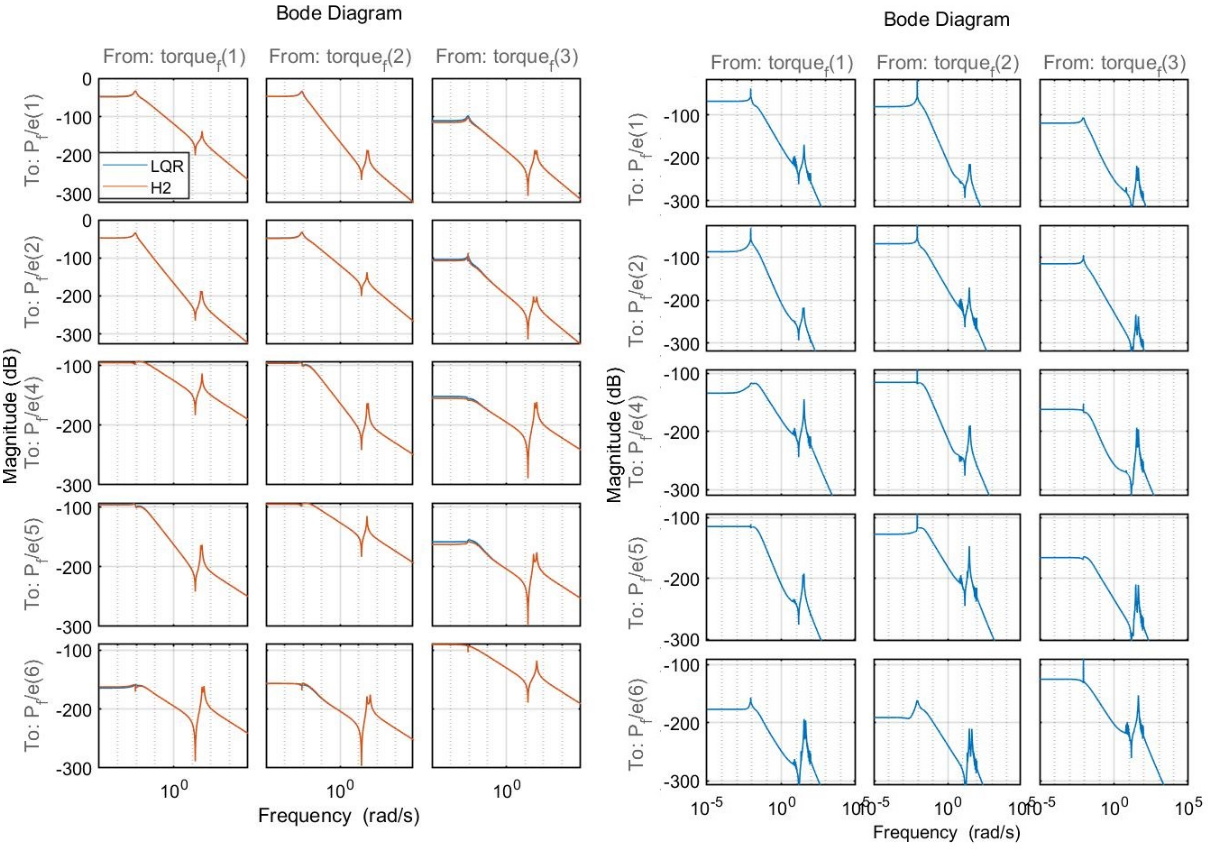

Figure I.2: Comparison of the performance of H_2 and LQR controller. Responses in the left, difference in response in the right. Extended figure I.2.

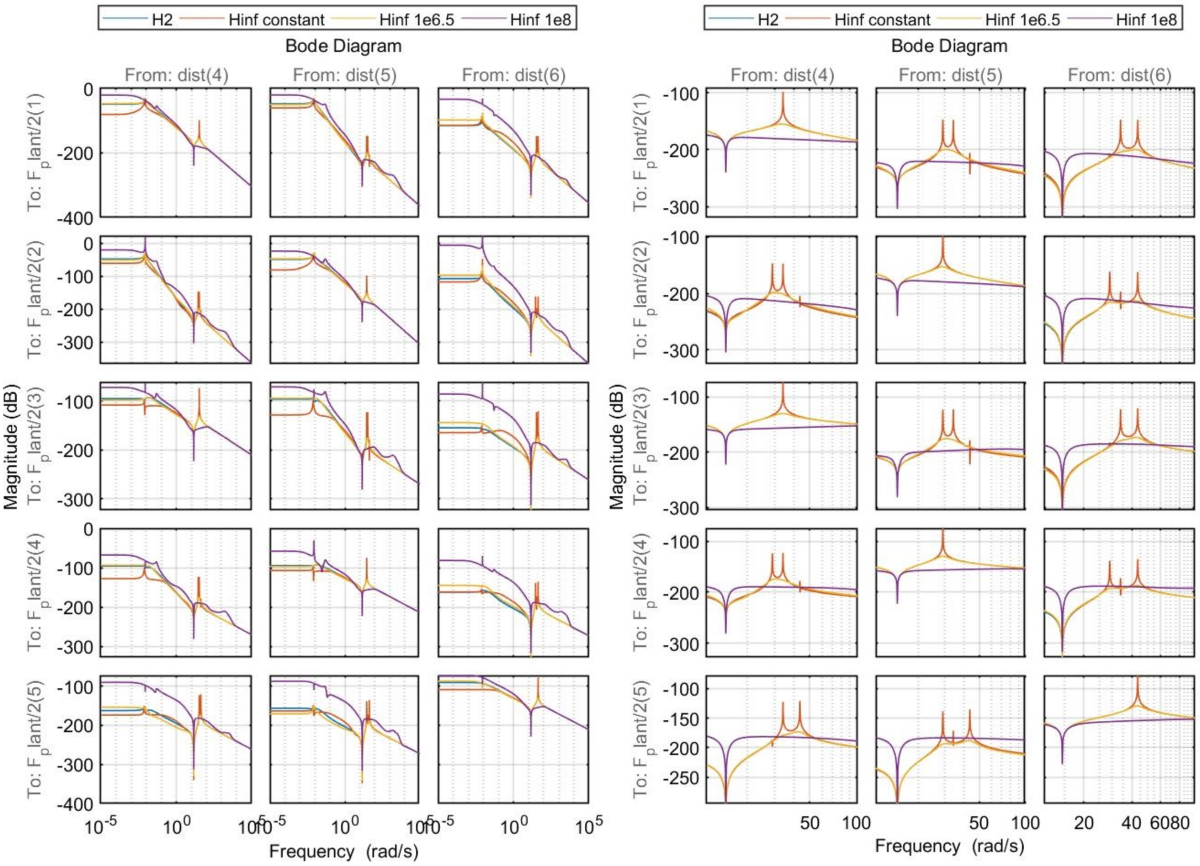

Figure I.3: Comparison of the performance of robust controllers computed with different error weighting functions ($f(s) = af_0(s)$, where a is the number in the legend) and LQR controller. Extended figure 5.15.

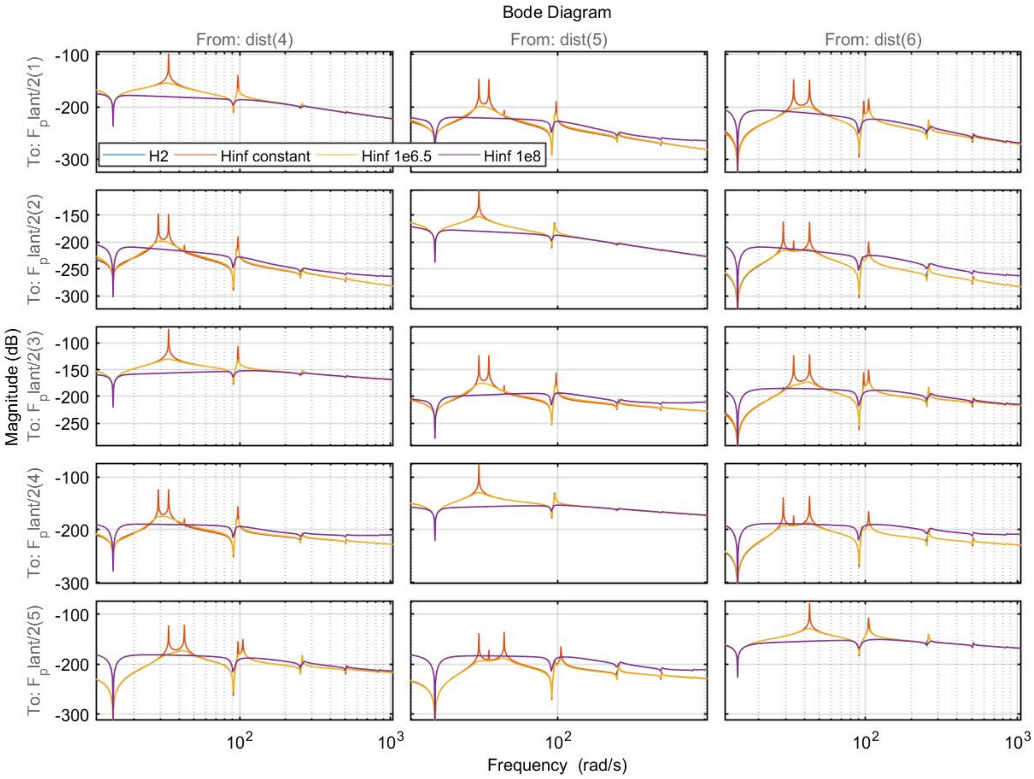

Figure I.4: Analysis shown in figure 5.15, including the first 5 modes. Extended figure 5.16

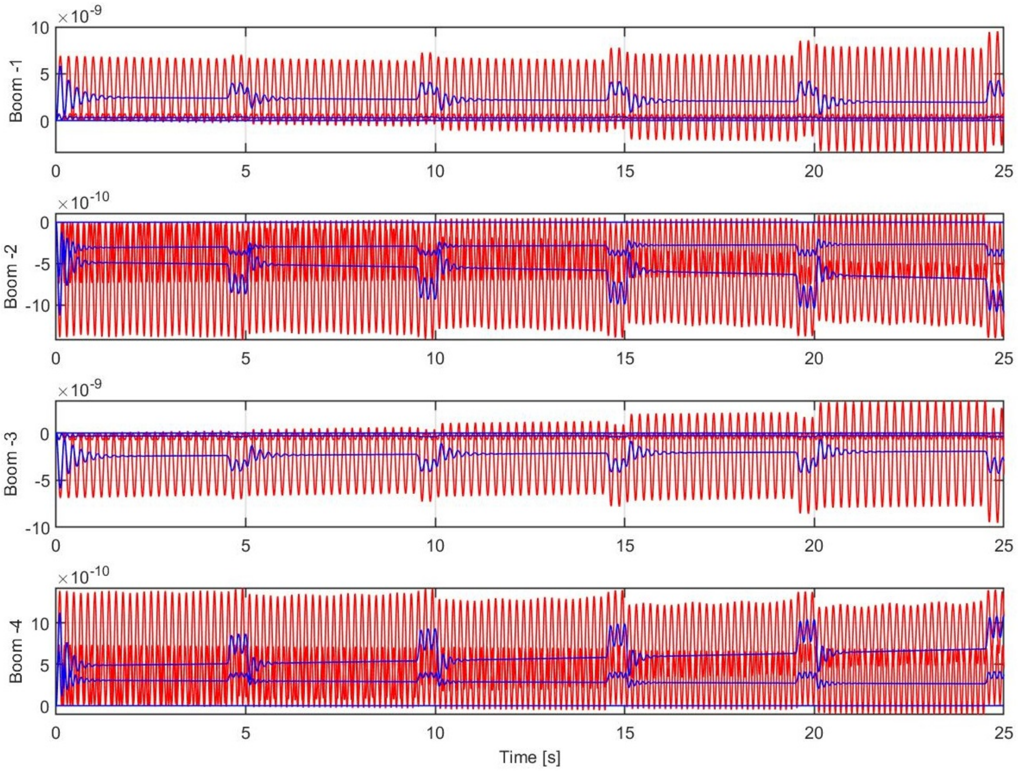

Figure I.5: Comparison of the the boom deformation for H_∞ (blue) and H_2 (red). Extended figure 5.19.

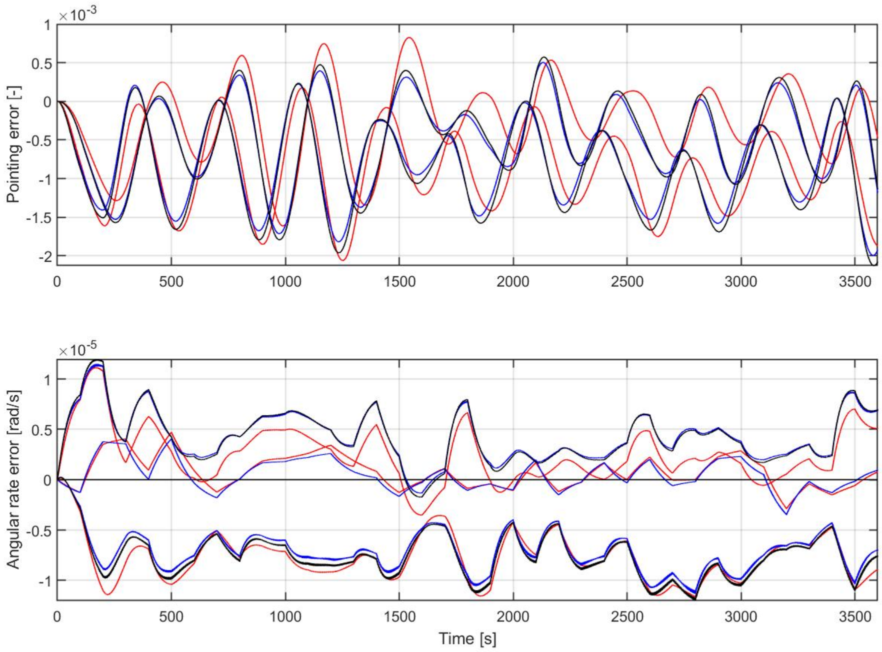

Figure I.6: Evolution of measurements under the action of disturbance force and torque for H_∞ (red), H_2 (blue) and LQR (black) controllers.

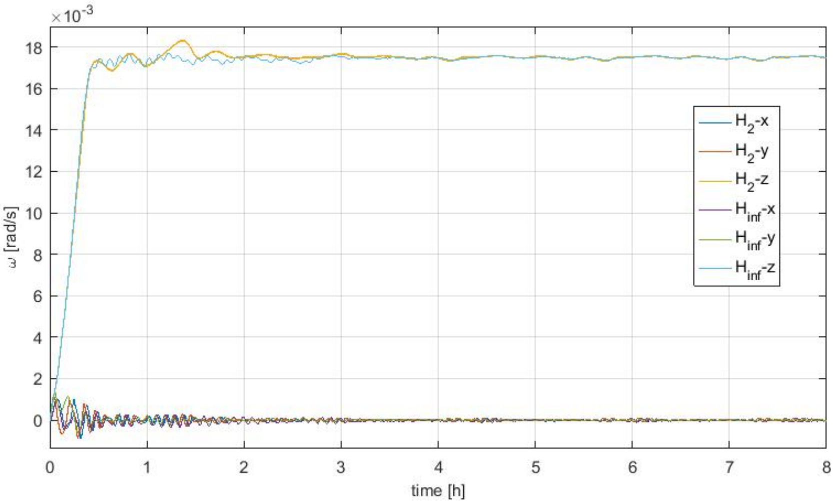

Figure I.7: Evolution of the angular rate error during the pointing phase, using H_∞ and H_2.

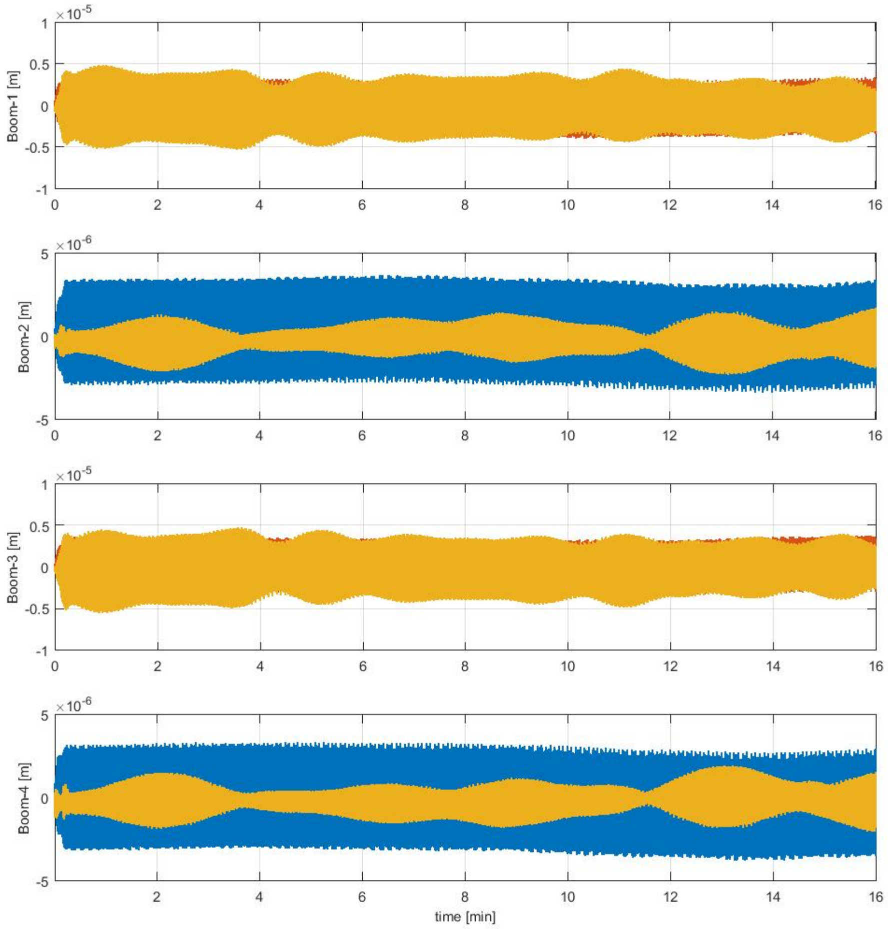

Figure I.8: Evolution of the deformation in the booms, using H_2.

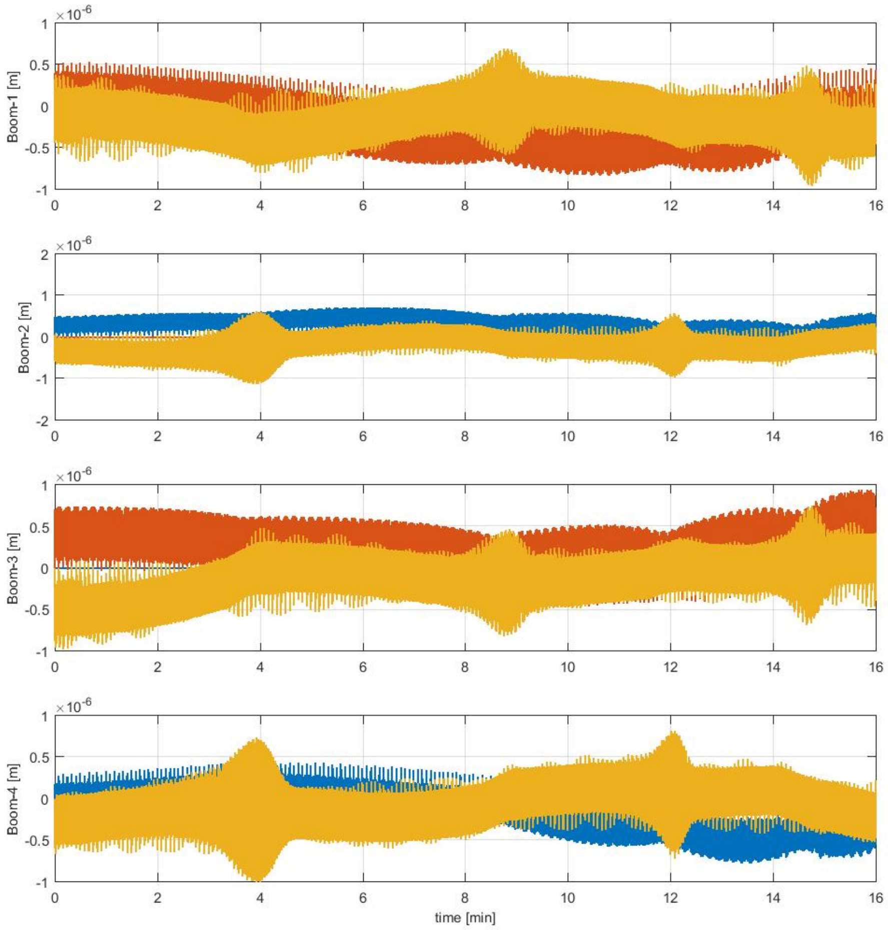

Figure I.9: Evolution of the deformation in the booms, using H_∞.

J

Extend state vector's estimations

In order to enable actively damping the vibration of the booms, the possibility of using an extended state vector was considered. This vector would include an estimation of the deformation of the booms. This appendix give a brief (conceptual) introduction to some of the possibilities that can lead to this extended vector.

There are several options for estimating the complete state vector, including the decomposition of the bending deformation between the deformation modes. These options are depicted in figure J.1 and will be briefly discussed here. On a top level, there are two main options: direct and indirect estimation. Direct estimation involves the use of sensors measuring the variables to be estimated, while indirect involves the use of information regarding other the external and internal disturbances in combination with a model of the dynamics. Within direct estimation the number of sensors and their characteristics is the main aspect to be considered. Regarding indirect estimation, it is necessary to defined the model which is to be used. The main pros and cons of each possibility are pointed out below.

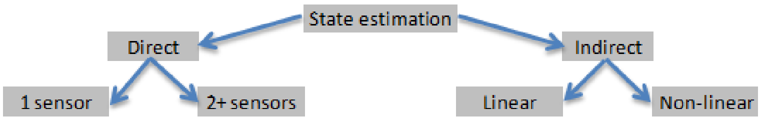

Figure J.1: Options for obtaining a more complete estimation of the state vector.

- Direct estimation. Additional weight and hardware complexity, proportional to the number of sensors. Each additional sensor along the length of the boom allows to estimate an additional mode. The number of sensors would therefore depend on the accuracy requirements. Regarding the type of sensor to be used, accelerameters seem to be the most logical choice due to their low weight and cost.
- Indirect estimation. Requires a fair estimation of the disturbance forces. Defining an initial condition is not trivial and requires a period with relatively stable external and internal forces and torques. When using a linearized model its validity is limited to the surroundings of the linearization point but the computational cost decreases considerably.

The most promising option appears to be to position one accelerometer in the tip of each boom, leading to an estimation of the deformation at the tip of the boom.

K

Extended results of non-linear controller

The figures contained in this section extend the results of the non-linear controller based in the Udwadia-Kalaba approach (see section 5.5). Figure K.1 shows the evolution of the pointing error for different initial conditions. Figures K.2 and K.3 compare the non-linear controller to the LQR controller. Figure K.4 analyses the improvement in the pointing error distribution when the constraint in the torque (magnetorquer) is introduced into the controller. Figure K.5 shows the evolution of the angular rate, pointing out the vibrations due to the magnetorquer duty cycle. Figure K.6 shows the deformation of the booms in the Z-axis with different degrees of zoom and figure K.7 in the X and Y axes. Finally, figure K.8 shows the force generated (by one of the long linear controllers) in order to damp the vibrations due the eclipses.

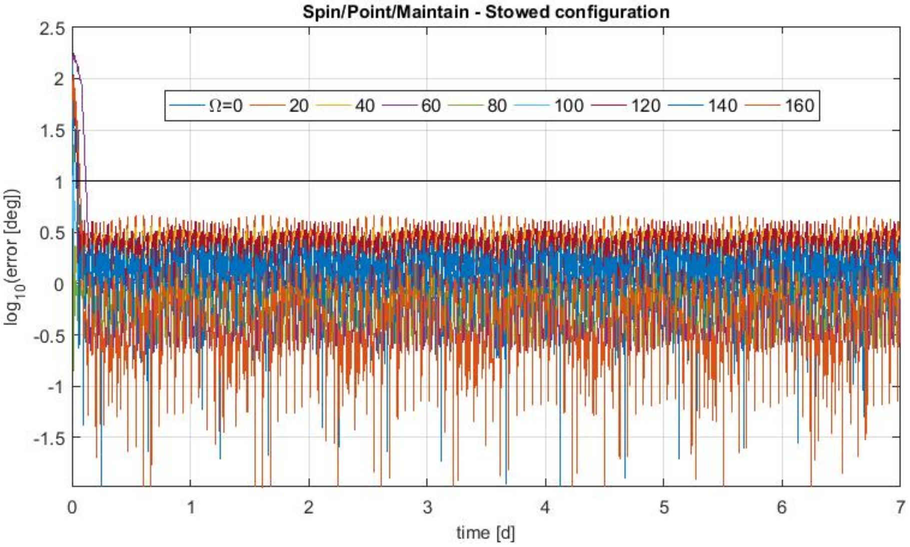

Figure K.1: Evolution of the pointing error for 9 different initial conditions (angular rate, attitude and Ω). Deployed configuration. h: 600 km, i: 97 deg.

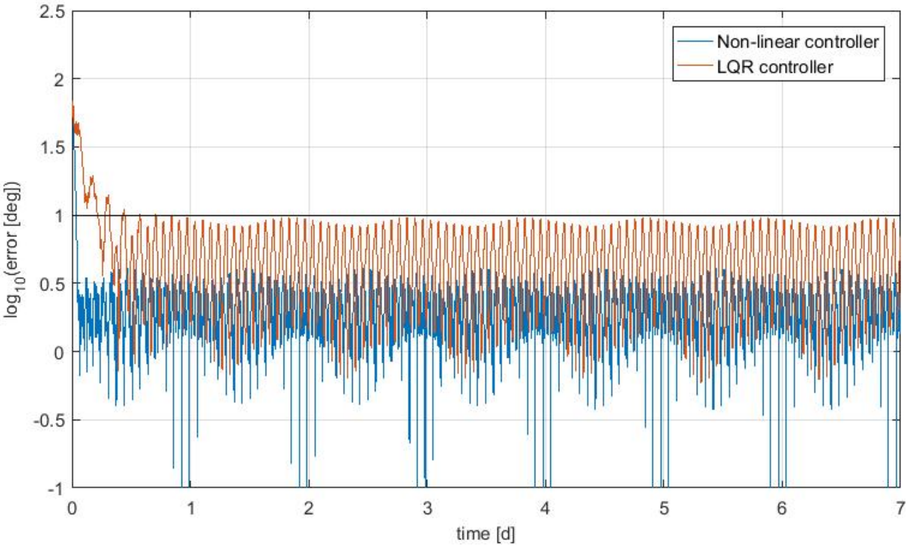

Figure K.2: Evolution of the pointing error under LQR and non-linear controllers. Deployed configuration. h: 550 km, i: 97 deg, Ω: 0.

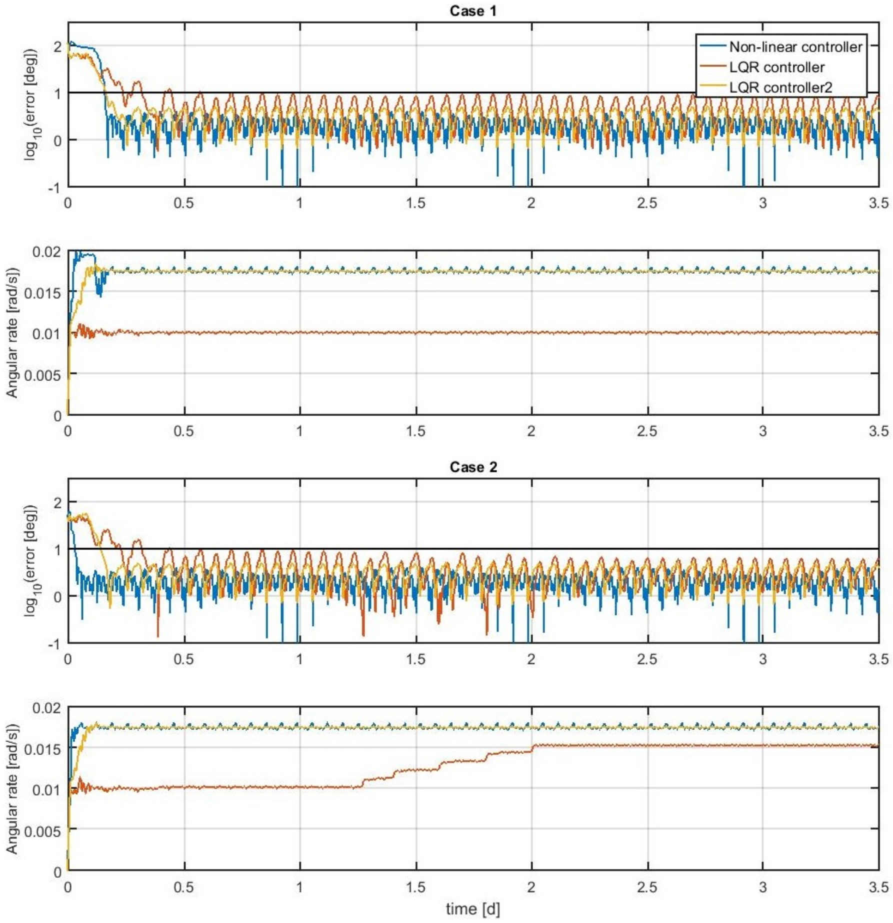

Figure K.3: Additional comparison based in figure K.2. h: 600 km, i: 60 deg, Ω: 0.

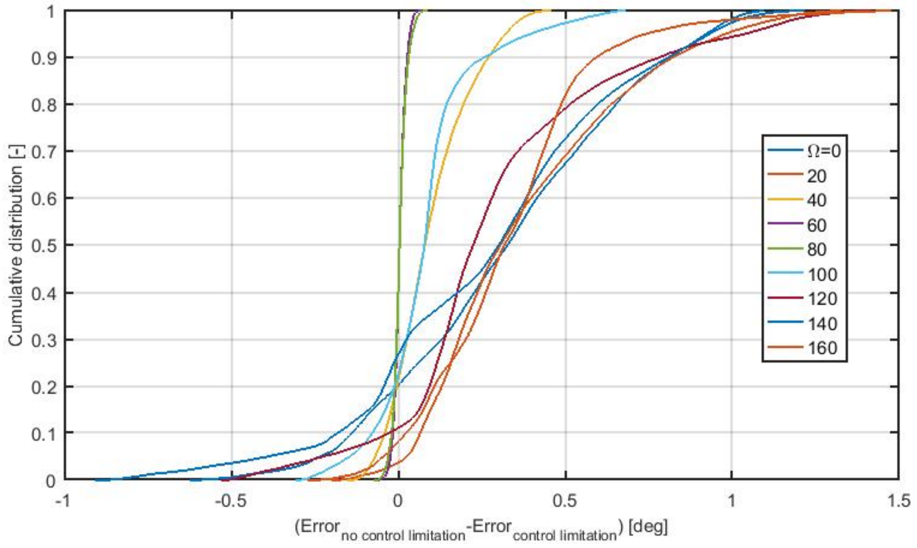

Figure K.4: Consequences of adding the constrain on the torque (expression 5.31)

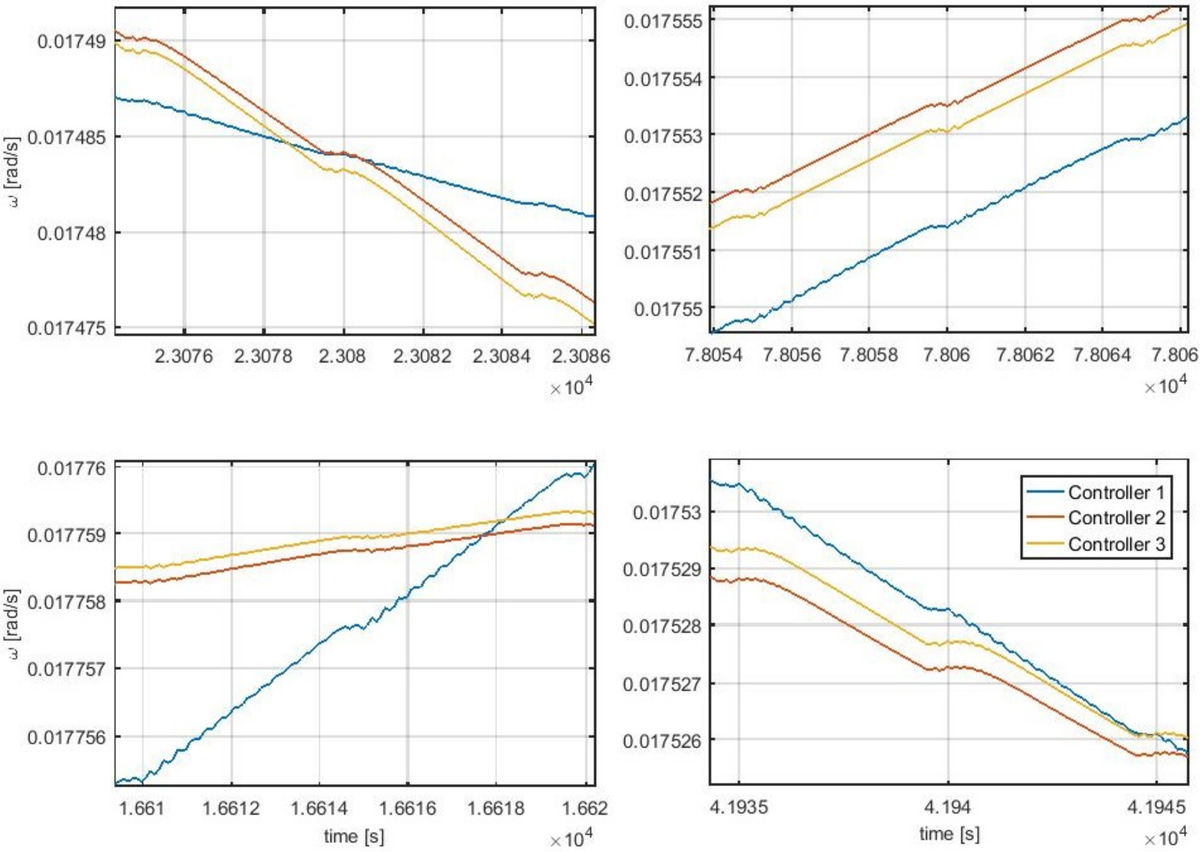

Figure K.5: Analysis of the short term oscillations of the angular rate under non-linear controller with different specifications. Deployed configuration. h: 600 km, i: 97 deg, Ω: 0. Extended figure 5.28

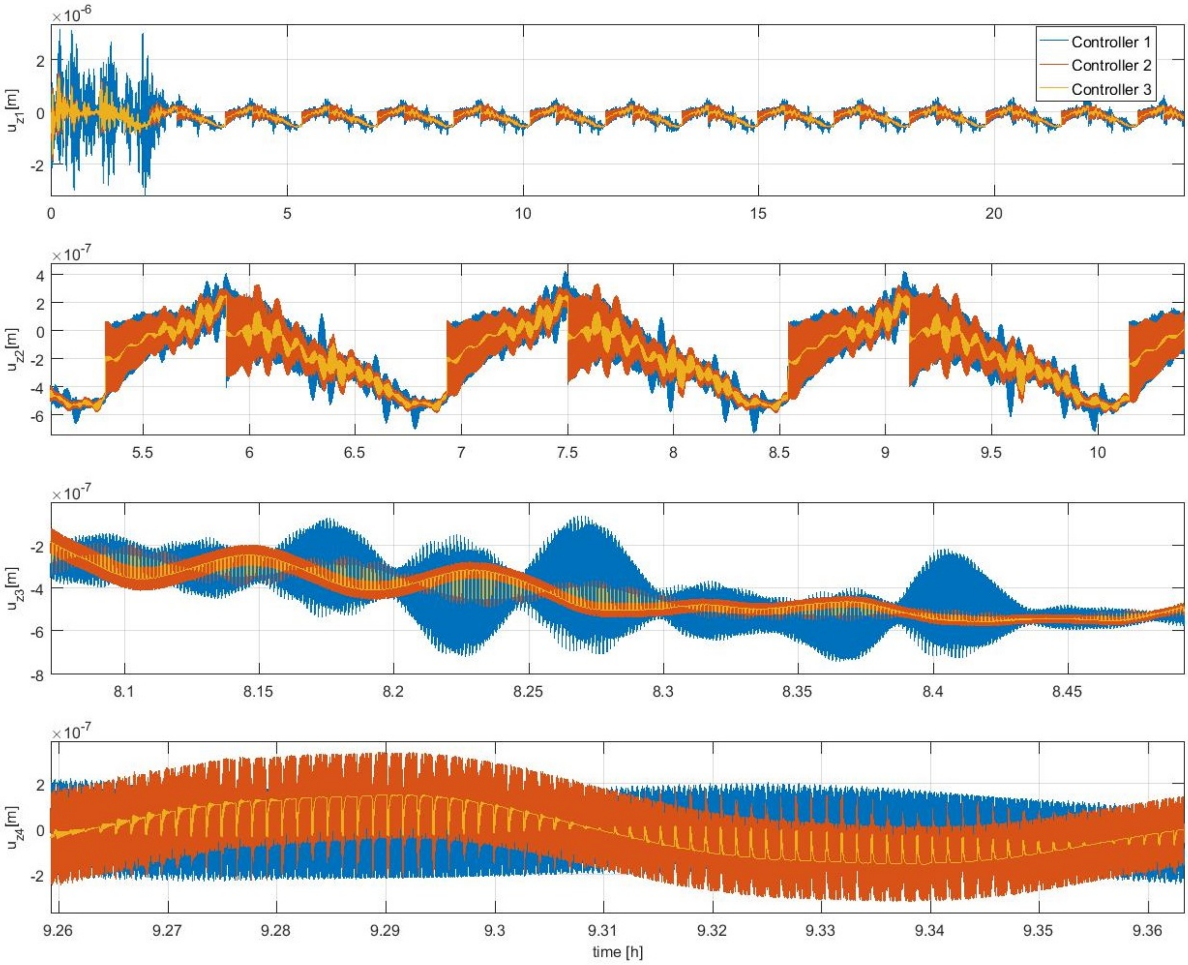

Figure K.6: Analysis of the evolution of the boom's deformations under non-linear controller with different specifications. Z-axis. Deployed configuration. h: 600 km, i: 97 deg, Ω: 0. Extended figure 5.29

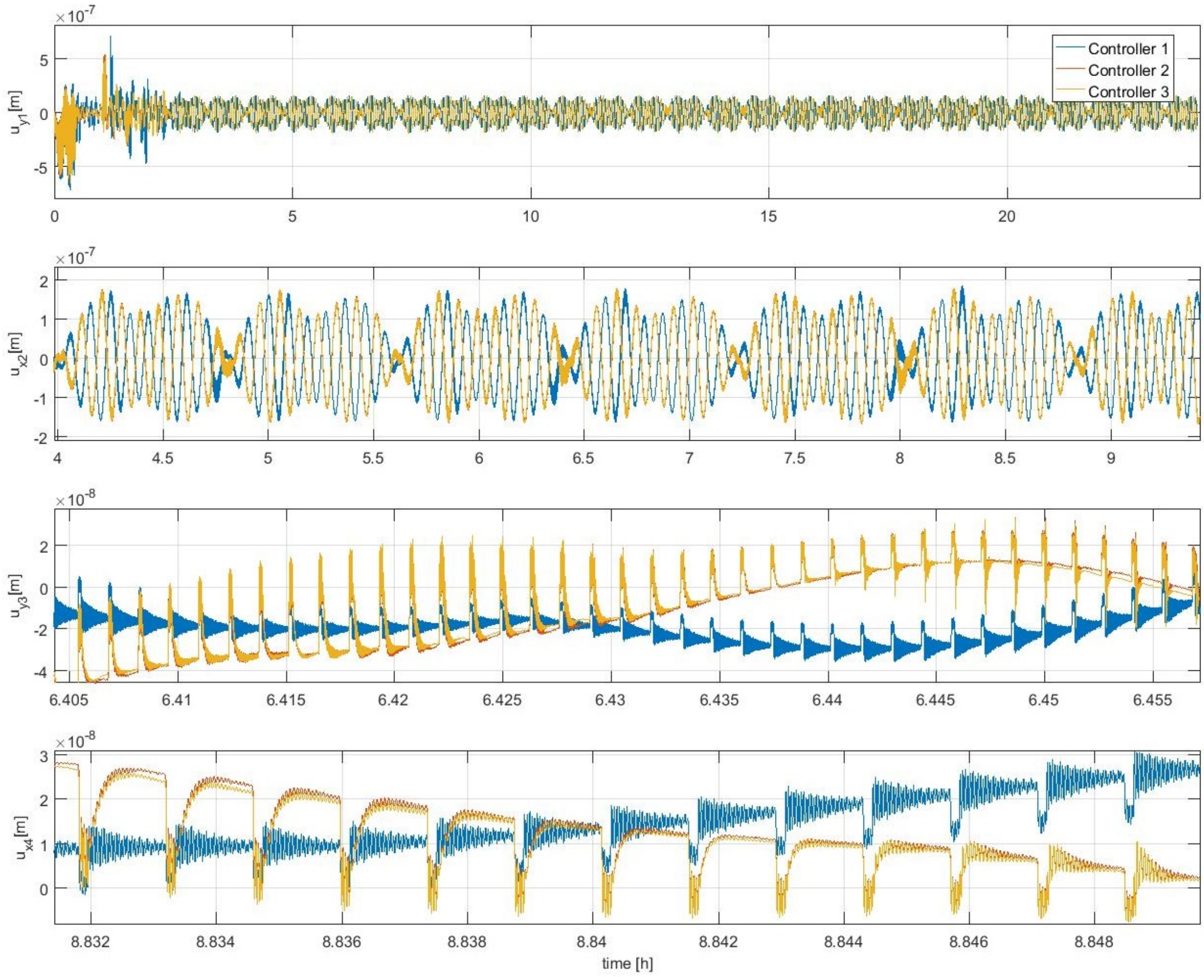

Figure K.7: Analysis of the evolution of the boom's deformations under non-linear controller with different specifications. X,Y-axes. Deployed configuration. h: 600 km, i: 97 deg, Ω: 0. Extended figure 5.30

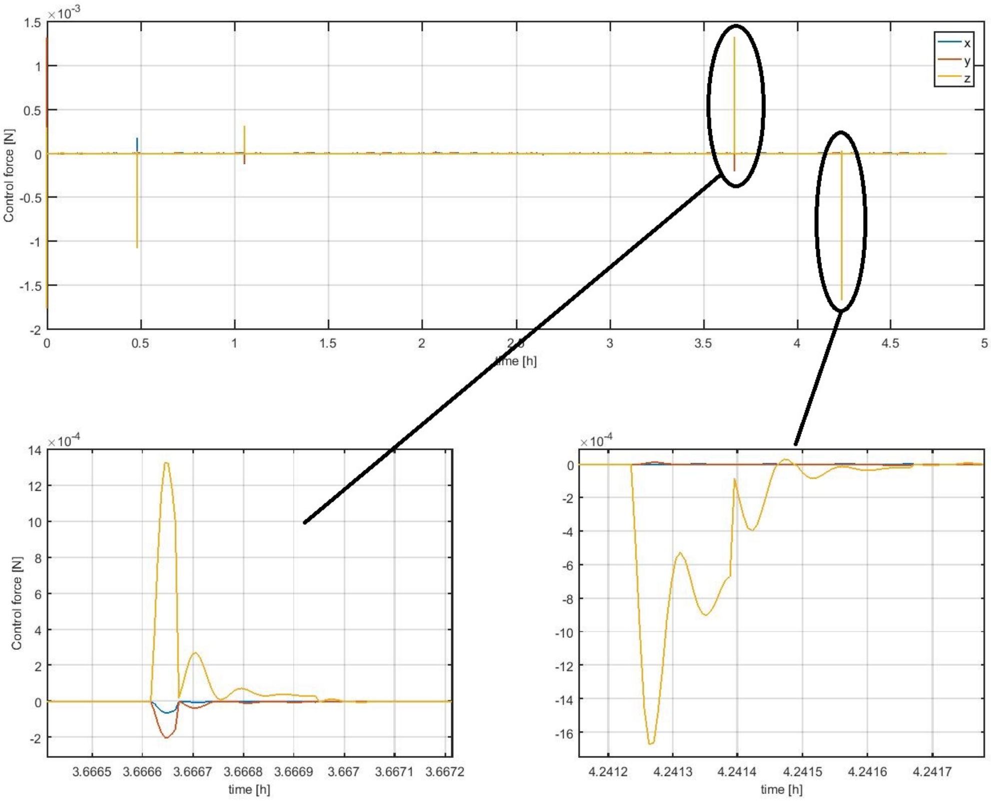

Figure K.8: Analysis of the control force exerted over the spacecraft by controller 3. X,Y-axes. Deployed configuration. h: 600 km, i: 97 deg, Ω: 0. Extended figure 5.31

L

Extended results of the sensibility analysis

The figures included in this appendix contains the additional results of the sensibility analysis explained in section 5.6.1. Figures L.1 to L.4 show the differences that appear in the pointing error due to errors in the moment of inertia (and related variables) for the different controllers studied. Figures L.5 to L.6 study this same difference but caused by noise in the measurements. Figures L.7 and L.8 focus in the difference in the vibration of the booms (i.e. analysing effectiveness of the active damping) due to errors in difference variables (e.g. bending stiffness) and noise.

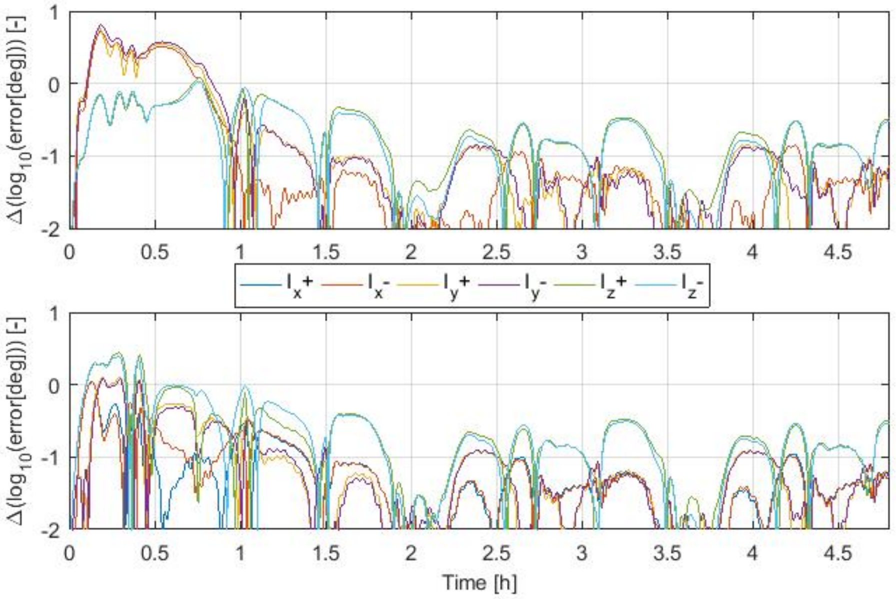

Figure L.1: Difference in the pointing accuracy due to errors in the estimation of the moment of inertia. Non-linear rigid controller. 2 different initial conditions.

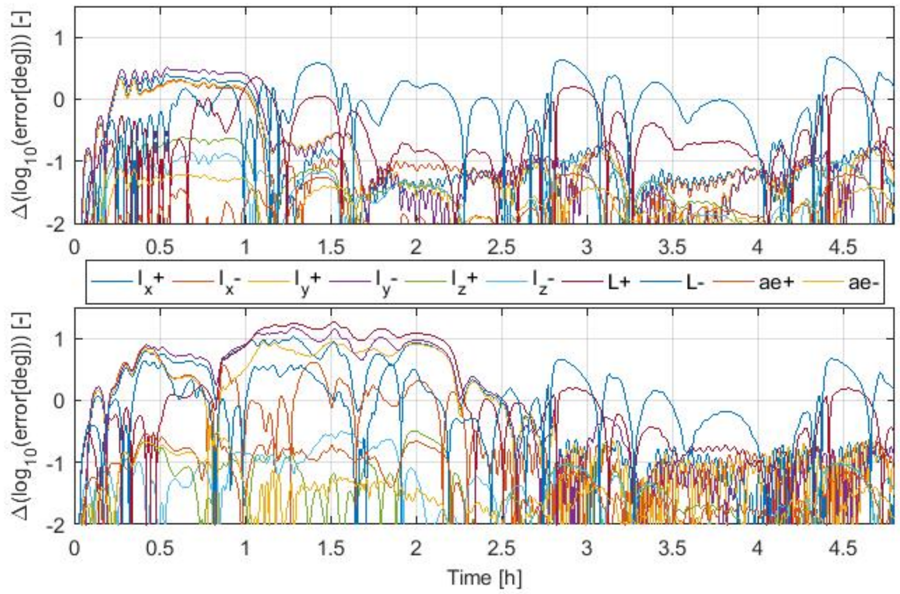

Figure L.2: Difference in the pointing accuracy due to errors in the estimation of the moment of inertia of the central part of the satellite and in the length and linear density of the booms. Non-linear flexible controller. ae states for linear density. 2 different initial conditions.

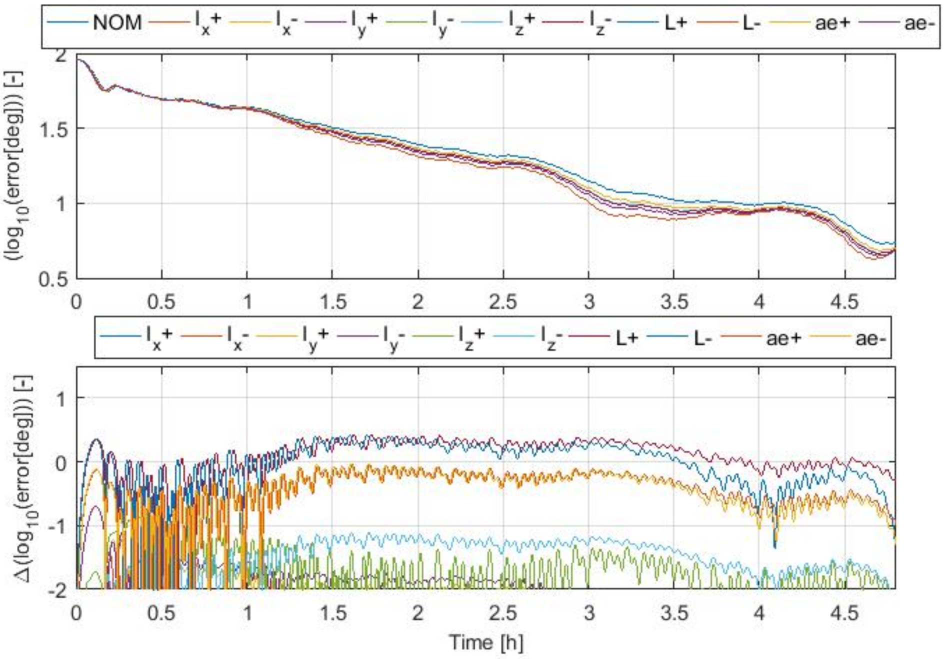

Figure L.3: Pointing accuracy and difference in the pointing accuracy due to errors in the estimation of the moment of inertia of the central part of the satellite and in the length and linear density of the booms. H_∞ controller. ae states for linear density.

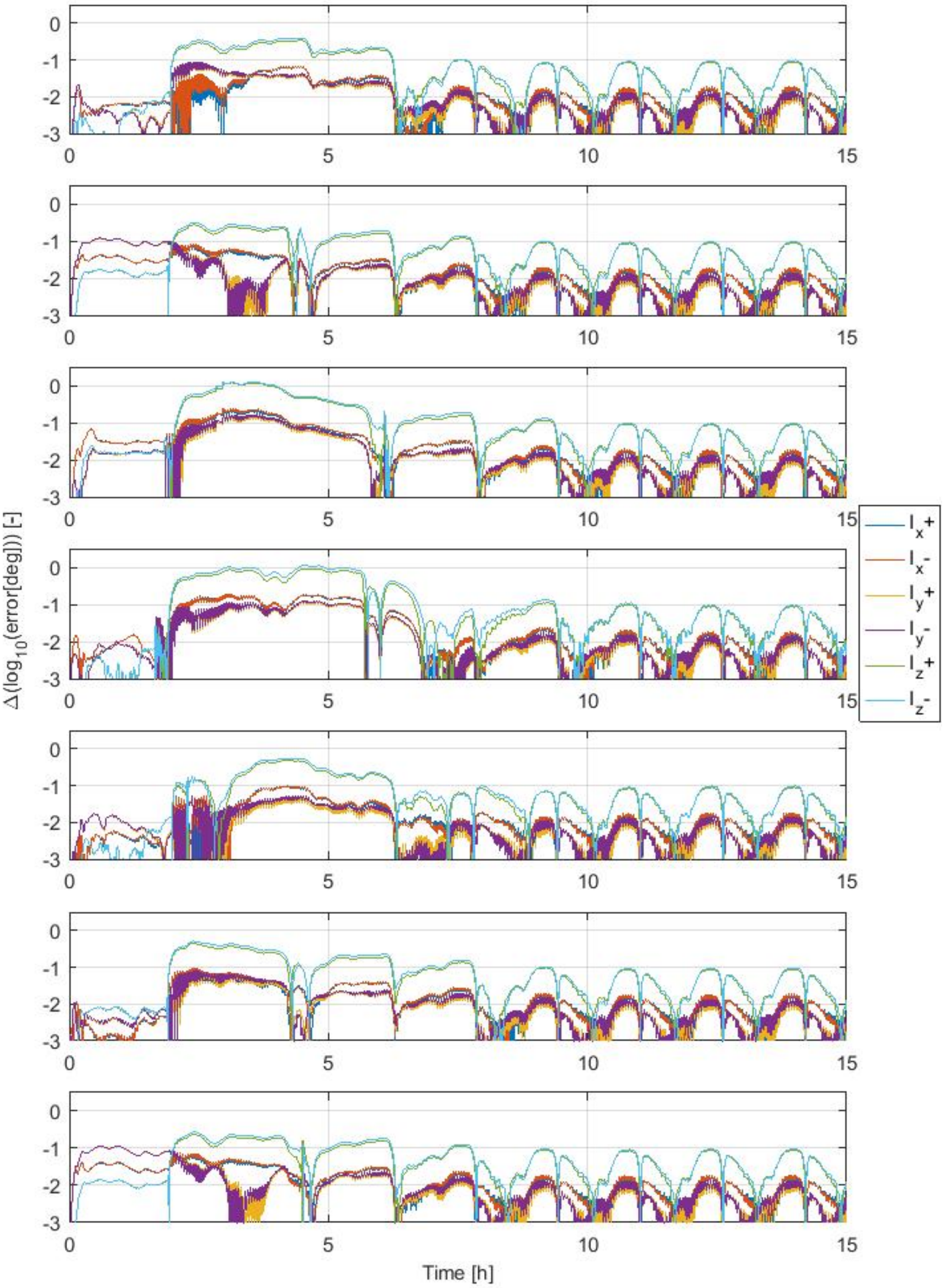

Figure L.4: Difference in the pointing accuracy due to errors in the estimation of the moment of inertia. LQR controller. 7 different initial conditions. Additional cases in relation with figure 5.32.

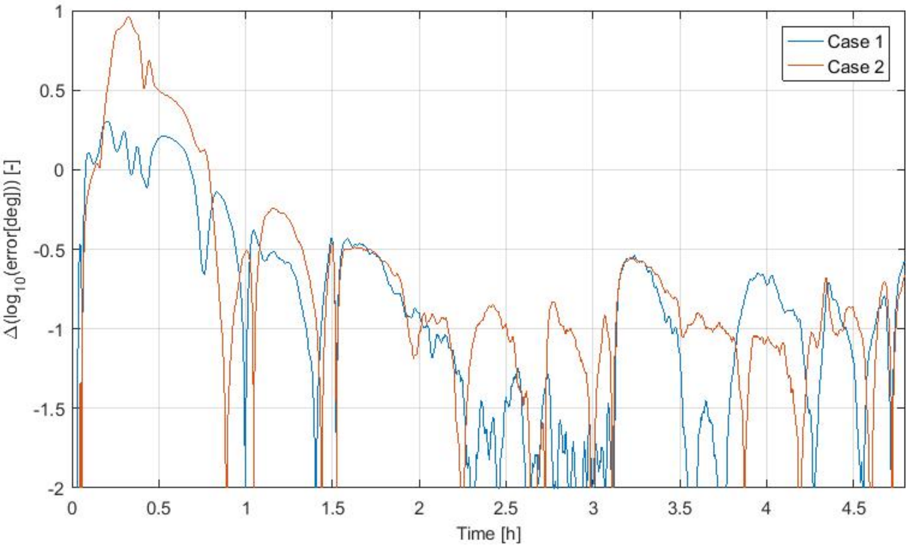

Figure L.5: Difference in the pointing accuracy due to the addition of noise to the measurements. Non-linear rigid controller. 2 different cases.

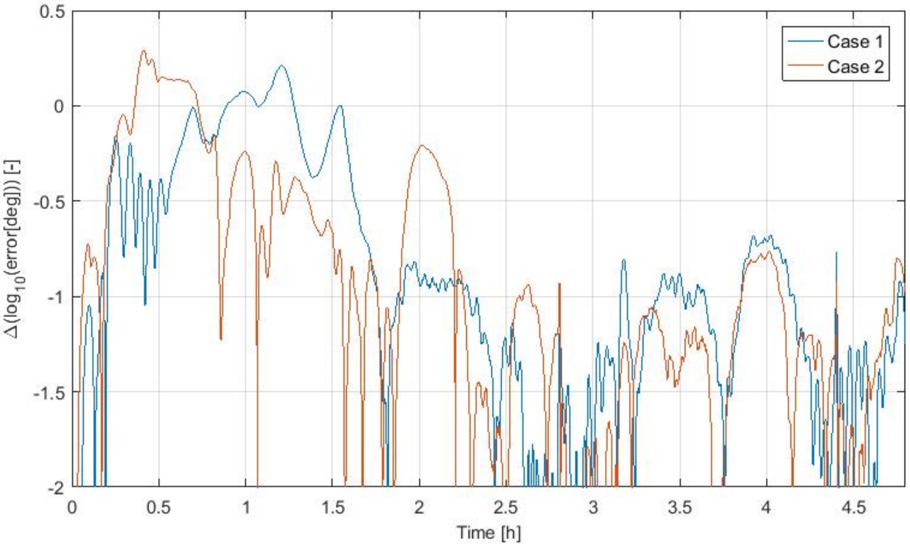

Figure L.6: Difference in the pointing accuracy due to the addition of noise to the measurements. Non-linear flexible controller. 2 different cases.

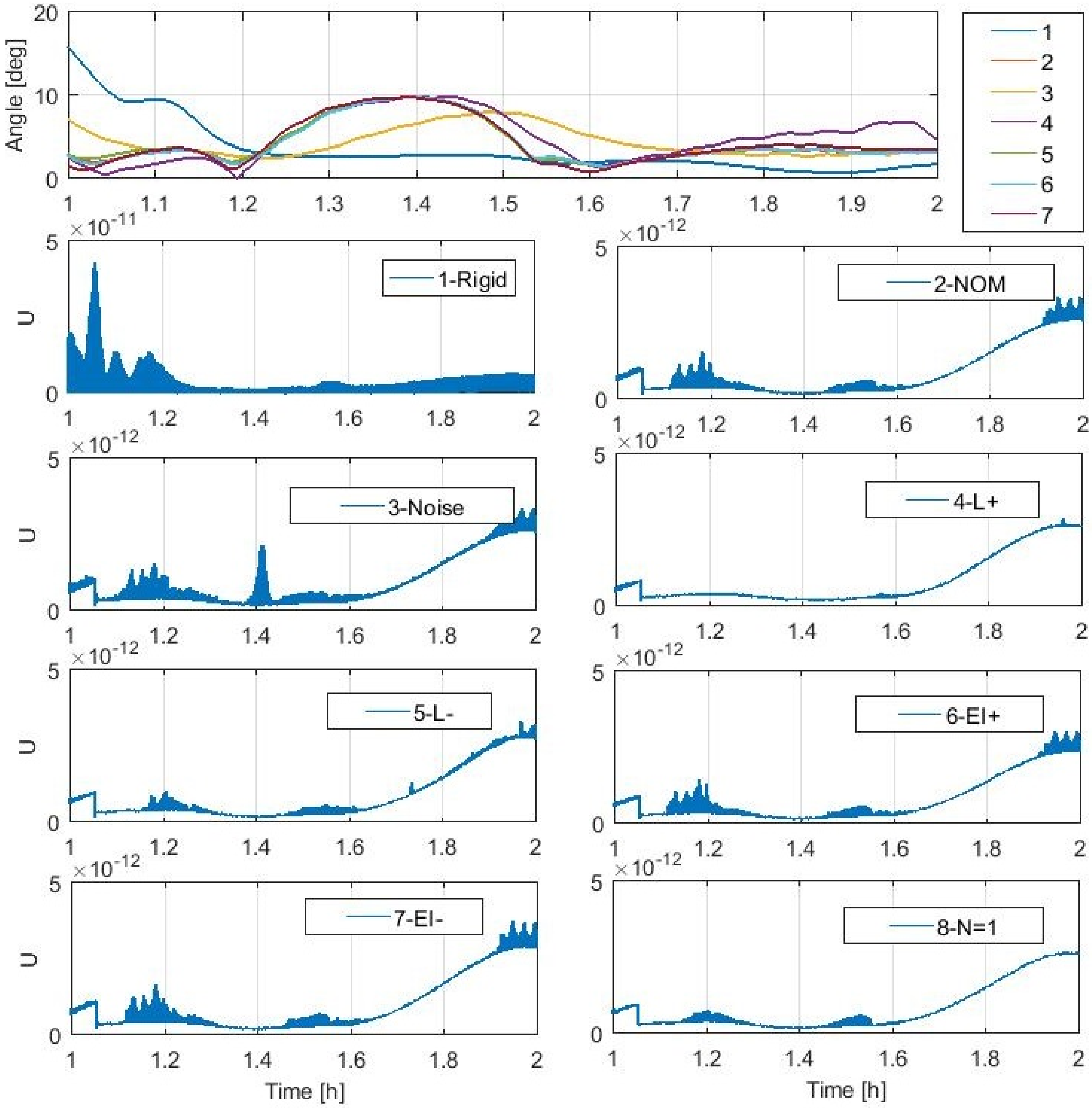

Figure L.7: Zoom in figure 5.35.

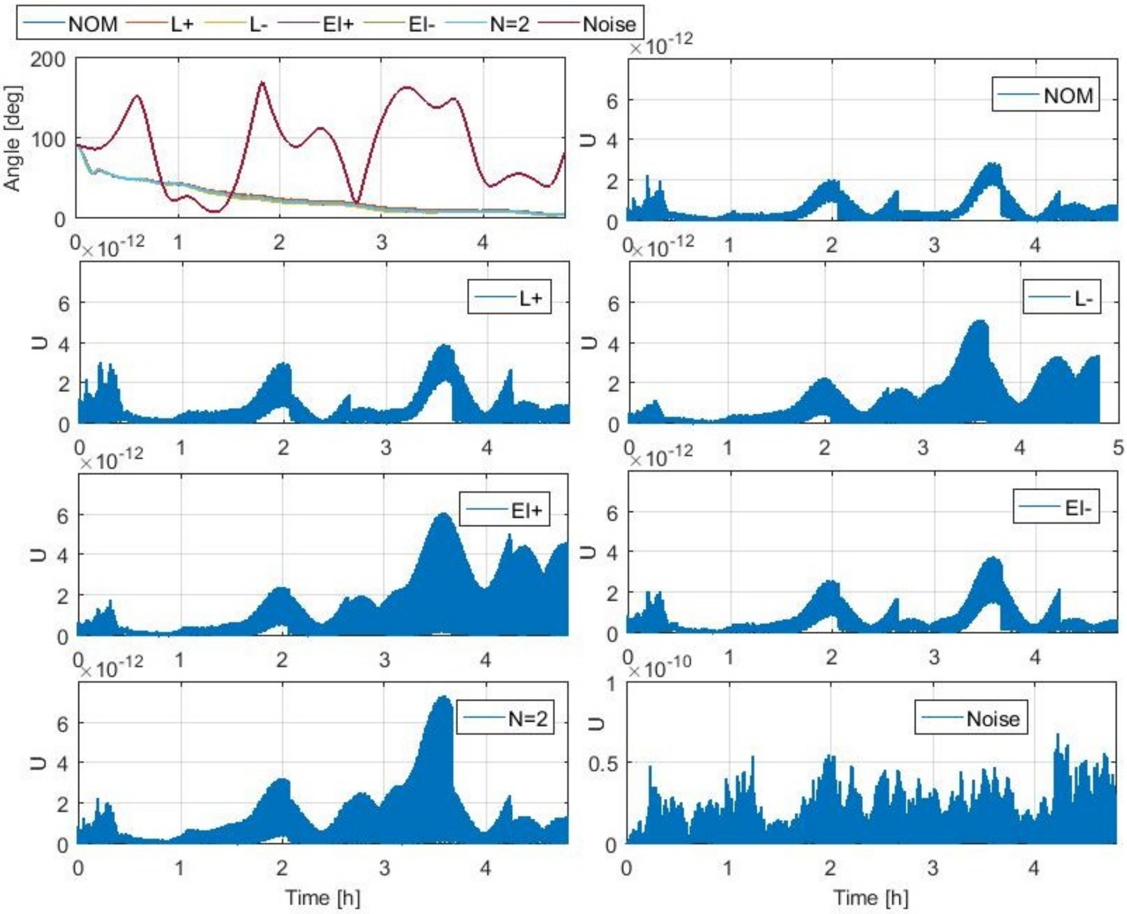

Figure L.8: Difference in the pointing accuracy and in the vibration of the booms (U) due to errors in the estimation of bending stiffness (EI) and length of the booms (L) and limitation in control information. H_∞ controller.